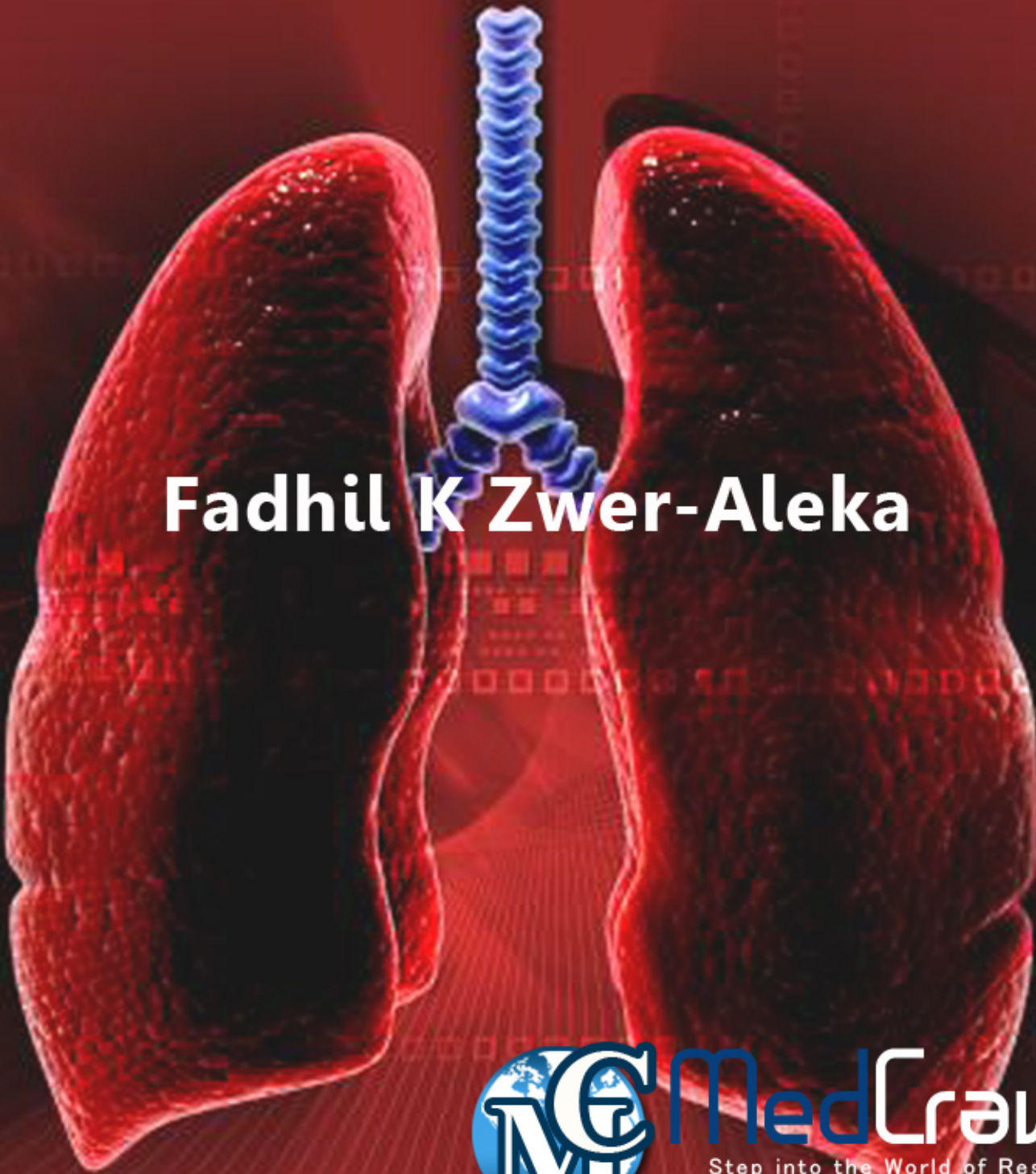


Acute Lung Injury & Acute Respiratory Distress Syndrome-Part II (Applied physiology) [Extensive Basic and Clinical Study]

An anatomical illustration of the human respiratory system. The lungs are shown in a reddish-pink color, and the spine is shown in a blue color. The lungs are positioned on either side of the spine, and the spine is shown in a vertical orientation. The background is a dark red color with a grid pattern.

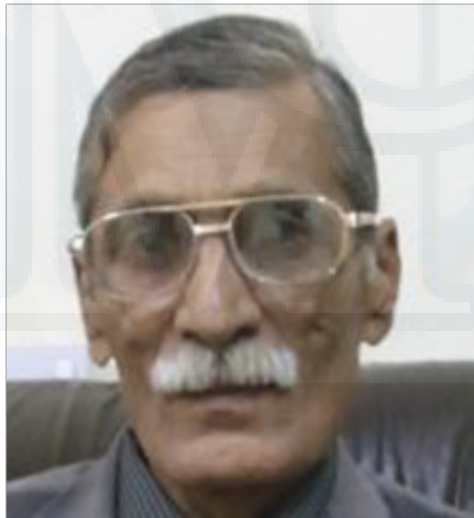
Fadhil K Zwer-Aleka

Acute Lung Injury & Acute Respiratory Distress Syndrome-Part II (Applied physiology) [Extensive Basic and Clinical Study]

Fadhil K Zwer-Aleka
by
MB ChB DAICM
Retired at private practice

Dedication

This book is dedicated for every physician that the patients need from him a high efficiency, fair scientific management, safety and a merciful outcome.



Published By:
MedCrave Group LLC
April 30, 2016

Contents

Pulmonary fluid balance.	1
Alveolar epithelium.	4
Mechanisms of alveolar protein clearance in the intact lung.	7
Distribution of blood flow and ventilation in the lung.	13
Morphological changes of carotid bodies in acute respiratory distress syndrome.	21
Pulmonary vascular permeability.	23
Regulation of alveolar epithelial function by hypoxia.	41
Pulmonary injury, oxidant stress, and gap junctional communication.	43
The roles of keratinocyte and hepatocyte growth factors in lung development, inflammation and repair.	47
Assessment of respiratory mechanics.	59
Pulmonary mechanics in intensive care patients.	68
Respiratory muscle functions during critical illness.	74
Work of breathing and breathing pattern in ALI/ARDS.	77
The normal alveoli.	79
Nasal potential difference to detect Na ⁺ channel dysfunction in acute lung injury.	80
References.	83

Pulmonary fluid balance

The proper regulation and maintenance of pulmonary fluid balance is crucial to health. In utero, the lungs are net fluid secretors with the volume of fluid being vital for optimal lung growth. Pulmonary hypoplasia occurs when too little fluid is produced, such as in oligohydramnios, whereas excess fluid produces pulmonary hyperplasia. Importantly, fetal fluid secretion is under the control of Cl^- secretion by the respiratory epithelium. At birth the sudden dependency on pulmonary gas exchange requires a dramatic change in lung fluid dynamics. As gaseous exchange requires a relatively dry alveolus the respiratory epithelium transforms to a net fluid absorber in a remarkably short space of time. In the few days before birth the lungs begin to produce less fluid, and during labor the physical passage of the fetus through the birth canal forces fluid from the lungs. Simultaneous increases in fetal sympathetic output and catecholamine levels help activate alveolar Na^+ channels necessary for fluid absorption. Additionally, the manifold increase in fetal oxygenation ex utero further stimulates Na^+ channels. The optimal alveolar gas exchange is dependent on an even thinner alveolar lining fluid of 0.1- 0.2 μm height. The alveolar lining fluid consists of an analogous dual layer, with surfactant covering an aqueous subphase. Alveolar lining fluid evens the air-liquid interface, enables surfactant precursors to reach the surfactant layer, and allows movement of surfactant within this layer. Pulmonary edema results in fluid deposition in the alveolar region. The resolution of pulmonary edema is vitally dependent on the active absorption of Na^+ and Cl^- from the alveolar air space into the interstitium creating an osmotic gradient for the movement of water out of the alveolar air space and thereafter from the interstitium, water is cleared by the lymphatic system (Ware 2005). Generally the ALI/ARDS were results from an inflammatory injury to the alveolar epithelial-interstitial-endothelial complex caused by either a pulmonary or extrapulmonary insult. The neutrophil-mediated disruption of this physical barrier causes increased permeability pulmonary edema. The alveolar flooding is commonly dependent on the balance of pulmonary edema formation and clearance, so that the dysfunction of any of the components needed for alveolar fluid clearance can promptly predispose to the development of pulmonary edema.

The types alveolar epithelial cell

The alveolar epithelium constitutes ~99% of the internal surface area of the lung and is one of the tightest epithelia in the body forming transepithelial resistances of $>2000\Omega \cdot \text{cm}^2$. It is ~0.1- 0.2 μm thick and is composed of two cell types: large, squamous type 1 alveolar cells (AT1) with a diameter of 50-100 μm and smaller cuboidal type 2 alveolar cells (AT2) with a diameter of 10 μm . Alveoli are ~250 μm in diameter and at its thinnest the alveolar interstitium consists of only a fused basement membrane between the epithelial and endothelial layers. Although AT1 cells compose 66% of the cell population of the alveolus, because of their large size they constitute $>95\%$ of the alveolar surface. Alveolar

epithelial cells form tight junctions, which represent a barrier between the functionally different apical and basolateral cell membranes with specifically localized ion channels and pumps. This functional division of apical and basolateral membranes is an essential for vectorial transport of ions and water across the alveolar epithelial layer.

Major alveolar channels, transporters and receptors

Na^+ channels: Apical membrane Na^+ channels are expressed in the alveolar epithelium and

contribute to Na^+ absorption (Figure 2). Two main classes of Na^+ channels have been found: the epithelial Na^+ channel (ENaC) and the cyclic nucleotide-gated channel. Nevertheless, there are three subtypes of ENaC have been described on the basis of the subunit composition: a highly selective cation channel (HSC) that is usually referred to as the ENaC channel; two types of poorly selective cation channel (PSC), types 1 and 2 differentiated by their unit conductance; and a nonselective cation channel (NSC). ENaC channels are present in the apical membranes of both AT1 and AT2 cells. Highly selective cation channel is a heterotrimeric channel composed of α , β and γ ENaC subunits. It has a unit conductance of 4-5 picoSiemens (pS; a measure of the ease of movement of ions through the ion channel) and a Na^+/K^+ selectivity of >40 . Poorly selective cation channel is composed of a combination of α - with either β - or γ -ENaC subunits and has a Na^+/K^+ selectivity of 5-8, with type 1 poorly selective cation channels having unit conductance of 8-9 pS and type 2 poorly selective cation channels a unit conductance of 56 pS. Nonselective cation channel is composed solely of α -ENaC subunits, has a Na^+/K^+ selectivity of 1.5 and a

unit conductance of 19 - 24 pS. Indeed efficient Na^+ transport requires all three subunits. It had been found that the highly selective cation channel, poorly selective cation channel and nonselective cation channel are inhibitable by amiloride. One isoform of the nucleotide-gated channel, nucleotide-gated channel 1, is present in the distal airway and AT1 cells and is likely to be involved in distal airway and alveolar fluid balance. This channel is nonselective, amiloride insensitive, but pimozone sensitive and has a unit conductance of 2-8 pS. Other Na^+ - dependent co-transporters, such as glucose or amino acid co-transporters, may contribute to amiloride-insensitive Na^+ absorption. In addition, atypical ENaC channels, composed of different subunit stoichiometries, rendering them potentially insensitive to amiloride, could also contribute to amiloride-insensitive Na^+ transport [1].

Cl^- channels: The cystic fibrosis transmembrane conductance regulator (CFTR) is a cAMP-regulated apical membrane Cl^- channel expressed in both AT1 and AT2 cells. Alveolar cystic fibrosis transmembrane conductance regulator has a unit conductance of ~4 pS (AT1, similar to airway CFTR) to 8 pS (AT2) and can be stimulated by forskolin. Cystic fibrosis transmembrane conductance regulator consists of two membrane-spanning domains, two nucleotide-binding domains, and a regulatory domain.

Both airway and alveolar cystic fibrosis transmembrane conductance regulator-mediated apical Cl^- movement may be bidirectional and under the control of adenosine. Although the absence of cystic fibrosis transmembrane conductance regulator does not hinder basal alveolar fluid balance, it is necessary for maximal alveolar fluid clearance during β -agonist therapy. In addition the cystic fibrosis transmembrane conductance regulator activation increases amiloride-sensitive Na^+ absorption, suggesting that both Na^+ and Cl^- transport determine alveolar fluid absorption. However, the exact interaction between cystic fibrosis transmembrane conductance regulator and ENaC remains to be determined.

K^+ channels: Respiratory epithelial K^+ channels mediate a diverse range of physiological functions including oxygen sensing, inflammation, and epithelial repair. The primary role of these channels is to regulate the cell membrane potential to allow maintenance of the transepithelial driving force for ion movement and subsequent regulation of the airway and alveolar liquid layers. K^+ channels have been localized to the apical and the basolateral membrane where they serve differing functions. Apical K^+ channels support K^+ secretion into the alveolar lining fluid resulting in the relatively high K^+ concentration of the alveolar lining fluid. In contrast, basolateral K^+ channels support recycling of K^+ across the basolateral membrane in support of the Na^+ - K^+ -ATPase and to hyperpolarize the cell. Classes of K^+ channels found in alveolar cells include inwardly rectifying K^+ channels (K^+ ir), Ca^{2+} -activated K^+ channels, and voltage-gated K^+ channels (K^+ v). K^+ ir channels have been localized to the basolateral membrane, and the α -subunit of the K^+ v channel has been localized to the apical membrane. A barium-sensitive K^+ channel with a unit conductance of 5-6 pS has been identified in the apical membrane of AT1. ATP-sensitive K^+ channels (K^+ ATP) have also been described in the alveolus. Inhibition of K^+ ATP reduced amiloride-sensitive Na^+ currents and forskolin-stimulated Cl^- currents in AT2, whereas K^+ ATP activation increased both ion fluxes. Similarly, ENaC and cystic fibrosis transmembrane conductance regulator expression responded to K^+ ATP modification, with increased expression occurring with K^+ ATP activation and decreased expression seen with K^+ ATP inhibition. Furthermore the interplay between K^+ , ENaC, and cystic fibrosis transmembrane conductance regulator provides further evidence for the complexity of the relationship between epithelial ion channels [2].

Na^+ - K^+ -ATPase: The Na^+ - K^+ -ATPase is expressed and is the primary active transport process that generates the gradients necessary for epithelial Na^+ absorption. It is a heterodimeric protein composed of an α - and a β -subunit and is located in the basolateral membrane of AT1 and AT2 cells. The α -subunit allows exchange of three intracellular Na^+ for two extracellular K^+ during ATP hydrolysis. The β -subunit is required for protein assembly and insertion into the cell membrane. Four α - and three β -subunits exist and different associations of an α - and a β -subunit, plus different posttranscriptional processing, creates a range of Na^+ - K^+ -

ATPase isoenzymes with different functional characteristics. It was found that the AT1 cells contain $\alpha 1$ -, $\alpha 2$ -, and $\beta 1$ -subunits, whereas AT2 cells express $\alpha 1$ - and $\beta 1$ -subunits. The regulation of Na^+ - K^+ -ATPase and ENaC occurs in parallel, with increased apical Na^+ transport being matched by increased Na^+ - K^+ -ATPase activity. Upregulating stimuli, such as glucocorticoids and catecholamines are increase expression and function of both proteins. Likewise, down-regulating stimuli, such as hypoxia, reduce levels and function of these membrane transporters.

Water channels: The aquaporins (AQP) are a family of small (~30-kDa monomer), integral membrane proteins that function as mercury-sensitive water channels. AQP5 has been located in the apical membrane of both AT1 cells and AT2 cells, AQP3 is located in the basolateral membrane of AT2 cells, and AQP1 is located in microvascular endothelia. AQP4 is also probably present in AT1 cells. Water permeability is required in both apical and basolateral membranes for efficient transcellular water transport, although paracellular water transport also occurs. However, the AQPs increase the water permeability of epithelial membranes by 5-50-fold with AT1 cells having the highest water permeability of any mammalian cell.

β -Adrenergic receptors: There are four β -adrenergic receptor subtypes exist, with over 90% of all pulmonary β -receptors being located in the alveoli, predominantly in the form of the $\beta 2$ -receptor. Both $\beta 1$ - and $\beta 2$ -receptors are expressed on the cell membranes of both AT1 and AT2 cells. Anyhow, the β -stimulation may increase the activity of ENaC or Na^+ - K^+ -ATPase, improve pulmonary lymphatic flow, or enhance cystic fibrosis transmembrane conductance regulator function. Basal rates of alveolar fluid clearance may not be dependent on β -adrenergic receptor signaling. Upregulated alveolar fluid clearance is largely dependent on $\beta 2$ -adrenergic receptor signaling, although $\beta 1$ -adrenergic stimulation may also increase alveolar Na^+ transport. β -stimulation increases rates of alveolar fluid clearance in normal lungs, in models of hydrostatic pulmonary edema and in models of ALI/ARDS. Furthermore overexpression of alveolar $\beta 2$ -receptors increases alveolar Na^+ transport and alveolar fluid clearance.

Respiratory ion transport and fluid balance

Traditionally alveolar fluid clearance was thought to be under the control of Starling forces, i.e. hydrostatic and oncotic forces. Work from the early 1980s onward, however, has shown that alveolar fluid clearance is an active osmotic process dependent on the epithelial absorption of Na^+ and Cl^- . Both AT1 and AT2 cells allow passive diffusion of Na^+ through apical membrane ENaC channels along its electrochemical gradient into the cells, and active extrusion of Na^+ via the Na^+ - K^+ -ATPase in the basolateral membrane. It was found that the Na^+ also enters AT1 cells via apical cyclic nucleotide-gated channels-1 and possibly AT2 Cells. Nevertheless, the apical membrane Na^+ channels are the rate-limiting step for Na^+ absorption accounting for 90% of the resistance to Na^+ movement. Approximately 30% of rat

AT1 and AT2 cell Na^+ transport is inhibited by amiloride and correspondingly, up to 60% of alveolar fluid clearance is amiloride insensitive. The contribution of amiloride-sensitive Na^+ transport varies across species and is ~40-50% for humans. It was found that the transepithelial electrolyte transport from the alveolar space toward the interstitium is followed by osmotically obliged water via both cellular and paracellular pathways resulting in clearance of pulmonary edema. The contribution of aquaporins is felt to be of minor significance as aquaporins do not appear to contribute to either regulation of the airway surface liquid or alveolar fluid

clearance. Thus, although all components of alveolar fluid clearance are important, it would seem that the function of ion channels, or β -adrenergic receptors, are likely to be of greater significance than $\text{Na}^+\text{-K}^+$ -ATPase or aquaporins in determining alveolar fluid clearance abilities.

Mechanism of alveolar Na^+ transport and fluid absorption: The following explanations are clarifying the mechanism of alveolar Na^+ transport (Figure 1) [the numbered paragraphs below refer to circled numbers in the figure]:

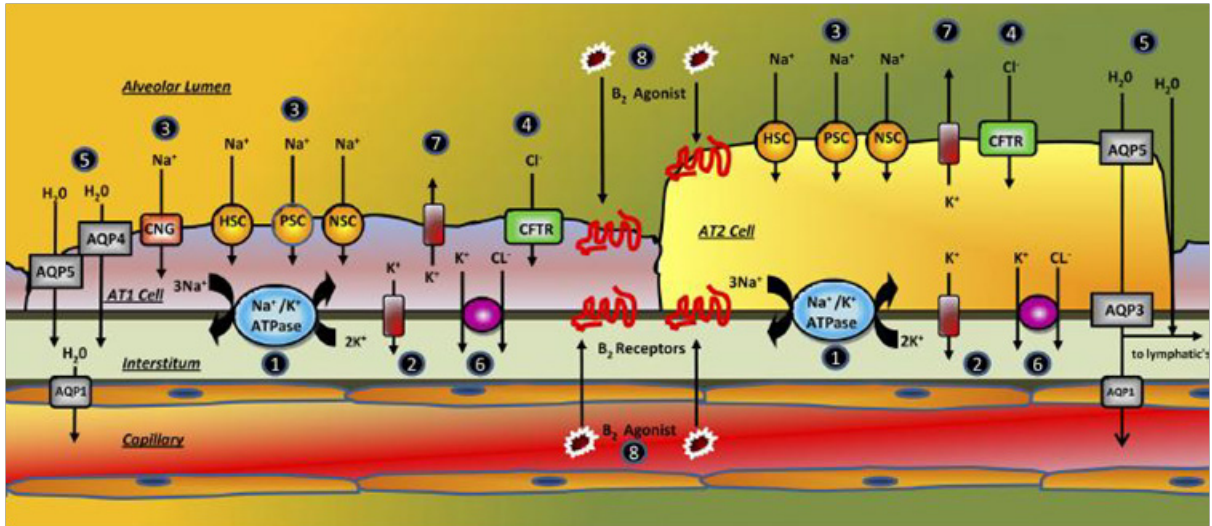


Figure 1: Schematic diagram of alveolar type 1 and 2 cells showing distribution of ion channels, pumps,

aquaporins (AQP). HSC: Highly Selective Cation Channel; PSC: Poorly Selective Cation Channel; NSC: Nonselective Cation Channel; CNG: Cyclic Nucleotide-Gated Channel; CFTR: Cystic Fibrosis Transmembrane Conductance Regulator [3].

- a) The $\text{Na}^+\text{-K}^+$ -ATPase pump exchanges intracellular Na^+ for extracellular K^+ . The activity of the $\text{Na}^+\text{-K}^+$ -ATPase hyperpolarizes the basolateral membrane potential and establishes an outward K^+ and an inward Na^+ gradient.
- b) Intracellular K^+ follows its chemical gradient across basolateral K^+ channels, which hyperpolarizes the basolateral membrane. In an epithelial setting, basolateral hyperpolarization results in apical hyperpolarization by electrical coupling of the two membranes across the tight junctions.
- c) This creates a large electrochemical gradient for entry of luminal Na^+ through the apical membrane Na^+ channels, including highly selective cation channel, poorly selective cation channel, nonselective cation channel and cyclic nucleotide-gated channels.
- d) The resulting Na^+ absorption depolarizes the apical membrane potential to allow for Cl^- entry across the cystic fibrosis transmembrane conductance regulator.
- e) The osmotic gradient created by the movement of Na^+ and Cl^- causes water to move from the air space to the interstitium both transcellularly and paracellularly.
- f) Cl^- leaves the basolateral membrane through an as yet undetermined pathway thought to be a Cl^-/K^+ cotransporter to maintain electroneutrality.
- g) K^+ secretion through the apical membrane enables maintenance of the transepithelial electrochemical gradient needed for ion and water movement.
- h) Alveolar fluid clearance may be upregulated in a catecholamine-dependent or independent fashion. Na^+ movement occurs by using the same $\text{Na}^+\text{-K}^+$ -ATPase driven mechanism, but in an upregulated manner. The exact means of upregulation remains unclear but several theories have been suggested. The upregulation may be primarily due to an increase in Na^+ absorption caused by an increase in any of the following: ENaC delivery to the apical membrane, ENaC open probability, $\text{Na}^+\text{-K}^+$ -

ATPase delivery to the basolateral membrane, $\text{Na}^+\text{-K}^+\text{-ATPase}$ α -phosphorylation and $\text{Na}^+\text{-K}^+\text{-ATPase}$ activity. In addition, the increase, in alveolar fluid clearance may be mediated through cystic fibrosis transmembrane conductance regulator and Cl^- conductance. Increased Cl^- movement may be required electrically to initiate or maintain increased Na^+ movement.

ALI/ARDS as an ion channelopathy

It is confirmed that a disorder of any of the components necessary for the regulation of the respiratory tract surface liquid layer could be implicated in disorders of pulmonary fluid balance. Decreased expression of ENaC has been reported in experimental models of ALI including bleomycin-induced injury, viral pneumonia and canine ischemia-reperfusion injury. The ability to maintain a maximal or submaximal rate of alveolar fluid clearance and similarly a smaller magnitude of extravascular lung water has been associated with improved survival in ALI/ARDS. Although this varying ability to resorb edema fluid could represent differing degrees of alveolar injury, it is also possible that it could represent underlying Na^+ channel function, with those with the most functional Na^+ channels having the best outcome. Cardiogenic pulmonary edema serves as a useful comparative model as it is a condition with much less physical injury to the alveolus. Patients with this condition who maintain an intact rate of alveolar fluid clearance also have superior outcomes to those who do not. This suggests that rates of alveolar fluid clearance in the critically ill may depend on more than just the degree of alveolar epithelial injury. Consistent with this theory of a spectrum of Na^+ channel activity being associated with abnormal pulmonary fluid handling, genetic variation in the β_2 -adrenergic receptor has been associated with a susceptibility to the development of pulmonary edema. Really a large body of evidence exists linking Na^+ channel activity with pulmonary edema.

Potential difference of ion channel function

The movement of ions across epithelia results in a transepithelial voltage, or potential difference. The transepithelial potential difference is determined by the sum of apical and basolateral membrane potential differences. As transepithelial conductances or ion gradients change, the potential difference changes accordingly. Placing electrodes on both sides of an epithelial membrane allows this potential difference to be measured via a high-impedance voltmeter [3].

Alveolar Epithelium

In the human lungs, the alveolar epithelium is populated by squamous alveolar type I and cuboidal alveolar type II cells. There are similar numbers of alveolar type I and alveolar type II cells; however, alveolar type I cells are elongated, with long thin cytoplasmic extensions, and cover 95% of the surface area. Alveolar type II cells, which produce, secrete and recycle surfactant, cover the remaining 5% of the surface area and are thought to differentiate into alveolar

type I cells. Recent studies have demonstrated that both alveolar type I and alveolar type II cells express sodium-potassium adenosine triphosphatase ($\text{Na}^+\text{-K}^+\text{-ATPase}$) and the amiloride-sensitive epithelial sodium channel (ENaC), and thus contribute to active Na^+ transport and alveolar fluid resorption. However, interactions between adjacent epithelial cells through domains such as tight junctions and adherens junctions provide a physical barrier between the alveolar airspaces and the interstitium (Figure 2). Tight junctions surround the cells like rubber O-rings, preventing large molecules from crossing the epithelial layer. The relative impermeability of the alveolar epithelium to paracellular solute diffusion is predominantly regulated by tight junctions. Tight junctions consist of integral membrane proteins: occludins, claudins and junctional adhesion molecules.

Cytoplasmic plaque proteins transduce signals between tight junctions and cytoplasmic signaling molecules or the actin cytoskeleton. In addition, tight junctions divide the epithelial plasma membrane into the apical and basolateral domains. Ion transporters and other membrane proteins are asymmetrically distributed in these two domains. Alveolar fluid resorption is accomplished through active Na^+ transport across alveolar epithelium. As depicted in (Figure 2) [4], Na^+ is taken in on the apical surface of alveolar epithelial cells, primarily through ENaC. Subsequently, Na^+ is actively extruded through the basolateral surface into the lung interstitium by the $\text{Na}^+\text{-K}^+\text{-ATPase}$, generating a transepithelial osmotic gradient. Water then follows the osmotic gradient into the interstitial space and pulmonary circulation, leading to the resorption of alveolar fluid. The apical surface of epithelial cells expresses the ENaC, which is a major Na^+ transporter and widely distributed in the lung, kidney and colon. It comprises three subunits (α , β and γ) and usually exists as a tetramer made up of two α -subunit, one β -subunit and one γ -subunit or a much larger complex containing three of each subunit. Maximal transport requires the presence of all three subunits. ENaC-mediated ion transport is voltage-dependent, activated by calcium ions (at high doses) and inhibited by $1\ \mu\text{M}$ amiloride. It had been found that in animal studies the α -ENaC knockout mice die due to pulmonary edema immediately after birth, whereas β -ENaC or γ -ENaC knockout mice show a compromised rate of fluid clearance.

The ENaC inhibitor amiloride does not completely inhibit Na^+ transport in alveolar epithelial cells, suggesting the presence of amiloride-insensitive pathways that contribute to fluid resorption. Among these are cyclic nucleotide-gated cation channels, the $\text{Na}^+\text{-glucose}$ transporter and other co-transporters (e.g. $\text{Na}^+\text{-amino acid}$) (see the above section for more details). The $\text{Na}^+\text{-K}^+\text{-ATPase}$ resides in the basolateral membrane of the cells. It utilizes the energy released from adenosine triphosphate (ATP) hydrolysis to pump 3Na^+ out of cells in exchange for 2K^+ into cells, generating Na^+ and K^+ gradients across the plasma membrane [5]. $\text{Na}^+\text{-K}^+\text{-ATPase}$ is a heterodimer of α -subunit and β -subunit, both of which are necessary for its activity. It is believed that the

α -subunit and β -subunit are synthesized independently and then assembled into a dimer in the endoplasmic reticulum and delivered to the plasma membrane. The α -subunit is a transmembrane protein that catalyses ATP hydrolysis and contains the binding sites for Na^+ , K^+ and the inhibitor ouabain. Four α -subunit isoforms, α 1- α 4, have been described. These isoforms are highly conserved, each containing a >77% identical primary amino acid sequence. The α 1-isoform is found in most tissues, whereas the other isoforms are tissue-specific. It was found that animals with

deletion of either the α 1- or α 2-isoform do not survive, suggesting a fundamental role of the α 1- isoform or α 2-isoform in organ development. Loss-of-function mutations in the α 2- subunit are associated with familial hemiplegic migraine type 2, and missense mutation of the α 3-subunit causes dystonia-Parkinsonism. The α -subunit has four isoforms and contains three glycosylation sites. It controls heterodimer assembly and insertion into the plasma membrane.

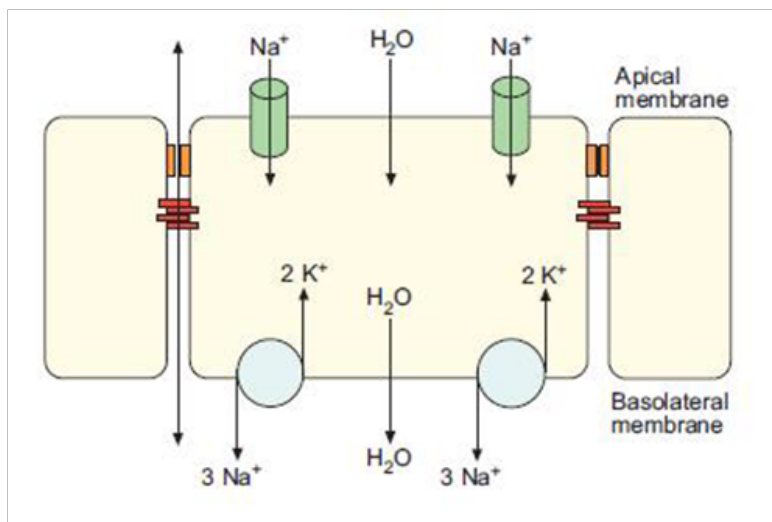


Figure 2: Schematic diagram of the alveolar epithelium. Tight (in orange) and adherens junctions (in red) on adjacent epithelial cells provide a restrictive barrier in order to maintain selective permeability. The asymmetrically distributed epithelial sodium channel (in green) and sodium–potassium adenosine triphosphatase (in light blue) confers the vectorial transport of sodium ions, which is crucial for alveolar fluid resorption. \updownarrow : paracellular transport [4].

Gap junctions in the lung's alveolar epithelium

It has long been appreciated that gap junctions are available in most mammalian tissues, and the lung is one of them. Gap junctions are composed of proteins known as connexins, which form channels that enable neighboring cells to be interconnected. Gap junction channels serve multiple functions by enabling the diffusion of signaling molecules and metabolites throughout interconnected cells. This, in turn, enables cells in a tissue to function in a coordinated manner. The ability to share metabolites and antioxidant molecules through gap junctions enables the tissue to have a robust response to stress and injury. A functional gap junction channel is composed of two connexin hexamers (or hemichannels) in two adjacent cells, which act to form a complete channel. Gap junction channels are typically arranged in semicrystalline arrays, known as plaques, at sites of cell-cell contact where intercellular communication occurs. However, free connexin hemichannels dispersed throughout the plasma membrane, enabling the exchange of aqueous molecules between the cytoplasm to the extracellular environment.

Connexin expression in the lung: Of the 20 mammalian connexins, several are differentially expressed throughout the lung. The pattern of expression depends on cell phenotype, which influences connexin transcription (Table 1) [7]. In normal lung, most epithelial cells express Cx32 and Cx43, whereas endothelial cells express predominantly Cx37, Cx40, and Cx43. The major connexins expressed by alveolar epithelial cells are Cx26, Cx32, Cx43, and Cx46. Others are expressed at low levels, such as Cx30.3 and Cx40. Expression of Cx37 by alveolar epithelial cells in situ is also low, but is consistently detectable by immunohistochemistry. Considerably more Cx37 is expressed by bronchiolar epithelium, but this is still less than the level observed for pulmonary endothelial cells. Cx43 is fairly ubiquitous and is the major connexin functionally interconnecting type II and type I cells. By contrast, Cx32 is expressed exclusively by type II alveolar epithelial cells in normal lung. Interestingly, type I cells cannot form functional gap junctions with cells expressing only Cx32. Type II cells form primarily heterocellular junctions in the normal lung (e.g., with type I cells). Thus, the role for Cx32 in alveolar epithelial physiology is not clear, because it is not likely to be participating in type I-type II cell gap junctions, and few type

II-type II cell junctions exist. However, a hemichannel role for Cx32 expressed by type II cells is exist [7]. It had found that the connexins have a relatively rapid half-life of 1-5 hours, suggesting that gap junction turnover is a constant process. Moreover, cells that express multiple connexins, including cells in the lung, have the potential to form heteromeric or mixed gap junction channels. Whether connexins form heteromeric channels is determined by their biochemical compatibility. For instance, Cx32 and Cx43 are incompatible and cannot form heteromeric channels. However, cells also regulate the formation of mixed gap junctions by compatible

connexins. For instance, two of the compatible connexins expressed by alveolar epithelial cells, Cx43 and Cx46, form heteromeric channels when expressed by type I alveolar epithelial cells, yet type II cells prevent Cx43 and Cx46 from interacting. Other examples of cells that regulate connexin assembly include endothelial cells that restrict formation of mixed gap junctions containing Cx37 and Cx40/Cx43. However, it is clear that by regulating connexin interactions, cells have the ability to form discrete functional zones of communication within the pulmonary system.

Table 1: Connexin expression in the lung [6].

Cell Type	Connexin Expression
Airway epithelium: trachea	Cx26, Cx30, Cx31, Cx32, Cx37, Cx43, Cx26, Cx43, Cx46
Alveolar epithelium: type II	Cx26, Cx32, Cx37, Cx43, Cx46
Alveolar epithelium: type I	Cx26, Cx37, Cx40, Cx43, Cx46
Pulmonary endothelium	Cx37, Cx40, Cx43
Smooth muscle	Cx37, Cx40, Cx43
Lung fibroblasts	Cx43, Cx45

Intercellular communication in the lung: Gap junctions serve several functional roles in the lung (Figure 2). By extension, any condition that disrupts gap junctional coupling can have a deleterious effect on lung function. In the airways, gap junctional coupling can contribute to calcium signaling between ciliated epithelial cells to coordinate ciliary beating. Coordinated ciliary movement is needed to ensure the directional flow of mucus out of lungs to clear environmental toxicants and microorganisms. Mechanical stimulation of primary airway epithelial cells in culture induces an intercellular calcium wave, which is transmitted from one cell to another by inositol 1,4,5-triphosphate (IP₃) diffusing through gap junctions. However, in addition to the gap junction-mediated pathway, intercellular calcium transients between airway cells can be generated by extracellular nucleotide release and paracrine stimulation of purinergic receptors. In this case, connexins may help regulate ciliary beat frequency by acting as plasma membrane hemichannels to promote ATP secretion. Gap junctions also play an important role in regulating secretion of pulmonary surfactant produced by type II alveolar epithelial cells. Pulmonary surfactant is a mixture of lipid and protein that performs the dual purposes of decreasing alveolar surface tension and regulating host defense in the lung. It is known that direct mechanical stimulation of type II cells can stimulate surfactant secretion through the calcium-dependent fusion of lamellar bodies to the plasma membrane. Although this would imply that cell stretch induced by a deep breath could directly stimulate type II cell secretion, type II cells are localized to areas of the lung where they are shielded from direct mechanical stress, as compared with type I cells. This helps protect the alveolus, because type II cells are significantly more sensitive to mechanical stress than are type I cell.

Instead, the alveolus regulates surfactant secretion as an integrated system in which type I cells act as mechanical sensors that transmit calcium transients to type II cells via gap junctions. Strong evidence for this pathway comes from in situ fluorescence microscopy analysis of the intact lung. These calcium signals can be induced by inflation or by changes in pulmonary vascular pressure and require gap junctional communication between type I and type II cells. Gap junctions also enable intercellular signals, which can propagate from one alveolus to the next. Again, it is important to note that intercellular calcium transients are not exclusively transmitted through gap junctions because alveolar calcium waves generated by extracellular ATP release and paracrine stimulation of purinergic receptors also contribute to mechanically regulated surfactant secretion (Figure 3). However, given the ability of gap junction blockers to inhibit calcium waves in situ, whether the paracrine pathway can fully compensate for a loss of connexin function indeed is not known.

Nevertheless, of relevance to the pulmonary circulation, calcium waves that propagate along pulmonary vessels through gap junctions have been imaged in the intact perfused lung. The requirement for Cx43 in pulmonary endothelial calcium waves was confirmed. One surprising result from in situ imaging was the discovery of spontaneous calcium signals generated from a subset of endothelial cells, referred to as pacemaker cells, localized to pulmonary branch points. Pacemaker cells are significantly more sensitive to mechanical stress, which results in a calcium wave of increased amplitude as compared with that of nonpacemaker cells. However, the frequency of the calcium oscillations in mechanically stressed vessels still matches the frequency in unstimulated vessels, underscoring the role of pacemaker cells in establishing signal-oscillation

frequency. Calcium waves induced by mechanical stimulation have been shown to increase pulmonary endothelial P-selectin expression at the cell surface, suggesting a link to the inflammatory response. This potentially injurious effect of endothelial Cx43 contrasts with pulmonary epithelium, where Cx43 is beneficial.

Interestingly, the proinflammatory role for endothelial Cx43 is counterbalanced by an antiinflammatory role for Cx37 expressed by circulating monocytes. In this case, Cx37 inhibits inflammation by forming hemichannels that mediate ATP release and reduce monocyte adhesion to endothelial cells [6].

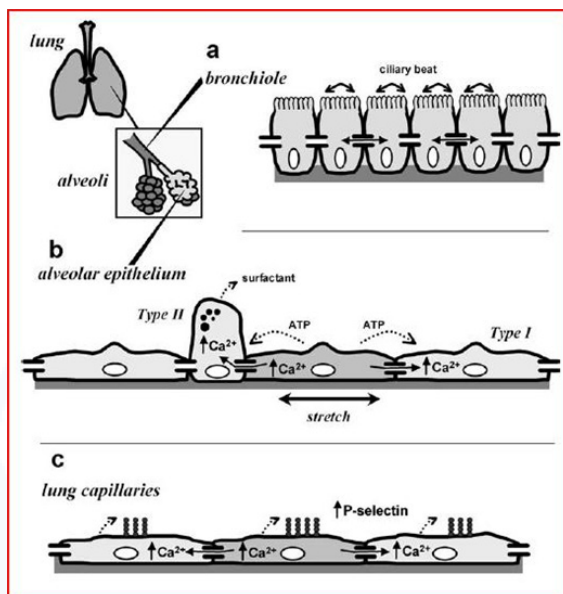


Figure 3: Intercellular communication in the lung. The lung consists of several distinct functional compartments. Shown in the inset are the terminal airspaces, alveoli, and bronchioles.

(a) In the airways, including bronchioles, diffusion of IP₃ through gap junctions enables the propagation of calcium waves, which help synchronize ciliary beating to allow directional transport of mucus.

(b) The alveolar epithelium is a heterogeneous monolayer consisting of type II cells and type I cells. The alveolus acts as an integrated system in which type I cells respond to mechanical stimulation with an increase in intracellular calcium, which, in turn, is transmitted to type II cells via gap junctions to induce lamellar body fusion and secretion of pulmonary surfactant. Also shown is the alternative pathway, mediated by ATP secretion and paracrine stimulation via purinergic receptors.

(c) In lung capillaries, transmission of calcium waves through pulmonary endothelial cell gap junctions upregulates the transport of P-selectin to the plasma membrane, thus transmitting a proinflammatory stimulus [6].

Mechanisms of Alveolar Protein Clearance in the Intact Lung

The clearance of serum proteins from the alveolar space is an important process in recovery from pulmonary edema. Albumin and immunoglobulin G (IgG) are present in pulmonary edema fluid in concentrations that are 40-65% of plasma levels in hydrostatic pulmonary edema and 75-95% in lung injury pulmonary edema. Concentrations of albumin, for example, may be 5 g/100 ml or more. Protein concentrations rise even higher during the recovery phase from alveolar edema because the salt and water fraction of edema fluid is cleared much faster than albumin and IgG. High protein concentrations are significant because increased protein osmotic pressures slow alveolar fluid clearance. For example, soluble protein concentrations in alveolar liquid rose from 5.9 ± 0.4 g/100 to 10.2 ± 1.2 g/100 ml over 12 hours after instillation of autologous serum into

the distal spaces of lungs, and calculated protein osmotic pressure in alveolar liquid increased from 40 to 53 cm H₂O. Alveolar liquid clearance slowed from 8%/h in the first 4 hours to 3%/h at the end of this period. In addition to limiting liquid clearance, highly concentrated alveolar protein may precipitate, necessitating clearance of insoluble as well as soluble protein. Inability to clear alveolar protein may play a role in poor outcomes after pulmonary edema. Patients dying with acute lung injury and the acute respiratory distress syndrome have large quantities of insoluble protein in their air spaces, and non-survivors of lung injury after ARDS have three times as much protein in their alveoli as survivors. Accordingly, the mechanism of alveolar protein clearance is a physiologically and clinically significant problem. Several mechanisms have been proposed for the removal of protein from the alveoli, including clearance by the mucociliary escalator, phagocytosis by macrophages, intraalveolar catabolism, passive diffusion between cells

in the epithelial barrier, and endocytic transport across the epithelial cells in vesicles, a process known as transcytosis. However, recently showed that liquid microinjected into small groups of surface alveoli of gas-inflated lungs redistributed within seconds to adjacent alveoli. This movement appeared to be convective flow because it was unaffected by inhibitors of active fluid transport. Convection from alveoli to distal airways could occur during initial alveolar flooding but would not necessarily contribute to clearance from the lung. In contrast, the other mechanisms have received considerable attention. For example, the rate of alveolar protein clearance is unchanged by the presence or absence of a cuffed endotracheal tube, indicating that the mucociliary escalator is an insignificant route for escape of protein from the lung. Only small amounts of alveolar tracer protein are found in macrophages, and most alveolar protein reaches the bloodstream intact in the first few days after instillation of solutions of protein in the air spaces, suggesting minimal impact for these processes. The importance of the first three mechanisms has been discounted in acute alveolar protein clearance. Thus paracellular diffusion and transcytosis across the distal lung epithelium remain the two most likely mechanisms for clearance of soluble protein from alveolar edema fluid in normal lungs. Net diffusion of protein from the air spaces to the interstitium would be supported by the positive protein concentration gradient between alveolus and plasma, established by more rapid clearance of alveolar liquid than alveolar protein during the resolution of pulmonary edema. Macrophages and catabolism could play a role in long-term clearance of precipitated protein.

Vesicles vs. channels

It had been reported that alveolar type I and type II cells contained endogenous albumin and immunoglobulins in intracellular vesicles. Micrographs of protein in vesicles demonstrate that the alveolar epithelium is capable of endocytosis of serum protein but do not establish whether the protein is transported across the epithelium, indicate the direction of transport, nor quantify how much protein is transported. Vesicles do not necessarily transport their contents across a barrier. Protein in vesicles could be returned to the alveolar space with no net transport across the epithelium, akin to type II cell recycling of surfactant phospholipid between intracellular and extracellular compartments. It had been found that type II cells transported cationic ferritin from alveolar liquid to organelles of the secretory pathway, supporting the operation of recycling routes in the lung. Microscopy studies also provide no information about how the protein entered the alveolar vesicles. More recent work suggests that albumin may undergo receptor-mediated uptake through binding to the albumin glycoprotein binding protein (gp60) on alveolar epithelial cells. It had been also shown that cultured pneumocytes internalize fluorescent albumin into plasmalemmal vesicles together with gp60 and that albumin and gp60 are located in caveolae, vesicles coated with the protein caveolin. Furthermore, cross-linking gp60 with

anti-gp60 antibodies and secondary antibodies stimulates endocytosis of gp60 and albumin, whereas prolonged stimulation with the cross-linking antibody depletes the type II cell surface of gp60 and abolishes endocytic albumin uptake. Albumin undergoes receptor-mediated transcytosis bound to gp60 in pulmonary capillary endothelium. Thus gp60 could play a role in alveolar albumin clearance.

The alveolar epithelium is a tight epithelium and is the primary barrier restricting passage of solutes and water into or out of the alveolar space. Consequently, some authorities have questioned whether molecules as large as serum proteins can pass through the epithelium through paracellular channels. Direct microscopic observation of proteins passing through paracellular passages in the epithelium has not been reported, but the slow rate of transalveolar protein flux may indicate that channels of sufficient size to transmit large macromolecules would be rare and exceedingly unlikely to be encountered by electron microscopy. However, the investigators had previously shown no difference in alveolar epithelial albumin permeability in lungs inflated with low volumes compared with lungs inflated to total lung capacity. Transcytosis of particles 85-95 nm in radius is unlikely because they are so large compared with the dimensions of endocytic vesicles. Vesicles typically have radii on the order of 25-75 nm. It had been found that some vesicles in the alveolar epithelium with radii as large as 130 nm but reported that the radius of the large majority of vesicles was <90 nm. It was reported that alveolar epithelial vesicles averaged 35 ± 2 nm in radii. Thus it was argued that large pores must be present to provide a passage for their large tracers. These pores were localized to the distal airway epithelium in the region of the alveolar ducts, respiratory bronchioles, or their associated alveoli. The presence of pores of adequate size shows that paracellular passage of alveolar protein is possible but says nothing about the contribution of this mechanism to alveolar clearance of serum proteins.

Size dependence

The rate of absorption from the alveoli *in vivo* is size dependent for most proteins. Investigators had assembled measurements of alveolar epithelial protein permeability from many sources. The combined data demonstrated a consistent inverse relationship between permeabilities and the corresponding molecular weights (MW) (Figure 4) [8]. It had been reported that the alveolar epithelial permeabilities of sucrose, inulin, and dextran (60-90 kDa) in saline-filled lungs varied inversely with molecular size and directly with the free diffusion coefficient in water. Other investigators had found that a larger permeability-surface area product for sucrose than for albumin in lungs. However, it had been found that the absorption of intratracheally instilled proteins and peptides were varied inversely with MW. In a study of pulmonary absorption of different-sized fluorescein isothiocyanate (FITC)-labeled dextrans, it was found that rate of absorption decreased with increasing molecular size. Anyhow, the transport of different-sized hetastarch

molecules out of the alveoli could be modeled by a system of epithelial pores of at least two sizes, 5 and 17 nm in radius, allowing size-dependent variation in the rate of passage. It was reported that an inverse relationship between the Stokes radius and the amount of radiolabeled protein tracer that remained in the lungs 8 hours after instillation. These investigators also examined size selectivity of protein clearance humans during the resolution phase of pulmonary edema. The fraction of total protein concentration made up of albumin was greater in edema fluid than in plasma

initially, consistent with size-dependent sieving of protein during edema formation. In patients who showed resolution of the edema in the ensuing hours, the albumin fraction decreased with time. This observation meant that albumin was being cleared more rapidly than the other protein in edema fluid. These other proteins for the most part would be proteins such as immunoglobulins that are larger than albumin. Thus all studies provide evidence that protein clearance from the air spaces of the lung is size dependent.

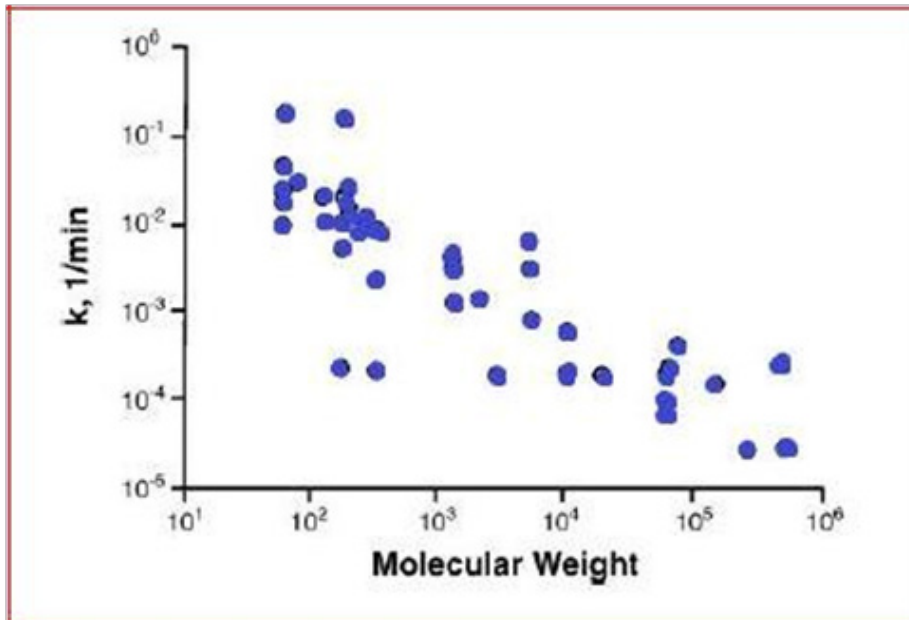


Figure 4: Alveolar protein clearance is size dependent for a wide range of proteins over a wide range of molecular weights. Plot of data is showing inverse relation between rate of lung clearance and molecular weight over a wide range [8].

Not all proteins, however, display the inverse size-clearance relationship demonstrated by the forgoing work. Some proteins are cleared from the lung more rapidly than expected for their size. For example, the plasma concentration-time curves obtained for human growth hormone (MW = 22,000) after intratracheal instillation demonstrated a more rapid clearance from the respiratory tract than expected compared with clearance of albumin. Surprisingly rapid clearance also held true if human growth hormone was aerosolized into the lung. These observations suggest that human growth hormone may utilize a different transport mechanism than other proteins. Because the rate is faster than expected and is subject to saturation kinetics, the mechanism is probably receptor-mediated endocytosis.

What does size-dependent alveolar protein clearance mean relative to mechanism? Simply put, diffusive paracellular transport, fluid phase and receptor-mediated transcytosis may differ in the influence of molecular size. Variation relative to size is a hallmark of diffusive transport. Diffusion is related to size because diffusivity varies inversely with

molecular mass. Diffusion through water-filled channels shows additional size effects for particles whose diameter approaches the diameter of the channel, a phenomenon referred to as restricted diffusion. The rate of transport by endocytosis, on the other hand, should not necessarily be size dependent. Fluid-phase endocytosis begins with vesicles formed from caveolae, clathrin-coated pits that close around fluid adjacent to the cell. The protein concentration in the vesicle would be expected to match the concentration of the outside fluid regardless of size, unless other factors such as unstirred layer effects or steric hindrance to caveolar access imparted sieving properties. Experimental studies support independence of size for fluid phase endocytosis in the distal lung epithelium. It was reported that 70-kDa dextran and 150-kDa dextran particles undergo pinocytosis across alveolar epithelial monolayers at the same rate, whereas other investigators observed that vesicles in alveolar epithelial cells *in vivo* took up similar amounts of 70-kDa dextran and two lectins with limited epithelial binding, concanavalin A (108 kDa) and agglutinin (58 kDa). There are reasons to expect that the

rate of receptor-mediated endocytosis should not depend on size either. Receptor binding can concentrate proteins in the vesicle above concentrations in the extracellular fluid, so the transport rate may be greater than expected for ligand size, as is the case for human growth hormone and other proteins. For example, vasoactive intestinal peptide (VIP, MW 3,450), which undergoes receptor-mediated endocytosis, appears to escape the lungs with a half-time of 19 minutes, nearly as fast as pertechnetate (MW 163) at 10 minutes and almost 10 times faster than diethylene triamine pentaacetate (MW 492), a much smaller molecule. The calculated kinetic constant for VIP is $3.7 \times 10^2 \text{ min}^{-1}$, nearly an order of magnitude greater than would be predicted for its size (Figure 4). Thus the observation that albumin and IgG permeate the alveolar epithelial barrier at a rate expected for their size is consistent with a paracellular mechanism but would not necessarily be anticipated for clearance by transcytosis.

Saturation kinetics

When receptors become fully occupied by ligand, increases in concentration do not increase the rate at which ligand

is taken up by endocytosis. Thus lung protein clearance by receptor-mediated endocytosis or transcytosis should exhibit saturation kinetics. Human growth hormone clearance demonstrates this relationship. The appearance of human growth hormone in the blood circulation after lung instillation increases nonlinearly with instilled dose (Figure 5A) [8], consistent with clearance, at least in part, by a receptor-mediated mechanism. Albumin transport across the upper airway epithelium follows saturation kinetics also and may therefore depend on an endocytic transport process. The half-maximal flux across bronchial epithelium occurs at $\sim 1 \text{ g}/100 \text{ ml}$ albumin. However, unlike the situation for passage across upper airway epithelium, saturation kinetics does not hold for clearance of serum proteins out of the alveoli over comparable protein concentrations. For example, clearance of instilled albumin is proportional to concentration between 3 and 25 g/100 ml (Figure 5B), and clearance of ^{125}I -albumin is unaffected by unlabeled albumin between 5 and 10 g/100 ml. The failure to observe saturation kinetics argues against a receptor-mediated mechanism for absorption of large quantities of serum proteins out of alveolar edema fluid [9].

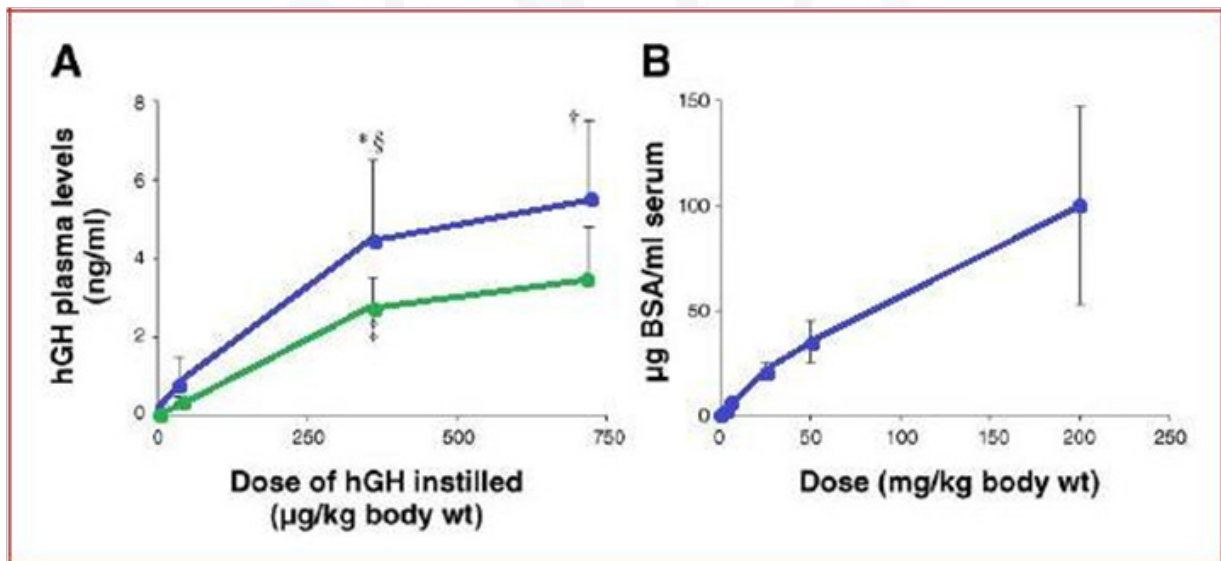


Figure 5: Kinetics of lung to blood passage of human growth hormone (hGH) and bovine serum albumin (BSA).

A: plasma levels of human growth hormone 24 hours after instillation were nonlinearly related to intratracheal dose over a range of 36-720 µg/kg body wt.

B: plasma albumin levels were nonlinearly related to dose at low concentrations of instilled albumin between 0 and 37 mg/kg. In contrast to low-dose albumin and to human growth hormone, plasma appearance was directly related to instilled load at higher doses, between 37 and 200 mg/kg. These doses correspond to albumin concentrations in the instilled liquid of 3.8-20 g/100 ml [8].

Receptor-mediated absorption of albumin may be important in the distal air spaces at lower albumin concentrations. Researchers had compared the permeability-surface area product for transport of ^{125}I -albumin out of the alveolar space of isolated perfused lungs with no unlabeled albumin and with total unlabeled albumin concentrations from ~ 0.001

to 10 g/100 ml. The permeability-surface area product fell when unlabeled albumin was increased from 0-5 g/100 ml. At higher concentrations, the product was constant, indicating that albumin clearance increased in proportion to concentration. These results show that albumin transport occurred by two processes depending on concentration:

- a) A saturable component predominated at low albumin concentrations, consistent with absorption mediated by cell surface albumin binding sites.
- b) Unlabeled albumin competed for these binding sites with a half-maximal inhibitor concentration of 0.3 g/100 ml. Non-saturable albumin clearances at higher concentrations were consistent with paracellular transport.

Temperature dependence

The magnitude and pattern of temperature dependence distinguish between endocytic and diffusive transport. Diffusion through aqueous channels slows as temperature decreases due to increases in the viscosity of water and a decrease in the diffusion coefficient. The rate of diffusion would decrease by ~40% for a fall in temperature from 37-17°C, assuming that the dimensions of the channel and the molecule remained constant. Temperature dependence is described conveniently by the Q_{10} , the ratio of the rates of a biological process with a 10°C change in temperature. The Q_{10} for diffusion would be ~1.6. On the other hand, endocytic transport requires energy and should demonstrate a much greater dependence on temperature, generally a $Q_{10} > 2$. Furthermore, endocytic uptake is abolished at a temperature between 10 and 20°C. Thus a plot of the rate of transcytosis as a function of temperature should show an inflection point somewhere in that range. In contrast, diffusive transport should demonstrate a monotonic relationship with temperature. Hostetter and colleagues aerosolized ^{125}I -albumin, total albumin concentration 0.02 g/100 ml, into isolated rabbit lungs and compared clearance at two temperatures, 37 and 12°C. Clearance decreased 89% between the two temperatures ($Q_{10} = 2.4$), much more than the 40-50% decrease expected for diffusion above. Thus these data suggested that transport of low concentrations of albumin out of the alveolar space occurred by transcytosis.

However, there may be a relation exist between the concentration and temperature on tracer albumin clearance. The investigators studied the effects of temperature on clearance of 0.05 g/100 ml albumin, representing saturable transport, and 5 g/100 ml albumin, the non-saturable component. At 0.05 g/100 ml albumin, the permeable-surface area product for ^{125}I -albumin decreased slightly over 50% when temperature was reduced from 37-27°C, a Q_{10} of 2.1. At 5 g/100 ml, the permeable-surface area product fell by ~40%, a Q_{10} of 1.6. Thus temperature sensitivity was greater at the lower albumin concentration, corresponding to saturable transport, than at the higher concentration corresponding to non-saturable albumin clearance. Anyhow, the temperature dependence at higher concentrations and the absence of saturation were both consistent with albumin transport by a paracellular route.

Pharmacological manipulation of endocytosis

Effects of monensin and nocodazole on albumin transport: Several investigators have evaluated the role of transcytosis in alveolar protein clearance by attempting

to increase or decrease the rate of endocytosis in vivo with pharmacological agents. It had found that inhibiting endocytosis should block alveolar protein clearance if endocytosis is the major pathway. Monensin is an ionophore that interferes with vesicular Na^+/H^+ exchange. It blocks acidification of endocytic compartments and disrupts recycling of membrane components to the plasma membrane, thus inhibiting endocytosis. Nocodazole reversibly disrupts microtubules, which are necessary for vesicle translocation across the cell. It inhibits transcytosis in kidney epithelial cells, Caco-2 intestinal epithelial cells, and tracheal epithelial cells.

The investigators performed four control experiments to demonstrate that monensin and nocodazole were active in whole lung and that they effectively reduced endocytosis:

- a. Electron microscopy with morphometric techniques demonstrated that the inhibitors increased the numerical density of vesicles in the alveolar epithelium and capillary endothelium. Thus the two drugs increased the size of internal membrane compartments as expected if membrane traffic were disrupted.
- b. The inhibitors were studied for effects on clearance of surfactant apoprotein A (SP-A) from the alveolar space. SP-A is a positive control for endocytosis inhibition because type II cells remove SP-A from the air spaces by receptor-mediated endocytosis. SP-A binds selectively to the apical surface of type II cells in a dose-dependent and saturable fashion.

After internalization, the protein dissociates from its receptor and progresses through vesicles, endosomes, multi-vesicular bodies, and lamellar bodies. Eventually, SP-A is recycled back to the alveolar space. Monensin increased the quantity of SP-A associated with the lung tissue after 2 hours (Figure 6). Thus monensin inhibited recycling of SP-A from the epithelial cells to the air spaces by either blocking dissociation from the receptor or interfering with intracellular sorting. In either case, the action was consistent with the pattern expected for a compound that inhibited endocytosis. Endocytosis of FITC-labeled albumin uptake was studied in cultured alveolar epithelial cell monolayers. Monensin and nocodazole reduced uptake by 20-50% over 4 hours and 8 hours, verifying that they were active against alveolar epithelial cells. Immunohistochemical techniques were used to evaluate the effect of inhibitors on parenchymal uptake of 5 g/100 ml human albumin from the air space. Albumin immunoreactivity appeared in the epithelium in the absence of inhibitors but was not found in alveolar epithelium treated with monensin or nocodazole (Figure 7). Because the inhibitors would not block paracellular transport, monensin and nocodazole must have blocked endocytic uptake of albumin. In summary, it was demonstrated that the two drugs blocked transport by cultured alveolar epithelial cells and disrupted alveolar membrane traffic in whole lung. Furthermore, monensin and nocodazole reduced transport of SP-A and albumin, indicating that they inhibited endocytosis of protein by the alveolar epithelium in vivo.

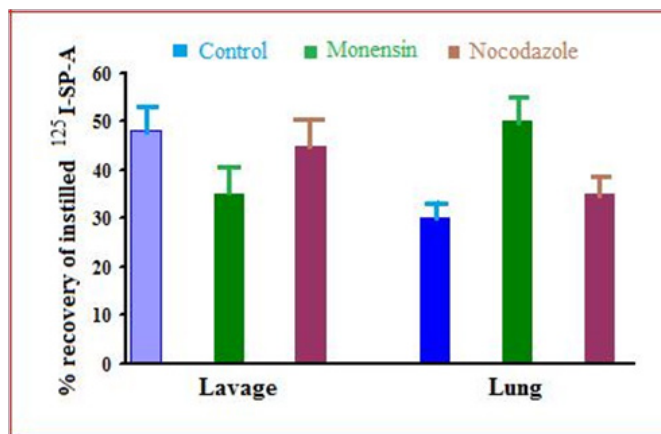


Figure 6: Monensin interferes with surfactant apoprotein A (SP-A) endocytosis. The chart shows recoveries of ^{125}I -SP-A in rabbit lung and lavage liquid 2 h after instillation. Lavage recoveries represent tracer still present in the air spaces, while lung recoveries are the amount of tracer taken up by alveolar epithelial cells or transported into the interstitium. Monensin increased the amount of SP-A in the lung, indicating that it interfered with dissociation of SP-A from its receptor, interrupted recycling of endosomal or vesicular membrane to the cell surface, or both. In either case, the data indicate inhibition of endocytosis. * $P < 0.05$ vs. control.

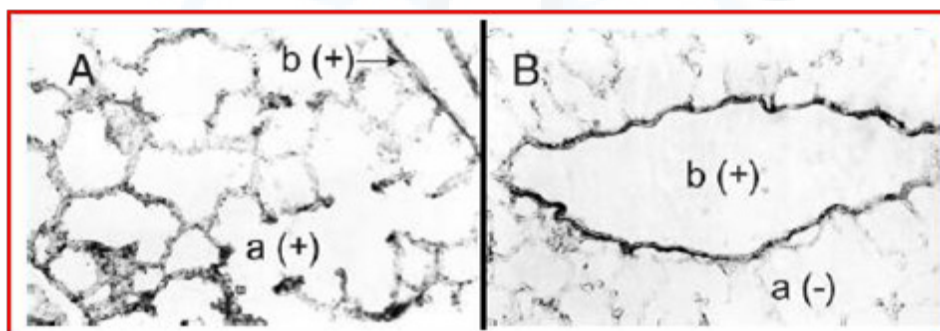


Figure 7: Albumin uptake from the alveolar space across airway epithelium. Shown are lung sections immune histochemically stained for human albumin after instillation of albumin plus DMSO vehicle (A) or albumin plus nocodazole (B). Labels mark the alveolar region (a) and a bronchus (b) and indicate the presence or absence of immunoreactive human albumin (+ or -). Nocodazole reduced uptake of immunoreactive human albumin by the alveolar parenchyma (B) compared with uptake in untreated control lung (A), suggesting inhibition of endocytic uptake by the alveolar epithelium. However, albumin immunoreactivity was present in larger airways regardless of treatment with DMSO or nocodazole (B). Because endocytosis was inhibited, the bronchial uptake may represent paracellular transport of albumin into the interstitium. The upper airway epithelium is thought to contain large pores in the region of the alveolar ducts or respiratory bronchioles. This micrograph suggests that these pores could support diffusive clearance of serum proteins from the alveolar space.

Effects on transport of riboflavin-albumin vs. albumin:

Riboflavin-conjugated albumin (riboflavin-albumin) and sucrose had been studied extensively. Riboflavin-albumin was tested because many cells possess riboflavin receptors and it was believed that the conjugate might undergo receptor-mediated transcytosis utilizing this receptor. In fact, tracer ^3H riboflavin-albumin was cleared twice as fast as ^3H albumin when instilled into the lungs in 0.5% unlabeled protein, indicating that it was transported differently from unconjugated albumin. In isolated perfused lungs, nocodazole and monensin decreased the permeability-surface area product of riboflavin-albumin by >50%, consistent with absorption by transcytosis mediated by riboflavin receptors. The permeability-surface area product of sucrose, a marker for paracellular transport, and the permeability-surface area product for albumin were unaffected by the endocytosis inhibitors. Thus transcytosis

was quantitatively important for riboflavin-albumin but did not play an important role in alveolar clearance of 0.5% albumin.

Alveolar degradation

Alveolar macrophages: Alveolar macrophages are well known for their capacity to endocytose and degrade exogenous protein and peptides. Their endocytic capacity is greater than that of type II alveolar epithelial cells. However, alveolar macrophages do not appear to play a major role in clearing protein over 24-48 hours from the alveoli of the normal lung. For example, the number of alveolar macrophages increased by 10-fold over 24 hours after autologous serum was instilled into lungs, but the rate of protein clearance remained constant during this period. Less than 10% of the instilled ^{125}I -albumin was associated with alveolar macrophages 24 and 48 hours

after the instillation. Alveolar macrophages may become important in alveolar protein clearance after 48 hours. Some researchers followed alveolar protein clearance for 6 days after instilling ^{125}I -albumin into the lungs. The influx of macrophages into the air spaces increased substantially between the 2nd and 6th days. Increased quantities of protein tracer were associated with macrophages by the 4th day, and phagolysosomes with staining characteristics similar to that of the instilled serum were present in the macrophage cytoplasm. On the 6th day, the quantities of protein-free ^{125}I in lung lavage, urine, and feces increased 4-5folds compared with the quantity at 48 hours. Thus as time progressed, resident cells in the air spaces (and/or alveolar epithelial cells) appeared to catabolize more proteins. In summary, macrophages may not play a major role in the short-term removal of excess protein from the intact lung, but they may be more important for long-term protein clearance or for clearance of surfactant apoproteins.

Peptidases and proteases: Catabolism by the airway epithelial cells with absorption of smaller protein fragments was first proposed as a mechanism for alveolar protein clearance. Various peptidases, such as neutral endopeptidase and cathepsin H, are present on the apical surface of the airway and alveolar epithelium and may be important for clearing small peptides. It had been suggested that aminopeptidases in the apical cell plasma membranes of the alveolar epithelial cells cultured on porous substrates could degrade a model dipeptide, glycyl-L-phenylalanine. Protein might also be degraded after endocytosis and transport to lysosomes in the epithelial cells. Intra-alveolar degradation is not a major clearance mechanism in the uninjured lung for most proteins, including serum proteins. The vast majority of studies indicate that >95% of the protein instilled into the distal air spaces of the normal lung reaches the blood circulation intact. However, peptidases and lysosomes could participate in metabolism of specific peptides or larger proteins, such as vasoactive intestinal peptide, gastrin, or insulin. Vasoactive intestinal peptide is cleared from the air spaces more rapidly than expected for its size and is completely degraded during transit across the pulmonary epithelium into the vascular spaces. Gastrin is also degraded in the passage from the air spaces into blood. Although cultured pneumocytes degrade substantial quantities of insulin, insulin is cleared intact at a rate consistent with its size relative to larger proteins in lungs.

Insoluble protein clearance

From a clinical perspective, hydrostatic pulmonary edema and increased permeability pulmonary edema (acute lung injury) represent the most important clinical settings in which large quantities of soluble protein collect in the distal air spaces of the lung. In the presence of severe acute lung injury, some of the protein in the air spaces of the lung precipitates out of solution and forms an insoluble matrix in conjunction with extracellular matrix proteins and fibrin. Microscopically, the insoluble protein is identified pathologically as hyaline membranes, a classic hallmark of

diffuse alveolar damage in patients with acute lung injury. Recent work indicates that the mechanism for accumulation of the insoluble protein components in the distal air spaces of the lung is probably a product of both pro-coagulant and proinflammatory mechanisms that are activated in the presence of acute lung injury. However, removal of the insoluble protein fragment will be much slower than the removal of soluble protein components. Alveolar macrophages probably play a primary role in the removal of insoluble proteins, matrix, and cell debris, although there is very little quantitative information regarding this process. Observational studies in experimental conditions, such as bleomycin-induced lung injury, indicate that the process probably requires weeks for removal of insoluble protein in the distal air spaces of the lung. The resolution process may also be complicated by the presence of intra-alveolar fibrosis and potentially by a loss of capillary blood flow and destruction of some lung lymphatics.

Distribution of Blood Flow and Ventilation in the Lung

Understanding the regional differences in ventilation and perfusion of the lung should assist understanding and management of different respiratory disorders. Several current textbooks state that gravity has either an exclusive or a predominant influence on pulmonary blood flow, although some texts present alternative accounts. Recent research has shown that factors such as the basic structure of the pulmonary vessels and airways may be as important as gravity in determining regional differences in blood flow and ventilation distribution.

The gravity effect on ventilation and perfusion distribution

Early studies using radio-labeled gases showed that regional ventilation was greater in the dependent part of the lung. The gradient in pulmonary ventilation was explained by the gradient of pleural pressure that was considered to be predominantly caused by the effects of gravity. In the upright position, there is a gradient in pressure from the apex to the base of the lung. In the resting state, the pleural pressure is less than the atmospheric pressure, but it is less sub-atmospheric at the base. These regional differences are attributed to two factors:

- I. The weight of the lung itself, which is considered to be semi-fluid.
- II. Differences between the shape of the lung tissue and the surrounding pleural space.

The transpulmonary pressure at the base of the lung is therefore less, and the lung tissue less expanded, than that at the apex. The less expanded basal lung tissue has a greater compliance and, consequently, has greater relative ventilation, when inspiration starts from FRC and when these measurements are made under static or quasi-static conditions. The effects of gravity on the distribution of blood

flow in the lung are attributed to the hydrostatic pressure difference between the top and bottom of the pulmonary arterial system. At the uppermost parts of the lung, the pressure within the vessels may be less than the alveolar pressure. Therefore, these vessels collapse and the alveoli that these vessels traverse will receive little blood flow. This accounts for some wasted ventilation or physiological dead space. In the gravitational middle zone, pulmonary

arterial pressure is greater and pulmonary artery pressure exceeds the alveolar pressure, and, similarly, in the lower zone pulmonary venous pressure also exceeds alveolar pressure. West describes these regions as zones 1, 2, and 3 (Figure 8). This well-established gravitational model has shaped the understanding of differences in the matching of ventilation to blood flow in the lung, which affects the efficiency of gas exchange [10].

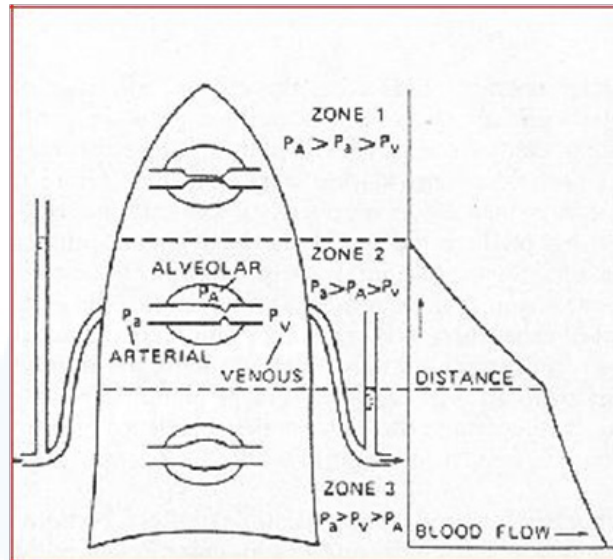


Figure 8: From West et al.'s paper. Left: the classic diagram of the three zones of the lung (zones 1–3) is showing the Starling resistor model for each of the three zones inside the outline of the lung. Middle: relationship of pulmonary artery pressure, pulmonary vein pressure, and alveolar pressure for each of the three zones. Right: graph of distance up the lung versus blood flow [10].

Other factors that affect distribution of pulmonary ventilation and perfusion

If the gravity is playing an important rule in distribution of pulmonary perfusion or not [considering a unique factor], really there are many explanations and/or theories act to reaching the factors that controlling the pulmonary perfusion.

Regional ventilation: Early studies of regional ventilation were done using radioactive gases, measured by external detectors that were directed at different lung regions. Xenon was used because it is almost insoluble and has a useful isotope, ^{133}Xe . However, the precision of these external detectors was limited, breath holds had to be imposed to allow sufficient time to acquire the data, and the original studies of regional ventilation were done with very slow maneuvers. Theory predicted that the distribution of ventilation would be affected by greater flow rates. When the distribution of inspired gas was studied using greater inspiratory flows, the regional differences were less than with very slow inspiration (Figure 9) [11].

Such studies were done in upright normal humans. The flow dependence found in the upright position was more marked than when the subjects were supine. This

suggests that there are differences in pleural pressure swings between the different regions, and such differences can affect regional ventilation and its dependence on the inspiratory flow. Indeed, voluntary changes in breathing movements and diaphragm activity clearly affect regional ventilation and reduce the differences between lung regions. However, measurements made with more precision show more variation in regional ventilation. CT scan allows measurements to be made of small regional differences in lung tissue expansion. Enhancement of CT measurements with xenon showed that ventilation was greater in the central lung than in the peripheral lung of mechanically ventilated dogs placed in the supine position. In a careful study of the lung, where CT density was used to measure the relative air and tissue content of each voxel. Anyhow, with both methods, it was found a considerable heterogeneity in expansion, which was not attributable to anatomical or gravitational gradients, at a scale of 1.5 mm^3 . At a slightly larger scale, two independent methods of measurement, using CT and aerosolized microspheres, showed good agreement. With both methods, there was considerable heterogeneity within each lung region, as much as between regions, and it was confirmed that the ventilation was greater in the central lung regions and be less in the periphery.

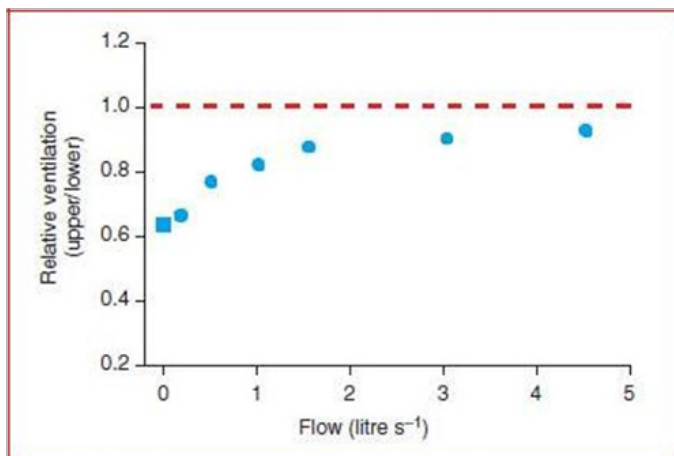


Figure 9: Change in distribution of ventilation (upper to lower ratio) caused by changes in inspiratory flow rate. The filled square shows the quasi-static value [11].

Blood flow distribution at iso-heights: The implication of the effects of gravity is that blood flow to regions of the lung at the same vertical height (isoheights) should be equal. The consequences of the vertical flow gradient might apply irrespective of posture. Under conditions of zero gravity or weightlessness, variations in ventilation and perfusion should be abolished. These predictions are not supported by investigations.

In upright human, there is a cephalad to caudal gradient of blood and gas flow distribution. The early studies used radio-labelled indicators and external counters of radioactivity that gave an averaged value for each horizontal level within the lung. Really such methods gave a two-dimensional picture of what is in fact a complex three-dimensional structure. Evidence that blood flow was not uniformly distributed within horizontal planes emerged from studies in the 1970s. Reed and Wood and later Greenleaf and colleagues used radioactive microspheres to determine regional blood flow in dogs placed in different positions. Microspheres were injected into the right ventricular outflow tract and lodged in the lung capillary beds in proportion to local blood flow. Analysis of the segments from the excised dried lung gave a three-dimensional record of blood flow distribution at the time of the injection of the tracer. These researchers found that blood flow varied within planes at the same vertical height and that there was a gradient of blood flow from apex to base, when dogs were in both the supine and the lateral position. However, recently, with higher resolution technology using fluorescent microspheres, it had found that a considerable blood flow heterogeneity within planes at iso height (Figure 10) [11]. In some studies, flow differences in lung samples at the same vertical height were 10 times greater than the flow differences at different heights. The same methods gave high resolution of regional ventilation. Inhaled fluorescent microspheres show that regional ventilation in pigs varies considerably within the same vertical level. Despite the varied distribution of pulmonary blood flow, variations in the

blood flow patterns with time are remarkably small, with flow distribution patterns remaining relatively stable over days. The strongest determinant of flow to any region of the lung at any given time was the flow to that region at a previous or subsequent point in time. This suggests that under conditions of constant total blood flow (cardiac output) and perfusion pressure, variations in blood flow arise from the basic architecture of the pulmonary vessels. The underlying divisions of the bronchial/pulmonary vessels may have a fractal pattern.

Variation in blood flow in different postures: Studies of regional perfusion in dogs placed in different positions show that anatomy and gravity affect the distribution. Regional ventilation and blood flow were measured in the right and left lateral postures, using aerosolized and intravenous microspheres. A gravity-dependent gradient of flow was present in both postures, but the variation with gravity was greater in the right lateral position than in the left lateral position. A similar pattern was also seen with ventilation, with an even greater difference in the vertical gradients in the two lateral postures.

In fact, in the left lateral position, total blood flow and alveolar ventilation were less in the dependent left lung than in the non-dependant right lung. Adding 10 cm H₂O PEEP reduced the differences in perfusion associated with gravity, in both postures. These differences in regional blood flow gradients between the two lateral positions do not accord with the concept that gravity alone determines blood flow distribution. It was suggested that lung volume affected the vascular diameter and that vascular resistance was the primary determinant of blood flow distribution, with gravity playing a secondary role. Lung distortion by the weight of the heart and mediastinum is greater in the left lateral position than in the right lateral position. The dependent lung has a smaller volume and a greater pulmonary vascular resistance in the left lateral position, and this reduces the magnitude of the vertical gradient of flow. Even though moderate reduction in lung volume is usually associated

with a reduction in pulmonary vascular resistance, the non-uniform distortion of the lung parenchyma in the left lateral position may increase pulmonary vascular resistance and reduce blood flow to the dependent lung in the left lateral position. PEEP reduced pulmonary vascular resistance by increasing ventilated lung volume, so that the V/Q ratio increased in the dependent left lung, and decreased in the nondependent right lung, and hence the overall V/Q matching improved [12].

The influence of gravity on flow distribution may be more important in bipeds than in the quadrupeds, so that the

dog studies, such as the one discussed above, may not be applicable to the variations in ventilation and perfusion in humans. Consequently, similar experiments were done in baboons, which spend most of their time upright. Only 7, 5, and 25% of variation in perfusion heterogeneity was attributable to gravity in the supine, prone, and erect postures, respectively. As the pulmonary vascular anatomy, including the serial distribution of vascular resistances resistance (the proportion of resistance offered by the arterioles, capillaries and venules) is similar, however, the investigators concluded that similar considerations would apply to humans (Figure 11).

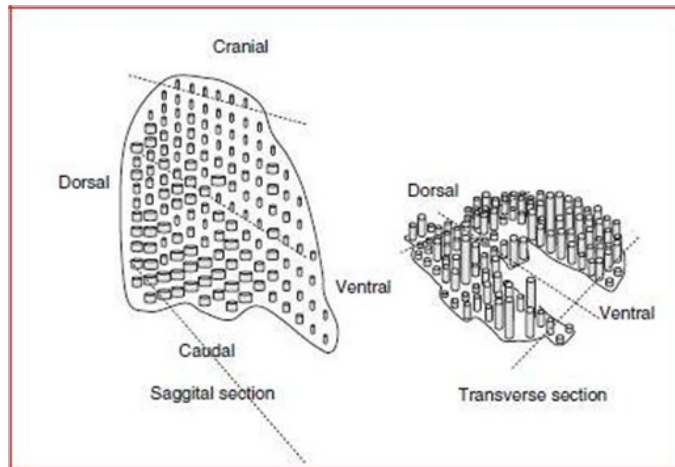


Figure 10: Relative blood flow in the sagittal and transverse planes of an upright baboon, measured using microsphere injection. The relative blood flow is shown in equal proportional steps, in relation to the mean, from 0.2 to 3 times. In the sagittal plane, the flow is shown by increasing diameter, and in the transverse section, by increasing height [11].

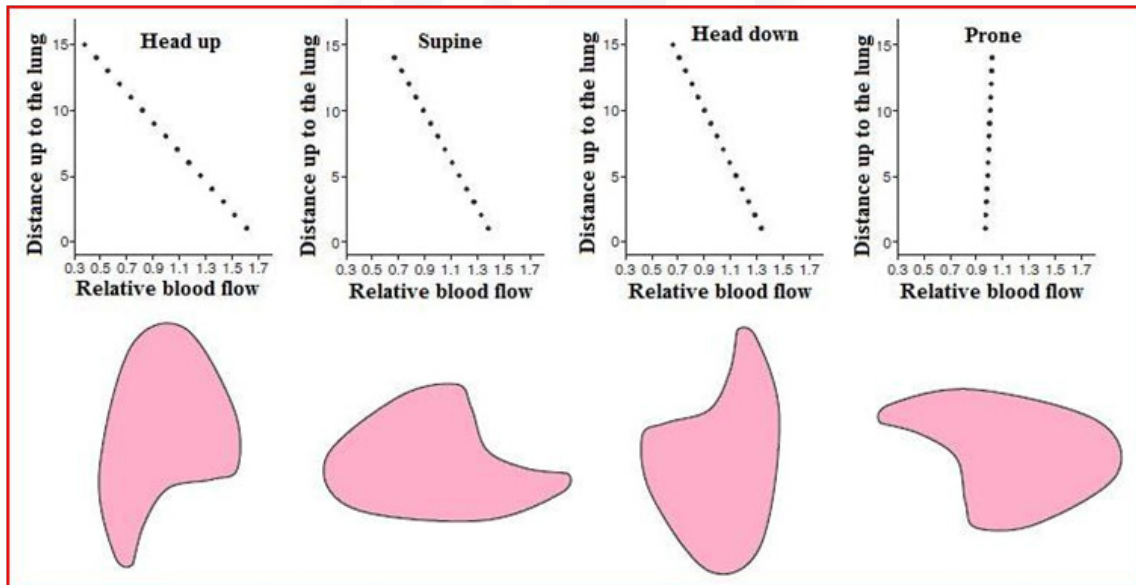


Figure 11: The vertical gradient of blood flow in four different postures. Measurements were made using microsphere injections. In the upper panels, the linear regression of blood flow (expressed as a fraction of the overall flow) in relation to the vertical height is shown. This depiction resembles conventional diagrams, but it is important to note that height is the independent variable. The lower diagram indicates the orientation of the lung in relation to gravity. The influence of gravity on blood flow is greatest in the head up position and least in the prone position. However, it should be noted that the confidence limits of these relationships are may be very large [11].

The effects of gravity: For instance in dogs, ventilation and perfusion were greater in the dependent lung in the lateral position. However, after correction for absolute lung weight, the total blood flow and ventilation were greater in the right, non-dependent lung when the animal was placed in the left lateral position. This finding cannot easily be reconciled with the gravitational model. However, in animals or in human the total blood flow is the product of mean regional blood flow and lung volume, whereas total ventilation is the product of regional ventilation and alveolar regional volume. Both measurements therefore have a direct relationship to lung volume. In the left lateral position the dependent lung has a smaller volume than in the right lateral position, and the magnitudes of the vertical gradients of blood flow and ventilation are less. The relatively small variation in blood flow and ventilation with gravity does not compensate for the greater loss of lung volume in this position. Thus, total blood flow and alveolar ventilation in the dependent lung is less than in the non-dependent lung in the left lateral position, because the decrease in lung volume outweighs any gravity dependent increase in ventilation and perfusion.

Reduced gravity: Volunteers were hyperventilated, held their breath, and then the amplitude of the cardiogenic oscillations and the height of phase-4 in expired CO_2 were recorded in a single expired breath. These measurements indicate variations in intrapulmonary perfusion. There was a significant reduction in perfusion heterogeneity, consistent with the traditional gravitational model. Unfortunately, the single breath exhalation technique does not provide satisfactory spatial resolution for an accurate quantitative analysis of pulmonary blood flow distribution. In structures with underlying fractal geometry, the ability to demonstrate heterogeneity depends on the scale of measurement. Indirect methods such as the single breath analysis

measure relatively large areas of the lung and cannot detect heterogeneity in smaller lung units. Subsequently, the fluorescent microsphere method was used, with better spatial resolution. Different gravitational forces (0-1.8 G [$G = \text{Gravity}$]) were used in a study of pulmonary perfusion (NASA KC-135 aircraft) (Glenny 2000). Perfusion remained variable, from region to region, during weightlessness (0 G) and in increased gravitational conditions (1.8 G), suggesting that vascular structure is indeed important in determining blood flow distribution. In the light of these findings, the following questions can be laid:

- A. What factors influence distribution of ventilation and perfusion in the lung?
- B. Is the gravitational model obsolete?
- C. What are the clinical implications?

What factors influence distribution of ventilation and perfusion in the lung? The spatial distribution of ventilation and pulmonary blood flow remains relatively fixed over time, and the shape and structure of the bronchioles and pulmonary arterioles/veins are important determinants of flow distribution. The branching structure of the bronchi and arteries in the lung is a series of bifurcations (Figure 12). On average, the airways branch about 23 times. Alveoli are present after about the 14th branch point. The pulmonary arteries follow the airways closely and have a similar branching pattern. However, the arteries continue to branch for several more generations, as the vessels penetrate further into the alveoli. Consequently, the pulmonary arterial system has an average of 28 generations of branches. The branching of the pulmonary veins resembles that of the arteries.

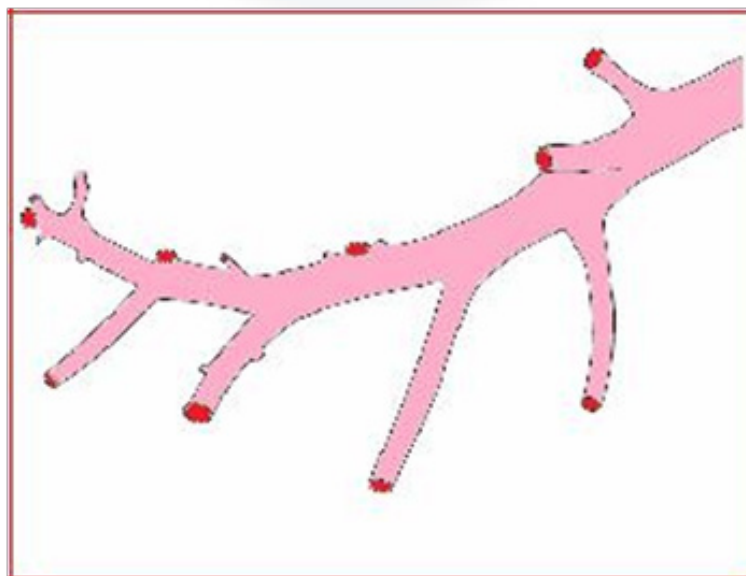


Figure 12: A bronchial cast showing the asymmetric branching structure typical of both airway and vascular branching in the lung [11].

It was found that the pattern of branching is asymmetric and follows consistent rules. At each bifurcation, the diameter and lengths of the daughter branches are reduced by a constant factor (Figure 13). This process of repeated branching can be described by a relatively simple set of rules (or a mathematical function). The repeated branching results in complex multi-dimensional structures and examples of such structures are widely distributed in nature. In the lung, it

provides an efficient mechanism to yield a vast surface area of approximately 130 m² within a limited volume of 5-6 liters. Benoit Mandelbrot had described fractal geometry, which was required for the accurate mathematical description of these objects. One of the basic concepts of fractal geometry is that the overall structure should be self similar at different scales of observation (Figure 14).

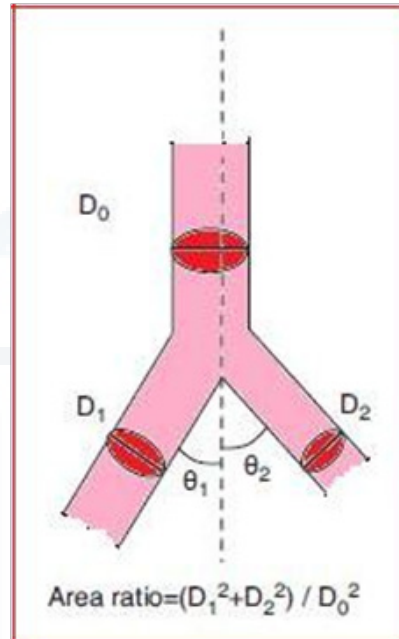


Figure 13: A method of quantifying asymmetry of branching. Both the branch angle and the relative diameters of the parent to the daughter branches can vary. The relative flow depends on these features, tube length, the nature of the flow, and considerations such as minimizing energy loss [11].

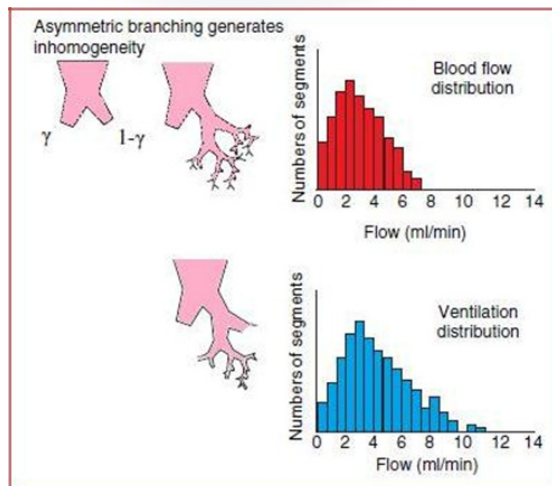


Figure 14: The consequence of asymmetry in branching. The total flow divides into two fractions in each of the branches. The greater fraction is γ and hence the remaining fraction is $1-\gamma$. When this asymmetrical pattern is continued for many generations of branches, these results in a distribution where different lung segments receive a wide range of flows (upper distribution histogram) and ventilations (lower distribution). The resultant blood flow and ventilation values in lung segments (samples) have a skewed normal distribution [11].

The size relationships at each bifurcation determine flow distribution in the bronchial and arterial systems. If, for example, the ratio of the diameter of the branches at each bifurcation is not equal, but is 1:1.1, then the flow difference between these two branches (assuming laminar flow) will be 1.1⁴:1 (i.e. 1.46:1). When this process is repeated through several generations, considerable variation in flow results within a small part of the lung (Figure 13). To detect this heterogeneity, a measurement of local blood flow (or ventilation) will require good spatial resolution. Using graded centrifugal forces to mimic different gravitational conditions (1, 2, and 3 G), workers in Seattle have studied how gravity affects pulmonary perfusion in conscious animals. They found variations in perfusion in all three conditions, at the same gravitational plane, and this heterogeneity is the most convincing argument against gravity being responsible for blood flow variation. More than 75% of blood flow variation was attributable to factors related to the basic vascular architecture under all gravitational conditions. The increase in heterogeneity with greater centrifugal forces was attributed to the stretching of the more peripheral vessels and the consequent increase in vascular resistance. Over the last two decades, researchers have gathered an impressive body of evidence supporting the concept that pulmonary vascular (and bronchiolar) architecture is the most important factor to determine the distribution of ventilation-perfusion in the lungs. This is an important change in the concept of applied respiratory physiology, incompletely recorded in the current texts, and the clinical implication of these observations remains to be assessed.

Is the gravitational model obsolete? Early studies used radioactive gases with collimated scintillation counters over the chest wall to detect the inhaled gases. Counts after a single breath of the radioactive gas were used to compare ventilation in different vertical zones, and the rate of removal of the isotope from the counting fields was used to measure the regional perfusion. Each counter measured at a single horizontal level and provided an averaged value for that level; hence, horizontal heterogeneity was not measured. These early studies reported ventilation-perfusion distribution only in the vertical dimension. With higher resolution methods, a more detailed three-dimensional picture of pulmonary perfusion has emerged. Fluorescent microspheres can show patterns of blood and gas flow within the lung. Given intravenously, they lodge in capillary beds in proportion to blood flow, and aerosol microspheres distribute themselves in the airways in proportion to gas flow. Different colors of microspheres can show differences in temporal, postural, or gravitational patterns. If smaller areas of lung are examined, the variation in blood flow between regions is found to be greater. Using an imaging cryomicrotome to determine the spatial distribution of fluorescent microspheres at a microscopic level, it appears that perfusion heterogeneity increases progressively and remains fractal down to the acinar level. In a study of the effects of different gravitational conditions on lung blood flow in pigs, a pattern of increasing and then decreasing

blood flow down the lung was confirmed. This observation correlated well with West's zones 1-4. However, this pattern persisted during weightlessness, suggesting that gravity was not wholly responsible for this effect.

What are the clinical implications? As the variation in ventilation and perfusion in normal lung is greater than that assumed previously, in both the horizontal and vertical planes, how are ventilation and perfusion matched to maintain efficient pulmonary gas exchange? Consider a part of the lung in which the blood flow has branched asymmetrically so that the distribution of blood flow has become heterogeneous. If this portion of lung is divided into small equal samples, these samples will show a range of different blood flows, with a divert distribution (Figure 14). A similar argument would apply to regional ventilation. If these blood flows and ventilations in each lung sample were matched in a random fashion, a very large range of ventilation to perfusion ratios would result, with a variance equal to the sum of the variances of ventilation and blood flow. However, this is not the case in practice. It had been shown that although regional ventilation and perfusion are heterogeneous, they are closely correlated with each other, ensuring efficient gas exchange. High-resolution maps of regional ventilation show that the strongest determinant of regional ventilation is regional blood flow. The correlation between blood flow and ventilation is of the order of 0.8, where 1 would be perfect (Figure 15). The way regional ventilation and perfusion are co-regulated, however, is not clear. In embryogenesis, the development bronchioles and pulmonary arterioles could be coupled, so that their relative dimensions are fixed at each bifurcation. In this way, the branching and development of the two systems could be linked, so that both ventilation and perfusion show proportionate changes through successive generations. It was found that a considerable convective mixing of gas in the alveoli, which could compensate for differences in alveolar gas composition caused by mismatching between ventilation and perfusion. However, because blood and air have very different flow characteristics, this delicate balance may be disturbed by effects such as gravity or acute lung injury. Hypergravity in humans increases heterogeneity of perfusion and worsening of gas exchange. Increased gravitational forces reduce P_{AO_2} and increase P_{ACO_2} . Increased gravitational forces also increase $P[A-a]O_2$.

The changes in the lung found in acute lung injury resemble, in many respects, the changes found with increased gravity. In both conditions, hydrostatic pressure gradients increase the bronchiolar-pulmonary arterial trees because of increased mucosal and interstitial edema formation. Endothelial damage contributes to edema formation in acute lung injury. These effects distort the precise matching of ventilation with perfusion, because atelectatic or collapsed tissue is not adequately ventilated, and perhaps more frequently, because there are asynchronous changes in gas and blood flow in the successive branches of the airways and pulmonary vessels. Even a small change in the division

of flow in one of the proximal branches of either system can be amplified in the subsequent generation of branches and generate considerable mismatch between ventilation and blood flow in the alveoli. The non-linear process makes the system extremely sensitive to initial conditions. This

could explain why the observed clinical signs or radiological changes in acute lung injury or aspiration pneumonia do not seem to be proportional to the extent of gas exchange impairment.

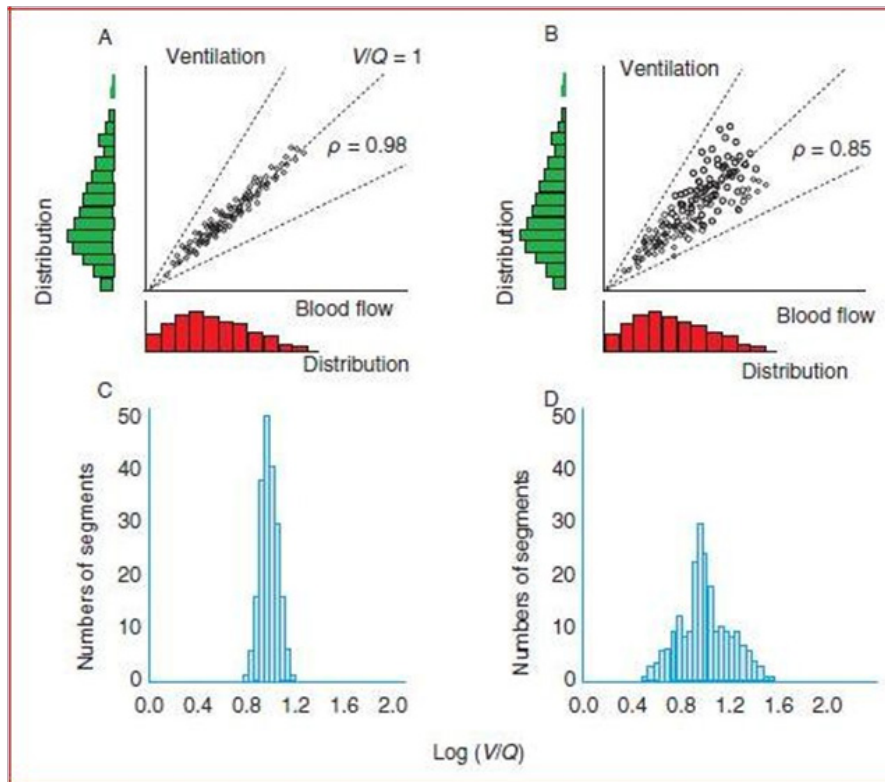


Figure 15: Two hypothetical models of correlation between ventilation and blood flow, using both the same number of lung samples and the same distribution of blood flow and ventilation [(A) and (B), distributions shown parallel to the axes] in each case. (A) The correlation between blood flow and ventilation in each lung sample is close, and the resultant scatter of V/Q values in the samples is small (C). Gas exchange is efficient. (B) Despite the same overall distribution of ventilation and blood flow values, the correlation is less close and the resultant distribution of V/Q values is broader (D) and gas exchange less good [11].

In the supine position, the relaxed diaphragm moves dorsally and cranially, reduces the lung volume, and moderately increases pulmonary vascular resistance, more so than in the prone position. Even in normal subjects, the prone position allows better conditions for pulmonary gas exchange. This is exaggerated in critically ill patients with acute lung injury and multiple organ failure. The increased volume of abdominal contents caused by edema or ascites commonly present in these patients may aggravate the effects of the supine position. It had been found that in human exposed to five times normal gravity, gas exchange was more efficient in the prone position. Pulmonary changes in these conditions mimic those seen in acute lung injury, and hypergravity has been used by several authors as a model of acute lung injury. In the supine position, vital capacity and diffusion capacity are reduced more, and there is a greater increase in V/Q mismatch than in the prone position. The prone position protects against hypoxemia during hyper-gravity (89.7 vs. 84.6% when supine). In

patients with ALI/ARDS the beneficial effect of the prone position is attributable to better alveolar ventilation in the dorsal regions of lung that preserves good V/Q matching. The fundamental structural features of the lung accord with evolution in which the upright position of the human race is a relatively recent event.

PEEP in other aspect is an accepted maneuver to improve oxygenation in ALI/ARDS. CT scan was used to show a direct relationship between the PEEP needed to re-open collapsed lung units with the distance below the ventral-dorsal axis of the lung in supine patients. This observation was consistent with a greater gradient in hydrostatic pressure because of pulmonary edema, with a greater effect in the dorsal and caudal regions of the lung. If gravity were the only important factor, then the beneficial effects of PEEP would be independent of posture. However, PEEP redistributes pulmonary perfusion to dependent lung regions in patients who are supine but not in patients when they are prone.

The traditional gravitational model suggests that in the lateral position, both blood flow and ventilation will be greater in the dependent lung. However, in the left lateral position, total ventilation, total blood flow, V/Q ratio, and regional oxygenation can be less in the dependent lung than in the non-dependent lung. Crucially, regional PO_2 in the lower parts of the dependent left lung was found to be sufficient to trigger hypoxic pulmonary vasoconstriction, and the V/Q ratio for the whole lung was greater in the left as opposed to the right lateral position. This may have important implications for gas exchange in patients in the left lateral position [11].

Morphological Changes of Carotid Bodies in Acute Respiratory Distress Syndrome

Carotid bodies are nodular structures found in the angle of the bifurcation of the common carotid arteries. They are considered to be chemoreceptors sensitive to changes in the partial blood oxygen pressure [PaO_2]. It had been showed that the innervation of the carotid body, originating from the glossopharyngeal nerve, was afferent in nature and probably with sensory function. The interpretation about the histological features of the carotid body is considered to be

the basis of the concept that this structure participates in blood gas monitoring. Later it was demonstrated that the carotid body responds to the fall in partial oxygen pressure, the increase in partial PCO_2 pressure and the fall in arterial blood pH, contributing to the genesis of the hyperventilation observed under these conditions. Other factors such as temperature, osmolarity and arterial pressure, can also stimulate the carotid body [13]. Morphologically, the carotid body shows two different types of cells:

- The cells which forming clusters, there are the chief cells, with three subtypes (light, dark and progenitor) observed by staining with hematoxylin and eosin (Figure 16A & B). These cells are considered to be the chemoreceptor cells of the organ. At the level of electron microscopy, the chief cells contain electron-dense granules in their cytoplasm. Many substances have been demonstrated in these granules, mainly biogenic amines (dopamine, noradrenaline) and some peptides, but the physiological significance of these findings remains unknown.
- The second type, surrounding the clusters of chief cells, is represented by the sustentacular cells that envelope the nonmyelinated nervous filaments and enclose them to the surface of the chief cells (Figure 16 C) [14].

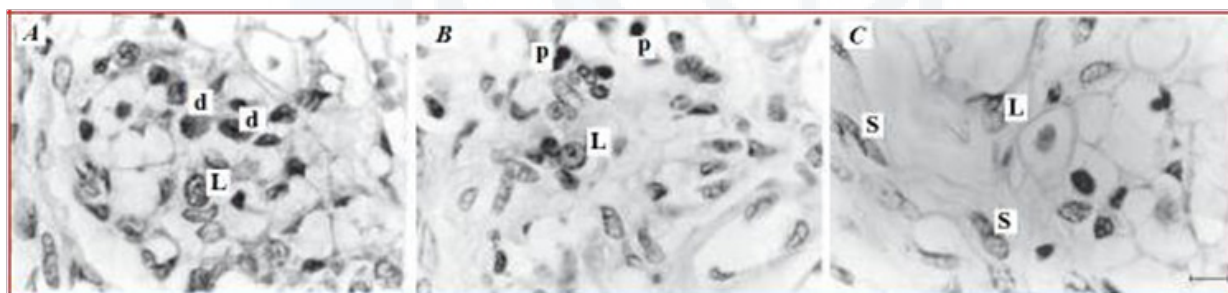


Figure 16: Photomicrographs of glomic cells. A, Light (L) and dark (d) cells in a cluster of chief cells, in a patient that died of acute myocardial infarction. B, Light (L) and progenitor (p) cells in a patient that died of ARDS and systemic lupus erythematosus. C, Light (L) and sustentacular (s) cells in a patient that died of COPD and rupture of aortic aneurysm (HE; bar = 10 μ m) [14].

There is considerable evidence that carotid bodies can have their structure modified under several conditions, such as normocapnic hypoxia, chronic obstructive pulmonary disease (COPD), aging, and arterial hypertension. In these situations, the changes in the histology of carotid bodies have been presumed to provide a reasonable structural basis for the functional abnormalities of respiratory control. For instance, chronic high altitude hypoxia has been associated with light cell hyperplasia; an increase of sustentacular cells has been clearly demonstrated in COPD. Thus, it is reasonable to assume that the cellular profile of carotid bodies can provide useful information about the physiopathology of the respiratory control. However, the relationship between the morphological and functional alterations of the structure in these situations remains obscure.

If chronic hypoxia modifies the histological profile of the carotid bodies, one can speculate that acute episodes of

hypoxia may promote histopathological changes as well. It has been well established that patients that survive acute respiratory distress syndrome may have abnormalities of respiratory control as demonstrated during weaning from mechanical ventilation.

A significant increase in the number of sustentacular cells in COPD was confirmed. Although the studies of carotid bodies in COPD patients previously performed did not use unbiased morphometric methods, proliferation of type II cells (sustentacular cells) but precisely in hypoxic patients has been reported. It was observed that the amount of glomic tissue in COPD was reduced in comparison to that of the connective tissue that limits the lobules within the carotid body, suggesting that the parenchyma of COPD patients shows reduced chemosensitivity. However, ARDS patients had had a different histological cells and an increase in dark cells when compared to controls (Table 2). It is interesting to note that the patients who complaining from ARDS

were younger than in the other groups. The difference in age could be a factor that affects the histological profile of carotid bodies since there is a predominance of dark cells in the chief cell population of children and young adults. However, even the three oldest patients with ARDS had an

increased dark cell population when compared to controls (mean values of $P_{\text{dark}} = 0.125$) and the COPD group. However, (Table 2 & 3) shows individual values of P_{dark} in ARDS patients.

Table 2: Morphometric parameters of carotid bodies in control, COPD and ARDS groups [14].

Group		Mean	Maximum	Minimum	Standard Deviation
Control	Plight	0.4372	0.5242	0.3477	0.061
	Pdark	0.1245	0.2683	0.0703	0.062
	Pprogenitor	0.0491	0.0796	0.0164	0.0221
	Psustent	0.3892	0.4441	0.3126	0.045
	Vc	0.6273	0.875	0.365	0.1942
COPD	Plight	0.3638	0.4237	0.3236	0.0299
	Pdark	0.0814	0.1556	0.0456	0.0249
	Pprogenitor	0.0416	0.1086	0.0201	0.0311
	Psustent	0.5133	0.5714	0.3728	0.0519
	Vc	0.3553	0.7875	0.168	0.2166
ARDS	Plight	0.3277	0.3744	0.2788	0.0332
	Pdark	0.2204	0.2927	0.1624	0.0545
	Pprogenitor	0.0663	0.1294	0.031	0.0329
	Psustent	0.3857	0.4985	0.2658	0.0881
	Vc	0.6527	0.82	0.363	0.1556

Table 3: Age and proportion of dark cells (P_{dark}) of patients with acute respiratory distress syndrome [14].

Age (y)	17	18	22	23	40	54	74
Pdark	0.286	0.279	0.163	0.18	0.179	0.192	0.239
Patient	1	7	3	2	6	4	5

P_{dark} is the mean value for each patient (10 microscopic fields for each patient).

What could be the mechanisms responsible for the increase of dark cells in ARDS? Since the increase in dark cells occurred at the same time as a decrease in light cells, it is tempting to consider that these two cell types are variants of the same cell. The increase in the dark cell population observed in ARDS could reflect a higher functional activity of carotid bodies in response to hypoxia. In an important study, Biscoe and Stehbens was investigating in detail the ultrastructural aspects of glomic cells, suggesting that dark cells have a highly complex secretory structure, presenting a large number of electron-dense granules, most probably containing biogenic amines. Furthermore, the number of electron-dense granules seemed to be increased in chief cells after exposure to acute hypoxia. It had been suggested that the increase in electron-dense granules was more pronounced in dark cells in a patient with arterial hypertension, leading to a darker cytoplasm at the ultrastructural level. In the human carotid body, dopamine is the biogenic amine present at the highest concentration in the electron-dense granules, but, interestingly enough,

dopamine is considered to decrease the respiratory response to hypoxia. The functional significance of these observations remains to be clarified. Since dark cells can represent a higher functional status of chief cells, an increased number of dark cells in ARDS could be seen as an adaptive response to low arterial oxygen tension. Consistent with the foregoing view is the report that dark cell hyperplasia was observed at an altitude of 3370 m for 3 months. However, the number of dark chief cells returned to normal values (11%) when the subjects were left at the same altitude for a period of 6 months. Furthermore, the carotid bodies from patients with asthma also present an increased number of dark chief cells and this response is considered the first morphological alteration of the carotid body cells after exposure to hypoxia.

In conclusion, the morphological changes observed in carotid bodies in ARDS indicate that functional alterations of respiratory chemosensitivity may be present in these patients. In this scenario, the results indicate that studies

focusing on respiratory control should be done in patients surviving ARDS in order to determine to what extent the difficulties of weaning from the ventilator are related to abnormal respiratory [14].

Pulmonary Vascular Permeability

Pulmonary capillary pressure

Pulmonary capillary pressure (P_{cap}) is the primary force determining the fluid flux across the pulmonary capillary wall. The hydrostatic pressure in the capillaries, representing the midpoint of the capillary bed, determines the filtration out into the interstitium and in the alveoli of the lungs, and controls lung fluid balance. Thus, increasing P_{cap} in the extreme induces lung edema. The driving pressure for blood flow in the pulmonary vasculature arises from the difference between pulmonary artery pressure and left atrial pressure. Accordingly, P_{cap}, which cannot directly be measured in human lungs, must range between the pulmonary artery pressure and the left atrial pressure, and is determined by the pulmonary artery pressure, pulmonary vascular resistance, and total blood flow.

In normal human lungs, left atrial pressure is somewhat less than pulmonary diastolic pressure. The P_{cap} is approximately 6 - 8 mmHg, increasing slightly with increasing blood flow and decreasing to near 0 at rest, when pulmonary blood flow almost ceases during each diastole. In many pathological states, such as acute respiratory distress syndrome, pulmonary hypertension, sepsis, inflammatory states, hypoxia or cardiovascular diseases, the pressure gradient between pulmonary arterial diastolic pressure and left atrial pressure is increased, and the distribution of the pulmonary vascular resistance from pre-capillary arterial to post-capillary venous compartments varies. Accordingly, at any given blood flow, the hydrostatic pressure in the pulmonary capillaries depends on the magnitude of the resistance to blood flow across the pulmonary circulation and its distribution between pre-capillary and post-capillary vessels.

Although quite a few thoroughly validated methods for estimating P_{cap} exist, not only in animal models but also under clinical conditions, the significance of the P_{cap} as a surrogate in controlling lung fluid balance is often ignored. In clinical practice, P_{cap} is seldom assessed, and pulmonary artery occlusion pressure (PAOP) - confusingly called pulmonary capillary wedge pressure or capillary pressure by Swan and Ganz - is commonly used to guide fluid therapy. The assumption that the widely used PAOP, and thus the left atrial pressure, reliably reflects pulmonary filtration pressure within the capillary bed is erroneous, particularly in patho- logical states, when the resistance in the post- capillary vessels, located between the capillaries and the left atrium, is increased.

Several studies have evaluated the relationship between P_{cap} and PAOP in critical illness and have found a high variability between them, with the risk of underestimation of filtration pressure and consequently the risk for lung

edema. In sepsis or severe inflammatory states, it is often mandatory to infuse large amounts of fluids to improve microcirculation and to establish appropriate oxygen delivery and tissue oxygenation. There is evidence that inadequate fluid management is associated with organ dysfunction and increased mortality. Hence, the crucial questions to be asked are: which hemodynamic parameters are particularly appropriate to promote optimal fluid management and what are the reasonable hemodynamic goals to be achieved. From the rational and physiological point of view, it is clear that the absolute value of PAOP is not an alternative for filtration pressure in neither the capillaries nor a substitute variable which consistently predicts the formation of lung edema.

As mentioned above the P_{cap} is the principal determinant of fluid flux across the pulmonary capillary wall, and thus of lung edema formation. The driving forces in the pulmonary capillaries determining the rate of fluid filtration from the intravascular to the interstitial compartment can be estimated by the Starling equation as follows:

$$\text{fluid efflux (Q)} = K_{fc} \times [(P_{\text{capillary}} - P_{\text{interstitium}})] - K_d [(P_{\text{capillary}} - P_{\text{interstitium}})]$$

where P is hydrostatic pressure, π oncotic pressure, K_{fc} capillary filtration coefficient (the product of capillary hydraulic conductivity and capillary surface area) and K_d reflection coefficient (values from 0 to 1; converging towards 0 when the microvascular wall is extremely permeable to proteins and converging towards 1 when the microvascular wall is impermeable to proteins) (Figure 17A) [15].

Under normal conditions, a small amount of fluid and protein is filtered through the capillary endothelium into the pulmonary interstitium and subsequently drained by the lymphatics into the systemic venous system. With an acute rise in P_{cap}, the lymphatics cannot rapidly increase the rate of fluid removal. As a consequence, the capacity of the lymphatics is exceeded; first interstitial and subsequently alveolar edema ensues. In states with an increased rate of transvascular fluid filtration, the lymph flow increases and consequently counteracts the development of edema. Over a wide range of varying capillary pressures, this system is self-adjusting. There is evidence that edema development does not occur until a P_{cap} of 15 - 20 mmHg above control values has been reached. As can be seen from the Starling equation, increased lymph flow decreases π interstitium by washing out interstitial protein, thus increasing the oncotic gradient for fluid flux back into the blood. By increased permeability to protein, the term K_d is reduced. By loss of protein into tissue, the term (π capillary - π interstitium) is decreased as well. However, the hydrostatic pressure in the capillaries may or may be not is the unique important determinant for fluid flux out of the capillaries and into the interstitium. This results in lung edema exceeding a certain level, notwithstanding the oncotic pressure gradient and the counteracting lymphatics. This close relationship between P_{cap} and development of pulmonary edema was first demonstrated in many experiments it was observed

that a linear increase in the development of edema when P_{cap} increased above 28 mmHg (Figure 17A). To study the effect of the oncotic pressure on the filtration rate within the pulmonary capillaries, investigators compared the filtration rates of whole blood and blood diluted to

50% of normal plasma oncotic pressure during increasing P_{cap} . Consequently it was found that pulmonary edema developed in diluted blood at a lower P_{cap} , but with the same rate of edema formation (Figure 17B).

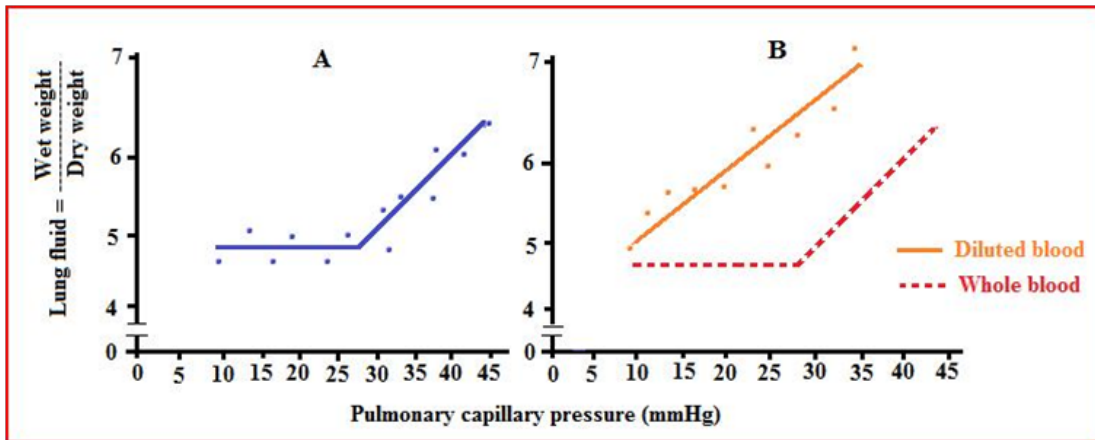


Figure 17: (A) Relationship between pulmonary capillary pressure and edema formation in the lung, which a linear increase in edema development above a critical capillary pressure of 28 mmHg. (B) Effect of diminished plasma protein on the relationship between pulmonary capillary pressure and edema formation [15].

Capillary hydrostatic pressure and capillary permeability interact in the lung and play a central role in the development of lung edema. In inflammatory disorders, most inflammatory mediators induce an increase in P_{cap} (vide supra). Simultaneously, a few mediators also cause an increase in pulmonary capillary permeability. Among these are oxygen radicals and cytokines which are induced by sepsis or ischemia (Interleukin-1, Interleukin-8, tumor necrosis factor) in part via the recruitment of neutrophils. However, data from isolated lung experiments suggest a possible increase in permeability due to an excessive increase in microvascular hydrostatic pressure. Nevertheless, in all types of lung edema, the major force that causes fluid efflux out of the capillaries into the interstitium is the hydrostatic pressure in the capillaries. Therefore, a differentiation between hydrostatic or cardiogenic lung edema and permeability or low-pressure edema when P_{cap} is unknown is to some extent arbitrary and artificial.

In other side an increase in P_{cap} results from an increase in the resistance in the pulmonary venous bed between the pulmonary capillaries and the left atrium. In cases of inflammatory disorders such as sepsis or ARDS, the pulmonary venous resistance is often increased. There is no longer a constant relationship between P_{cap} and PAOP, and thus between P_{cap} and left atrial pressure. Under these conditions PAOP may be used inaccurately as a therapeutic goal during fluid therapy: underestimation of the pressure responsible for pulmonary capillary filtration can lead to potentially dangerous interstitial edema and deteriorating oxygenation. Due to the important clinical impact of the close relationship between formation of lung edema and P_{cap} , methods have been developed to determine P_{cap} in humans. To date, only indirect measurements exist to assess P_{cap} reliably.

Increased transpulmonary pressure gradient: The transpulmonary pressure gradient is defined as the pulmonary artery diastolic pressure (PAPd) minus the left atrial pressure, or PAOP. It is not more than 6-8 mmHg in normal human lungs. At the same time, fluctuations in PAPd and PAOP are very similar. Pulmonary arterial pressure may be increased with a normal transpulmonary pressure gradient, as is the case in the classical cardiogenic or hydrostatic pulmonary edema, in which the transudation of excess fluid into the lungs develops secondary to an increase in left atrial, pulmonary venous and capillary pressures. This occurs in the absence of a primary change in the permeability of the capillaries or in the longitudinal distribution of the resistance over the pulmonary vasculature, with minimal resistance across the pulmonary veins. Because of that, P_{cap} may be approximated by the PAOP. In contrast, a widening of the transpulmonary pressure gradient results from an increase of pre-capillary arterial or post-capillary venous resistance, increased pulmonary blood flow, or both. This is the case in the classical non-cardiogenic pulmonary edemas such as ARDS (Figures 18) and high altitude pulmonary edema or neurogenic pulmonary edema, in which there is an increase predominantly of the venous pulmonary resistance [16]. As a consequence, a large increase in P_{cap} occurs, and there is no fixed relationship between the microvascular hydrostatic pressure in the lung and PAOP. Thus, in the presence of a normal or low left ventricular filling pressure and PAOP, the tendency for fluid efflux from the circulation and worsening pulmonary edema may be overlooked or considerably underestimated.

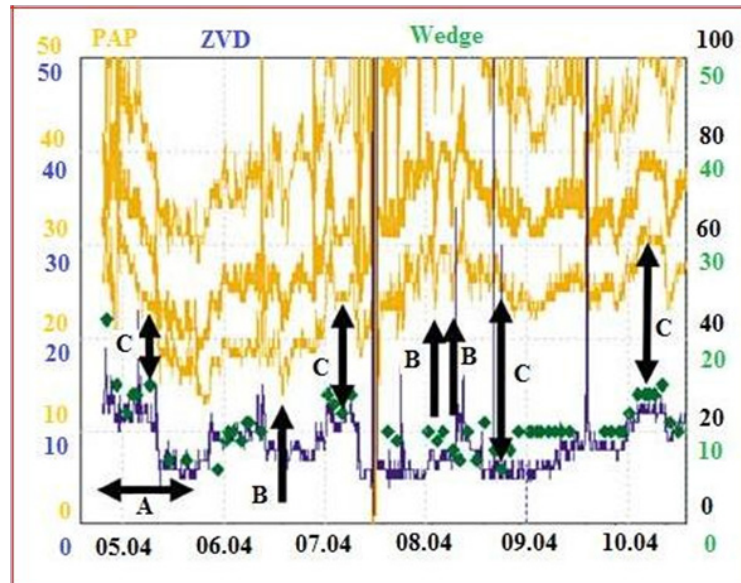


Figure 18: Evolution of ARDS in a patient after cardiac surgery (time scale 6 days): PAP (pulmonary artery pressure, trend displayed in orange), CVP (central venous pressure, trend displayed in blue) and PAOP (pulmonary artery occlusion pressure, green diamonds). A represents a dry-lung approach. A marked negative fluid balance has been achieved by strengthened fluid removal through continuous veno-venous hemodiafiltration. B: Inhalation of prostacyclin (PGI_2) in severe pulmonary hypertension. C: increased and highly variable transpulmonary pressure gradient [15].

Normally, the transpulmonary pressure gradient is divided into 60% pre-capillary and 40% post-capillary components. However, various compounds released into the circulation as a consequence of normal physiological responses, of disease states, or administered as pharmacologic agents, affect the distribution of the pulmonary vascular resistance. Some compounds are known to predominantly increase pre-capillary resistance, whereas others only affect post-capillary resistance. The variability in the locations where stimuli affect pulmonary vascular resistance has been revealed in many studies. For example, serotonin was found to predominantly increase the arterial resistance, whereas histamine was found to have a selective vasoconstrictive effect on the venous side of the vasculature in isolated blood-perfused lungs as well as in quasi-intact. In several studies, norepinephrine infusions constricted large and small veins and arteries in equal measure in the lungs. Hypoxia has been demonstrated to markedly increase the mean pulmonary artery pressure (PAPm) as a consequence of selective constriction of the pre-capillary vessels, with little effect on Pcap, in many experimental models of isolated lungs and intact lungs. Smoke inhalation resulted in an increase of arterial and venous pulmonary resistance, with a principal increase of the venous side. In acute lung injury, the distribution of pre-capillary and post-capillary pulmonary resistance may be altered as the result of inflammatory injury. Several inflammatory mediators, such as arachidonic acid, thromboxanes, leukotrienes, platelet-activating factor or histamine, have been shown to selectively increase pulmonary venous resistance and directly increase Pcap in proportion to blood flow with an elevated transpulmonary pressure gradient but unchanged

left atrial pressure and PAOP. Some of the compounds altering the pulmonary vascular resistance cause different effects and the response is dependent on receptor distribution and pulmonary vascular tone. Histamine, for example, constricts vessels (H1 receptors) with normal tone but dilates vessels (H2 receptors) with high vascular tone.

In sepsis the endotoxin has been demonstrated to induce pulmonary hypertension, with a marked increase in capillary pressure and transpulmonary pressure gradient. In acute respiratory failure, endotoxin resulted in sustained pulmonary hypertension and increased pulmonary arterial resistance, whereas Pcap and pulmonary venous resistance only temporarily increased. Hemodynamic parameters were measured in a septic shock and found that an increase of PAOP, mean pulmonary arterial pressure, and Pcap after endotoxin, while left atrial pressure and left ventricular end-diastolic diameter decreased. Pulmonary arterial resistance as well as venous resistance increased, with a predominance of the venous side, due to endotoxin. However, immediately after a subsequent resuscitation with lactated Ringer's solution, left atrial pressure and left ventricular end-diastolic diameter returned to baseline and pulmonary venous resistance transiently decreased, while PAOP remained increased. This dissociation between PAOP and left atrial pressure after the endotoxin has been suggested by the investigators to result from Starling resistor forces (venocompression) rather than from active venoconstriction. Therefore, these findings indicate that in sepsis-related pulmonary dysfunction, PAOP does not accurately reflect left ventricular filling pressure, and in the presence of Starling resistor forces PAOP overestimates left atrial pressure. However, based on the assumption of

a reliably fixed relationship between hydrostatic P_{cap} and PAOP or left ventricular filling pressure, the potential for inaccurate therapeutic interventions exists under conditions with both normal and elevated transpulmonary pressure gradients (vide supra).

ARDS is an inflammatory disease of the lung, characterized most prominently by pulmonary edema and increased permeability of the alveolar-capillary barrier, with accumulation of protein-rich fluid in the alveoli. The rise in microvascular permeability is the principal difference between the pulmonary edema in ARDS and the classic cardiogenic pulmonary edema. PAOP or other surrogates of left ventricular filling pressures are commonly used to distinguish between cardiogenic and non-cardiogenic lung edema. Although enhanced microvascular permeability is the hallmark of ARDS, in all types of pulmonary edemas the rate of edema development depends directly upon the hydrostatic pressure in the capillaries, which is the main determinant for transvascular fluid filtration. In the presence of a capillary leak, as occurs in ARDS, pulmonary edema is more likely to develop at any given P_{cap} than in conditions with normal vascular permeability. Thus P_{cap} and permeability always interact in the development of pulmonary edema. Moreover, P_{cap} is related to post-capillary venous resistance, and varies directly with blood flow. In ARDS, post-capillary resistance has been found to be elevated, and cardiac output, particularly in sepsis, is often increased. Therefore, in ARDS, the hydrostatic pressure in the capillaries may be the crucial factor for net filtration of fluid out of the pulmonary capillaries. However, in clinical practice, PAOP remains a common hemodynamic target to guide fluid management and cardiovascular support, whereas P_{cap} is seldom assessed, even though it is physiologically evident that PAOP is not a substitute for the hydrostatic P_{cap}. In ARDS, it has been well documented that the transpulmonary pressure gradient, the pulmonary vascular resistance mainly in the venous bed, and the P_{cap} are typically increased, with dissociation between P_{cap} and PAOP.

Recently, in a study on ARDS patients, the evolution of P_{cap} from acute to late ARDS was investigated. A decrease of PAPd, P_{cap} and PAOP towards late ARDS was found, whereas the post-capillary pressure gradient of the pulmonary vasculature (P_{cap}-PAOP) remained unchanged. PAPd, P_{cap}, PAOP and P_{cap}-PAOP increased with higher PEEP levels throughout the course of ARDS, while the proportion of the post-capillary pressure drop to total transpulmonary pressure gradient (P_{cap}-PAOP)/(PAPd-PAOP) tended to increase during established ARDS and with higher PEEP levels. The rise of (P_{cap}-PAOP)/(PAPd-PAOP) was attributed to the restricted fluid administration resulting in a stronger decrease of PAPd and PAOP than P_{cap}. The increase of P_{cap}-PAOP with higher PEEP levels did not seem to be associated with increased blood flow. Furthermore, the relationship between P_{cap} and PAOP has been demonstrated to be highly variable, and P_{cap} cannot be predicted from PAOP. Accordingly, in the

presence of a normal PAOP, the P_{cap} and the tendency toward development of pulmonary edema may substantially be underestimated.

In ARDS, a therapeutic strategy of reducing pulmonary edema formation with diuretics, dialysis, and restrictive fluid administration [the so-called dry-lung approach (Figure 18)] can improve pulmonary function and probably outcome, even in patients who are not volume overloaded. Anyhow, there is evidence that high P_{cap} aggravates fluid accumulation. In patients with acute lung injury, lowering P_{cap} has been demonstrated to reduce trans-capillary protein flux. In one retrospective analysis of 40 ARDS patients, survival was superior in patients with a large reduction in PAOP compared to patients with little reduction in PAOP (75% versus 29%, respectively). The difference in survival remained statistically significant after patients were stratified by age and APACHE II severity of illness.

Inflammatory insult to the alveoli resulting in diffuse alveolar damage has been recognized as the primary injury in ARDS. High quantities of neutrophils, the predominance of proinflammatory cytokines and low levels of anti-inflammatory cytokines in the bronchoalveolar lavage fluid, as well as pulmonary fibrosis, correlate with poor outcome in ARDS. However, many inflammatory mediators contributing to the pathogenesis of ARDS, such as arachidonic acid, thromboxanes, leukotrienes and platelet-activating factor, have been shown to selectively increase pulmonary venous resistance and P_{cap}. These findings have prompted interest in agents capable of suppressing inflammation and promoting lung repair. Various anti-inflammatory agents, such as corticosteroids, prostaglandin E1, and inhibitors of arachidonic acid metabolism, have all been investigated. However, the effect on the P_{cap} has only been studied for PGE1, which is not only a potent, endogenous anti-inflammatory mediator but also an efficient vasodilator. A hallmark of severe ARDS is pulmonary hypertension (Figure 18), with an increase of P_{cap}, subsequent increase of transvascular filtration rate, and severe hypoxemia caused by physiological shunts and ventilation/perfusion mismatch. Many attempts have been made to reverse pulmonary hypertension and ameliorate oxygenation with vasodilators. Prostaglandin E1 and nitroglycerine infusions have been shown to reduce PAPm, P_{cap}, right atrial pressure, and PAOP without changing the longitudinal distribution of the pulmonary vascular resistance in ARDS patients, whereas gas exchange was impaired as a result of increased shunting. Two randomized, double-blind, placebo-controlled clinical trials investigating the effect of PGE1 on survival of ARDS patients have yielded conflicting results. Hence, the role of PGE1 in clinical practice remains uncertain. Infusions of prostacyclin (PGI₂) have been found to lower PAPm and P_{cap} without impairing oxygenation and to maintain the proportion of arterial to venous pulmonary resistance in ARDS patients. Inhaled PGI₂, causing an almost identical physiological effect as nitric oxide (NO), has been demonstrated in most clinical studies to improve oxygenation and lower pulmonary hypertension (Figure 17)

in the same manner as NO. The administration of inhaled PGI₂ requires distinctively less complex equipment than the administration of inhaled NO; however, no reduction in mortality has been observed. Inhaled nitric oxide (NO) has been investigated extensively, and a decrease of P_{cap} has been demonstrated in animal models of pulmonary hypertension and in patients with ARDS as well. Inhalation of 40 ppm NO has been found to predominantly decrease venous pulmonary resistance and thereby lower P_{cap}, while arterial pulmonary resistance did not change. Furthermore, inhaled NO is acting to reduce transvascular albumin flux in ARDS patients which indicating a diminished vascular permeability. Nevertheless, large randomized trials did not demonstrate any benefit on mortality or duration of mechanical ventilation, although short-term improvements in oxygenation have been observed [15].

Alveolar epithelial fluid transport in acute lung injury and acute respiratory distress syndrome

Pulmonary edema is a life-threatening condition resulting from an imbalance between forces driving fluid into the airspaces and biological mechanisms for its removal. Although, for many years, Starling forces (hydrostatic and protein osmotic pressures) were thought to play a major role in maintaining the alveolar space free of fluid, there is now strong evidence that active ion transport across the alveolar epithelium creates an osmotic gradient that leads to water reabsorption both during the perinatal period and in the adult lung.

Sodium and water transport across the normal respiratory epithelium: Results from several studies indicate that sodium can enter the apical membranes of alveolar epithelial cells through amiloride-sensitive cation channels, such as the amiloride-sensitive epithelial sodium channel (ENaC), and is then transported across the basolateral membrane into the interstitium by the ouabain-inhibitable sodium/potassium adenosine triphosphatase (Na⁺/K⁺-ATPase). Water follows passively, probably

through water channels [the aquaporins (AQPs)], although the presence of these water channels is not required for maximal alveolar epithelial fluid transport in the lung. Really it had been identified the presence of messenger ribonucleic acid (mRNA) encoding all the three subunits of the ENaC in alveolar epithelial cells both in vivo and in vitro. Consistent with this idea, studies of alveolar epithelial cells have failed to identify the classical amiloride-sensitive sodium channel in alveolar epithelial cells, suggesting that apical sodium entry may also be mediated by other cation channels with different single channel conductance. Nevertheless, several other cation channels have been identified in alveolar type II cells. One of these, the nonselective cation channel, can be inhibited by amiloride, further suggesting that, in parallel with the ENaC, it could contribute to sodium transport across the alveolar epithelium.

Na⁺ /K⁺-ATPase is a ubiquitous plasma membrane, ion-transporting ATPase that maintains transmembrane gradients of Na⁺ and K⁺ by pumping Na⁺ out of the cell and K⁺ into the cell against their respective concentration gradients. It is widely believed that a heterodimeric form comprising the α₁-subunit and β₁-subunit is the predominant sodium pump isoform expressed in alveolar epithelial type II cells, although expression of the α₂-subunit has also been reported. The catalytic α-subunit binds to and cleaves the high-energy phosphate bond of adenosine triphosphate, whereas the β-subunit is apparently responsible for the assembly and normal insertion of the enzyme complex into the plasma membrane.

Studies in vitro have indicated that there is usually parallel independent regulation of apically localized sodium transport processes and basolaterally located Na⁺/K⁺-ATPase in response to a variety of stimuli, including hormones, such as catecholamines, dopamine, glucocorticoids, thyroid hormone and insulin, and growth factors (Figure 19 & Table 4) [17]. The intracellular sodium concentration appears to be responsible, in certain cases, for the coupling of the sodium pump and cation channel activities [18,19].

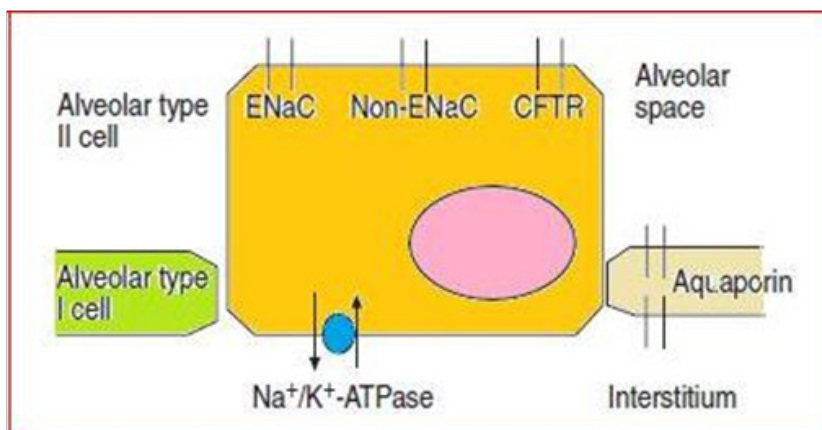


Figure 19: Schematic representation of the possible transporters involved in ion and water transport in alveolar cells. ENaC: Apical Amiloride-Sensitive Epithelial Sodium Channel; CFTR: Cystic Fibrosis Transmembrane Conductance Regulator [19].

Table 4: Summary of possible mechanisms of regulation of ion and water transport in the lung [17].

Simulation	Inhibition	Possible Implicated Mechanisms
Catecholamines and β -agonists.	Hypoxia.	Transporter gene expression.
Growth factors (EGF, KGF, HGF).	Oxidants.	Intracellular trafficking.
Cytokines (TGF- α).	Nitric oxide.	Membrane abundance.
Hormones (glucocorticoids, thyroid hormone, insulin).		Degradation/ubiquitination.
Oxidants.		Transporter activity, open probability and conductance.
Serine protease (CAP1).		Cell proliferation.

EGF: Epidermal Growth Factor; KGF: Keratinocyte Growth Factor; HGF: Hepatocyte Growth Factor; TGF: Transforming Growth Factor; CAP1: Channel-Activating Protease 1.

Catecholamine-dependent mechanisms are the most extensively studied stimulatory mechanism of transepithelial sodium transport and alveolar fluid clearance. It had been demonstrated that β_2 -adrenergic agonists can upregulate alveolar fluid clearance. It was found that a rise in alveolar protein concentration in the distal airspaces of the lungs provided an index of alveolar fluid clearance since alveolar fluid is removed much more rapidly than protein. The β_2 -agonist effect is mediated in part by cyclic adenosine monophosphate (cAMP) - dependent mechanisms, is partially inhibited by amiloride and seems to be unrelated to the increased pulmonary blood flow simultaneously induced by these drugs. It is noteworthy that endogenous catecholamines do not play a major role under normal conditions, as demonstrated by the unaltered alveolar fluid clearance in adrenalectomised animals, as well as in studies showing no effect of β -blockers on basal alveolar clearance in human lung. β_2 -Adrenergic agonists are effective when delivered intravenously or directly into the distal airspaces of the lung. Although early studies indicated that the primary stimulating effect was mediated by β_2 -receptors, recent work indicates that β_1 stimulation is also effective in upregulating alveolar fluid clearance. Consistent with these data, β_1 -receptors and β_2 -receptors are present on both the apical and basolateral surface of alveolar epithelium. Several studies have indicated that β_2 -adrenergic agonists markedly enhance the rate of alveolar fluid clearance in human lung preparations. The magnitude of this effect is similar to that observed in other species, with a β_2 -agonist-dependent doubling of alveolar fluid clearance over the baseline level.

Proposed mechanisms for stimulation of active sodium absorption across the alveolar epithelium include increases in sodium pump α -subunit phosphorylation and quantity delivered to the basolateral cell membrane, augmented apical sodium channel (both ENaCs and nonselective cation channels) abundance and open probability, augmented α -ENaC and α_1 - Na^+/K^+ -ATPase gene expression and increased transport of the ENaC from the cytoplasm to the cell membrane. However, other reports indicate that, in the airways, cystic fibrosis transmembrane

conductance regulator (CFTR) can regulate the ENaC. This hypothesis has gained new strength recently. Indeed, indirect stimulation of transcellular sodium movement by stimulation of an apical chloride conductance in the presence of β_2 -agonists or cAMP has been reported by different studies. This hypothesis suggests that a critical factor in upregulating fluid clearance might be chloride, rather than simply transepithelial sodium absorption.

Sodium channels and sodium pump activity in the plasma membrane can be regulated by other mechanisms, including acute regulation by covalent or allosteric modification, and acute intracellular trafficking between the endoplasmic reticulum, intracellular endosomal pools and the plasma membrane. Colchicine, which impairs intracellular microtubular transport of proteins from intracellular stores to the plasma membrane, inhibits the increase in Na^+/K^+ -ATPase subunit abundance induced by β_2 -agonists, suggesting that upregulation is achieved, at least in part, by recruitment of preformed ion-transporting proteins from intracellular pools to the plasma membrane. Recent data also indicate that β_2 -agonists can increase in Na^+/K^+ -ATPase activity by insertion of increased numbers of α -subunits, recruited from late endosomes, into the plasma membrane. Chronic regulation of the abundance of channels and pumps in the membrane is mediated not only by changes in channel synthesis but also by their rates of degradation. Indeed, ENaC activity appears to depend on channel stability at the membrane, a process regulated by degradation via ubiquitination. Finally, there is increasing evidence supporting a new, previously undiscovered, mechanism for autocrine regulation of the ENaC by a serine protease (channel-activating protease 1) expressed in kidney, gut, lung, skin and ovary.

In addition, it was found that the dobutamine markedly upregulates alveolar epithelial fluid clearance by stimulating β_2 -receptors, whereas dopamine upregulates alveolar fluid transport by stimulating the dopaminergic D_1 receptor. Glucocorticoids and thyroid hormone in other way increases respiratory transepithelial sodium transport during the foetal and perinatal period. Recent observations suggests that these hormones may modulate ENaC and Na^+/K^+ -ATPase

gene expression in the lung and also play a significant role in upregulating fluid clearance in adult. Insulin can also cause an increased sodium transport across cultured alveolar type II cells, especially when added to the basolateral membrane, by increasing the open probability of ENaCs. There is also some data showing that oestrogens may increase ENaC expression. However, it is not clear whether the concentrations needed to increase sodium transport in vitro occur in the lung interstitium in vivo.

In addition to the well-studied effects of β_2 -adrenergic agonists, several catecholamine-independent pathways can increase the rate of alveolar fluid clearance. For instance incubation of epidermal growth factor with isolated alveolar type II cells for 24-48 hours increases their capacity to transport sodium; it also upregulates alveolar fluid clearance. Keratinocyte growth factor (KGF), an important alveolar epithelial type II cell mitogen, induces a similar effect, primarily by stimulating alveolar type II cell proliferation. Recently, it is found that one dose of KGF (5 mg/kg body weight) produced sustained upregulation of alveolar fluid clearance over 5 days. Interestingly, addition of terbutaline, a β_2 -adrenergic agonist, further accelerated the rate of alveolar fluid clearance by 50% per hour. Transforming growth factor- α (TGF- α) can also increase the alveolar fluid clearance acutely. Anyhow, since eAMP levels were only minimally increased in alveolar type II cells isolated from lungs exposed to TGF- α , it is possible that the TGF- α effect may be mediated by an alternative signal transduction pathway that does not require elevation of cAMP levels. Since the effect was inhibited by genistein, the mechanism may involve a tyrosine kinase pathway.

Downregulation of alveolar fluid transport can occur with reactive oxygen or nitrogen species or with severe hypoxia. Reactive oxygen/nitrogen at concentrations similar to the one potentially released by activated macrophages downregulates the activity of alveolar type II cell sodium channels as well as amiloride-sensitive currents in oocytes injected with ENaCs. Similar effects have been observed in alveolar type II cells exposed to hypoxia for 12-18 hours.

Initial immunocytochemical evidence in situ demonstrated apical sodium channels and Na^+/K^+ -ATPase were present in type II cells, but not in type I cells. From these observations, it was initially inferred that alveolar transport was only regulated by type II cells and distal airway epithelial cells. Based on more recent data, however, this hypothesis may need to be re-evaluated. New data show that freshly isolated type I cells express subunits of both Na^+/K^+ -ATPase and the amiloride-sensitive ENaC, suggesting that this cell type might also play a role in active vectorial ion and water transport. Moreover, freshly isolated type I cells exhibited the highest known water permeability of any mammalian cell type, thereby probably explaining the very high water permeability of the lung.

Water transport across the alveolar epithelial barrier occurs during fluid absorption from the alveolar spaces because a miniosmotic gradient is created by the vectorial

transport of sodium, and perhaps chloride, that results in water absorption across the alveolar epithelium. Water permeabilities have been measured across several of the major barriers in lung. Osmotically-driven water movement across pulmonary epithelial barriers in the lung is fast, weakly temperature-dependent and inhibited by mercurials.

It was found that there are a four specialized water-transporting proteins, AQPs, which have been localized in lung:

- a) AQP1 in microvascular endothelia and some pneumocytes.
- b) AQP3 in basal cells of the nasopharynx, trachea and large airways.
- c) AQP4 at the basolateral membrane of airway epithelium.
- d) AQP5 at the apical membrane of type I alveolar epithelial cells.

In order to define the role of AQP water channels in water transport across the various barriers in the intact lung, each of the four lung AQPs has been deleted. The deletion of AQP1 or AQP5 produced any ~10-fold decrease in osmotically driven water transport between the airspace and capillary compartments, thus, demonstrating major roles in osmotically driven water movement across the alveolar endothelial and epithelial barriers, respectively. AQP1 deletion also caused a moderate decrease in isosmolar transcapillary water movement in response to a modest increase in lung vascular pressure. AQP4 deletion alone had little effect on airspace- to-capillary water permeability. Interestingly, and most importantly, isosmolar alveolar fluid clearance was not affected by AQP1 or AQP5 deletion, even under conditions in which the clearance rate was maximized by pretreatment with isoproterenol and KGF. Consistent with these observations, recent studies show no effect of AQP1, AQP4 or AQP5 deletion, alone or in combination, on the formation or clearance of lung edema following lung injury from hyperoxia, thiourea or acid instillation. Thus, although the precise role of AQPs in lung physiology remains uncertain, the studies to date demonstrate that active isosmolar alveolar fluid clearance in the newborn or adult lung does not require lung water channels. Current studies are focused on the possible role of AQPs in movement of water across the conducting airways of the lung.

Fluid transport across the respiratory epithelium in acute lung injury: Two separate barriers form the alveolar/capillary barrier, the microvascular endothelium and the alveolar epithelium. The acute phase of ALI/ARDS is characterized by the influx of protein-rich edema fluid into the airspaces as a consequence of increased permeability of the alveolar/capillary barrier. The severity and outcome of ALI depends in part on the balance between vascular endothelial and/or alveolar epithelial injuries and their repair mechanisms. The importance of endothelial injury and increased vascular permeability to the formation of

pulmonary edema in this disorder is well established. The critical importance of epithelial injury to both the development of and recovery from alveolar flooding has recently become better recognized. Several observations confirm that transepithelial sodium transport plays a major role in the clearance of fluid from the airspace not only under normal conditions but also during experimental lung injury:

- a. As already explained, for example α -ENaC-deficient mice die shortly after birth due to lung edema. Transgenic expression of α -ENaC in α -ENaC (-/-) mice rescues the lethal pulmonary phenotype, but results in a subclinical defect of transepithelial sodium transport. This defect is associated with an ~50% lower rate of alveolar fluid clearance and significantly greater hypoxia- and thiourea-induced pulmonary edema.
- b. Instillation of phenamil (an irreversible blocker of epithelial sodium channels) into the lungs exposed to hyperoxia resulted in a significant increase in extravascular lung fluid volume.
- c. Systemic administration of amiloride facilitates the development of thiourea-induced pulmonary edema.
- d. Pharmacological stimulation of this transport facilitates recovery from lung injury in
- e. several experimental models of ALI.

It had been found that in many but not all of the existing models of ALI, sodium and fluid transport are upregulated. This interesting finding is well established in conditions such as some models of hyperoxia, thiourea-induced injury, hemorrhagic shock, septic shock and neurogenic pulmonary edema. Besides a possible, direct stretch-sensitive mechanism in the alveolar wall for detecting volume overload, the major underlying mechanism responsible for such stimulation appears to be increased endogenous release of catecholamines (for example, as in the case of short-term studies of septic and hypovolaemic shock or in the early phase of neurogenic pulmonary edema). Consistent with this hypothesis, adrenalectomy reduces alveolar fluid clearance and facilitates thiourea-induced pulmonary edema in lung injury models.

Proliferation of alveolar epithelial type II cells provides another catecholamine-independent mechanism for accelerating fluid transport across the alveolar epithelial barrier as shown in the subacute phase of bleomycin-injured lungs. This mechanism may be very important as it can result in sustained upregulation of alveolar fluid clearance. Finally, there may also be an oxidant-dependent mechanism that can increase the sodium transport capacity of individual type II cells exposed to hyperoxia for several days.

In contrast, conditions associated with lung injury may down-regulate transepithelial sodium transport. Hypoxia affects respiratory epithelial function and inhibits transepithelial sodium transport in alveolar type II cells in lungs by impairing both amiloride-sensitive and amiloride-insensitive sodium transport. Moreover, exposure to

prolonged hypoxia has been shown to decrease both nasal potential difference and alveolar fluid clearance and Na^+/K^+ -ATPase hydrolytic activity. Recently it had been shown that hypoxia downregulates alveolar fluid clearance by ~50% but α -ENaC expression and mRNA levels are modestly upregulated, not down-regulated. Interestingly, terbutaline increased alveolar fluid clearance to high levels, suggesting that perhaps cAMP agonists increase insertion of ENaC into the cell membrane of type II cells.

Ventilator-associated lung injury decreases the ability of the lung to clear edema. Moreover, sodium pump activity in alveolar type II cells isolated with ventilator-associated lung injury is significantly down-regulated compared with non-injured lungs. The mechanisms involved are not clear but may involve an increase in lung endothelial and epithelial paracellular permeability and/or down-regulation of alveolar transport proteins. In addition a release of nitric oxide (NO) by activated alveolar macrophages can contribute to inhibition of sodium transport in lung injury models associated with airways inflammation. However, administration of NO inhibitors can reverse the effect of pulmonary hypotension on down-regulation of alveolar fluid clearance.

Even when lung endothelial injury occurs, the alveolar epithelial barrier may remain normally impermeable to protein and retain a normal or upregulated fluid transport capacity with confinement of the edema to the pulmonary interstitium. However, more severe systemic and pulmonary endothelial injury may be associated with a marked increase in epithelial permeability to protein and inability to transport fluid from the airspaces of the lung which, in turn, lead to alveolar flooding. The inability to remove excess fluid from the airspaces in these conditions may be related to both a marked increase in paracellular permeability due to injury to the epithelial tight junctions and loss or inhibition (NO or other oxidants) of the transport capacity of the alveolar epithelium. In some cases, epithelial integrity may recover rapidly (e.g. after parenteral oleic acid administration) or gradually (e.g. bleomycin-induced lung injury). In other cases, however, the injury to the epithelial barrier is so severe that its function is compromised and recovery may not occur (e.g. severe acid aspiration-induced lung injury).

During ALI/ARDS the ability to remove alveolar fluid rapidly is associated with improved oxygenation, shorter duration of mechanical ventilation and increased likelihood of survival. The alveolar epithelium is remarkably resistant to injury, particularly compared to the adjacent lung endothelium. Even when mild-to-moderate alveolar epithelial injury occurs, the capacity of the alveolar epithelium to transport salt and water is often preserved. As discussed earlier, several mechanisms may result in upregulation of the fluid transport capacity of the distal pulmonary epithelium. However, this upregulation may not be sufficient to counterbalance alveolar flooding. Therefore, efforts to attenuate the lung endothelial injury and alveolar epithelial injury are as important as treatments that might enhance the reabsorptive capacity of the alveolar epithelium.

As had been mentioned above the β_2 -Agonists are attractive as therapeutic agents because they are already in widespread clinical use and have minimal side-effects, even in critically ill patients. Treatment with β_2 -agonists may also increase the secretion of surfactant and perhaps exert an anti-inflammatory effect, thus, helping to restore the vascular permeability of the lung. The previously discussed upregulation of alveolar fluid clearance by endogenous β -adrenergic stimulation has been clearly demonstrated in several clinically relevant animal models. In addition to endogenous upregulation, there is growing evidence that alveolar fluid clearance can be further stimulated by exogenous β -adrenergic therapy in the presence of lung injury. Nevertheless, aerosolized salmeterol resulted in effective treatment, with high concentrations of the drug in the alveolar edema fluid. β_2 -Adrenergic agonists have also been reported to augment the rate of alveolar epithelial fluid transport in the presence of moderate lung injury due to hyperoxia and to restore the ability of the lung to clear edema in ventilator-associated lung injury. In the latter studies, disruption of the cell's microtubular transport system by colchicine inhibited this stimulatory effect. In contrast, following prolonged hemorrhagic shock the reactive oxygen species can inhibit the response of alveolar epithelium to β_2 -agonist stimulation. This suggests that, under certain circumstances, the epithelium may not respond to β_2 -agonist stimulation because of extensive injury and loss of alveolar type II cells or because of a reactive effect of the inflammatory environment on the normal ability of type II cells to increase alveolar fluid clearance [20].

Since acute injury to alveolar epithelial type I cells frequently causes denudation of the alveolar epithelium, an additional approach to hastening the resolution of ALI and ARDS would be to accelerate re-epithelialisation of the alveolar barrier. The provision of a new epithelial barrier with alveolar type II cells may have beneficial effects in addition to restoration of the air-liquid interface. Indeed, the rate of alveolar epithelial fluid clearance in the subacute phase of bleomycin-induced ALI was increased by >100% over baseline levels. The enhanced alveolar fluid clearance depended mainly on the extensive proliferation of alveolar epithelial type II cells. Recent information suggests that hepatocyte growth factor (HGF) and KGF are major mitogens for alveolar epithelial type II cells. Intratracheal pretreatment with KGF before induction of lung injury with radiation, thiourea, bleomycin, hyperoxia or acid instillation decreased the severity of lung injury and overall mortality. This effect required high doses of the growth factor delivered by the intratracheal route and the maximal effect occurred only after 48-72 hours. After 48 hours, however, KGF produces sustained upregulation of alveolar fluid clearance for several days. The mechanism of protection is thought to be due to an increase in alveolar fluid transport secondary to increased numbers of alveolar type II cells even though other mechanisms (including cytoprotection, antioxidant effect, increased release of surface-active material and, perhaps, reduction of lung endothelial injury) may play additive roles. However, the combination of KGF and β_2 -agonist treatment results in

additive upregulation of alveolar fluid clearance. This suggests that there may be mechanisms for providing both short-term (β_2 -agonists) and longer-term (growth factor) upregulation of alveolar fluid transport that might hasten the resolution of clinical pulmonary edema.

Several experimental studies have demonstrated that alveolar edema clearance may correlate with Na^+/K^+ -ATPase activity in both normal and acutely injured lungs. Thus, another potential approach to increasing sodium transport and alveolar fluid reabsorption would be to overexpress the Na^+/K^+ -ATPase gene in the alveolar epithelium. Accordingly, it was found that the overexpression (via adenoviral gene transfer) of the β_1 - subunit or α_2 -subunit increased sodium pump expression and function in the lung. Furthermore, pretreatment of the lungs was associated with increased survival from lung injury due to exposure to hyperoxia for 64 hours exposure to thiourea. Surprisingly, for unknown reasons, overexpression of the catalytic α_1 -subunit of the pump did not induce a similar effect.

Alveolar epithelial transport: The study of the role of alveolar epithelial sodium and water transport in human clinical medicine is a new area of research. Although only limited data exist, currently available results confirm that active alveolar epithelial transport plays a critical role in maintaining lung fluid balance in humans (Table 5). Several approaches have been used to assess such importance in clinical medicine:

- In the ex vivo human lung, standard agonists and antagonists have been employed to demonstrate that active alveolar transepithelial sodium transport in the human lung is inhibited by amiloride and/or ouabain and stimulated by β_2 -adrenergic agonists. Furthermore, this transport is preserved in resected human lungs that are exposed to rewarming after severe hypothermia (7°C).
- The cellular content and protein composition of samples of undiluted edema fluid collected from mechanically ventilated patients with ALI/ARDS have been compared to those of appropriate control samples collected from ventilated patients with hydrostatic pulmonary edema. Thus, markers of endothelial and epithelial lung injury have been detected and their appearance correlated with clinical outcome.
- Alveolar fluid clearance has been measured in patients with ALI/ARDS and compared to control patients with hydrostatic pulmonary edema.
- In vivo respiratory transepithelial sodium transport has been evaluated by measurement of nasal transepithelial potential difference (a marker of this transport in the distal airways [vide supra]) in a small number of patients with defined clinical diseases such as neonatal respiratory distress syndrome and high-altitude pulmonary edema.

Several studies have compared the concentrations of different biologically active substances in pulmonary edema fluid collected from patients with ARDS versus controls with hydrostatic pulmonary edema. These studies indicate that,

in patients with ALI, edema fluid concentrations of several substances are increased compared to control subjects. For example, the concentration of intercellular adhesion molecule-1 (ICAM-1), an adhesion molecule found in high concentrations on the alveolar endothelium and epithelium and released in soluble form into the alveolar space in the setting of lung injury, was 2-fold higher in the pulmonary edema fluid of ALI patients than in that of control patients

with hydrostatic edema. In contrast, plasma concentrations of ICAM-1 were similar in both groups, suggesting that this substance is released directly into the alveolar space when the lungs are injured. Also, preliminary data indicate that high pulmonary edema fluid levels of ICAM-1 were associated with impaired alveolar fluid clearance and prolonged duration of assisted ventilation [21].

Table 5: Potential clinical applications of treatments designed to enhance the resolution of alveolar edema [17].

Intervention	Substance	Potential Clinical Condition*
Systemic β -agonists	Dobutamine (intratracheal and intravenous).	Congestive heart failure.
Aerosolized β -agonists	Salmeterol.	High-altitude pulmonary edema.
	Salmeterol.	Hydrostatic pulmonary edema; experimental.
	Isoproterenol/terbutaline.	Acute lung injury from hyperoxia.
	Isoproterenol/terbutaline.	Ventilator-associated lung injury.
Vasoactive agents	Dopamine.	Acute lung injury from hyperoxia.
	Adrenaline.	
Growth factors	Keratinocyte growth factor (intratracheal).	Radiation.
		Thiourea.
		Bleomycin.
		Hyperoxia.
		Acid instillation.
Glucocorticoids	Solumedrol/dexamethasone.	Acute lung injury.
Gene therapy	Na ⁺ /K ⁺ -ATPase β_1 -subunit overexpression.	Hyperoxia.
	Na ⁺ /K ⁺ -ATPase α_1 -subunit overexpression.	Hyperoxia.

Similarly, the concentration of biologically active HGF (but not KGF) was 7-fold higher in the edema fluid than in the plasma of patients with ALI. Moreover, the edema fluid concentration of HGF was higher in patients with ALI than in those with hydrostatic pulmonary edema, and higher edema fluid levels of HGF were associated with higher mortality in patients with ALI. From other side the soluble TGF- α is also present, in biologically significant concentrations, in the pulmonary edema fluid of patients with ALI but not those with hydrostatic pulmonary edema. The concentrations of TGF- α in pulmonary edema have potent in vivo and in vitro effects on alveolar epithelial sodium transport and alveolar epithelial cell mobility. Two properties of the epithelial barrier can be assessed clinically:

- i. Since the epithelial barrier is normally impermeable to protein, the ratio of edema fluid to plasma protein concentration is a good index of epithelial permeability.
- ii. Since the concentration of protein in alveolar fluid reflects net clearance of alveolar fluid, the measurement of protein concentration in sequential alveolar edema

fluid samples provides a useful estimate of the ability of the epithelial barrier to remove alveolar edema fluid.

With this method, it has been shown that clearance of alveolar fluid can occur surprisingly early and is often apparent within the first few hours after intubation and initiation of mechanical ventilation in patients with either hydrostatic or increased permeability edema.

In many investigations were found that ~ 40% of patients with ARDS were able to reabsorb some of the alveolar edema fluid within 12 hours after intubation. These patients showed more rapid recovery from respiratory failure and lower mortality. In contrast, patients with no evidence of net reabsorption of alveolar edema fluid in the first 12 hours following ALI experienced protracted respiratory failure and higher mortality. In contrast, 75% of 65 mechanically ventilated patients with severe hydrostatic pulmonary edema showed intact alveolar fluid clearance. However, impaired alveolar fluid clearance was associated with lower arterial pH and higher Simplified Acute Physiology Score II at the time of edema fluid sampling. Both of these factors

may be markers of systemic hypoperfusion, which has been reported to impair alveolar epithelial fluid transport by oxidant-mediated mechanisms. Conversely, administration of β_2 -agonist (albuterol) had a positive predictive value of 85% for the presence of intact alveolar fluid clearance, although this finding did not reach statistical significance. Finally, intact alveolar fluid clearance was associated with a greater improvement in oxygenation at 24 hours, along with a trend towards shorter duration of mechanical ventilation and lower hospital mortality.

Intact and rapid alveolar fluid clearance was also found in a group of patients with ischemia/reperfusion pulmonary edema after lung transplantation, confirming that a functionally intact alveolar epithelium may be preserved despite clinically severe reperfusion lung injury. Furthermore, alveolar epithelial fluid transport was preserved in most patients despite evidence of marked lung endothelial injury with a substantial increase in alveolar-capillary barrier permeability. Intact alveolar fluid clearance was correlated with less histological injury, rapid resolution of hypoxemia, more rapid resolution of radiographic infiltrates, and a trend towards a shorter duration of mechanical ventilation and a shorter intensive care unit stay [22].

Newborn infants with either transient tachypnea or neonatal distress syndrome demonstrate a lower nasal potential difference, a marker of transepithelial sodium transport across the epithelium in the distal airways. In these patients, the nasal potential difference is reduced weakly by amiloride. These results suggest that impairment of sodium absorption across the respiratory epithelia of very premature infants may be one factor contributing to the pathogenesis of neonatal respiratory distress syndrome. It was therefore, hypothesized that a similar mechanism may contribute to susceptibility to pulmonary edema in adults. High-altitude pulmonary edema (HAPO) was chosen as a paradigm of pulmonary edema because it occurs in predisposed, but otherwise healthy, subjects, making it possible to study underlying mechanisms in the absence of drugs or cardiac dysfunction. At low altitude, the nasal potential difference was ~ 30% lower in HAPO-prone than in HAPO-resistant subjects.

Amiloride superfusion induced a significantly smaller decrease in nasal potential difference in HAPO-prone than in HAPO resistant subjects. These findings provide the first evidence for genetic impairment of respiratory transepithelial sodium and water transport, at least in part related to ENaC dysfunction, in a human form of pulmonary edema. However, the ENaC may not be the only important cation channel facilitating alveolar fluid clearance [17].

Cytoskeletal regulation of pulmonary vascular permeability

Pulmonary vascular barrier regulation: Despite recent therapeutic advances, inflammatory pulmonary conditions such as acute lung injury, acute respiratory distress syndrome, and sepsis continue to result in high rates of patient morbidity and mortality. Centrally involved in the pathogenesis of these processes and now recognized

as a cardinal feature of inflammation, increased vascular permeability contributes to the profound pathophysiological derangements observed in these disorders. Because of the enormous surface area of the pulmonary vasculature, the pulmonary endothelium, which functions as a semipermeable cellular barrier between the vascular compartment and the interstitium, is particularly sensitive to the dynamic features of barrier regulation. Endothelial barrier properties are not uniform throughout the pulmonary vasculature, with greater macromolecule diffusion in postcapillary venules compared with pulmonary arterioles in whole lung, whereas cultured microvascular endothelial cells [ECs] exhibit 10-fold higher barrier properties than macrovascular endothelial cell as measured by electrical resistance across monolayers.

The integrity of the pulmonary endothelial cell monolayer is a critical requirement for preservation of pulmonary function, with two general pathways described for the movement of fluid, macromolecules, and leukocytes into the interstitium and subsequently the alveolar air spaces. The transcellular pathway utilizes a tyrosine kinase-dependent, gp60-mediated trans-cytotic albumin route, whose regulation and function are unclear but which may serve to uncouple protein and fluid permeability. However, there is general consensus that the primary mode of fluid and trans-endothelial leukocyte trafficking occurs by the paracellular pathway (Figure 20), whose essential role in endothelial permeability has been well supported by an impressive body of research, including electron microscopy studies, which demonstrate the formation of paracellular gaps at sites of active inflammation within the vasculature. Mechanistic approaches designed to understand endothelial cell paracellular gap formation and barrier function have revealed the complexity of these processes; however, several valuable attempts have been developed. One useful model describes paracellular gap formation as regulated by the balance of competing contractile forces, which generate centripetal tension, and adhesive cell-cell and cell-matrix tethering forces, which together regulate cell shape changes. As outlined in (Figure 21), both competing forces in this model are intimately linked to the actin-based endothelial cytoskeleton by a variety of actin-binding proteins that are critical to both tensile force generation as well as to linkage of the actin cytoskeleton to adhesive membrane components [23].

Endothelial cell cytoskeleton: The cytoskeleton is composed of three primary elements: actin microfilaments, intermediate filaments, and microtubules. Actin filaments are of critical importance to endothelial cell permeability, as demonstrated by the findings that cytochalasin D, a well-described disrupter of the actin cytoskeleton, increases endothelial cell permeability in cultured cells, whereas phalloidin, an actin stabilizer, prevents agonist-mediated barrier dysfunction. The actin microfilament system is focally linked to multiple membrane adhesive proteins such as cadherin molecules, glycocalyx components, functional intercellular proteins of the zona occludens (ZO) and zona adherens, and focal adhesion complex proteins (Figure 21). Actin structures are also intimately involved in endothelial cell tensile force generation. endothelial cells contain

an abundance of the molecular machinery necessary to generate tension via an actomyosin motor, actin and myosin represent ~16% of total endothelial protein, and focally distributed changes in tension and relaxation can be accomplished by regulation of the level of myosin light chain (MLC) phosphorylation and actin stress fiber formation.

There is excellent association between the development of transcellular actin cables, stress fibers, increased MLC phosphorylation, and enhanced tension development, with a key regulator of the endothelial cell contractile apparatus being the Ca^{2+} /calmodulin (CaM)-dependent MLC kinase (EC MLCK).

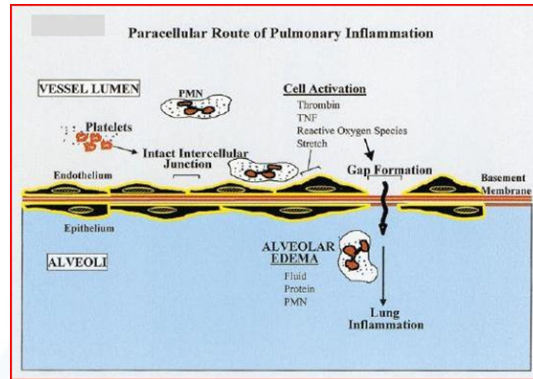


Figure 20: Paracellular route of pulmonary inflammation. Under basal conditions, endothelial cells of the pulmonary vasculature form a semipermeable barrier that restricts the flow of luminal contents into the alveolar air spaces. The important roles of flow and platelets/platelet-derived phospholipids in maintaining these intact intercellular junctions are becoming increasingly recognized. During inflammation, the endothelium is activated by biophysical alterations (stretch or increased shear) or by stimuli such as thrombin, tumor necrosis factor (TNF), and/or reactive oxygen species to form paracellular gaps. In concert with a break in the endothelial cell barrier, fluid, proteins, and polymorphonuclear neutrophils (PMNs) flow into the alveoli to produce pulmonary edema via this paracellular route [23].

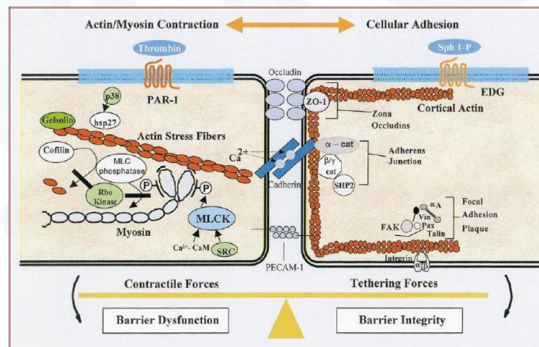


Figure 21: Actomyosin contractile elements and cellular adhesive forces regulate endothelial paracellular gap formation. In this working model of endothelial cell barrier regulation, under basal conditions, a balance exists between actomyosin contractile and cellular adhesive forces. When contractile forces predominate, as depicted in the thrombin-stimulated model (left), endothelial cells pull apart to form paracellular gaps, favoring barrier disruption. Left: schematic representation of the major components involved in regulating endothelial actomyosin contraction. Thrombin binding to its receptor increases intracellular Ca^{2+} , which via Ca^{2+} /calmodulin (CaM) interaction activates myosin light chain kinase (MLCK) to phosphorylate (P) myosin light chains (MLCs), leading to increased actomyosin interaction, force development, and subsequent contraction. Also depicted are other representative regulatory proteins whose activity either increases (green background) or decreases (white background) endothelial cell tension. Tyrosine phosphorylation of EC MLCK catalyzed by pp60^{src} (SRC) increases MLCK kinase activity, whereas Rho kinase augments endothelial cell contraction by inhibiting both MLC phosphatase and the actin-depolymerizing protein, cofilin. Inhibition of heat shock protein (HSP) 27 activity by p38 mitogen-activated protein kinase (MAPK)-catalyzed phosphorylation induces actin stress fiber formation, and the actin capping/severing protein gelsolin is likewise involved in stress fiber-dependent contraction. Right: cell-cell and cell-matrix contacts that link endothelial cells into a functional barrier between the vasculature and the airways. When these tethering forces predominate, as in the sphingosine 1-phosphate (Sph -1-P) model, a thick cortical actin ring is observed, whereas endothelial cells maintain tight connections with each other and the underlying matrix to tilt the balance toward increased barrier integrity. Cell-cell connections include tight junctions composed of transmembrane occludin proteins linked to the endothelial cell actin cytoskeleton by the zona occludens family (ZO-1), adherens junctions mediated by Ca^{2+} -dependent association of cadherin proteins in turn linked to the α -, β -, γ -catenin (cat) complex, and platelet endothelial cell adhesion molecule-1 (PECAM-1)-associated junctions. An example of the complicated regulation of these adhesive sites is provided by the tyrosine phosphatase SHP2, which appears to help stabilize adherens junctions by decreasing tyrosine phosphorylation of catenins. Cell-matrix tethering is maintained by focal adhesion plaques composed of α - and β -integrin transmembrane proteins linked to the actin cytoskeleton by a complex of proteins, including talin, paxillin (Pax), vinculin (Vin), α -actinin (α A), and focal adhesion kinase (FAK). PAR-1: Protein-Activated Receptor-1; EDG: Endothelial Differentiation Gene [23].

The actin cytoskeleton is a dynamic structure that undergoes rearrangement under the control of various actin binding, capping, nucleating, and severing proteins, which are intimately involved in regulating the contractile status of cells:

1. For example, the actin-depolymerizing activity of cofilin is inhibited by Rho-GTPase pathway activation during stress fiber formation. In addition, reduction in either expression or activity of the abundant actin-severing protein gelsolin significantly decreases stress fiber-dependent contraction in cultured cells. Another actin-binding protein involved in cellular contraction is the 27-kDa heat shock protein (HSP27), whose actin-binding properties are altered by phosphorylation through a p38 mitogen-activated protein kinase (MAPK)-driven pathway. Reduction of HSP27-induced inhibition of actin polymerization alone can produce stress fiber formation. Undoubtedly, important roles for additional F-actin binding proteins in regulating cell contraction, potentially in a splice-variant-specific manner, will continue to be explored.
2. The roles of microtubules and intermediate filaments in endothelial cell barrier regulation are much less defined. Microtubules are polymers of α -tubulin and β -tubulin that form a lattice network of rigid hollow rods spanning the cell in a polarized fashion from the nucleus to the periphery while undergoing frequent assembly and disassembly. It was viewed that these elements as a separate and distinct cytoskeletal systems but microtubules and actin filaments are now known to interact functionally during dynamic cellular processes. Microtubule disruption with agents such as nocodazole or vinblastine induces rapid assembly of actin filaments and focal adhesions, isometric cellular contraction, which correlates with the level of MLC phosphorylation, increased permeability across endothelial cell monolayers, and increased trans-endothelial leukocyte migration, whereas microtubule stabilization with paclitaxel attenuates these effects. The mechanisms involved in these effects are likely to be mediated through interaction with actin filaments, suggesting significant microfilament-microtubule cross talk and an intriguing role for the microtubule cytoskeleton in endothelial cell barrier regulation.
3. Intermediate filaments represent the third major element involved in endothelial cell cytoskeletal structure. Although they exhibit much greater diversity than the highly conserved components of either actin microfilaments or microtubules, intermediate filament proteins share a common dimer structure containing two parallel α -helices, which combine to form a polar fibrils that associate with an array of intermediate filament-binding proteins while connecting to the nuclear envelope, peripheral cell junctions, and other cytoskeletal components. Intermediate filament proteins are expressed in a highly cell-specific manner, with vimentin representing the primary protein found in

endothelial cell and other cells of mesenchymal origin. Vimentin phosphorylation occurs rapidly in thrombin- or phorbol-stimulated endothelium. However, data suggest that potential roles for intermediate filaments in endothelial cell cytoskeletal structure, and more specifically barrier function, are likely to be subtle and subject to compensation by biologic increment.

Regulation of vascular permeability by the endothelial cell contractile apparatus:

Multiple studies have demonstrated a critical role for activation of the contractile apparatus in specific models of agonist-induced endothelial cell barrier dysfunction. A well-studied model is that evoked by thrombin, a central regulatory molecule in the coagulation cascade. The dual finding of microthrombi in the pulmonary microvasculature of patients expiring from acute lung injury and recent success of anticoagulant strategies at microcirculatory sites of inflammation illustrates the relevance of this model to the study of acute lung injury and barrier regulation. Thrombin increases pulmonary lymph flow and also increases lung weight gain and reduces the sigma reflective coefficient in the isolated perfused lung, consistent with enhanced permeability. In vitro, thrombin induces a profound increase in endothelial cell albumin permeability and a reduction in electrical resistance reflective of a loss of barrier integrity through rapid actin cytoskeletal rearrangement and force generation dependent on actomyosin interaction, effects confirmed by fluorescent microscopy and biophysical measurements. A key endothelial cell contractile event in several models of agonist-induced barrier dysfunction is the phosphorylation of regulatory MLCs catalyzed by Ca^{2+} /CaM-dependent MLCK, which is sufficient to produce endothelial cell contraction and barrier dysfunction. The inflammatory agonists thrombin and histamine both produce rapid increases in MLC phosphorylation, actomyosin interaction, and endothelial cell permeability, which can be significantly attenuated by treatment with MLCK inhibitors. In addition, MLCK inhibition prevents transforming growth factor- β_1 -stimulated endothelial cell permeability and abolishes barrier dysfunction in lung models of ischemia-reperfusion injury and ventilator-induced lung permeability. The endothelial cell contractile apparatus is activated by polymorphonuclear neutrophil (PMN) adherence and diapedesis with increased MLC phosphorylation, whereas reduction in endothelial cell MLCK activity significantly attenuates leukocyte migration.

The regulation of the MLCK isoform in the endothelium is complex and differs significantly from smooth muscle MLCK regulation. The only MLCK isoform expressed in endothelial cells is a 1,914-amino acid high-molecular-mass (214 kDa) protein derived from a single gene on chromosome 3 in humans, which also encodes the smaller (130-150 kDa) smooth muscle MLCK isoform. EC MLCK shares essentially identical catalytic and CaM regulatory motifs with smooth muscle MLCK but in addition includes a unique 922-amino acid NH_2 terminus containing multiple sites for protein-protein interactions as well as sites for p60^{src} -catalyzed tyrosine phosphorylation, which regulate enzyme

activity. Protein tyrosine phosphorylation status appears to play an important role in regulation of endothelial cell permeability, as demonstrated by the modest enhancement of barrier function with the nonspecific tyrosine kinase inhibitor genistein. More specifically, p60^{src}-induced tyrosine phosphorylation is critical for diperoxovanadate-induced endothelial cell barrier dysfunction through increased contraction and altered focal contacts. EC MLCK may provide the link between tyrosine phosphorylation events and permeability changes because tyrosine phosphorylation of endothelial cell MLCK evokes significant increases in MLCK activity, endothelial cell contraction, and subsequent endothelial cell barrier dysfunction while promoting the development of a contractile complex containing EC MLCK, actin, myosin, CaM, p60^{src}, and the actin-binding protein cortactin.

Recently, the critical importance of the small GTPase Rho in regulation of the contractile apparatus has been demonstrated in several models of agonist-induced endothelial cell barrier dysfunction. The Rho family of small GTPases is involved in signal transduction linking extracellular stimuli to dynamic actin cytoskeletal rearrangement, and activation of Rho specifically produces stress fiber formation in cultured cells. Through its downstream effector, Rho kinase, Rho activation leads

to phosphorylation of the myosin binding subunit of MLC phosphatase (PP1), thereby inhibiting its phosphatase activity and resulting in increased MLC phosphorylation, actomyosin interaction, stress fiber formation, and subsequent endothelial cell barrier dysfunction (Figure 22) [24]. Nevertheless, the relative contributions of the EC MLCK and Rho pathways in regulating endothelial cell permeability are not well understood: inhibition of either MLCK activity or Rho activation attenuates thrombin-induced endothelial cell barrier dysfunction. A recent report suggests that Rho/Rho kinase and MLCK may differentially regulate MLC phosphorylation according to spatial localization within cultured cells. Additional complexity in the system is provided by the contribution of the p21-activated kinase (PAK) family, downstream effectors of the small GTPases Rac and Cdc42. Isoforms PAK1 and PAK2 have both been shown to phosphorylate smooth muscle MLCK and decrease MLCK activity in cultured cells, but whether PAK regulates the high-molecular-mass MLCK present in endothelium in this fashion is not very clear. However, conversely, PAK2 can directly phosphorylate MLC to produce endothelial cell contraction. A complex interplay exists among these processes in regulating MLC phosphorylation status, cell tension, and subsequent endothelial cell permeability.

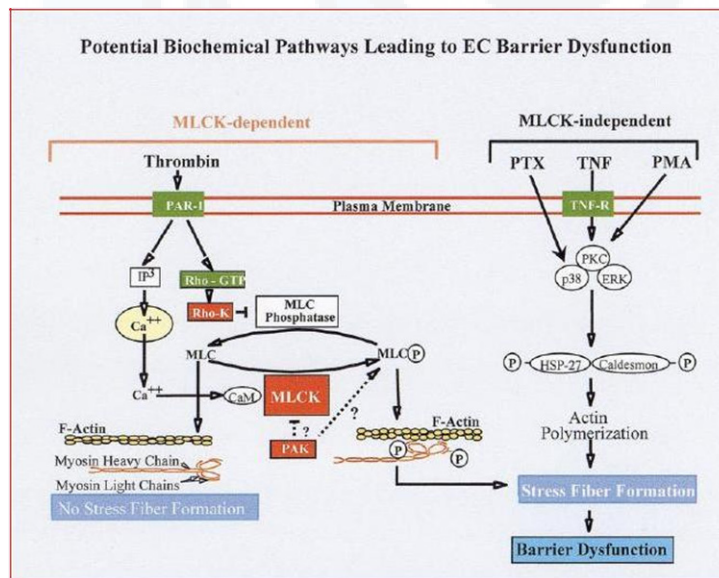


Figure 22: MLCK-dependent and MLCK-independent pathways are involved in endothelial cell [EC] barrier dysfunction. MLCK-dependent barrier disruption is represented by the thrombin model outlined at *left*. Thrombin binding to its receptor results in inositol trisphosphate (IP₃) production and a subsequent increase in intracellular Ca²⁺, which via Ca²⁺/CaM interaction activates MLCK to phosphorylate MLCs, leading to increased actomyosin interaction and subsequent contraction. Thrombin also increases MLC phosphorylation through Rho/Rho kinase pathway inhibition of MLC phosphatase activity. Examples of MLCK-independent barrier disruption are depicted at right. Pertussis toxin (PTX) activates p38 MAPK via an unknown mechanism, resulting in phosphorylation of HSP27, whose inhibitory effect on actin polymerization is thereby attenuated, allowing stress fiber formation to occur. Phorbol myristate acetate (PMA) induces a protein kinase C (PKC)-dependent increase in bovine pulmonary EC permeability without significantly increasing MLC phosphorylation, possibly through extracellular signal-regulated kinase (ERK)-catalyzed caldesmon phosphorylation and subsequent alteration of actomyosin cross bridging. Likewise, the cytokine TNF- α through its receptor (TNF-R) appears to mediate cytoskeletal rearrangement and eventual barrier dysfunction through a PKC-dependent pathway. Although TNF- α produces an increase in MLC phosphorylation, this effect does not appear to contribute to the subsequent increase in EC permeability [23].

Despite the clear contribution of MLCK/Rho kinase-driven increases in MLC phosphorylation to tension development and increased vascular permeability, MLCK-independent pathways are also involved in the regulation of cellular contraction (Figure 22). Protein kinase C (PKC)-mediated pathways exert a prominent effect on barrier regulation in a time- and species-specific manner. For example, phorbol myristate acetate induces a PKC-dependent increase in pulmonary endothelial cell permeability without significantly increasing MLC phosphorylation and without inducing formation of actin stress fibers, whereas PKC activation in umbilical vein endothelial cells does not have this barrier-disrupting effect. PKC-mediated increases in endothelial cell permeability may occur through phosphorylation of caldesmon, an actin-, myosin-, and CaM-binding protein present in smooth muscle actomyosin cross bridges as a 145-kDa protein and in endothelial cell as a 77-kDa protein. The phosphorylation of caldesmon is known to alter smooth muscle cross-bridge activity. Caldesmon distributes along stress fibers and is phosphorylated in endothelial cell after thrombin and phorbol myristate acetate challenge. Caldesmon-mediated regulation of actomyosin ATPase in smooth muscle is also modified by the actin cross-linking protein filamin and gelsolin. Although filamin participates directly in barrier regulation via CaM kinase II activation, its effects on actin cytoskeletal rearrangement are regulated through Rho family GTPases, thereby providing another link with a known modulator of endothelial cell barrier function. Tumor necrosis factor- α (TNF- α) slowly induces barrier disruption in cultured endothelial cell, which is independent of MLCK activity. As well as the p38 kinase activation has also been linked to contractile regulation in smooth muscle, endothelial cell migration and lipopolysaccharide-induced endothelial cell permeability. The mechanism through which p38 exerts these effects may involve the actin binding protein HSP27, a known p38 MAPK target whose actin polymerization-inhibiting activity dramatically decreases after phosphorylation in association with stress fiber development.

Adhesive protein-cytoskeleton linkages: Cell-cell and cell-matrix adhesions are essential for barrier maintenance and restoration and exist in dynamic equilibrium with endothelial cell contractile forces. Intercellular contacts along the endothelial monolayer consist primarily of two types of complexes, adherens junctions and tight junctions, which link to the actin cytoskeleton to provide both mechanical stability and transduction of extracellular signals into the cell. Adherens junctions are composed of cadherins bound together in a homotypic and Ca²⁺-dependent fashion to link adjacent endothelial cell. Cadherins interact through their cytoplasmic tail with the catenin family of intracellular proteins, which in turn provide anchorage to the actin cytoskeleton. The primary adhesive protein present in human endothelial adherens junctions, vascular endothelial (VE) cadherin, is critical to maintenance of endothelial cell barrier integrity as demonstrated by increased vascular permeability induced after infusion of VE-cadherin-blocking antibody. Similarly in cultured endothelial cell, VE-cadherin-

blocking antibody increased permeability and enhanced neutrophil trans-endothelial migration while producing reorganization of the actin cytoskeleton. The observation that VE-cadherin-blocking antibodies produce barrier disruption primarily in the alveolar capillary bed suggests that differential adherens junction functioning exists within segments of the pulmonary vasculature. The MAPK pathway may be involved in regulating adherens junction/VE-cadherin function because MAPK inhibitors attenuate vascular endothelial growth factor (VEGF)-mediated VE-cadherin rearrangement and subsequent endothelial cell monolayer permeability.

Tyrosine phosphorylation may provide an additional regulatory link between actin cytoskeletal rearrangement and adherens junction function. Pervanadate treatment of cultured cells resulted in tyrosine hyperphosphorylation of catenins, partial dissociation of the catenin-cadherin complex, and subsequent decreased cell-cell adhesion. Similarly, the anti-adhesive protein thrombospondin-1-induced tyrosine phosphorylation of adherens junction proteins, actin rearrangement, and increased albumin flux across endothelial cell monolayers, whereas tyrosine kinase inhibition attenuated these effects. Recent work suggests that, in addition to increasing contractile forces, thrombin also alters endothelial cell permeability through dissociation of the tyrosine phosphatase, SHP2, from VE-cadherin complexes to produce increased tyrosine phosphorylation of catenins and subsequent destabilization of adherens junction linkage to the cytoskeleton. However, a certain level of basal tyrosine phosphorylation is likely necessary for maintenance of cell-cell contacts since selective inhibition of specific tyrosine kinases can disrupt these attachments.

Anyhow, a critical function of the endothelial cell barrier is the regulation of neutrophil (PMN) margination and migration into sites of acute inflammation, a complex process involving cytokine/chemokine signaling and interaction of specific recognition molecules (e.g., platelet endothelial cell adhesion molecule-1) on PMNs and endothelial cells. As evidence for an integral role for the endothelial cell cytoskeleton and its connections in PMN diapedesis, disruption of either the endothelial cell actin cytoskeleton with cytochalasin B or stabilization of microtubules with paclitaxel decreases leukocyte trans-endothelial movement, whereas disassembly of microtubules increases PMN migration. The ability of activated PMNs to increase endothelial cell permeability suggests that cross-cellular signaling pathways are employed during the cytoskeletal rearrangements of PMN trans-endothelial migration. Binding of PMN to endothelial cell causes disruption of adherens junctions, as evidenced by the disappearance of VE cadherin and catenins from cell-cell contacts. Adherens junctions appear integral to this process because VE-cadherin-blocking antibodies increase PMN diapedesis, whereas conversely tight junctions remain intact during this migration. Tyrosine phosphorylation pathways also appear important because activated PMNs increase the phosphotyrosine content of

VE cadherin and β -catenin in association with adherens junctions disruption and hyperpermeability.

As mentioned above the tight junctions consist of transmembrane proteins such as occludin, the claudins, and junctional adhesion molecules coupled to cytoplasmic proteins, including the zona occludens [ZO] family. Tight junction-associated cytoskeletal proteins such as ZO-1 appear to participate in signal transduction and to provide a link between occludin and the actin cytoskeleton. The functional significance of confocal microscopy-observed colocalization of F actin and ZO-1 is supported by the finding that cytochalasin D inhibits cytokine-induced fragmentation of ZO-1 inter-endothelial staining. Alterations in tight junctions may be signaled through the MAPK pathway, as both VEGF and H_2O_2 -induced occludin dissociation from cell junctions and EC barrier dysfunction were partially blocked by MAPK inhibitors. In other way the focal adhesions comprise extracellular matrix (ECM) proteins (collagen, fibronectin, laminin, vitronectin, proteoglycans), transmembrane integrin receptors, and cytoplasmic focal adhesion plaques (containing α -actinin, vinculin, paxillin, and talin), which combine to provide additional adhesive forces in barrier regulation and form a critical bridge for bidirectional signal transduction between the actin cytoskeleton and the cell-matrix interface. ECM protein composition modulates basal endothelial cell permeability as well as TNF-induced barrier dysfunction, whereas antibodies to β_1 -integrin alter endothelial cell attachment, cell spreading, and permeability. Extracellular stimuli can be transmitted to the cytoskeleton through focal adhesion rearrangement linked to integrin ligation. Unliganded integrins are not associated with the cytoskeleton; however, ECM binding induces the attachment of integrins to intracellular actin fibers, a process in endothelial cell that stimulates tyrosine phosphorylation of multiple proteins [including paxillin, cortactin, and focal adhesion kinase (FAK)] as well as tyrosine phosphorylation-dependent Ca^{2+} influx. Integrin binding also targets activated extracellular signal-regulated kinase to newly formed focal adhesion sites. Reciprocally, intracellular signaling pathways that regulate cytoskeletal rearrangement can also modulate cell-matrix contacts. Rho inhibition dissociates stress fibers from focal adhesions, decreases phosphotyrosine content of paxillin and FAK, and enhances endothelial cell barrier function. Similarly, v-Src-induced tyrosine phosphorylation of focal adhesion proteins is a well-established stimulus for disassembly of these adhesive structures; however, some basal level of tyrosine phosphorylation appears necessary to maintain focal adhesions because selective tyrosine kinase inhibition will disrupt these contacts. In support of a barrier maintenance function for tyrosine phosphorylation of focal adhesions is a recent report describing the association of diperoxovanadate-induced transient endothelial cell barrier enhancement with phosphotyrosine incorporation into FAK [25].

Pulmonary vascular cytoskeletal and barrier regulation by mechanical forces: The study of endothelial cell in

static culture provides the opportunity to mechanistically evaluate the role of cytoskeletal components in physiological functions. However, it has been increasingly appreciated that this approach may have major limitations given that the pulmonary endothelium in its native state is continuously exposed to mechanical forces that greatly influence cellular structure and function. Shear stress activates signaling pathways (e.g., MAPK), leading to upregulation of transcription factors and subsequent gene expression of various vasoactive substances, growth factors, and adhesion molecules. Active cytoskeletal rearrangement begins rapidly and continues to occur over several hours as endothelial cells orient themselves to reduce both peak shear stresses and shear stress gradients. The cellular mechanisms for sensing flow and transducing its signal are still unclear, but recent reports suggest that both apical actin stress fibers linked to cell-cell contact sites and integrin-mediated signal transduction are involved.

However, when endothelial cell in static culture are exposed to shear stress, multiple signaling pathways implicated in cytoskeletal rearrangement are stimulated, including Ca^{2+} mobilization, G-protein activation, increased tyrosine phosphorylation, and MLCK and MAPK activation. These pathways interact downstream to produce the complex cellular effects of flow. For example, during shear stress, the GTPases Rho and Cdc42 combine to activate MAPKs; anyhow, individually, Rho is necessary for flow-induced stress fiber formation and cell alignment and Cdc42 activates transcription factors. The integrated effects of these shear-induced signals on endothelial cell barrier function are variable depending on the magnitude, duration, and gradient of flow. Shear stress maximally increases protein expression of integrins after 12 hours of exposure and significantly enhances cell-matrix attachment, suggesting that flow helps maintain the endothelial cell monolayer through augmentation of focal adhesions. However, endothelial cells exposed to high shear gradients, or turbulent flow, develop increased permeability relative to areas of either constant laminar flow or no flow. One mechanism by which shear stress may alter barrier function is by inhibition of endothelial cell apoptosis; however, the recent work using a TNF model under static conditions suggests distinct signaling and cytoskeletal involvement in cytokine-induced apoptosis and permeability [26].

Ventilator-induced lung injury is a highly morbid clinical entity believed to be caused by excessive mechanical stretch of pulmonary airways and vasculature, producing fluid flux across capillaries primarily through an active endothelial response. Similarly, the contribution of capillary rupture in this process has recently been confirmed. Intracellular Ca^{2+} and tyrosine phosphorylation-dependent pathways appear to mediate the response to cell stretch. In addition, reduction in endothelial tensile forces by MLCK inhibition significantly attenuates capillary leak illustrating the importance of the endothelial cell contractile apparatus in stretch-induced pulmonary edema. However, the mechanism by which mechanical signals are transduced

to the endothelial cell cytoskeleton may involve the complex array of proteins that constitute the endothelial cell glycocalyx. The glycocalyx is a meshwork of glycoproteins and glycolipids that combine to form a cell-surface layer of anionic polymers that is variable across the vasculature. The components of the glycocalyx have been implicated in cytoskeletal organization as syndecan, the primary heparin sulfate proteoglycan, and podocalyxin, the primary sialoprotein, modulating cell-cell and cell-matrix adhesion through their cytoplasmic domains. NMR techniques have demonstrated that cell-surface proteoglycans behave as viscoelastic anionic polymers, undergoing shear-dependent conformational changes, which may function as blood-flow sensors to transduce signals into the endothelial cell [23].

Protein kinase C modulates pulmonary endothelial permeability

In human studies and in experimental models of acute lung injury, pulmonary edema is induced by increases in microvascular hydrostatic pressure [Pmv] capillary filtration coefficient [Kfc] and by a decrease in protein reflection coefficient [σ]. During ARDS, the compromised pulmonary endothelium maintains, at least in part, a decrease in protein

selectivity (i.e., decrease in σ), an increase in transvascular fluid flux (i.e., increase in Kfc), and an altered metabolism of inflammatory mediators [e.g., angiotensin I, bradykinin, endothelin, prostacyclin, thromboxane A2, superoxide ($\bullet O_2^-$) and nitric oxide ($\bullet NO$)] (Figure 23). The increase in Pmv is caused by a decrease in the ratio of the pre-capillary to postcapillary resistance arising from the altered levels of a number of endothelium-dependent mediators that have been implicated in ARDS, such as angiotensin II, endothelin, thromboxane A2, prostacyclin, reactive nitrogen species [e.g., $\bullet NO$, peroxynitrite (ONOO⁻)], and reactive oxygen species [e.g., hydrogen peroxide (H_2O_2), $\bullet O_2^-$, hydroxyl radical ($\bullet OH$)]. The increase in Kfc and the decrease in σ are due, in part, to the response to inflammatory mediators such as $\bullet NO$, H_2O_2 , thrombin and tumor necrosis factor (TNF)- α . Isolated lung studies indicate that the increase in Kfc is primarily due to an increase in permeability to water, in addition to heterogeneous increases in surface area. In lung injury that progresses toward alveolar flooding, the extra-alveolar and alveolar epithelium also exhibits a decrease in barrier function and an increased generation of inflammatory mediators [e.g., inducible nitric oxide synthase (iNOS) $\rightarrow \bullet NO$].

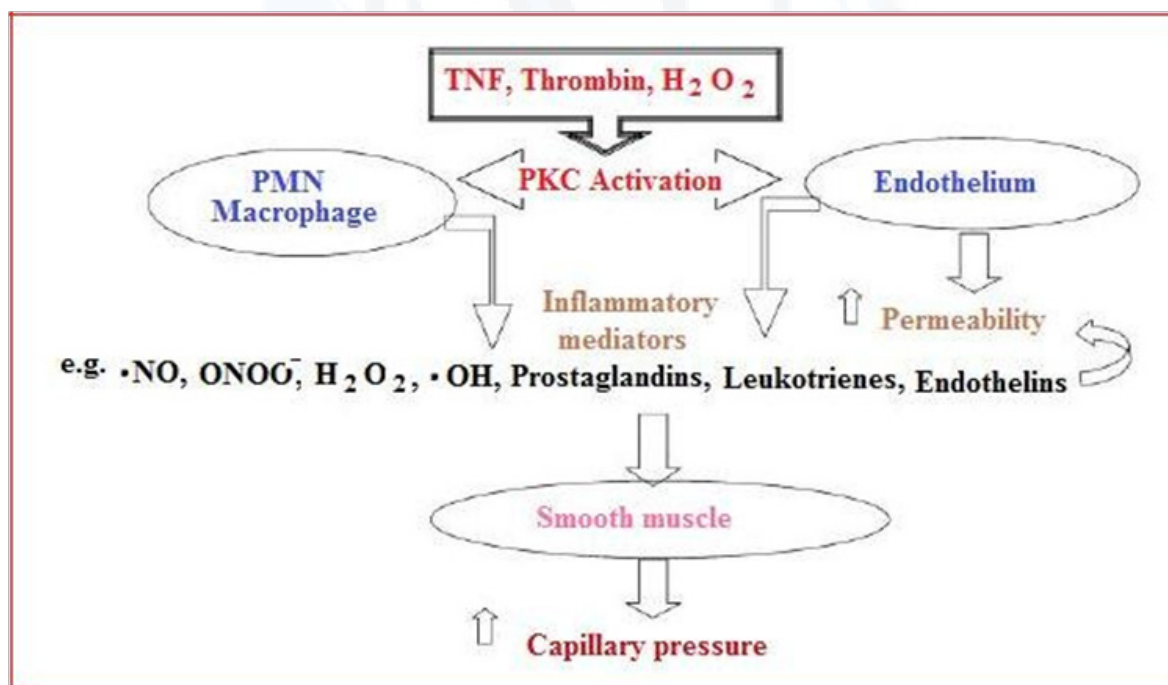


Figure 23: The cell types and mediators involved in the protein kinase C (PKC) paradigm of lung injury. PMN, neutrophils; NO, nitric oxide; ONOO⁻, peroxynitrite; OH, hydroxyl radical [27].

The basics of protein kinase C [PKC]: PKC is a family of serine/threonine kinases characterized by at least eleven different isotypes. PKC isotypes are differentially regulated by calcium (Ca^{2+}), diacylglycerol, and phospholipids and differ in structure, expression, intracellular localization, substrate utilization, and mechanisms of activation. PKC is

composed of four conserved (C1-C4) and five variable (V1-V5) domains (Figure 23). C1 and C2 constitute the regulatory domain and contain binding sites for phospholipids (e.g., phosphatidylserine), Ca^{2+} , diacylglycerol, and phorbol esters. The C3 and C4 regions contain the catalytic domain that has binding sites for ATP and different PKC substrates.

The conserved region of the regulatory domain, within residues 19-36, has structural features of a pseudosubstrate; therefore, it maintains PKC in the inactive form during the absence of phospholipid activators. The activation of PKC begins with the release of membrane phospholipids in response to phospholipase activity [e.g., phospholipase C (PLC)]. The phospholipids interact with the C1 and C2 domains, which provides the free energy required for the dissociation of the NH₂-terminal pseudosubstrate from the active site, which allows substrate binding. The C1 and C2 domains each have their own determinants for membrane recognition, and the C1 domain is present in most PKC isoforms. PKC isoforms are involved in signal transduction pathways that govern a wide range of physiological processes, such as differentiation, proliferation, gene expression, brain function, membrane transport, and the organization of cytoskeletal and extracellular matrix proteins. The PKC isoforms are subdivided into three groups: the classical, novel, and atypical. This subdivision is based on the structural and functional differences in the conserved domains C1-C4 (Figure 24). The classical PKC- α , PKC- β 1/2, and PKC- γ isoforms are Ca²⁺ and diacylglycerol

dependent. These PKC isoforms have the conserved diacylglycerol-binding C1 domain and the Ca²⁺-binding C2 domain. The C1 domains consist of a tandem C1A and C1B arrangement that can bind the endogenous diacylglycerol and exogenous phorbol esters. The novel PKC- ϵ , PKC- δ , PKC- η , PKC- θ and PKC- μ isoforms contain C2 domains that lack Ca²⁺-binding ability but still retain functional C1A and C1B domains that can bind the endogenous diacylglycerol and exogenous phorbol esters (Figure 24). The atypical PKC- τ , PKC- λ and PKC- ζ isoforms lack a functional C2 domain and contain a single C1 domain that lacks the ability to bind diacylglycerol and phorbol esters. Therefore, the mechanism of activation of the atypical PKC isoforms is both Ca²⁺ and diacylglycerol independent and involves other lipid-dependent pathways. Thus for example the phorbol ester 2-O-tetradecanoylphorbol-3-acetate or the lipid diacylglycerol would activate the classical and novel PKC isoforms but not the atypical PKC isoforms. The activation of the novel PKC isoforms will persist in the presence of EDTA, but the classic PKC isoforms would not exhibit activity.

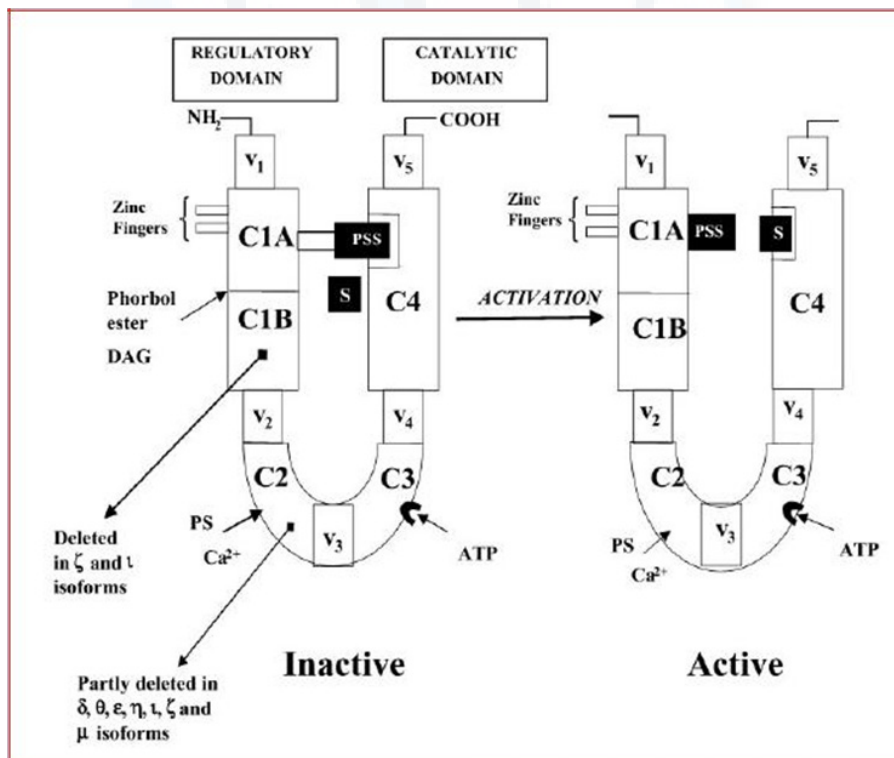


Figure 24: A molecular model for PKC isoforms and PKC activation. C1–C4: Conserved Domains; V1–V5: Variable Domains; DAG: Diacylglycerol; PSS: NH₂-Terminal Pseudosubstrate; PS: Permeability-Surface Area Product; S: Substrate [27].

In addition to the classic activation mechanisms indicated above, other PKC activation mechanisms have been proposed. It had been shown that PKC- α activation is also dependent on lack of a C1-C2 domain interaction, corresponding to a transition of PKC- α from a closed

inactive state to an open active state (Figure 24). It had been also showed that PKC- α isoform bound specifically and with high affinity to an α C1A-C1B fusion protein of PKC- α . The α C1A-C1B domain activated the isozyme in a phorbol ester- and diacylglycerol-dependent manner

comparable with activation resulting from membrane-phosphatidylserine association. Interestingly, the α C1A-C1B domain also activated the classical PKC- β 1/2, and PKC- γ isoforms, but not the novel PKC- δ or PKC- ϵ isoforms that were each activated by their own C1 domains. PKC- α , PKC- β 1/2, and PKC- γ isoforms were unaffected by the C1 domain of the PKC- δ isoform and only slightly activated by that of PKC- ϵ isoforms. Thus the activation mechanism of the novel PKC isoforms may be similar to that of the classic isoforms. PKC- ζ isoform activity was unaffected by its own C1 domain and those of the other PKC isoforms. Another key determinant of PKC activity is the phosphorylation of the PKC molecule, its intracellular localization, and proteolytic degradation. Phosphorylation is controlled by PKC-mediated autophosphorylation and the phosphorylation mediated by other kinases such as 3-phosphoinositide-dependent kinase-1 and tyrosine kinases.

The distribution of PKC activity is regulated by its direct interaction with accessory proteins (e.g., receptor for activated C protein) that target the movement of the PKC molecule to different intracellular compartments, which confers selectivity by associating individual isoforms with specific substrates. PKC activity is also determined by its degradation. The literature indicates that the calcium-lipid-dependent protease calpain- μ can degrade PKC to a catalytically active PKM by cleaving off the regulatory domain. PKM may be a constitutively active enzyme that mediates long-term phosphorylation activity of PKC. Yet the regulation of PKC activity is maintained because of further degradation into inactive degradation products by calpain-m.

PKC in lung injury: PKC is implicated in many cellular responses associated with lung injury, including endothelial permeability, cell contraction, migration, proliferation, apoptosis, mucous secretion, gene expression and the organization of cytoskeletal and extracellular matrix proteins. Throughout the last five decades, investigation into the pathogenesis of the increased endothelial permeability associated with ARDS has indicated a role for many mediators, such as cytokines (e.g., IL-1, TNF- α), growth factors [e.g. vascular endothelial growth factor (VEGF)], peptides (substance P, bradykinin), proteases (e.g., elastase), complement activation (e.g., C5a), intravascular coagulation (e.g., thrombin), reactive oxygen and nitrogen species (e.g., H_2O_2 , $\cdot\text{OH}$, $-\text{O}_2$, $\cdot\text{NO}$, ONOO) and lung sequestration of neutrophils (Figure 22). The intracellular signal pathways that cause an increase in endothelial permeability are still not completely defined despite extensive study of the effect of the above mediators of endothelial dysfunction. Importantly, however, PKC is now known to be a necessary part in the regulation of endothelial permeability and edema formation induced by three known mediators of ARDS: H_2O_2 , thrombin, and TNF- α [27].

Regulation of Alveolar Epithelial Function by Hypoxia

The alveolar epithelium contributes to the maintenance of surface tension, basic host defense properties, gas exchange and edema clearance. It is normally well oxygenated since oxygen is exchanged across the alveolocapillary membrane. However, under a number of conditions, the alveolar epithelium is exposed to low oxygen levels (hypoxia). For example, during ascent to high altitude, the partial pressure of oxygen drops due to the decline in barometric pressure, which can contribute to high-altitude pulmonary edema (HAPE). In turn, HAPE exaggerates alveolar hypoxia as a consequence of alveolar flooding. In addition, patients with acute respiratory distress syndrome or congestive heart failure develop pulmonary edema, resulting in impaired oxygen transfer from the airspaces into the pulmonary circulation. Patients who cannot clear edema efficiently have worse outcomes, suggesting that hypoxia plays a deleterious role in alveolar epithelial function.

Cellular adaptation to hypoxia

During hypoxia, cells respond to this stress through adaptive mechanisms. One response is to increase the level of expression of genes responsible for angiogenesis, in order to provide more efficient blood flow, and of genes involved in glycolytic pathways. This regulation of gene expression during hypoxia is carried out by turning on the master transcription factor, hypoxia-inducible factor (HIF), a dimer consisting of the subunits HIF- α and HIF- β . HIF- α is a short-lived protein, whereas HIF- β is constitutively expressed. Under normoxic conditions, oxygen- and iron-dependent prolyl hydroxylase hydroxylates HIF at prolines 402 and 564, two highly conserved amino acids within the oxygen-dependent degradation domain of HIF- α . In turn, von Hippel-Lindau protein (pVHL) recognizes and binds to the prolyl-hydroxylation sites, targeting HIF- α for ubiquitination [*a class of enzymes that catalyzes the ATP-dependent formation of a thioester bond between itself and ubiquitin*] and eventual degradation in the proteasome. Under hypoxic conditions, prolyl hydroxylase activity is inhibited; therefore, HIF- α is stabilized, since it is neither hydroxylated nor degraded in the proteasome. After stabilization, HIF trans-locates into the nucleus and activates downstream genes, such as vascular endothelial growth factor, erythropoietin, glucose transporter 1 and enzymes involved in the glycolytic cascade, to improve delivery of oxygen and glucose to cells. Cells can also adapt to hypoxia by maintaining ATP homeostasis. During hypoxia, insufficient oxygen limits ATP production through mitochondrial oxidative phosphorylation, and thus cellular ATP levels decrease. In order to maintain ATP homeostasis, cells can either increase ATP production via anaerobic glycolysis or decrease ATP demands via inhibition of ATP-consuming enzymes, such as Na, KATPase and the protein

synthesis machinery. Na, K-ATPase activity may account for ~ 40% of ATP consumption in cells, dependant upon cell type. It has been reported that hypoxia decreases ATP demand by reducing the amount of plasma membrane Na,K-ATPase.

Effects of hypoxia on alveolar fluid resorption

Hypoxia has been shown to impair alveolar fluid clearance by inhibiting transepithelial active Na⁺ transport (Figure 2). It has been demonstrated that exposure to hypoxia results in:

- A significant decrease in alveolar fluid resorption, which is associated with a decrease in ENaC, as well as Na, K-ATPase, activity.
- In cultured alveolar epithelial cells, hypoxia-mediated down-regulation of Na, K-ATPase is time and oxygen concentration-dependent.
- Short-term exposure to hypoxia decreases Na, K-ATPase activity and its protein abundance at the plasma membrane without significant changes in its total amount, suggesting that endocytosis of Na, K-ATPase occurs during hypoxia.

The endocytosis of Na, K-ATPase during hypoxia appears to be mediated by mitochondrial reactive oxygen species (ROS), since ROS scavengers prevented the hypoxia-

induced down-regulation of Na, K-ATPase. Moreover, treatment with hydrogen peroxide is sufficient to cause both Na, K-ATPase endocytosis from plasma membrane and a decrease in Na, K-ATPase activity. The source of ROS in this process was further assessed in mitochondrial-DNA-depleted (p⁰) A549 cells. These cells lack a competent electron transport chain and are thus incapable of generating ROS during hypoxia. In p⁰ A549 cells, hypoxia failed to induce Na, K-ATPase endocytosis and decrease Na, K-ATPase activity. Furthermore, an exposure to hypoxia, over expression of manganese superoxide dismutase inhibited mitochondrial ROS production and blocked the decrease in Na,K-ATPase abundance and alveolar fluid resorption. Together, these studies suggest a role for mitochondrial ROS in the hypoxia-mediated endocytosis of Na, K-ATPase. Nevertheless, during hypoxia, mitochondrial ROS activate protein kinase C ζ leading to Na, K-ATPase α 1-subunit phosphorylation at serine18. In addition, plasma membrane Na, K-ATPase was ubiquitinated; however, mutation of the four lysines surrounding serine 18 to arginine prevented Na, K-ATPase ubiquitination, implying that these are the ubiquitination sites. Mutation of serine 18 to alanine prevented ubiquitination and endocytosis of the Na, K-ATPase α 1-subunit, suggesting that serine 18 phosphorylation is a prerequisite for these processes (Figure 25).

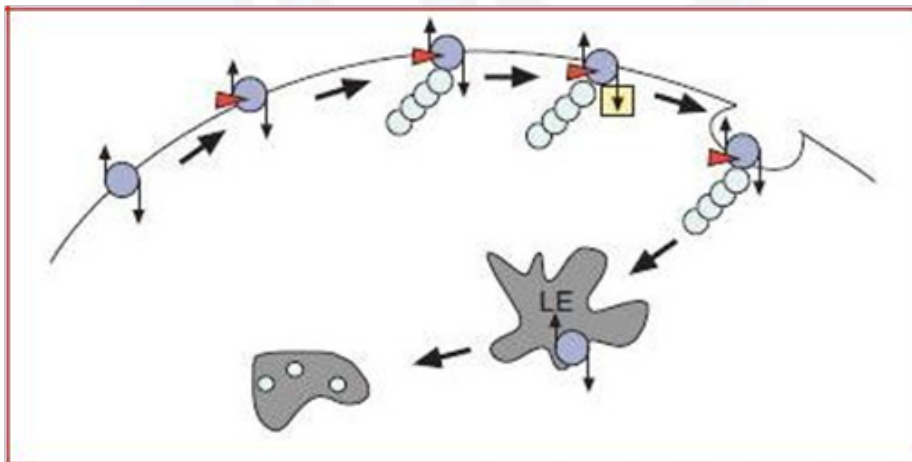


Figure 25: Hypoxia induces endocytosis and degradation of plasma membrane sodium–potassium adenosine triphosphatase (Na, K-ATPase; in purple). In alveolar epithelial cells exposed to hypoxia, generation of mitochondrial reactive oxygen species activates protein kinase C ζ , which phosphorylates (in red) plasma membrane Na,K-ATPase, leading to its ubiquitination (in light blue). This series of events triggers Na, K-ATPase endocytosis via clathrin (in yellow)-coated vesicles. Na, K-ATPase-containing endosomal vesicles merge to form the late endosome (LE) and Na, K-ATPase is degraded [4].

Endocytosis of Na, K-ATPase has been reported to be clathrin-dependent. In alveolar epithelial cells, hypoxia-induced endocytosis of Na, K-ATPase requires the binding of adaptor protein 2 to the tyrosine-based motif (tyrosine 537) located in the Na, K-ATPase α 1-subunit, leading to the incorporation of Na, K-ATPase into clathrin vesicles. Trafficking of clathrin vesicles requires the actin cytoskeleton in mammalian cells. Activation of Rho GTPase

leads to rearrangement of the actin cytoskeleton, thus regulating trafficking of clathrin vesicles. Rho GTPases can activate two types of actin nucleators that directly stimulate actin polymerization and also regulate cofilin to affect actin reorganization via Rho-associated protein kinase (ROCK)/p21-activated kinase/LIM domain kinase signaling. More recently, it has been suggested that hypoxia-mediated endocytosis of Na, K-ATPase is dependent upon the

activation of RhoA/ROCK signaling and actin stress fiber formation. During hypoxia, mitochondrial ROS activate the small GTPase RhoA, leading to the formation of actin stress fibers in alveolar epithelial cells, and dominant negative RhoA and ROCK inhibitor prevent the hypoxia-mediated Na, K-ATPase endocytosis.

Anyhow, the prolonged hypoxia may lead to the mitochondrial ROS-dependent degradation of plasma membrane Na, K-ATPase, and both the proteasome and the lysosome are involved in this process. Since the ubiquitination of plasma membrane Na, K-ATPase is required for its endocytosis, it is likely that Na, K-ATPase ubiquitination acts as a signal for its endocytosis, stimulating its merger with the proteasome and/or the lysosome for degradation. In contrast, hypoxia did not alter the half-life of total pool Na, K-ATPase, suggesting that degradation of total pool Na, K-ATPase is not affected by hypoxia. Recent studies reported that loss of pVHL prevented hypoxia-mediated degradation of plasma membrane Na, K-ATPase. Although this process required the pVHL E3 ligase activity, HIF stabilization was not required, indicating a role for pVHL in hypoxia-mediated Na, K-ATPase degradation independent of HIF. These studies suggested that pVHL may play a dual function during hypoxia:

- a) Hypoxia inhibits pVHL-HIF interaction, resulting in stabilization of HIF and upregulation of HIF-responsive genes for glycolytic ATP production and better oxygen delivery.
- b) pVHL facilitates plasma membrane Na, K-ATPase degradation to decrease ATP demands through an HIF-independent mechanism.

Taken together, these data suggest that hypoxia increases mitochondrial ROS generation and induces endocytosis and degradation of plasma membrane Na, K-ATPase, resulting in the inhibition of Na, K-ATPase activity and impaired alveolar fluid clearance.

Effects of hypoxia on keratin intermediate filaments

Keratin intermediate filaments (IFs) are the major cytoskeletal component of epithelial cells and play a crucial role in maintaining the structural integrity of cells. Although it was originally thought that the IF is a static structure, accumulating data suggest that keratin IFs can undergo rapid deformation/displacement in epithelial cells in response to stress, suggesting that the IF cytoskeleton transmits mechanical signals from the cell surface to all regions of the cytoplasm. Keratin IFs are assembled as heteropolymers of type I and type II IF proteins. Keratins consist of a conserved central α -helical domain, a non- α -helical N-terminal head and a C-terminal tail domain containing all of the known phosphorylation sites. Lung alveolar epithelial cells primarily express keratins K8 and K18 in equal amounts. Phosphorylation of K8 and K18 promotes their depolymerisation and redistribution.

Exposure to hypoxia caused a time-dependent disassembly of K8 and K18, which was associated with an increase in phosphorylation of K8. In alveolar epithelial cells, the hyperphosphorylation and disassembly of keratin during hypoxia was mediated by mitochondrial ROS, which activate PKC and phosphorylate keratin, leading to disassembly of the keratin IF network. An exposure to hypoxia, was lead to a significant decrease in keratin in alveolar epithelial cells compared to normoxic state, due to degradation of keratin IFs. Keratin was degraded in alveolar epithelial cells exposed to hydrogen peroxide, suggesting that ROS are necessary for the degradation of keratin. The proteasome inhibitor MG132 (carbobenzoxy-L-leucyl-L-leucyl-L-leucinal) prevented the degradation of keratin IFs in alveolar epithelial cells exposed to hypoxia, suggesting that keratin degradation was mediated via the ubiquitin/proteasome pathway. These data suggest that keratin IF dynamics may play a role in adaptation to hypoxia in alveolar epithelial cells.

Potential therapies for epithelial function improvement during hypoxia

Since down-regulation of Na, K-ATPase contributes to alveolar epithelial dysfunction, its upregulation may improve epithelial function during hypoxia or other pathological conditions. Indeed, over expression of the Na, K-ATPase β 1-subunit via viral and non-viral gene transfer resulted in an increase in alveolar fluid resorption in normal and injured lungs. These studies suggest a potential therapeutic application of Na, K-ATPase gene transfer in the improvement of epithelial function and lung edema clearance. In addition, an administration of catecholamines, such as dopamine, terbutaline and isoproterenol, has been shown to be effective in increasing Na, K-ATPase activity and alveolar fluid resorption. Parallel to this, treatment with dopamine and isoproterenol was associated with increases in Na, K-ATPase protein abundance at the cell basolateral membrane. This increase in protein abundance was mediated by exocytosis of Na, K-ATPase from endosomal compartments into the basolateral membrane. More importantly, the impaired alveolar function of injured lungs can be reversed by administration of dopamine, terbutaline and isoproterenol in lungs with hypoxia, hyperoxia, increased left atrial pressure or ventilation-induced lung injury. The data from these studies led to the development of a clinical trial, in which patients receiving salbutamol, a β -adrenergic agonist, showed a significant reduction in extravascular lung water. Moreover, inhalation of salmeterol has been shown to prevent HAPE in susceptible subjects. These findings support the hypothesis that β -adrenergic agonists accelerate the resolution of alveolar edema and may improve survival [28].

Pulmonary Injury, Oxidant Stress, and Gap Junctional Communication

Gap junctions and lung injury

ALI/ARDS can develop in response to stresses as diverse

as sepsis, trauma, gastric aspiration, and pneumonia. Hallmarks of ARDS include increased oxidant stress, lung inflammation, surfactant dysfunction, and disruption of the alveolar and endothelial barriers. Because optimal lung function requires functional cell-cell contacts, even partial disruption of an epithelial monolayer can be a significant contributor to the severity of ARDS. Significantly, >85% of patients with ARDS have at least a partial defect in lung-fluid clearance, which contributes to a high degree of patient morbidity and mortality. Compromised barrier function is a particular concern, because patients with impaired lung fluid balance are 3 times more likely to die of ARDS than are patients with a maximal ability to clear lung fluid. Alveolar flooding directly compromises gas exchange; unfortunately, the requirement for mechanical ventilation to improve tissue oxygenation causes direct alveolar cell injury, which further exacerbates lung function.

Cross talk between connexins and tight junctions: It is documented that the lung barrier function is commonly controlled by tight junctions. Although gap junctions are not a direct structural component of tight junctions, they are frequently seen adjacent to tight-junction strands with freeze-fracture electron microscopy. However, connexins do not necessarily colocalize with tight junctions, and the gap junction content of some tight junctions is low. Functionally, treatment of lung endothelial cell line with the gap junction inhibitors glycyrrhetic acid or oleamide decreased barrier function by ~50 - 75% as compared with controls, based on trans-endothelial resistance and small-molecule flux measurements. Cx40 and Cx43 (vide supra) are biochemically associated with several tight-junction proteins, including occludin, claudin-5, and ZO-1, based on co-immunoprecipitation analysis. Because lung endothelial cells are claudin deficient, experiments were done with cells in which claudin expression was reconstituted. Nonetheless, results with the lung endothelial cells were consistent with primary brain endothelium, expressing endogenous claudins. As an example from epithelia, expression of transfected Cx32 induced a ~25% increase in the barrier function of immortalized hepatocytes. In this system, Cx32 expression enhanced localization of ZO-1 and JAM-A to the plasma membrane, suggesting an increase in tight-junction formation. Interestingly, Cx26-transfected hepatocytes show a reduction in the ability of ouabain to decrease barrier function; however, Cx26 had no effect on baseline transepithelial resistance (TER). This underscores the notion of different connexins having specific roles for regulating tight junctions.

This specificity is due in part to differences in the ability of connexins to interact with different junction scaffold proteins. Because Cx40 and Cx43 interact with ZO-1, a protein that also directly interacts with claudins and occludin, any role for Cx40 or Cx43 in regulating tight junctions is likely to involve ZO-1, either as a cross-linking scaffold protein, via ZO-1 recruitment to cell junctions or via an effect on the distribution of the ZO-1 pool between gap and tight junctions. In contrast, whereas Cx32 can also co-immunoprecipitate with tight-junction proteins, it does not directly bind to ZO-1.

Instead, interactions between Cx32 and tight junctions may be mediated by another scaffold protein, such as discs large homologue 1 (Dlgh1), which directly interacts with Cx32. As another distinct mode of interaction, Cx26 binds directly to the hydrophilic surface of the coiled-coil C-terminal domain of occludin, which does not interact with Cx32.

What role can gap junctions have in regulating other classes of cell junctions? One possibility is that gap junctions transmit intercellular signals to coordinate junction assembly. A related possibility is that gap junctions serve to balance the concentration of metabolites between cells (such as calcium or GTP), so that junction-regulatory proteins are exposed to comparable microenvironments. Alternatively, connexins may structurally regulate junctions through a direct interaction with other tight-junction proteins. Given the heterogeneity of gap junction and tight junction protein expression and assembly really need further work.

Connexins in lung injury: Connexin expression in the lung changes during the injury response. In the injured lung, type II cell hyperplasia increases the frequency of type II cells in direct contact with other type II cells, both of which express Cx32. Because type I-type II cell communication is mediated through Cx43-compatible connexins and is not mediated by Cx32, this has the potential to provide type II cells with an independent pathway for communication that does not involve type I cells and may be used to regulate the injury response. During the acute phase of lung injury, connexin expression in the alveolus is altered, where Cx43 and Cx46 expression is elevated. Conversely, Cx40 expression at the whole-lung level decreases during the acute phase of injury (Rignault 2007). Some Cx46-expressing alveolar epithelial cells do not express typical type II cell markers and thus may represent a distinct subtype of cells proliferating in response to injury. Cx46 has relatively limited permeability, as compared with Cx32 and Cx43, suggesting a possible role for Cx46 in limiting metabolic depletion or intercellular transmission of toxic agents. Interestingly, lung fibroblasts isolated from patients with idiopathic pulmonary fibrosis have decreased Cx43 expression and function. The downstream effects of impaired fibroblast communication and whether epithelial Cx43 expression is decreased in late stages of fibrotic lung disease are not yet known.

Oxidant stress and signaling in the alcoholic lung

Although alcohol abuse is classically associated with liver disease, recent evidence has confirmed that chronic alcohol abuse is also a major risk factor contributing to the severity of ARDS. In a study of ICU patients, it was found that after adjusting for smoking and hepatic dysfunction, patients with a history of alcohol abuse were more than twice as susceptible to ARDS than were nonalcoholic patients. In large part, the increased susceptibility to ARDS caused by prolonged ethanol ingestion is due to a fundamental defect in lung-barrier function as a result of impaired tight-junction formation between type I alveolar epithelial cells. As described earlier, decreased barrier function (e.g. a leaky lung) contributes to the severity of ARDS.

It had been found that the dietary ethanol causes oxidant stress in the lung. The lung is particularly sensitive to oxidant stress, which is minimized by the antioxidant glutathione in the alveolar airspaces. Thus, one source of oxidant stress is from ethanol metabolism to acetaldehyde, which directly depletes the reduced glutathione pool (Figure 26). The prominent role for oxidant stress and reactive oxygen species (ROS) in alcoholic lung suggests that antioxidant therapy could be a useful therapeutic approach. In animal models of alcohol ingestion, a diet enriched in the glutathione precursor procystine prevents the alcoholic lung phenotype. However, complete reversal of the alcoholic lung phenotype requires several weeks of treatment and is not a suitable approach for an immediate treatment regimen for alcoholic lung. However, different studies have demonstrated that ethanol treatment of cells in vitro inhibits gap junctional communication. The ability of ethanol to inhibit gap junctions could be due to direct partitioning into cell membranes, analogous to the inhibitory effect of long-chain alcohols on connexins. Ethanol-induced depletion of the glutathione pool and increased oxidant stress can also inhibit gap junctional communication. The effect of ethanol on connexin expression is more variable, where ethanol was shown to inhibit Cx43 expression, but had little effect on Cx26 or Cx32.

Hormone signaling in alcoholic lung: In addition to its metabolic effects on the antioxidant glutathione pool, ethanol also induces cell-signaling pathways that contribute to oxidant stress. In particular, ethanol stimulates angiotensin II activity which, in turn, upregulates NADPH oxidase (Nox). Interestingly, angiotensin II has also been shown to upregulate cardiovascular and epithelial Cx43 expression and function and can antagonize the effect of ethanol on gap junctional communication. In contrast, Cx40 appears to be less affected by angiotensin II. Given the role for endothelial Cx43 in inflammation, this is consistent with the notion that angiotensin II is proinflammatory as well. Clearly, inflammation and the concomitant infiltration of neutrophils and activation of alveolar macrophages contribute to oxidant stress in response to acute lung injury. The intense oxidant load on alcoholic lung provides a condition in which the alveolar epithelium is prone to injury and apoptosis. As a response to oxidant stress, alveolar epithelial cells increase expression and secretion of TGF- β , the majority of which is the TGF- β 1 isoform. In the otherwise healthy alcoholic lung, most of this TGF- β is inactive; however, a significant increase in active TGF- β is also found as compared with normal lung. This has influences on alveolar epithelial function by promoting the cells to undergo an epithelium-to-mesenchyme transition (EMT) and is consistent with models in which TGF- β influences the acute phase of lung injury as well as the chronic phase. Further, the large latent pool of TGF- β induced by prolonged ethanol ingestion plays an important role in exacerbating the influence of other insults on the lung. In essence, the alcoholic lung is primed to have an exaggerated response to the effects of subsequent insults that promote TGF- β activation (Figure 26).

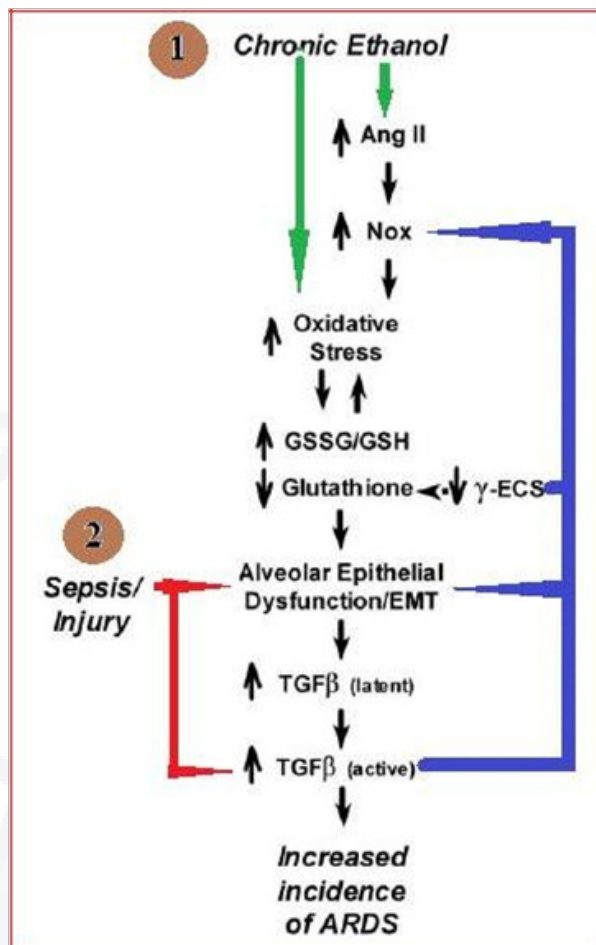


Figure 26: Oxidant and hormone stress responses in the alcoholic lung. Prolonged ethanol ingestion initiates and exacerbates oxidant stress via several pathways. Here is depicted a two-hit model for the role of alcoholic in ARDS. (1) Prolonged alcohol abuse causes direct oxidant stress because of the metabolism of ethanol to acetaldehyde. Ethanol also induces angiotensin II, which stimulates both the endothelium and epithelium to upregulate Nox activity. Oxidant stress depletes the alveolar epithelial glutathione pool, which induces cell damage and stimulates the cells to undergo an epithelial-to-mesenchyme transition (EMT) as a compensatory mechanism. Alveolar epithelial cells undergoing EMT increase production and secretion of TGF- β and have impaired alveolar barrier function, which adds further stress to the lung. (2) A second hit, such as direct trauma, infection, or sepsis, has an exaggerated effect on the alcoholic lung because of impaired alveolar epithelial function and the presence of a large pool of latent TGF- β , which is readily activated and exaggerates the normal injury response. Note the feedback loops in the diagram (blue lines), indicating the potential for “runaway” activation of a deleterious injury response [6].

TGF- β can also increase oxidant stress by decreasing γ -glutamylcysteine synthetase expression, thus reducing the antioxidant glutathione reserves of the lung. TGF- β also increases ROS production by increasing Nox expression and H_2O_2 production. In addition to ROS, reactive nitrogen species, including peroxynitrite, are generated during acute

lung injury, which can inhibit gap junctional communication. Increased oxidant stress has the added potential to exacerbate alveolar injury and TGF- β expression by creating a positive-feedback loop, particularly if TGF- β expression and activation are driven by a second insult, such as sepsis or direct trauma. TGF- β can directly influence gap junctional communication; however, this effect varies depending on cell type. Studies have demonstrated that TGF- β 1 increases, decreases or has no effect on gap junctional communication. TGF- β 1 has also been found to simultaneously upregulate Cx43 and suppresses Cx37 expression by endothelial cells, suggesting that differential regulation of connexins by TGF- β can provide a mechanism to alter intercellular communication.

Relevant to the lung injury response, investigators were examined the effect of TGF- β on gap junctional communication between type I alveolar epithelial cells (Figure 27). Primarily alveolar epithelial cells were isolated and cultured for 6 days to generate a model type I cell monolayer. The cells were then treated for 16 hours with varying amounts of activated TGF- β 1, and the level of intercellular communication was assessed by microinjecting calcein into individual cells and measuring the extent of dye transfer 5 minutes after microinjection. Consistent with previous reports, control cells were highly coupled and transferred calcein to nearly 20 cells through gap junctions [29]. Treatment with increasing levels of TGF- β inhibited gap junctional communication by ~50%. Thus, alveolar epithelial cells decreased intercellular communication in response to TGF- β . This suggests that if a similar phenomenon occurs in situ, then one effect of TGF- β would be to dampen the intercellular communication required to regulate surfactant secretion and thus potentially further to promote acute lung injury.

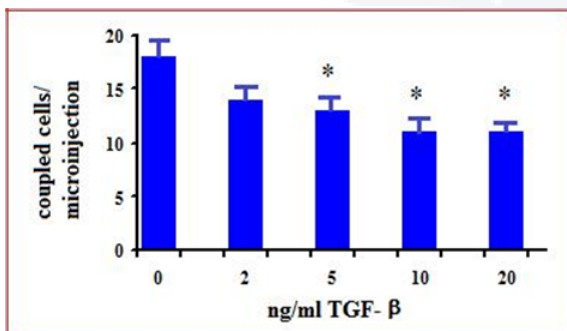


Figure 27: TGF- β 1 inhibits gap junctional communication between alveolar epithelial cells. Primarily type II cells were isolated and cultured for 6 days in minimal essential medium to produce a model type I cell monolayer. The cells were then treated with varying amounts of TGF- β 1 for 16 h; then the extent of gap junctional communication was determined by visualizing the intercellular transfer of calcein microinjected into individual cells with fluorescence microscopy. Dye transfer was quantified by counting the number of calcein-labeled cells per microinjection. Data were combined from two independent experiments counting ≥ 20 microinjections/treatment. Increasing concentrations of TGF- β 1 significantly decreased intercellular communication, as determined by t test (* $p < 0.05$) [6].

Role of pulmonary surfactant in acute lung injury

The alveolus acts as a coordinated system to regulate pulmonary surfactant secretion. Pulmonary surfactant is a mixture of lipids and proteins synthesized by type II cells, which lines the alveolar airspace to reduce surface tension at the air/liquid interface. The majority of surfactant lipid is phosphatidylcholine (PC), with phosphatidylglycerol (PG) and phosphatidylethanolamine (PE) as the other major phospholipids present. It was found that the most mammalian surfactant lipid is saturated [e.g. dipalmitoylphosphatidylcholine (DPPC)], which can form a barrier to inhaled oxidants, such as ozone. Conversely, unsaturated lipids present in surfactant are reactive and can act as an antioxidant sink. Extensive lipid oxidation, including damage to cell-membrane lipids is deleterious. Oxidant damage to type II cells alters their ability to synthesize surfactant lipids, which further compromises the surface activity. Consistent with this, overexpression of the antioxidant enzyme peroxiredoxin 6 is protective, because it can reduce phospholipid hydroperoxides in a glutathione-dependent reaction. Pulmonary surfactant also contains significant catalase and superoxide dismutase activity, which contributes to its ability to quench oxidant stress. In addition, surfactant lipids can have a direct role to help attenuate oxidant stress associated with inflammation by inserting into neutrophil membranes, which, in turn, inhibits Nox activity [30].

However, the other major components of pulmonary surfactant are four surfactant proteins, SP-A, SP-B, SP-C, and SP-D. SP-B and SP-C are hydrophobic and directly contribute to the biophysical properties of surfactant. By contrast, SP-A and SP-D are members of the collection protein family and are largely hydrophilic. Although these proteins can bind to surfactant lipids and help organize them into higher-level structures, such as tubular myelin, they are largely dispensable from the standpoint of surfactant biophysics. Conversely, SP-A enhances surfactant lipid turnover, by enabling uptake of DPPC by type II cells. SP-D also helps regulate the surfactant lipid pool size, although the mechanistic basis for regulation of surfactant metabolism by SP-D remains unclear. Anyhow, SP-A and SP-D are playing a key roles in regulating lung inflammation, which can have downstream effects on oxidant stress and alveolar damage. Consistent with an immunoregulatory role for SP-A and SP-D, these proteins are required for efficient clearance of bacterial infections. Both SP-A and SP-D have carbohydrate-recognition domains that recognize bacterial polysaccharides, whereas the collagenous stalk region of the proteins binds to neutrophils, macrophages, and type II cells. SP-A and SP-D also bind viruses. Thus, the collectin surfactant proteins act as co-receptors, or opsonizing agents, by coating pathogens and enabling them to be recognized and destroyed by the innate immune system in the lung.

Importantly, several examples show that the stressed and/or inflamed alveolus upregulates SP-A and SP-D while simultaneously decreasing SP-B and SP-C expression.

This has the dual effect of both increasing inflammation and depressing surfactant surface activity, which can further compromise lung function. However, the success of surfactant therapy for premature infants, has led to the notion that natural and pulmonary surfactants can be used as part of a treatment regimen for ARDS. However, treatment of adults with exogenous surfactant has had limited success:

- a) In part, this stems from a focus on using surfactant to recover the biophysical function of surfactant in adults, who have a large mature airspace as opposed to infants.
- b) Conversely, exploiting the immunomodulatory function of surfactant may ultimately be a more fruitful approach to treating adults with ARDS.

Conclusively, a net decrease in gap junctional communication will have a negative impact on surfactant and lamellar body secretion. However, evidence suggests that type II cells secrete the majority of SP-A and SP-D through a distinct vesicular pathway from the hydrophobic surfactant proteins and lipids packaged into lamellar bodies. Consistent with this, the SP-A content of lamellar bodies is low, and SP-D is largely undetectable. Although a complete lack of surfactant production and secretion is clearly deleterious, an imbalance in the regulation of surfactant secretion, which increases the relative level of SP-A and SP-D in the airspace at the expense of surface-active and antioxidant components of pulmonary surfactant can also compromise lung function. Whether this is due to decreased or altered intercellular communication in the alveolus during injury or infection remains to be controversial [6].

The Roles of Keratinocyte and Hepatocyte Growth Factors in Lung Development, Inflammation and Repair

Since the discovery and characterization of the epithelial-specific growth factors keratinocyte growth factor (KGF) and hepatocyte growth factor (HGF), their roles in lung development, lung inflammation, and repair have been widely investigated. Over the past more than 10 years, it has become increasingly clear that KGF and HGF play important roles in both the normal and the injured lung and ultimately may have therapeutic potential in lung disease.

Keratinocyte growth factor (KGF)

Interest in identifying epithelial-specific growth factors that might be oncogenic led to the isolation of KGF from a human embryonic lung fibroblast line by Rubin et al. in 1989. The factor was termed keratinocyte growth factor because of its potent mitogenic activity on epidermal keratinocytes. Subsequent studies showed that KGF is a member of the FGF family (and is also designated FGF-7) and, like other members of the family, has heparin-binding capability. Unlike other members of the fibroblast growth factor (FGF) family, KGF has epithelial specificity; KGF is expressed predominantly by mesenchymal cells,

and its receptor (KGF receptor; KGFR) is expressed only in epithelial cells. This epithelial specificity suggests that KGF may play an important role in mesothelial-epithelial interactions. Nevertheless, attempts to find new FGFs with sequence homology to KGF and other FGFs led to the discovery of FGF-10 in 1996. Initial studies indicated that its sequence had significant homology to KGF and that it was expressed preferentially in the lung. Like KGF, human FGF-10 is mitogenic for keratinocytes but not fibroblasts and is highly induced in the skin after wounding. This similarity to KGF has led some researchers to label it KGF-2 but however, it will be referred to as FGF-10.

A comparison of the basic properties and receptor specificity of KGF and FGF-10 is shown in Table 6. Unlike other members of the FGF family that bind to a variety of FGF receptors, KGF binds only to a splice variant of FGF receptor (FGFR)2 termed FGFR2-IIIb or KGFR. Like KGF, FGF-10 binds with high affinity to FGFR2-IIIb but has also been shown to have a weaker affinity for FGFR1-IIIb. These receptors are expressed only in epithelial tissues, thus conferring the unique paracrine epithelial specificity of these growth factors. KGF also interacts with low-affinity cell surface heparan sulfate proteoglycan receptors. This interaction has a potentiating effect on the interaction of KGF with KGFR. Heparan sulfate proteoglycan may also bind to the KGFR, further modulating the KGF/KGFR interaction. The interaction of FGF-10 with cell surface heparan sulfate proteoglycan has not been as well studied but is likely similar. FGF-10 does have 4-fold higher affinity for pericellular matrix heparan sulfate than KGF [31].

Role of KGF in the developing lung: A role for KGF in lung development was first suggested when it was reported that FGFR2 is expressed in the epithelial cells of the developing lung. Targeting a dominant negative FGFR2 to the lung led to the total absence of lung development. KGF is expressed in mesenchymal cells of the developing lung and other organs. Overexpression of KGF in the lung epithelium either constitutively or conditionally caused embryonic pulmonary malformation with histological similarities to pulmonary cystadenoma (Figure 28). Embryonic lungs had dilated saccules lined with columnar epithelial cells and no normal alveolar architecture, and the embryos died before reaching term. Studies in explanted lungs have provided further evidence for the importance of KGF in lung morphogenesis. Both the addition of exogenous KGF and blocking KGF or KGFR expression using antisense oligonucleotides disrupt normal branching morphogenesis in fetal lung explants. The effects of KGF in lung development depend on the stage of gestation. When KGF was expressed in the liver late in gestation using an apolipoprotein E promoter, the predominant effect in the lung was type II cell and bronchiolar cell hyperplasia rather than pulmonary malformation. Interestingly, although these studies suggest a role for KGF in normal lung morphogenesis, KGF null mice had histologically normal lung development and survival.

Table 6: Possible mechanisms to explain the protective effects of KGF and HGF in acute lung injury [31].

Factor	Protective Effects
KGF	Effects on alveolar type II and airway epithelial cells
	· Increased proliferation.
	· Increased surfactant protein and phospholipid production.
	· Enhanced spreading and motility.
	· Altered release of matrix metalloproteinases and urokinase-type plasminogen activator.
	· Resistance to mechanical injury.
	· Resistance to oxidant-induced injury.
	· Enhanced alveolar epithelial fluid transport.
	· Enhanced DNA repair.
	· Decreased apoptosis.
	· Release of cytokines and growth factors with autocrine and paracrine effects.
	Other effects
	· Enhanced endothelial cell barrier function, motility, and resistance to injury.
HGF	Effects on alveolar epithelial type II cells
	· Increased proliferation.
	· Increased motility.
	· Enhanced fibrinolysis with increased production of urokinase and plasmin.
	Other effects
	· Enhanced organ repair/regeneration through systemic actions of HGF.
	· Increased proliferation of bronchial epithelial cells.

The lack of an effect of the KGF null mutation can now be partially explained by the discovery that FGF-10 also binds to KGFR and is an important mediator of branching morphogenesis in the developing lung. FGF-10 is highly expressed at the sites where distal buds will appear in the embryonic lung and acts as chemoattractant for epithelial lung buds in concert with KGF. In addition to its role in lung morphogenesis, KGF has important effects on epithelial differentiation in the developing lung. In isolated fetal lung epithelial cells, type II cell maturation and surfactant synthesis appear to be under the control of mesothelial-epithelial interactions. It is recently reported that at least one-half of the stimulation of surfactant synthesis by fibroblast-conditioned media in isolated fetal lung epithelium could be abrogated by a KGF-neutralizing antibody. Administration of KGF to fetal type II cells led to increased synthesis of all surfactant components including disaturated phosphatidylcholine and surfactant proteins A, B, and C. Similar findings have been reported in a mesenchyme-free lung epithelial culture system where KGF administration promoted distal epithelial differentiation and surfactant

protein expression. In vivo, intratracheal, intravascular, or intramuscular KGF administration significantly increased lung-tissue saturated phosphatidylcholine.

Glucocorticoid effects in the fetal lung may also be mediated by KGF. Administration of dexamethasone, known to enhance fetal type II cell maturation and surfactant synthesis, was accompanied by a 50% increase in KGF mRNA in fetal lung fibroblasts. In fetal lung explants cultured with dexamethasone, an increase in KGF and KGFR expression was measured along with increases in surfactant protein expression and mature type II cell phenotype. However, both KGF and FGF-10 also play an important role in fetal lung fluid secretion, a process that is closely linked to lung morphogenesis. The fetal airway and alveoli actively secrete fluid, and normal lung development is dependent on this process. Experimental studies indicate that active chloride secretion is the driving force for fetal lung fluid secretion and that the fetal mesenchyme can produce soluble factors that alter fetal lung distal epithelial ion transport. It had been found that in fetal lung explants, administration of KGF led

to increased fluid secretion that was independent of cystic fibrosis transmembrane conductance regulator (CFTR) and could be inhibited by ouabain and bumetanide. Similar findings have been reported in fetal lung for both KGF and FGF-10. Thus both KGF and FGF-10 appear to enhance CFTR-independent fluid accumulation in the fetal lung. A candidate chloride channel for this effect is CLC-2, a fetal lung epithelial chloride channel that exhibits increased expression on the apical surface of the respiratory epithelium after KGF administration. KGF also inhibited expression of the α -subunit of the epithelial sodium channel (ENaC) in fetal lung explants, suggesting that KGF may inhibit sodium absorption in the fetal lung in addition to its effects on chloride secretion [28].

Effects of KGF in the injured lung:

Endogenous KGF: It seems likely, on the basis of the key role that endogenous KGF has been shown to play a role in wound healing in the skin, that endogenous KGF plays an important role in epithelial repair in the lung as well. For instance in hyperoxia, KGF mRNA expression was increased 12-fold in whole lung homogenates at about 6 days. This rise in KGF mRNA was followed, at 8-12 days, by an increase in type II cell proliferation, suggesting that increased expression of KGF led to alveolar epithelial type II cell hyperplasia in response to hyperoxic injury. In a case of increased permeability pulmonary edema due to exposure to α -naphthylthiourea (ANTU), pretreatment with a small dose of ANTU leads to resistance to pulmonary edema when a larger dose is administered. It had been showed that a single low dose of ANTU caused an upregulation of KGF gene transcription in the lung, suggesting that KGF-induced hyperplasia might underlie the induced resistance to ANTU. In acute lung injury due to bleomycin injection, KGF levels in bronchoalveolar lavage (BAL) increased markedly after injury, peaking at 7-14 days, coincident with peak type II cell proliferation. Thus in several different injuries, the available evidence indicates that KGF expression is increased after acute lung injury and may be an important endogenous stimulus for alveolar epithelial proliferation and repair.

Exogenous KGF: The protective effect of exogenous KGF in a model of acute lung injury was first reported in 1995 by Panos et al. In animals pretreated intratracheally with 5 mg/kg of recombinant human KGF had far better survival and virtually no histological changes when exposed to 120 hours of hyperoxia compared with untreated animals. For example, in an acid instillation model, pretreatment with intratracheal KGF 72 hours before intratracheal acid instillation reduced mortality, histological changes, inflammatory cell influx, procollagen mRNA levels, and hydroxyproline accumulation (Figure 29). In an ANTU experimental model of increased permeability pulmonary edema, pretreatment with KGF reduced alveolar-capillary barrier permeability and pulmonary edema formation. Similar beneficial effects on vascular permeability and pulmonary edema formation have been reported in ventilator-induced lung injury model. Intratracheal KGF has also been shown to ameliorate

radiation pneumonitis, bleomycin-induced lung injury, lung injury from bleomycin and radiation (Figure 30), and *Pseudomonas aeruginosa* pneumonia, when given before the insult. Recently, intravenous KGF (5 mg/kg) has also been shown to protect against bleomycin- and hyperoxia-induced lung injury, even though it stimulated less alveolar epithelial proliferation than intratracheal KGF. However, subcutaneous administration of KGF may also ameliorate graft-vs.-host disease and idiopathic pneumonia syndrome in allogeneic bone marrow transplant models.

Anyhow, several important observations can be made from a comparison of KGF in lung injury models:

- KGF was protective for a wide variety of mechanisms of lung injury, including direct epithelial injury (e.g., acid aspiration), direct endothelial injury (e.g., ANTU), and T cell-mediated injury (graft-vs.-host disease).
- The beneficial effects of KGF were apparent on multiple levels from cellular to whole body organs. These beneficial effects included reduced or absent histological changes, decreased fibrosis and deposition of collagen precursors, reduced physiological indices of lung injury including vascular permeability and formation of pulmonary edema, and improved survival.
- In all studies, pretreatment with KGF was necessary for the protective effect. Simultaneous or post-treatment was not efficacious.

These observations suggest that the mechanisms by which KGF exerts its protective effects on lung injury are probably multiple, not immediate, and affect multiple cell types within the lung.

Mechanisms of protection in acute lung injury: KGF has a wide variety of effects on lung epithelial cells that may mediate its protective effect in acute lung injury. One of the earliest observations was that both in vivo and in vitro administration of KGF causes alveolar epithelial type II cell proliferation (Figure 31). In vivo, intratracheal administration stimulates reproducible type II cell hyperplasia that peaks at 2-3 days. Proliferation of type II cells is accompanied by migration to cover the alveolar epithelial barrier with type II cells, a process that histologically resembles reactive type II hyperplasia seen in lungs after an injurious stimulus. Bronchial epithelial hyperplasia also occurs in response to KGF, both in vitro and in vivo. A similar response to intratracheal KGF has been observed in animals. By 7 days after a single intratracheal administration of KGF, the lung parenchyma returns to normal, a process that is mediated by both apoptosis and differentiation to type I cells. In this model, type II cell proliferation is accompanied by increased expression of surfactant proteins A, B, and D. Increases in surfactant protein secretion could have several beneficial effects in lung injury, including prevention of alveolar collapse by reduction of alveolar surface tension and augmentation of host defense. However, whereas in vitro KGF administration enhances surfactant protein expression on a per cell basis,

in vivo KGF administration enhances surfactant protein expression only on a whole lung basis. Individual type II cell levels of surfactant protein expression are decreased. The differential effect of KGF in vitro compared with in vivo probably has multiple explanations, including relative differences in dose and duration of exposure to KGF as well as complex environmental influences in vivo that are not present in a simple in vitro system. When KGF expression is increased via adenovirus-mediated gene transfer either in vitro in type II cells or in vivo, similar findings of type II cell hyperplasia and increased surfactant proteins A and D production have been reported.

One of the histological hallmarks of acute lung injury is sloughing and necrosis of the alveolar epithelium. In addition to type II cell proliferation, regeneration of a normal alveolar epithelium requires migration of type II cells along the denuded basement membrane to reconstitute an intact epithelium. KGF enhances the spreading and motility of alveolar epithelial type II cells, suggesting that improved alveolar repair may underlie some of the protective effects of KGF in lung injury. The beneficial effects of KGF on wound closure were first observed in the skin, bladder, gastric epithelium and cornea. In the lung, KGF enhances wound closure during cyclic mechanical strain in bronchial epithelial monolayers through enhanced cell spreading and motility. KGF also enhances the alveolar epithelial repair activity of alveolar epithelial type II cells when administered in vivo or in vitro. Altered migration and wound repair in KGF-treated epithelial cells may, in part, be a function of altered interaction with the extracellular matrix through increased expression of matrix metalloproteinases (MMPs) and urokinase-type plasminogen activator (UPA). In cultured human keratinocytes, KGF increased cell migration, UPA activity and MMP-10 (stromelysin-2) activity.

In addition to enhancing epithelial repair after a mechanical injury, KGF renders epithelial cells more resistant to mechanical injury. KGF-treated alveolar epithelial cells are inherently more resistant to injury from mechanical deformation (Figure 32), a factor that may contribute to KGF's protective effects in ventilator-induced lung injury [33]. KGF also renders airway epithelial cells more resistant to both hydrogen peroxide-induced and radiation-induced increases in cell permeability. Interestingly, in both of these in vitro studies, the protective effect was not limited strictly to pretreatment. In the radiation model, KGF was partially protective when given immediately after radiation. In the hydrogen peroxide model, as little as 1 hour of pretreatment with KGF was partially protective, suggesting that at least some of the KGF effects were posttranslational. In both these studies, KGF's protective effects were associated with stabilization of the F-actin cytoskeleton and could be inhibited by blocking protein kinase C. KGF also renders alveolar epithelial cells more resistant to cell necrosis induced by in vitro mechanical deformation. It was found that KGF treatment accelerated the in vitro transition from type II phenotype to type I phenotype, a transition that may have

conferred resistance to mechanical deformation; changes in the actin cytoskeleton and the secretion of extracellular matrix may have also played a role in that condition.

KGF also has effects on alveolar epithelial fluid transport in the adult lung. Unlike the fetal lung, which is a net secretor of fluid, the adult lung actively removes fluid from the alveolar space to maintain the gas exchange interface. Alveolar epithelial fluid transport is driven primarily by the active transport of sodium across the alveolar epithelial barrier by alveolar epithelial type II cells. The ability to clear fluid from the alveolar space is critically important to the resolution of pulmonary edema and to the restoration of adequate gas exchange in the setting of acute lung injury. Furthermore, in clinical acute lung injury, alveolar fluid clearance is impaired. KGF has been shown to increase alveolar epithelial fluid transport in both in vitro and in vivo studies in both the uninjured and the injured lung. In primary isolates of alveolar epithelial cells, addition of KGF enhanced active ion transport across monolayers primarily due to increased Na-K-ATPase α 1-subunit expression. In the normal lung, intratracheal pretreatment with KGF increased alveolar epithelial fluid transport both in vivo and in the isolated perfused lung. The primary mechanism was by type II cell hyperplasia since expression of the ENaC was diminished on a per cell basis. In patients with lung injury due to *P. aeruginosa* pneumonia, KGF pretreatment prevented the reduction in alveolar epithelial fluid transport observed in the untreated patients. Similar findings have been reported after ANTU injury in an isolated perfused lung model. The effects of KGF on alveolar epithelial fluid transport can be additive with other measures to stimulate alveolar fluid clearance. In one study, KGF treatment combined with the cAMP agonist terbutaline more than doubled the rate of alveolar fluid clearance (Figure 33).

Several groups have investigated the effects of KGF on DNA repair after oxidant injury. In A549 alveolar epithelial cells exposed to radiation, addition of KGF to the media ameliorated the formation of DNA strand breaks. This protective effect of KGF was blocked by the addition of inhibitors of DNA polymerases α , δ and ϵ , indicating that the effect was due to enhanced DNA repair. Similar findings were reported when A549 or primary isolates of alveolar epithelial cells were exposed to H_2O_2 . Again, the protective effect of KGF against DNA strand breaks was blocked by the addition of inhibitors of DNA polymerases (α , β , δ and ϵ). This protective effect was associated with the appearance of proliferating cell nuclear antigen, suggesting that the KGF may facilitate transition to a point in the cell cycle where DNA strand breaks can be repaired. KGF may also prevent epithelial cells from responding to proapoptotic stimuli.

Although KGF has a multitude of direct effects on epithelial cell proliferation, motility, fluid transport, and repair, some of the beneficial effects of KGF may be mediated by the release of downstream mediators that have both autocrine and paracrine effects. For example, in state of T cell-mediated idiopathic pneumonia after bone marrow transplantation,

KGF administration before bone marrow transplant suppressed T cell-dependent alveolar macrophage activation and production of inflammatory mediators. This finding suggests that KGF stimulated the release of an epithelial cell-derived mediator capable of down-regulating macrophage function. The protective effect of KGF in this state was blocked if a nitrating species was introduced by adding cyclophosphamide to the conditioning regimen. The investigators hypothesize that the generation of peroxy nitrite disabled downstream signaling from the KGF receptor by disabling tyrosine phosphorylation. KGF may also stimulate epithelial cells to produce other growth factors. In cultured keratinocytes, KGF stimulated the expression and secretion of TGF- α into the medium. Similarly, supernatants from alveolar epithelial cells isolated from KGF treated animal stimulated alveolar epithelial repair, consistent with an autocrine effect of KGF. This effect also appears to be mediated through the epidermal growth factor (EGF) receptor, perhaps due to the stimulation of production of soluble factors such as EGF or TGF- α . KGF treatment may also prevent the release of potentially harmful mediators. In a bleomycin-induced lung injury, pretreatment with KGF prevented the bleomycin-associated increase in profibrotic mediators including TGF- β and PDGF-BB.

However, recent reports indicate that KGF may have direct or indirect effects on endothelial cells that contribute to protection from acute lung injury. It had been reported that subnanomolar concentrations of KGF induced neovascularization in the cornea. In this study, KGF induced chemotaxis in capillary but not large vessel endothelial cells in culture. FGF-10 had similar effects. KGF also helped to maintain the barrier function of capillary endothelial cell monolayers, protecting against hydrogen peroxide-induced and vascular endothelial growth factor-induced increases in permeability. However, KGFR could not be localized to endothelial cells. The authors hypothesize that KGF may be acting through an as yet undiscovered high affinity receptor on endothelial cells since KGF administration led to rapid rises in mitogen-activated protein kinase activity in capillary endothelial cells. A protective effect of KGF on the endothelium was also suggested in an in vivo hyperoxia studies. In these studies, KGF administration prevented damage by hyperoxia to both the alveolar epithelium and capillary endothelium as measured by electron microscopy. The mechanism of the protective effect for the endothelium was not defined, although whole lung levels of the cell death-associated proteins p53, Bax, and Bcl-x all declined, as did levels of plasminogen activator inhibitor-1. In an isolated perfused lung model, intravenous KGF attenuated hydrostatic pulmonary edema, a finding that was associated with decreased alveolarcapillary barrier permeability and may have been due to effects on endothelial permeability.

Hepatocyte growth factor (HGF)

The identification of HGF was the result of a concerted effort to identify the growth factor responsible for hepatic regeneration after hepatectomy. Initially isolated from

multiple sources, it was later recognized that HGF was identical to another growth factor, scatter factor, which had been independently isolated and cloned. Like KGF, HGF has heparin-binding capability, but it is not a member of the FGF family. HGF is expressed as a single chain molecule of 728 amino acids that is cleaved proteolytically to an active heterodimer. The active heterodimer has four kringle domains and an inactive serine protease site and belongs to a group of fibrinolytic and coagulation-related proteins, which includes plasminogen and other blood proteases. The HGF receptor (Table 6) is a membrane-spanning tyrosine kinase that was identified as the *c-met* protooncogene product in 1991. Unlike the KGFR, *c-met* expression is not confined to the epithelium, although epithelial expression predominates. In addition to normal epithelial cells of almost every organ, *c-met* has been detected on fibroblasts, endothelial cells, microglial cells, neurons, and hematopoietic cells. Like KGF, HGF binds to cell surface heparan sulfate proteoglycans that serve as low-affinity receptors and modulate the interaction between HGF and the *c-met* receptor.

Role of HGF in the developing lung: HGF and its receptor are expressed in many developing organs. HGF expression is usually confined to the mesenchyme, and HGF receptor expression is usually confined to the epithelium. Some researchers had tested the effect of HGF on various epithelial cell lines and found that HGF could induce endogenous morphogenetic programs in epithelial cells from a variety of organs including the lung (LX-1 carcinoma cells). In embryonic lung organoids grown on three-dimensional collagen matrices, antisense HGF oligonucleotides blocked alveolar and bronchial morphogenesis. In fetal lung explants, exogenous HGF stimulated branching organogenesis. However, when fetal lung epithelial explants were grown in the absence of mesenchyme, HGF alone was insufficient to restore branching morphogenesis, whereas KGF alone or acidic FGF alone was sufficient. HGF had a synergistic effect with KGF or acidic FGF in this mesenchyme-free system. Thus while HGF appears to play an important role in branching morphogenesis in the lung, it is not essential, perhaps due to redundancy in the repertoire of mediators of mesenchymal-epithelial interactions. It had been found that in humans, amniotic fluid from women up to 31 weeks pregnant had a motogenic effect on a fetal feline lung cell line. This motogenic activity could be abolished by anti-HGF neutralizing antibodies, suggesting that HGF is present and probably functional in human lung development as well. After 31 weeks, human amniotic fluid was no longer motogenic for fetal lung cells [34].

Effects of HGF in the injured lung

Endogenous HGF: HGF is present in the BAL fluid of normal adult and is responsible for most of the mitogenic effects of lavage fluid on alveolar epithelial cells. In the first published study to examine the effect of acute lung injury on HGF expression in the lung, it was reported that HGF mRNA and HGF activity increased in whole lung at 3-6

hours after injury with intratracheal hydrochloric acid. This increase in HGF expression was followed at 24 hours by a peak in bronchial epithelial DNA synthesis and at 48 hours by a peak in alveolar epithelial DNA synthesis. An increase in whole lung HGF expression has also been reported in an animal model of ischemia-reperfusion. In that model, whole lung HGF mRNA increased by 24 hours after ischemia-reperfusion. This was followed by an increase in whole lung HGF protein that peaked at day 3 after ischemia-reperfusion. Administration of an anti-HGF antibody aggravated ischemia-reperfusion lung injury and reduced post-injury DNA synthesis in the lung, suggesting that endogenous HGF plays a role in the reparative response to lung injury. In recent studies attempted to localize the cellular source of HGF of *P. aeruginosa* pneumonia. Whole lung HGF mRNA increased at 3 hours after bacterial instillation and again at 24-72 hours. Immunohistochemistry suggested that the cellular source of HGF for the early peak was bronchial epithelial cells. This finding is surprising and was not confirmed by in situ hybridization but is in keeping with a report that normal human bronchial epithelial cells can produce HGF in culture as an autocrine mitogenic factor. The cellular source for the later peak of HGF production appeared to be alveolar macrophages and, in particular, those that had phagocytosed apoptotic neutrophils. The lung may also be a source of HGF after injury to other organs. For example, after partial hepatectomy, unilateral nephrectomy, or induction of hepatitis, HGF mRNA in the intact lung increased at 6 hours. In the setting of acute pancreatitis in, HGF mRNA and protein increased in the lung, liver, and kidney. These findings suggest that the lung may contribute to organ repair and regeneration in an endocrine fashion through production of circulating HGF.

The human HGF gene has an IL-6 response element and a potential binding site for nuclear factor IL-6 near the transcription initiation site, suggesting that IL-6 may promote transcription. This is potentially important because plasma levels of IL-6 are elevated in patients with acute lung injury. IL-1 α and IL-1 β have both been shown to increase HGF mRNA in cultured human skin fibroblasts. In addition to transcriptional regulation, local proteolytic activation of HGF may control its activity. It had been shown that an enzymatic activity that proteolytically activated the HGF precursor could be induced in the liver in response to tissue injury.

Exogenous HGF: In bleomycin-induced lung injury in the mouse, concomitant treatment with a continuous infusion of HGF repressed fibrotic morphological changes at 2-4 weeks after initiation of bleomycin (Figure 34). Interestingly, HGF infusion was also effective if it was started 2 weeks after the bleomycin was started, suggesting that HGF may be able to reverse some of the fibrotic changes induced by bleomycin. It had been recently reported that intratracheal HGF given at 3 and 6 days after (but not before) bleomycin could also reduce fibrotic changes in the lung. This reduction in fibrosis was associated with increased bronchial epithelial and alveolar epithelial proliferation. Alveolar epithelial type II cells express the *c-met* receptor, and HGF is a potent

mitogen for alveolar epithelial cells, both in vitro and in vivo. Human adult lung fibroblast-conditioned media are also mitogenic for alveolar epithelial type II cells. This mitogenic activity is predominantly due to HGF and KGF. HGF is also a potent in vitro mitogen for human bronchial epithelial cells. Unlike KGF, however, addition of HGF to primary isolates of alveolar epithelial cells inhibited the synthesis and secretion of phosphatidylcholine surfactant components. In addition to its potent mitogenic effects on alveolar epithelial cells, the addition of exogenous HGF may also modulate the alveolar epithelial response to other growth factors. For example, TGF- β is a potent growth factor associated with acute lung injury, fibroblast proliferation, and lung fibrosis that is known to inhibit epithelial cell proliferation. TGF- β dramatically downregulates HGF expression in human lung fibroblasts through regulation at the posttranscriptional level. In primary isolates of alveolar epithelial type II cells, addition of TGF- β did not inhibit HGF-induced proliferation. Thus exogenous HGF may restore a proliferative phenotype in type II cells that is down-regulated by TGF- β .

Another interesting mechanism by which HGF may ameliorate lung injury is through modulation of fibrinolysis. Clinical acute lung injury is associated with fibrin deposition and a reduction in fibrinolytic capacity in the airspace. An intact fibrinolytic system is also important to recovery from experimental lung injury. For example, intact fibrinolysis is required for recovery from bleomycin-induced lung injury and hyperoxia-induced lung injury. The alveolar epithelium is an active participant in maintaining the fibrinolytic balance in the lungs. It had been reported that administration of HGF to A549 alveolar epithelial cells in culture enhanced cell surface plasmin generation and expression of urokinase activity, thus enhancing the fibrinolytic capacity of this cell line. Anyhow, (Table 7) is summarized the possible mechanisms which protect lung injury by KGF and HGF (Ware 2002).

Variation in the PaO₂/FiO₂ ratio with FiO₂

The ratio of the partial pressure of oxygen in arterial blood (PaO₂) to the inspired oxygen fraction (FiO₂) has been used to quantify the degree of abnormalities in pulmonary gas exchange. The ratio has been used in numerous experimental studies to quantify pulmonary gas exchange before and after therapeutic intervention. The PaO₂/FiO₂ [in mmHg] ratio has also been used in the clinical setting to classify patients' pulmonary gas exchange status, including the definitions of acute lung injury (ALI) (202.5 ≤ PaO₂/FiO₂ < 300) and of adult respiratory distress syndrome (ARDS) (PaO₂/FiO₂ < 202.5). However, despite its widespread use, the validity of the PaO₂/FiO₂ ratio as a tool for assessing pulmonary gas exchange has been questioned. Using mathematical models describing gas exchange, previous authors have simulated values of the PaO₂/FiO₂ ratio and have shown them to vary with the FiO₂ level. These theoretical analyses could lead us to believe that the PaO₂/FiO₂ ratio is a poor indicator of a patient's pulmonary gas exchange status in the clinic. This hypothesis is only true, however, if the simulations performed are indeed able to

describe measured variations in the $\text{PaO}_2/\text{FiO}_2$ ratio, and if these variations happen within interesting ranges of FiO_2 . The latter of these conditions is crucial in determining whether this ratio is a useful scientific and clinical parameter.

Table 7: Comparison of the properties of keratinocyte growth factor, fibroblast growth factor-10, and hepatocyte growth factor [31].

Property	Keratinocyte Growth Factor	Fibroblast Growth Factor-10	Hepatocyte Growth Factor
Molecular mass	28 kDa	20 kDa	b-chain
Homology	Fibroblast growth factor family	Fibroblast growth factor	Related to plasminogen, has 4 kringle domains and an inactive serine protease site
Activation required	Single chain polypeptide is bioactive	Single chain polypeptide is bioactive	Single chain is cleaved proteolytically to active heterodimer
High-affinity receptor	FGFR2-IIIb	FGFR2-IIIb FGFR1-IIIb	c-met protooncogene product
Receptor type	Membrane-spanning tyrosine kinase	Membrane-spanning tyrosine kinase	Membrane-spanning tyrosine kinase
Low-affinity receptors	Heparan sulfate proteoglycans	Heparan sulfate proteoglycans	Heparan sulfate proteoglycans
Cells that produce growth factor	Mesenchymal cells including fibroblasts and vascular smooth muscle cells	Mesenchymal cells	Mesenchymal cells, bronchial epithelial cells, alveolar macrophages
Target cells that express receptor	Epithelial cells of all types; effects on endothelial cells suggest that an unidentified receptor may be present	Epithelial cells of all types	Primarily epithelial cells of all types but also endothelial cells, fibroblasts, microglial cells, neurons, hematopoietic cells

The ability of a particular simulation to accurately describe variation in the $\text{PaO}_2/\text{FiO}_2$ ratio depends upon the complexity of the mathematical models used. Gowda and Klocke were using the complex mathematical model included in the multiple inert gas elimination technique to simulate changes in the $\text{PaO}_2/\text{FiO}_2$ ratio on varying FiO_2 levels. This complex model has the advantage of describing pulmonary gas exchange accurately; however, its complexity means that the model is not useful for describing an individual patient in the intensive care unit. Aboab and colleagues used a simple mathematical model where an effective pulmonary shunt was used to describe all ventilation/perfusion (V/Q) abnormalities in the lung. This model has the advantage that values of effective shunt can be estimated from clinical data. Values of effective shunt, however, are well known to vary with FiO_2 , as shown previously. A single fixed value of effective shunt may therefore not be able to simulate changes in the $\text{PaO}_2/\text{FiO}_2$ ratio accurately. Mathematical models have been proposed recently that describe the gas exchange using two parameters: a shunt value, and a second parameter describing the V/Q ratio. These parameter values can be estimated simply and non-invasively in the clinic, and have been shown to fit data from a range of mechanically ventilated patients and spontaneously breathing patients. These models and techniques therefore provide tools that can both describe pulmonary gas exchange in the individual patient and potentially simulate changes in the $\text{PaO}_2/\text{FiO}_2$ ratio.

Anyhow, the data were analyzed using two mathematical models of gas exchange: the effective shunt model, used by Aboab et al.; and the two-parameter model. However, (Figure 35) [35] illustrates how these models differ in their representation of pulmonary gas exchange. The effective shunt model includes one ideally ventilated and perfused alveolar compartment plus a compartment representing pulmonary shunt. The two-parameter model includes two alveolar compartments incorporating V/Q inequality with the addition of a shunt compartment. In the effective shunt model, oxygenation problems are described by a single parameter (effective shunt) quantifying the blood flowing through the lungs without being oxygenated. In the two-parameter model, a shunt parameter is included along with the parameter fA2 describing the fraction of ventilation to a compartment receiving 90% of non-shunted perfusion. The fA2 value of 0.9 gives ideal V/Q matching, while lower fA2 values indicate V/Q mismatching. The fA2 value can be transformed into a

PO_2 value, which describes the drop in oxygen pressure from the ventilated alveoli to the mixed blood leaving the lung capillaries; that is, the value in blood prior to the mixing of shunt. As such, PO_2 describes the extra oxygen pressure required at the mouth to remove an oxygenation problem due to V/Q mismatch; that is, $\text{PO}_2 = 150$ mmHg (20 kPa) means air plus 20% inspired oxygen ($\text{FiO}_2 = 0.41$) is required. Interestingly, the effective shunt model and the two-parameter model were used in three ways:

- a) A theoretical comparison was performed between model simulations of changes in SaO_2 and the $\text{PaO}_2/\text{FiO}_2$ ratio with variation in FiO_2 using the two mathematical models. To do so, simulations were performed for different values of model parameters.
- b) The models were fitted to the data from each patient in turn using the least-squares method, and the root mean square of the residuals was calculated for each of the fits. Model fits were illustrated by plotting simulated and measured values of SaO_2 and the $\text{PaO}_2/\text{FiO}_2$ ratio versus FiO_2 . A statistical comparison of the goodness of fit of the two models to the data was performed using an F test.
- c) Both models were then used to analyze the variation in the $\text{PaO}_2/\text{FiO}_2$ ratio over a range of FiO_2 levels. This analysis had two aims: first, to evaluate the significance of any difference between the two models when fitted to the data; and second, to investigate whether the simulated variation in the $\text{PaO}_2/\text{FiO}_2$ ratio was relevant.

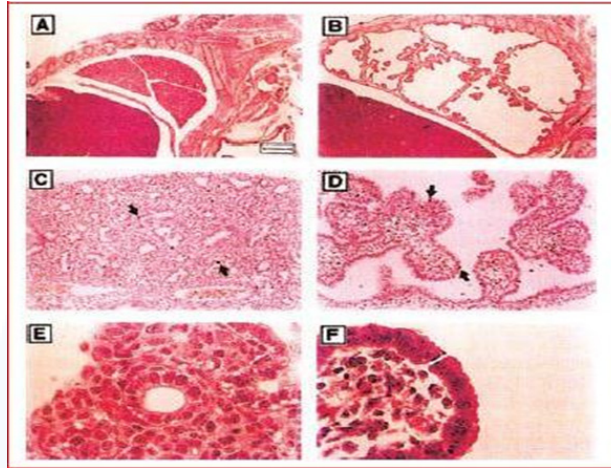


Figure 28: Effect of targeted over expression of human (h) keratinocyte growth factor (KGF) in the murine lung using a surfactant protein C (SP-C) promoter. Comparison of pulmonary development pattern and pulmonary epithelial proliferation and morphology in a normal mouse at gestational day 16.5 (E16.5; A, C, and E) compared with a littermate SP-C-hKGF transgenic embryo (B, D, and F). A: photomicrograph of a sagittal section showing lungs of a normal E16.5 mouse. B: photomicrograph of a sagittal section showing lungs of an E16.5 SP-C-hKGF transgenic mouse lung. C: staining of lungs from A for Ki-67, an endogenous marker of cell proliferation. D: Ki-67 staining of lungs from B. Arrows in C and D point to proliferating cells staining positive for Ki-67 expression. E: higher powered photomicrograph of a distal epithelial airway from A. Note the cuboidal shape characteristic of the distal airway epithelium in normal embryonic mouse lung. F: higher powered micrograph of the epithelial cells lining the large dilated saccules in B. Note the more columnar appearance of the epithelial cells, characteristic of more primordial or immature bronchial epithelium. Sections were stained with hematoxylin and eosin. Bar = 500 μm for A and B; 100 μm for C and D; and 25 μm for E and F [32].

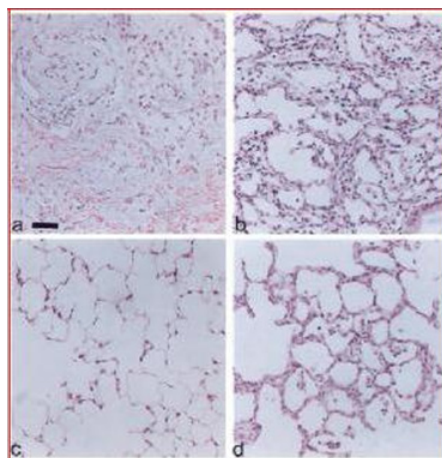


Figure 29: Representative photomicrographs of left lung tissue 7 days after unilateral HCl instillation. HCl (0.1 N, 0.5 ml) was instilled intra-bronchially into the left lung. Left intra-bronchial instillation of KGF (5 mg/kg) at 72 h (KGF 72 h/HCl) or saline (0.5 ml) at 72 h (Saline 72 h/HCl) was completed before HCl treatment. Microscopic lung injury after the saline 72 h/HCl treatment varied from severe injury consisting of consolidation, hemorrhage, inflammatory cell infiltration, fibroblast proliferation, and obliteration of alveolar architecture (a) to moderate injury consisting of focal areas of inflammatory cell infiltration and fibroblast proliferation (b). Pretreatment with KGF at 72 h before HCl instillation (KGF 72 h/HCl) completely prevented microscopic lung injury (c) or resulted in only mild focal areas of inflammatory cell recruitment and cell proliferation (d). Bar = 40 μm [32].

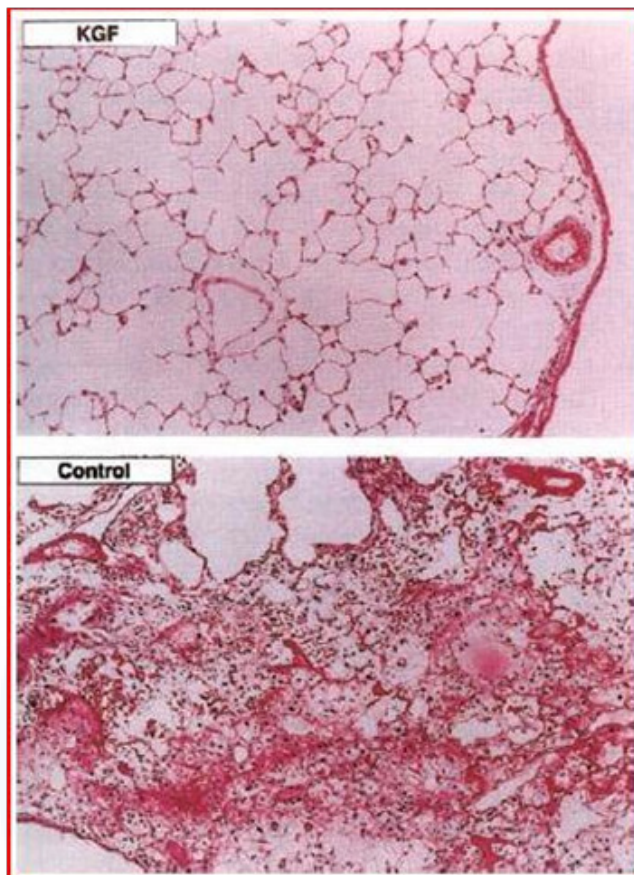


Figure 30: High magnification view of lung injury caused by the combination of bilateral thoracic radiation (18 Gy) and intratracheal instillation of bleomycin (1.5 U) shows that the intact pulmonary architecture in KGF-pretreated lung (intratracheal instillation) contrasted with the architectural disorganization and hemorrhage in the saline-pretreated lung [32].

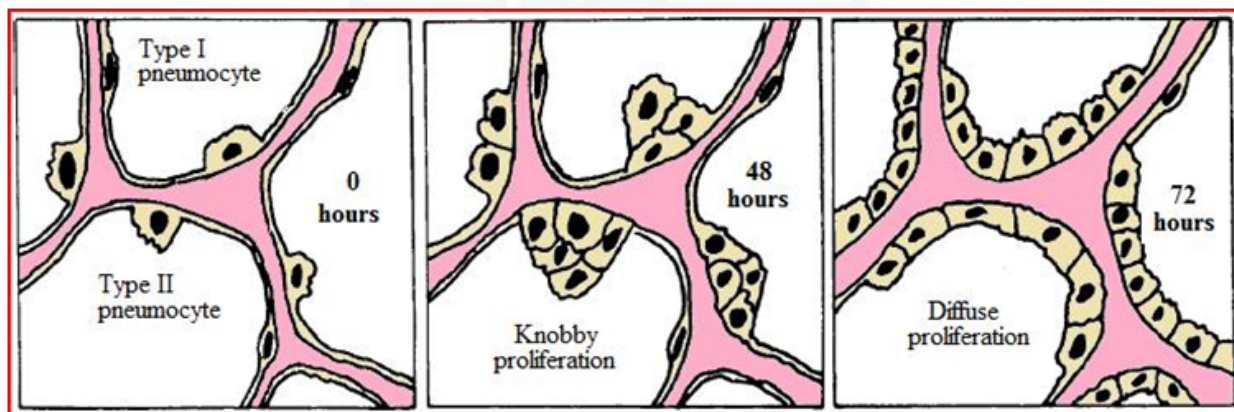


Figure 31: Schematic diagram shows the progression of type II pneumocyte hyperplasia in the lung after a single intratracheal injection of KGF [32].

The relevant range was defined on an individual patient basis as the FiO_2 range that resulted in a simulated value of SaO_2 within the range 92-98%. The variation in the PaO_2/FiO_2 ratio was then used to quantify the number of patients changing disease classification as a result of varying FiO_2 levels according to the two models across the defined FiO_2 range, these results being presented in a confusion

matrix. Patients were classified into disease groups at the lowest and highest FiO_2 level in the range, according to the following criteria: ARDS ($PaO_2/FiO_2 < 202.5$ [~ 200]), ALI ($202.5 \leq PaO_2/FiO_2 < 300$), and normal ($PaO_2/FiO_2 > 352.5$). Those patients falling outside these categories are defined here as having mild hypoxemia ($300 \leq PaO_2/FiO_2 < 352.5$) [36].

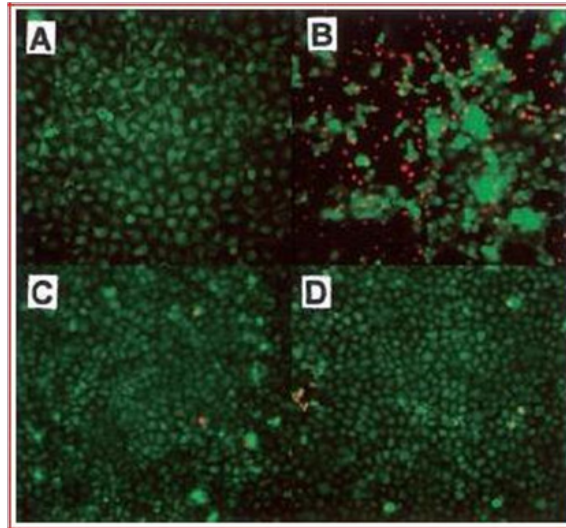


Figure 32: Enhanced viability after application of mechanical strain in KGF-treated alveolar epithelial cells. Intratracheal instillation of KGF was given 48 h before isolation of alveolar epithelial type II cells. Cytoplasm of viable cells was stained using calcein-AM (indicated in green), and nuclei of nonviable cells were stained using ethidium homodimer-1 (indicated in red). A: Saline vehicle-treated unstretched cells. B: Saline vehicle-treated cells after 1 h of cyclic stretch (25% change in surface area). C: KGF-treated unstretched cells. D: KGF-treated cells after same 1-h stretch protocol [32].

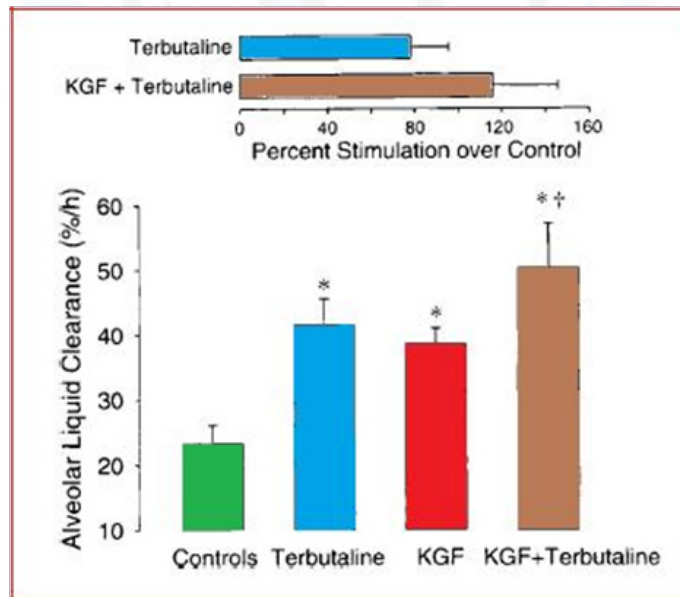


Figure 33: Effect of terbutaline on alveolar liquid clearance over 1 h and 72 h after KGF treatment. Data are also shown for alveolar liquid clearance over 1 h in control and in control treated with 10^{-4} M terbutaline. Data are means \pm SD. * $P < 0.05$ compared with control group. † $P < 0.05$ compared with 72 h after KGF treatment and $P < 0.05$ compared with terbutaline control.

Top: % stimulation (means \pm SD) by terbutaline with and without KGF [32].

Nevertheless, the (Figures 35&36) illustrate the results of the theoretical analysis showing the effects of varying F_{iO_2} on model simulated values of Sa_{O_2} and the Pa_{O_2}/F_{iO_2} ratio. The (Figure 36 a & b) illustrates the effects of varying either the effective shunt of the model of Aboab et al. or the shunt value included in the two-parameter model, these being equivalent for $PO_2 = 0$ mmHg. Simulated increased shunt depresses the shoulder of the F_{iO_2} versus Sa_{O_2} curve,

and depresses and deforms the shape of the F_{iO_2} versus Pa_{O_2}/F_{iO_2} ratio curve. As a result, the relevant range of F_{iO_2} (thick solid part of lines) broadens with increases in shunt. The deformation in the Pa_{O_2}/F_{iO_2} ratio curve has a characteristic shape whereby the Pa_{O_2}/F_{iO_2} first falls and then gradually rises, explained as follows. On increasing the F_{iO_2} level, the partial pressure of oxygen in the lung capillary blood increases. As the lung capillary blood mixes with that

shunted the increase in the partial pressure of oxygen in the lung capillary blood helps to oxygenate the shunted blood, so that the PaO_2 value increases little and the PaO_2/FiO_2 ratio falls. On increasing the FiO_2 level further, the mixture of shunted and lung capillary blood reaches an SaO_2 value of about 98% where the arterial blood hemoglobin is almost saturated. Further increases in FiO_2 translate into increased PaO_2 , and hence an increasing PaO_2/FiO_2 ratio. It should be noted that the range of FiO_2 giving 92-98% saturation

may extend below atmospheric oxygen levels ($FiO_2 = 0.21$) in patients with only mild gas exchange abnormalities or in normal subjects. The simulations in (Figure 35b) show how the PaO_2/FiO_2 ratio changes with FiO_2 as found by Aboab and colleagues. For example, for a shunt value of 20% (Figure 36b, points a & b) the PaO_2/FiO_2 ratio falls by 153.7mmHg, from 341-187.5 mmHg, over the relevant range of FiO_2 .

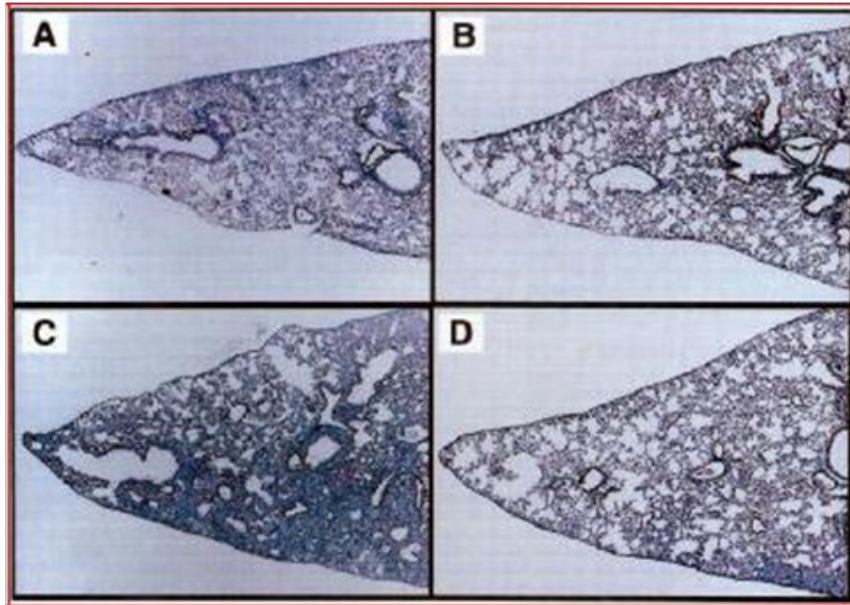


Figure 34: Microscopic findings in lungs 2 and 4 wk after treatment with bleomycin and/or low-dose hepatocyte growth factor (HGF). A: bleomycin (continuous subcutaneous administration from days 0 to 7) alone at 2 wk. B: bleomycin and low-dose HGF (continuous intraperitoneal administration from days 0 to 7) at 2 wk. C: bleomycin alone at 4 wk. D: bleomycin and low-dose HGF at 4 wk. Lungs were stained with elastica- Masson. Original magnification, $\times 10$ [32].

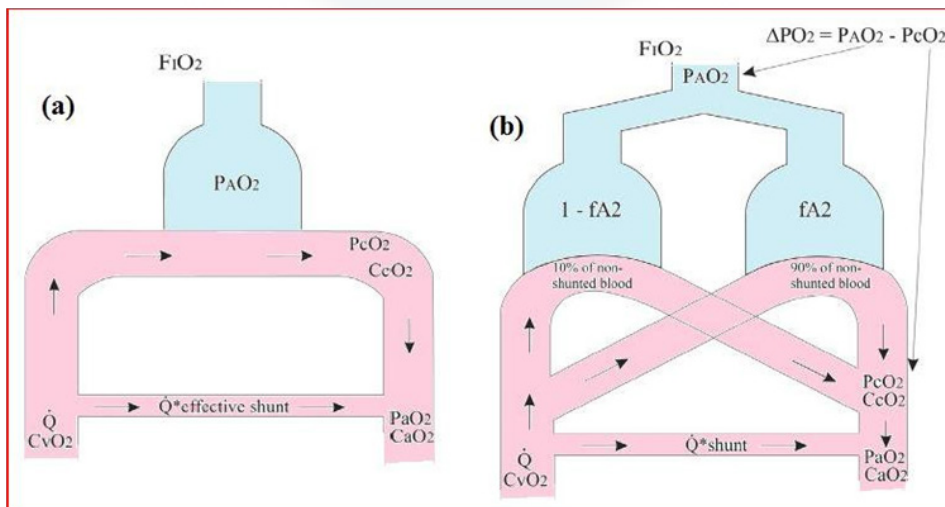


Figure 35: Mathematical models of pulmonary gas exchange. (a) The 'effective shunt' model. (b) The two-parameter shunt and ventilation/perfusion mismatch model. Data describing oxygen transport in the models are indicated: oxygen partial pressure in alveolar air (P_{AO_2}), oxygen partial pressure in capillary blood (P_{CO_2}), oxygen partial pressure in arterial blood (PaO_2), concentration of oxygen in venous blood (CvO_2), concentration of oxygen in capillary blood (CcO_2), concentration of oxygen in arterial blood (CaO_2), cardiac output (Q), shunt parameter (shunt), and parameters describing ventilation/perfusion mismatch (fA_2 , PO_2) [37].

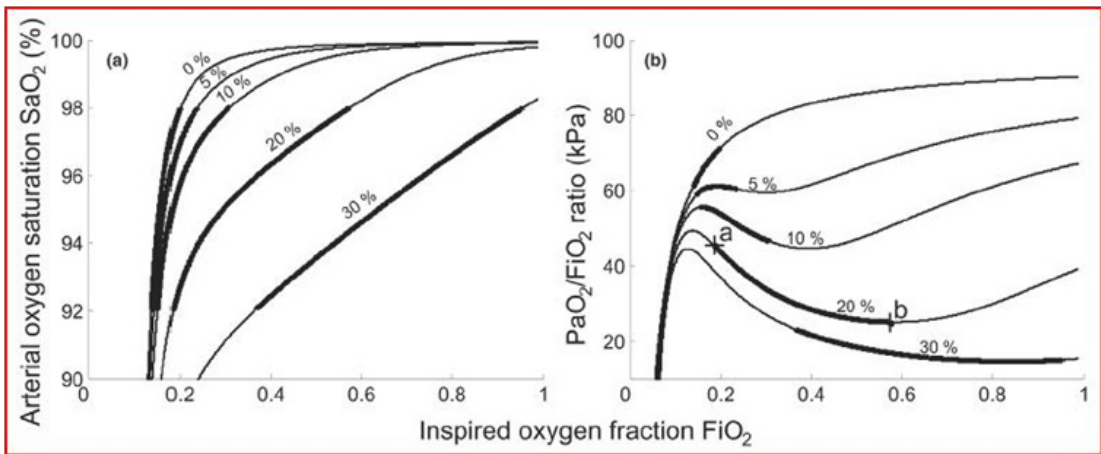


Figure 36: Model simulations of arterial oxygen saturation and arterial oxygen partial pressure/inspired oxygen fraction ratio. (a) Inspired oxygen fraction (FiO_2) versus arterial oxygen saturation (SaO_2). (b) FiO_2 versus the partial pressure of oxygen in arterial blood (PaO_2)/ FiO_2 ratio. Simulations performed using shunt = 0–30%, parameter PO_2 (fA2) = 0 mmHg (0.9), oxygen consumption = 0.26 l/min, alveolar minute volume = 5.25 l. Points a and b, the PaO_2/FiO_2 ratios for $FiO_2 = 0.19$ (point a) and $FiO_2 = 0.57$ (point b) – corresponding to the extremes of the relevant range of FiO_2 (thick solid line) [37].

The (Figure 37a & b) illustrates the effects of varying the degree of V/Q mismatch in the two-parameter model. The effects of a V/Q mismatch on the SaO_2 or the PaO_2/FiO_2 ratio are quite different from the effects of shunt. The FiO_2 versus SaO_2 curves are shifted horizontally along the FiO_2 axis with increasing V/Q mismatch. The PaO_2/FiO_2 ratio is increased with increasing FiO_2 levels, as the absence of significant shunt means that arterial hemoglobin is saturated

on small increases in FiO_2 . The small decline in the PaO_2/FiO_2 ratio seen in these curves, particularly at the 0 mmHg level, is due to the 5% shunt used in these plots. For the cases simulated in (Figure 36), the PaO_2/FiO_2 ratio is quite sensitive to changes in FiO_2 . Within the relevant range of FiO_2 (thick solid part of lines) for a PO_2 value of 75 mmHg (Figure 37b, points a and b), the PaO_2/FiO_2 ratio increases by 62 mmHg, from 246.7 to 309 mmHg.

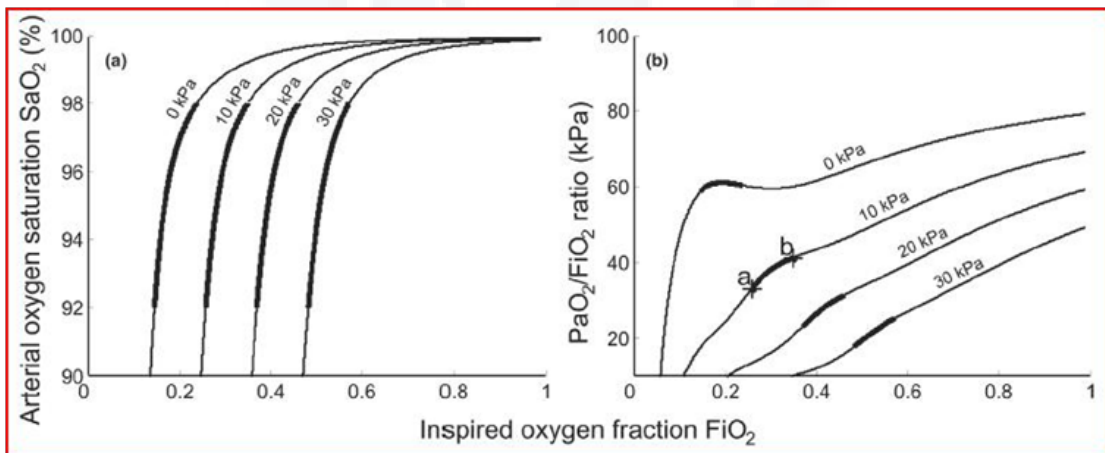


Figure 37: Model simulations of arterial oxygen saturation and arterial oxygen partial pressure/inspired oxygen fraction ratio. (a) Inspired oxygen fraction (FiO_2) versus arterial oxygen saturation (SaO_2). (b) FiO_2 versus the partial pressure of oxygen in arterial blood (PaO_2)/ FiO_2 ratio. Simulations performed using shunt = 5%, parameter PO_2 (fA2) = 0 – 225 mmHg (0.9–1.1), oxygen consumption = 0.26 l/min, alveolar minute volume = 5.25 l. Points a and b, the PaO_2/FiO_2 ratios for $FiO_2 = 0.26$ (point a) and $FiO_2 = 0.35$ (point b) – corresponding to the extremes of the relevant range of FiO_2 (thick solid line) [37].

In conclusion it has been shown that the PaO_2/FiO_2 ratio depends on both the FiO_2 level and the SaO_2 level, and that, for changes in FiO_2 corresponding to an SaO_2 range of 92–98%, 30% of patients change disease classification due to variation in the PaO_2/FiO_2 ratio. The clinical and scientific utility of the PaO_2/FiO_2 ratio therefore seems doubtful, and at the very least the FiO_2 level at which the PaO_2/FiO_2 ratio is

measured should be specified when quantifying the effects of therapeutic interventions or when specifying diagnostic criteria for ALI and ARDS. Perhaps more appropriate criteria would be to replace the single-parameter PaO_2/FiO_2 ratio description with two parameters, a parameter to describe the oxygenation problem due to V/Q mismatch and one to describe oxygenation problems due to shunt [35].

Assessment of respiratory mechanics

More than 30 years after its first description, mortality associated with the acute respiratory distress syndrome (ARDS) is still great, with reported rates between 30 and 60%. The range in mortality is partly because of the loose definition of both ARDS and acute lung injury (ALI), based on bilateral lung infiltrates on X-ray, a left ventricular filling pressure < 18 mm Hg and a $\text{PaO}_2/\text{FIO}_2$ of < 300 mm Hg (ALI) or < 200 mm Hg (ARDS). No factors relating to lung mechanics are used in these definitions. Use of PEEP can easily move the patient from ARDS to ALI or even out of the definition completely. The vagueness of the definition is also indicated when mortality is the same in ALI and ARDS, not related to ventilator settings. However, Amato and colleagues showed that a protective form of ventilation, in contrast to normal ventilator treatment, reduced mortality from 71 to 38% in ARDS, and the ARDSNetwork study found that mortality decreased from 40 to 31% when tidal volumes were decreased from 12 to 6 ml/kg. It may be argued that a tidal value of 12 ml/kg is not normal, and these studies may only show that the use of large tidal volumes is harmful, as seen in the study of Amato and colleagues, in which the control group mortality was very high (71%), rather than small tidal volumes being protective. A link between lung mechanics and morbidity and mortality was suspected in 1998, and in 1999 Ranieri and colleagues reported that inflammatory markers in lung lavage fluid and blood were less with a protective ventilatory strategy and that the risk of developing organ failure was reduced. The concept of ventilator-induced lung injury is well established. Lung injury can cause a systemic inflammatory reaction leading to multiple organ failure and death in patients with ARDS. Despite the clear link between lung mechanics and outcome in ALI and ARDS, ventilator settings are normally based on blood gases rather than measurements of lung mechanics. Rarely is the gap between research and clinical practice as wide as in the assessment of lung mechanics. In research, static measurements are considered ideal and the ventilator settings are supposed to be made on this basis, i.e. end-expiratory pressure should be above the lower inflection point and tidal volume below the upper inflection point on the static pressure-volume curve to avoid cyclic collapse, reopening of alveoli and overstretching. In clinical practice, however, lung mechanics are assessed during ventilation so that pressure measurements are affected by the resistance of the endotracheal tube. At best, the ventilation is set with an end-inspiratory pause giving semistatic conditions, so that an adequate plateau pressure indicates the maximal alveolar pressure. Intermittent application of a prolonged hold in expiration gives information about intrinsic PEEP. The discrepancy between the static methods used for research and clinical reality and the dynamic measurements of lung mechanics raises the question of whether static measurements are truly superior to dynamic measurements, if the latter could be obtained in such a way that the effects of endotracheal tube and airway resistance were minimized [37].

Airway pressure

In clinical practice, airway pressure, measured in the ventilator or at the patient connection, and tidal volume measurements are the most common values used for assessment of lung mechanics. However, pressure measured proximal to the endotracheal tube is affected to a great extent by the tube resistance. Peak inspiratory pressure (PIP) is much greater than peak tracheal or peak alveolar pressure. The magnitude of the difference depends on the tube resistance and the inspiratory flow at end of inspiration. This means that the smaller the inspiration:expiration (I:E) ratio, the greater the end-inspiratory flow and the more the PIP will overestimate the maximum alveolar pressure. If an end-inspiratory pause is used, the pressure during the pause (plateau pressure) represents the maximum pressure in the airway below the tube. Recording PIP only is inadequate, but recording both PIP and plateau pressure gives useful information; for example, increased resistance caused by narrowing of the tube (secretions, kinking) will increase PIP and not affect plateau pressure. If the increased resistance is caused by the lungs of the patient below the tube, then both the PIP and the plateau pressure may increase. In modern ventilators there is no end-inspiratory pause when pressure control mode is used and the proximal inspiratory pressure will always be greater than the maximum tracheal pressure. With normal I:E ratios (< 1:2) there is little risk of incomplete expiration and the proximal pressure will give correct information about the end-expiratory pressure of the patient. However, if the I:E ratio is greater, or the tidal volume is large, or the frequency is high, or respiratory compliance is great, or resistance is great, there may be incomplete expiration and intrinsic PEEP can develop. In such cases, the end-expiratory pressure can only be measured accurately if the end-expiratory pause is prolonged. This creates static conditions in the airway, so that airway pressure is the same from the proximal measurement point down to the alveoli. It is a disadvantage that this intrinsic PEEP level cannot be monitored continuously, as it affects oxygenation and outcome, recruitment of lung and the maintenance of recruitment. The efficacy of triggering the ventilator is enhanced in patients with intrinsic PEEP if the extrinsic PEEP is set just below the intrinsic level. Mean airway pressure calculated from the proximal pressure usually gives correct values as overestimates of pressure during inspiration are balanced by underestimates of pressure during expiration.

Calculated tracheal pressure: By using measurements of flow, proximal pressure measurements and an expression for the resistance of an endotracheal tube developed from laboratory testing of clean tubes and connectors, the tracheal pressure can be calculated continuously (Figure 38). This is a great step forward in the monitoring of ventilator patients. It has been used in commercially available ventilators for automatic tube compensation. Particularly during inspiration, ventilator flow is increased to overcome the endotracheal tube resistance. However, there are some drawbacks with this method. The

calculation of tube resistance is based on measurements with clean tubes and a specific set of connectors. Adding a humidifier increases resistance by 15% and different connectors can have different resistances, which affects the calculated tracheal pressure. It had been found that changes in position or angulation of the endotracheal tube caused large changes in resistance of the tube, so that calculated tracheal pressure may differ considerably from directly measured tracheal pressure. Clean tubes are rare in the intensive care unit environment. Secretions in the

tube will cause overestimation of the inspiratory pressure and underestimation of the expiratory pressure below the tube. In children, where small endotracheal tubes do not allow the use of catheters to measure pressure, Guttman and colleagues calculated tracheal pressure from proximal pressure and flow by using constants calculated from bench tests of endotracheal tubes of specified length, curvature and diameter. They included an expression for inertia that was not used in their adult method.

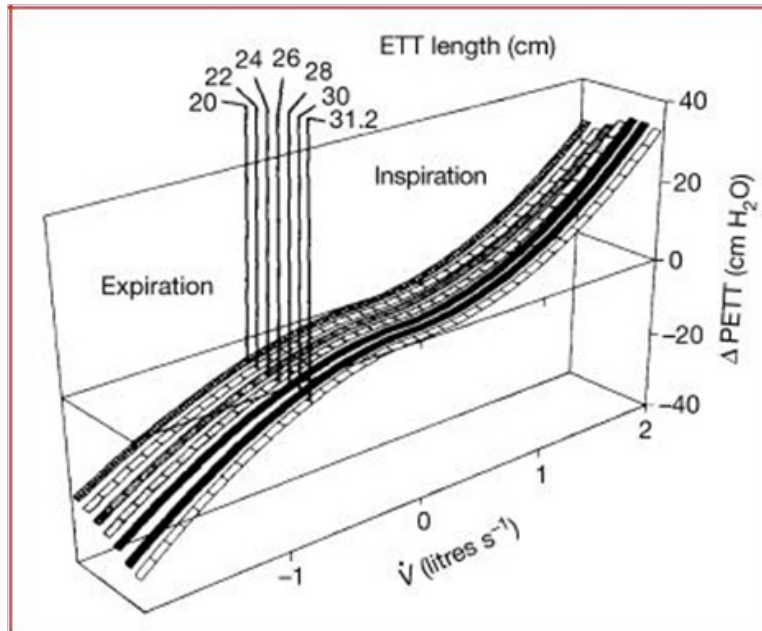


Figure 38: Decrease in pressure (ΔPETT) at different inspiratory and expiratory flows (V) over endotracheal tubes of different lengths with an inner diameter of 7.5 mm. The pressure difference increases with increasing length, as expected. The pattern is most prominent during expiration [37].

Direct tracheal pressure: Direct tracheal pressure measurements can be made by passing a catheter through the endotracheal tube and connecting it to a pressure transducer. It is not clear whether the catheter should have an end-hole or a side-hole, or what should be the exact position of the tip of the pressure catheter. It had been showed that there was a small difference in pressure readings between side-hole and end-hole catheters. It was also found that the difference depended on the position of the catheter tip, and also found large differences in pressure according to whether the catheter was inside the endotracheal tube or below the tip of the tube. Direct measurements are made to obtain values for the tracheal pressure in the trachea where flow changes caused by the transition from tracheal pipe diameter to endotracheal tube diameter are minimized. This is between 2 cm above the carina down to the carina, which is a reasonable place for a reference measurement. With a side-hole catheter, the pressure readings will indicate this reference value only if the side-hole is placed below the tip of the endotracheal tube. When the hole is inside the tube, the static (lateral) pressure will be much higher than the pressure in the trachea because the flow velocity is ~ 10

times greater inside an endotracheal tube with an inner diameter of 7 mm than in the trachea with a diameter of 22 mm. Thus, the correct position of a side-hole catheter is crucial and difficult to verify clinically. An end-hole catheter, on the other hand, measures static minus kinetic pressure during inspiration and static plus kinetic pressure during expiration. This would underestimate pressure during inspiration and overestimate pressure during expiration if the kinetic pressure was large. However, the kinetic energy of gas is so small that the effect on the pressure readings in comparison with the reference pressure is negligible [38].

The pressure catheter can be gas-filled or fluid-filled with a slow drip passing through to keep it clear of secretions. The advantage of a gas-filled catheter is that it gives correct absolute pressure readings irrespective of the transducer position, whereas the fluid-filled catheter requires that the transducer is at the same level as the catheter tip to measure absolute pressure accurately. The fluid-filled catheter is less sensitive to secretions and occlusion. The gas-filled catheter can be occluded or the signal can be dampened by secretions, and has to be flushed with air from a syringe.

It had been found that it is easy to detect occlusion from the pressure signal and waveform for long-term tracheal pressure monitoring, and flushing every 2 hours was necessary. The increase in airway resistance imposed by the pressure cannula in the trachea is small but intrinsic PEEP can occur if the resistance is increased too much. However, direct tracheal pressure measurements provide correct end-inspiratory and expiratory pressures, including intrinsic PEEP caused by ETT resistance, without stopping ventilation and irrespective of ventilatory mode. This is particularly important when an inverse I:E ratio or high respiratory frequencies are used. The difference between end-inspiratory and end-expiratory pressure is needed to calculate respiratory system compliance correctly, and correct values can be obtained only when intrinsic PEEP is considered in addition to the semistatic end-inspiratory pressure. In addition, the pressure waveform will show clearly that the changes in pressure during inspiration and

expiration below the tube are much slower than above the tube during mechanical ventilation (Figure 39). The difference is most marked during inspiration with pressure control ventilation, where proximal pressure increases promptly to the pressure value set in the ventilator and the tracheal pressure increases more slowly because of the endotracheal tube resistance. Anyhow, recently Söndergaard and colleagues described direct tracheal pressure monitoring using a fiber-optic pressure transducer with a fiber dimension of 0.25 mm, which has almost no effect on resistance when it is placed in the endotracheal tube, even with one as small as 3 mm in inner diameter. This method is still under development but it could be used in combination with proximal pressures and flow to measure inspiratory and expiratory tube resistance continuously. This could provide a warning for tube obstruction, which is a constant concern in pediatric intensive care.

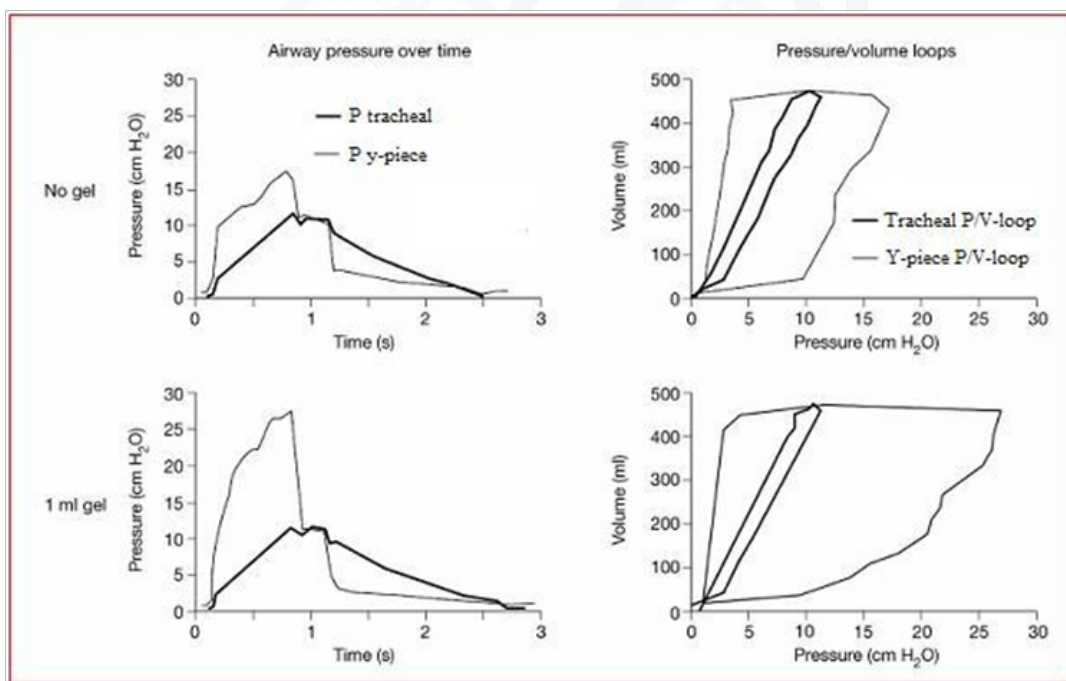


Figure 39: Proximal and distal airway pressure. The left column shows the directly measured tracheal pressure (thick black line) and Y-piece pressure (thin black line) in an endotracheal tube with inner diameter 7 mm without and with 1 ml of gel (mimicking secretions) deposited in the tube. The corresponding P-V loops are shown in the column to the right. Note that the peak tracheal pressure is not affected by the gel, but the peak inspiratory pressure measured at the Y-piece is markedly increased. The plateau pressure from the Y-piece measurement corresponds with the peak tracheal pressure because it is measured during static conditions. The decrease in tracheal pressure during expiration is much slower than the corresponding pressure at the Y-piece, which decreases almost immediately to the extrinsic PEEP level. In the P-V-loop graphs, a large increase in Y-piece loop area is noted after gel administration, but the tracheal P-V loop is almost unchanged. The main difference in the Y-piece loop is seen during inspiration, when the decrease in pressure across the tube is markedly increased by the gel in the tube [37].

Pressure- volume curves

A P-V diagram plots the change in pressure P with respect to volume V for some process or processes. Typically in thermodynamics, the set of processes forms a cycle, so that upon completion of the cycle there has been no net change in state of the system; i.e. the device returns to the starting

pressure and volume. The (Figure 40) shows the features of a typical P-V diagram. A series of numbered states (1 through 4) are noted. The path between each state consists of some process (A through D) which alters the pressure or volume of the system (or both). A key feature of the diagram is that the amount of energy expended or received by the

system as work can be estimated as the area under the curve on the chart. For a cyclic diagram, the net work is that enclosed by the curve. In the example given in the figure, the processes 1- 2-3 produce a work output, but processes from 3- 4-1 require a smaller energy input to return to the starting position / state; thus the net work is the difference between the two. Note that this figure is highly idealized, and a diagram showing the processes in a real device would tend to depict a more complex shape of the P-V curve. shows that the pressure-volume ratio (PVR) tracing of the respiratory system is not linear; rather, in general it is sigmoid in shape with two extremities where E is greater, and a relatively linear intermediate zone in which E is

smaller. The three segments of the inspiratory arm of the curve are separated by lower inflexion point (LIP) and upper inflexion point (UIP) (Figure 41) that allow us to identify the pressures at which recruitment and derecruitment begin and end. Accordingly, it has been postulated that tidal ventilation (TV) should occur in the central zone of the PVR tracing, between the two inflexion points. On a ventilator, pressure volume curves can be created. Compliance represents the proportion of change in volume to that of change in pressure. ($C = \text{Vol} / \text{Press}$). The pressure volume-curve plots the two components (inspiration and expiration) throughout the respiratory cycle.

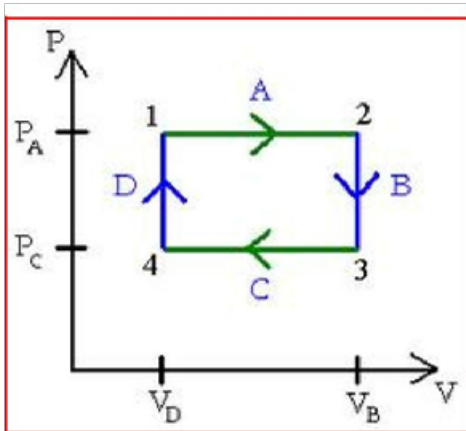


Figure 40: Author archive.

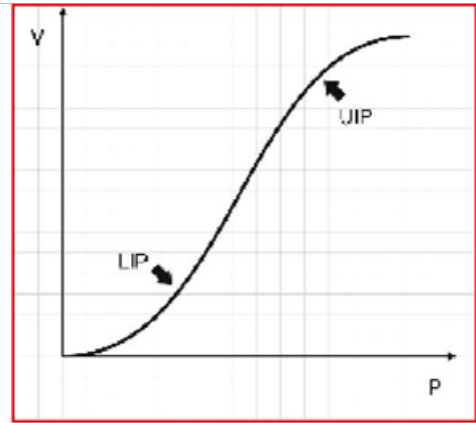


Figure 41: Author archive.

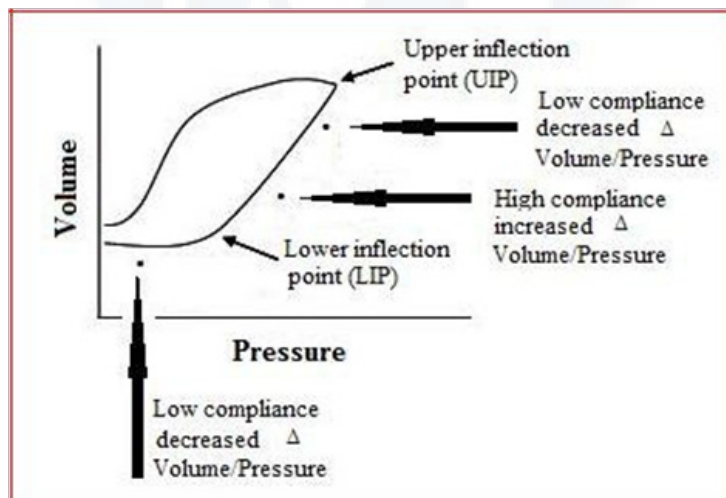


Figure 42: Effect of compliance on the Pressure-Volume curve (author archive).

With regards to alveolar recruitment, inspiration is considered as a key. Applying this to collapsed alveoli and static/dynamic resistance is demonstrated in (Figure 42). On the left side of the plots (just below the lower inflexion point [LIP]), compliance is low and a significant amount of pressure must be exerted to obtain a relatively small change in volume. However, the forces required to change

volume (i.e., high compliance) change dramatically at the lower inflexion point up to the upper inflexion point (UIP). Between these points, a relatively small change in pressure results in significant volume change. The inspiration between LIP and UIP represents optimal lung usage. In clinical terms, the goal is to keep patients inspiring between the LIP and UIP.

The total lung capacity was calculated as the upper asymptote of the curve. The maximum compliance was calculated as the maximal slope of the pressure-volume curve (as compliance is the first derivative of the pressure-volume curve, maximal compliance is the value where the second derivative equals zero). The inflection point and points of maximum curvature were calculated as the

pressure values where the second and third derivatives of the model equal zero respectively. Due to the sigmoid nature of the models, there are two points of maximum curvature [MC] in each limb (the so-called maximum curvature "lower" and "upper" inflection points [LPMC and UPMC]). The general values of the parameters are presented in (Figure 43).

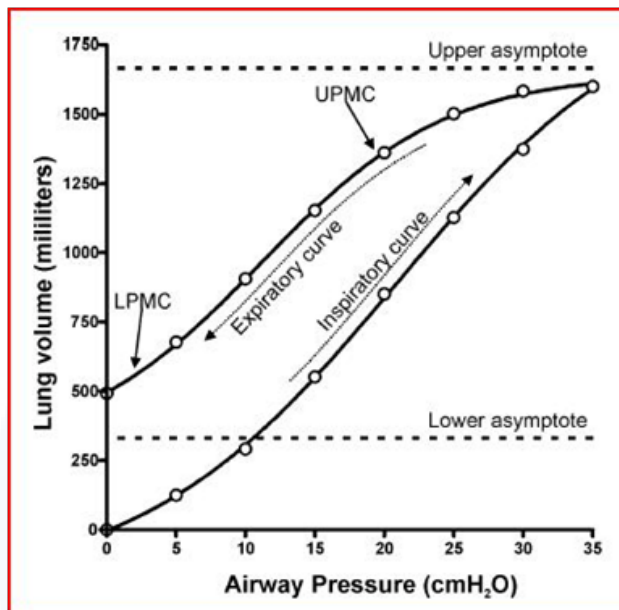


Figure 43: Author archive.

Rahn et al. and Fenn had established the modern analysis of respiratory mechanics by describing the pressure-volume curve of the respiratory system. They described a sigmoid static P-V curve where compliance was small below the functional residual capacity (FRC). At FRC, compliance was greatest and then decreased progressively with increasing lung volume. The transition from small compliance at low volumes to greater compliance is the lower inflection point (LIP), and the transition from greater compliance to smaller at the end of inflation is the upper inflection point (UIP). In subjects with normal lungs there is no LIP when starting inspiration from FRC. In 1984, Matamis et al. had related the pattern of the chest X-ray, the stage and the total respiratory system P-V curve in patients with ARDS. Very early in the disease, compliance was normal, with little hysteresis and no LIP. Normal compliance, increased hysteresis and an LIP were found in the early period, decreased compliance, marked hysteresis and an LIP occurred in the later stages of the disease, and in the end-stage a marked lowering of compliance, no increase in hysteresis and no LIP were noted. The lower inflection point was believed to reflect the pressure level at which collapse of alveoli occurred during expiration and then reopened during the next inspiration. This was considered to cause damage, referred to as atelectrauma. At the top of the P-V curve, compliance decreased and this upper inflection point was considered to occur when the lung was

over-inflated. It was considered that tidal ventilation and PEEP should be set so that end-expiratory pressure was above the lower inflection point to prevent cyclic collapse of alveoli and the end-inspiratory pressure kept less than the UIP to avoid over-stretching. It had been showed that avoiding collapse and overstretching reduced ventilator induced lung injury and multi-organ failure. However, there was no consensus on how to set PEEP. It is puzzling that the first portion of gas, often not more than 100-150 ml, is sufficient to create enough pressure to open a great number of alveoli or terminal bronchioli. The compliance of the P-V curve below the LIP is often not more than 10 ml/cm H₂O. If all terminal bronchioli were closed, the event could perhaps be explained, but if some airways are not closed and still in continuity with open alveoli, where compliance would definitely be >10 ml/cm H₂O, then the first part of the gas would be delivered to this part of the lung rather than the least compliant parts. Also, why are lung mechanics quite different during dynamic conditions, i.e. normal tidal breathing, compared with static measurements? It had been showed that the time to collapse alveoli is very short when pressure is reduced in the airways. When dynamic and semistatic P-V curves are compared (Figure 44), a lower inflection point that is quite visible during a low flow inflation P-V curve disappears when tidal breathing with a frequency of 20 is used. It seems that the time available for collapse is too short under these circumstances (Figure 45). There

are differences in dynamic and static P-V curves obtained with the SLICE method and the dynostatic algorithm, which are two breath- by-breath methods for alveolar P -V curves (vide infra). These show the greatest compliance at the start of inspiration and a progressive decrease in compliance during the whole inspiration. This contrasts

with the static P-V curve, where compliance is extremely low below the inflection and then increases after the LIP. The initial compliance of a dynamic P-V curve is often 5-10 times greater than in the static P-V curve. Assessment of respiratory mechanics seems to need dynamic, continuous monitoring rather than static, intermittent measurements.

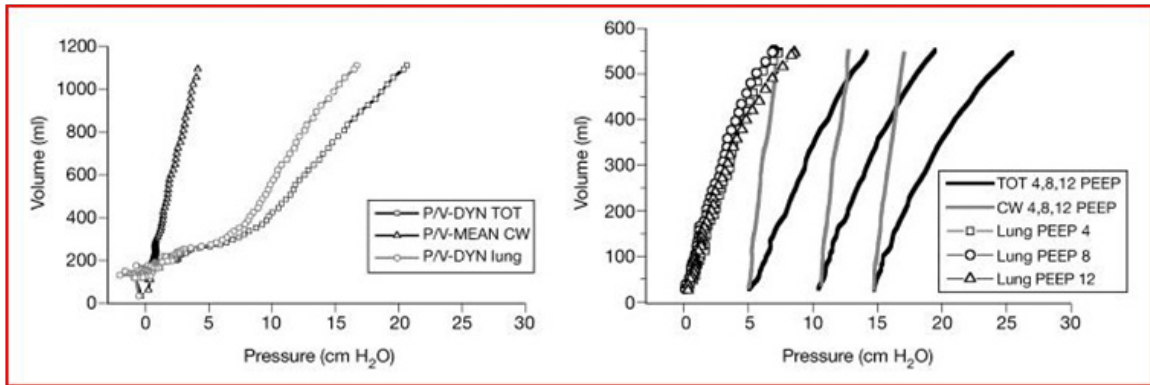


Figure 44: The left graph shows development of respiratory mechanics in a patient with ALI during low-flow inflation. Lower inflection points are noted at different positions in the total respiratory system (P/V-DYN TOT) and the lung dynostatic P-V curve (P/V-DYN Lung). In the P-V curve of the chest wall (P/V-MEAN CW) no LIP is seen. In the column to the right the respiratory mechanics are shown during normal tidal breathing in the same patient. No LIP can be seen in the P±V curves of the total respiratory system (TOT), chest wall (CW) or lung. The tidal breathing graph shows a successive decrease in volume-dependent compliance in the total respiratory system and lung within each breath [37].

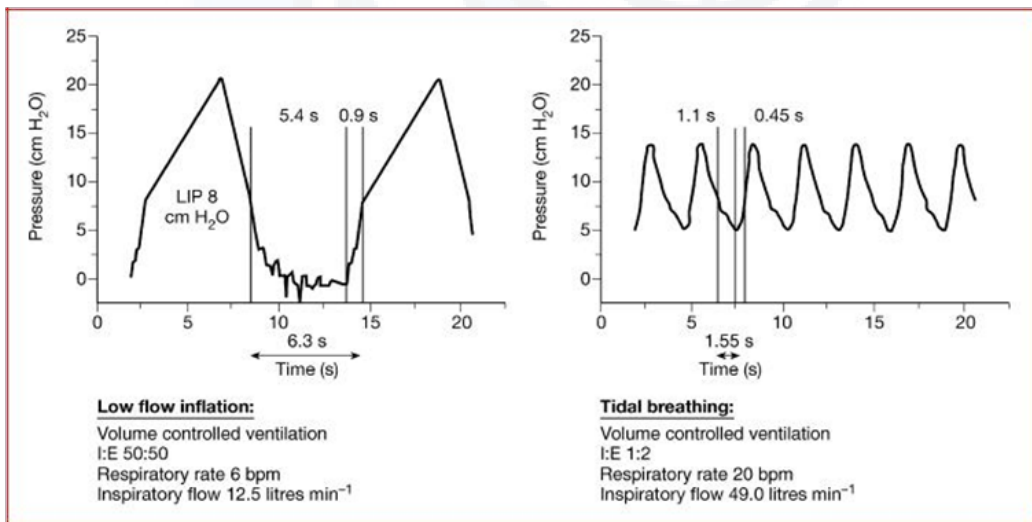


Figure 45: Changes in alveolar pressure over time in an ALI patient (same patient as in Figure 43) during low-flow inflation and normal tidal breathing. During low-flow inflation, the time when the alveolar pressure is below the lower inflection point (LIP) (~ 8 cm H₂O) is 6.3 s, but it is only 1.55 s during normal tidal ventilation. In CT studies of end-expiratory breath-holding at zero end-expiratory pressure, airway collapse begins after 0.6 s and is almost over after 4 s. During low-flow inflation, this allows time for the airways to collapse, but this might not be the case during normal tidal breathing. Thus, the respiratory system is not only volume- and pressure-dependent but also time-dependent [37].

Static/semistatic methods for P-V curves and loops:

The super -syringe: The static reference method is the super- syringe method, applying increments of volume with 50-100 ml gas up to a total volume of 1000- 2000 ml. After each increment, the static airway pressure is measured during a pause of a few seconds when there is no flow,

and the pressure is the same in the entire system from the super-syringe to the alveoli. The lung is then deflated in the same way and an inspiratory and expiratory P-V curve is plotted. The whole procedure takes 45-120 s, during which oxygen uptake will continue from the alveoli. Carbon dioxide elimination will be close to zero during the inflation. Inspiration resembles a long apnea, so that alveolar and

arterial carbon dioxide partial pressures increase. This reduces the evolution of carbon dioxide from blood to alveoli as the content of carbon dioxide increases with increasing partial pressure. Thus, during stepwise slow deflation the carbon dioxide output from the alveoli will be less than before the start of the measurement, while oxygen uptake will continue unchanged. This causes expired volume to be less than inspired volume and the P-V curve has a marked hysteresis. In a patient with ARDS, with a small functional residual capacity, and sepsis with an increased oxygen uptake of ~300 ml/min and carbon dioxide production of 250 ml/min, if the inflation-deflation procedure lasts for 60 s the deflation volume would be 200-300 ml smaller than the inflation volume. In addition to this apparent hysteresis, which is an artefact from the mechanical point of view, the slow, stepwise inflation to a high pressure will also cause hysteresis because very slow compartments of the lung will be inflated and collapsed alveoli will be recruited. Both these phenomena mean that the deflation volume will be substantially smaller than the inflation volume. Compression of inflated gas and changes in humidity and temperature may cause further artefacts. Mathematical correction of these factors is advised but may be insufficient. Thus, this method creates results which would not be seen during normal ventilator treatment.

The multiple occlusion technique: To mimic conditions during normal ventilation and ventilate the patient during the measurement, the multiple occlusion technique has been proposed. It uses a sequence of different-sized volume-controlled inflations with an end-inspiratory pause to allow semistatic pressure measurements. Pressure and volume are plotted for each end-inspiratory pause to form a static P-V curve. If expiratory interruptions are also done, a static expiratory P-V curve is obtained. In spite of the fact that these inspiratory and expiratory P-V curves are truly static, no hysteresis is found even in ARDS patients. This is explained by how the measurement points on the curves are obtained: they are obtained by a series of normal, but varying breaths and the artefacts caused by gas exchange do not occur. The largest tidal volumes used with this technique may cause recruitment, but this is limited because of the short time the pressure is very high during tidal breathing. The entire sequence of measurements may take 5-10 minutes and all the tidal volumes must be in volume control mode. The multiple occlusion technique is the superior semistatic method and the inherent measurement artefacts are minimal. This method can be regarded as static if the end-inspiratory pause is long enough also for viscoelastic pressure equilibrium. Even with a short end-inspiratory pause the pressure at the end of such a pause will be within 1 cm H₂O of a static measurement.

The low-flow inflation technique: The low-flow inflation technique uses a very small constant inspiratory flow to generate a large total volume. The low flow causes a minimal but recognizable pressure decrease over the endotracheal tube, which means that the dynamic inspiratory pressure volume curve will be shifted to the right depending on the endotracheal tube resistance and the flow selected compared with a true static P-V curve.

The slope (compliance) of the curve is parallel with a static P-V curve only if airway resistance is constant throughout the inspiration. This is doubtful, as reliable data show that resistance decreases as the lung is inflated and the airways widen. As the flow is low, the duration of the inspiration will be long and the same artefacts described with the super-syringe technique are present to some extent. If the total inflated volume is great, with a large end-inspiratory pressure, this procedure will recruit collapsed lung. The low-flow inflation method does not analyze expiration and no information on hysteresis, real or artefactual, is obtained. Another drawback of the method is that the procedure requires resetting the ventilator and only volume-control ventilation can be used. Thus, lung mechanics estimated with low-flow inflation do not reflect the lung mechanics of normal tidal breathing.

Generally a common feature of these static and semistatic methods is that they require stopping therapeutic ventilation for a longer (super-syringe) or shorter period (low-flow inflation) or using a sequence of breaths that is different from the selected therapeutic settings. Such intermittent and static or semistatic methods may not be relevant in predicting the mechanical behavior of the lung under dynamic conditions, where resistance and compliance depend on volume, flow and respiratory frequency.

Dynamic methods for P-V loops: The obvious advantage of dynamic methods is that they are continuous and can be used as ventilator treatment is applied. Dynamic methods are more methods of monitoring than of measurement, and their lack of precision is counterbalanced to some degree by their capacity to follow trends.

Dynamic, proximal (to the endotracheal tube) P-V loops: Continuous display of pressure from the patient connection or ventilator can be plotted against volume to give breath-by-breath P-V loops. The effect of endotracheal tube resistance makes the interpretation of these loops very difficult. In pressure control mode, the inspiratory part of the loop shows an immediate increase in pressure to the set inspiratory pressure level and then an increase in volume with constant pressure level. However, the pressure in the lungs increases much more slowly and the square waveform of the loop recorded from ventilator pressure has little in common with the P-V events in the alveoli during inflation. In volume-control mode the inspiratory part of the proximal loop has an almost parallel but right-shifted course compared with the alveolar P-V curve. The magnitude of the shift depends mainly on the endotracheal tube resistance and the flow through it. As the inspiratory part of the proximally recorded loop is parallel to the inspiratory part of a loop from pressures measured below the tube, changes in the waveform show events occurring in the lungs. Thus, a curving of the plot during late inspiration reflects decreasing compliance or even overstretching of the alveoli. In neither pressure-controlled nor volume-controlled ventilation does the upper end of the loop reflect true peak alveolar pressure, because the pressure decrease over the tube is not distinguishable. The expiratory part of the proximally recorded loop has the same form in pressure-control and

volume-control mode and mainly reflects the low resistance of the expiratory pathway of the ventilator. Pressure measured in the ventilator tube will decrease almost immediately to atmospheric pressure or the end-expiratory pressure level set in the ventilator. The pressure in the trachea decreases more slowly. Intrinsic PEEP cannot be detected in the proximal loop. Because neither peak airway pressure at end-inspiration nor end-expiratory pressure is measured accurately when the proximal pressure is taken, compliance will be underestimated.

The stress index method: It analyses the pattern of proximal pressure change during volume-controlled inspiration. A decrease or deflection of the slope during inspiration indicates increasing compliance and possible recruitment of lung, and an increase or inflection in the slope suggests over-inflation and a decrease in compliance. The technique assumes that airway resistance in the endotracheal tube and patient airway is constant during inspiration. This may not be correct in the patient airway, where airway resistance decreases as the airway widens with lung inflation, but endotracheal tube resistance will be almost constant during constant-flow inspiration. As the endotracheal tube contributes ~70% of the resistance between the Y-piece and the alveoli, changes in the resistance of the patient airway during inspiration probably have a negligible effect on the accuracy of this method.

Dynamic, distal (to the endotracheal tube) P-V loops: Plotting tracheal pressure against volume provides dynamic distal (tracheal) P-V loops (Figure 46) where the influence of endotracheal tube resistance during inspiration is removed, and during expiration endotracheal tube resistance is accounted for. Such a loop has an area that is only 30% of a loop made using proximal pressures, and the difference is caused by endotracheal tube resistance (Figure 47). With the distal loop, the inspiratory part increases more rapidly during pressure-control mode as the flow is great at first, compared with volume-control mode. The expiratory limb shows a slow decrease in pressure and volume as the endotracheal tube resistance delays the pressure decrease in the airways. Over-distension can be detected even in pressure-control ventilation with decelerating flow, not as an upper inflection point but rather as a progressively decreasing compliance with increasing inspiration-an over-distension zone. The endpoints of the tracheal loop give the pressure values used for calculation of conventional endpoint compliance. It is clear, especially where marked over-distension is present and the loop is convex upwards, that a line through the endpoints will lie outside the tracheal loop. Thus, compliance must vary with volume, and compliance will be greater at the beginning of the breath and then decrease with increasing volume.

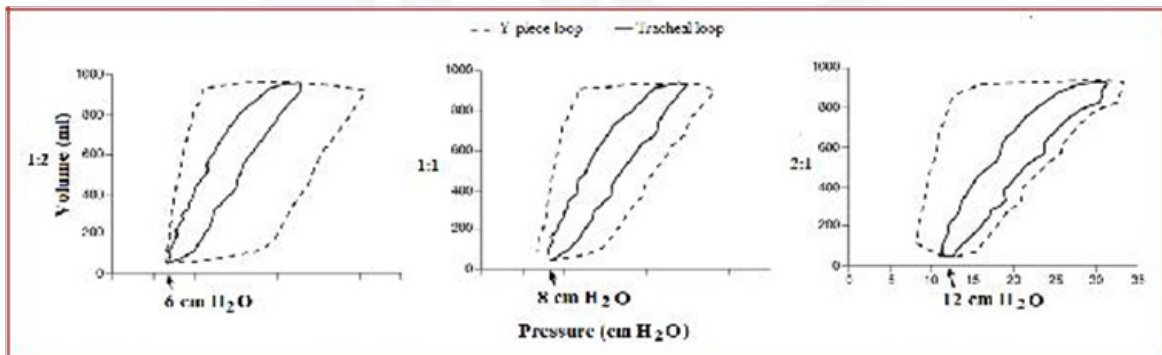


Figure 46: A patient with volume-controlled ventilation with extrinsic PEEP 8 cm H₂O and increasing I:E ratio. Development of intrinsic PEEP (indicated by arrows) is detected in the tracheal P-V loop but not in the Y-piece loop. Evidence of successive over-inflation and decreasing compliance after increasing the I:E ratio, despite unchanged tidal volume, is explained by the development of intrinsic PEEP [37].

Dynamic alveolar P-V curves:

Multiple linear regression: The equation of motion is:

$$P = V/C + V R + PEEP$$

Where V/C is the pressure necessary for expanding the lung, $V R$ is the pressure necessary to overcome the resistance of the airways and PEEP is the pre-existing pressure in the lungs. Values for C and R can be found by a statistical method, multiple linear regression, also known

as the least-squares fit method (LSF or LSM). This method assumes constant compliance and resistance throughout the whole breath or for the inspiratory and expiratory parts separately. Because this assumption may not be valid, the method has been developed by dividing the breath into six slices and applying the method for each slice (Figure 48). The assumption is that resistance and compliance remain constant within each slice. The method estimates changes in compliance in six parts of the breath. This forces the inflection points to be positioned at the intersection between the slices. The number of slices can be increased, but this reduces the data available for the multiple linear regression computation and the precision of the estimates of C and R .

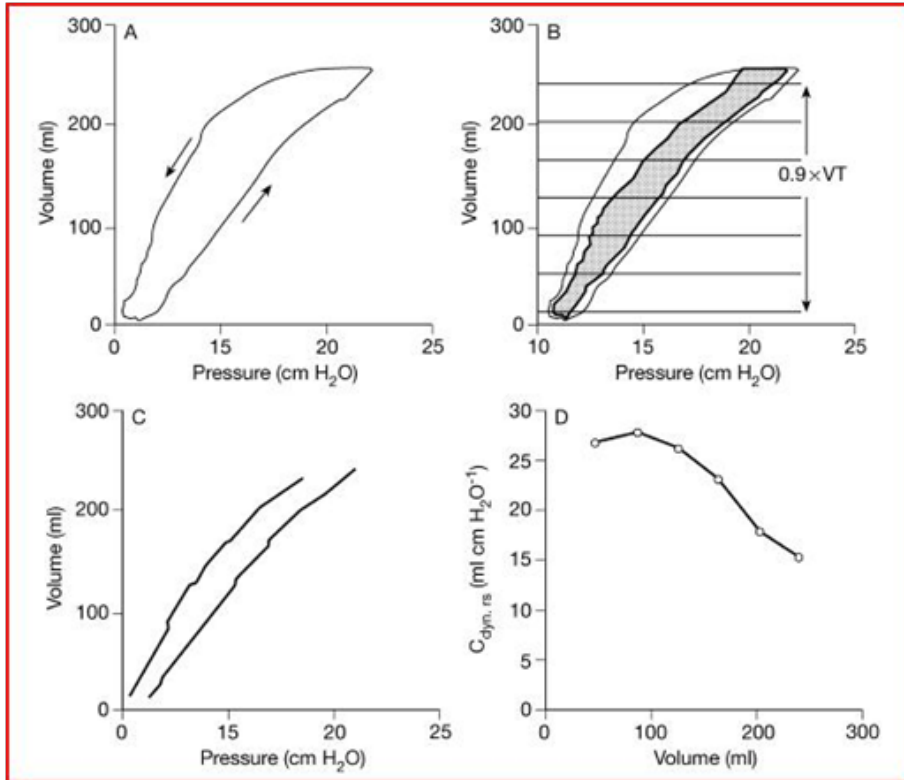


Figure 47: Proximal and tracheal loops and the SLICE method-based compliance-volume curve in a surfactant-deficient animal. (A) Proximal loop with up-arrow indicating inspiratory limb and down-arrow indicating expiratory limb of loop. (B) Calculated tracheal pressure vs. volume displayed inside the proximal loop. The 5% lowest and highest volume slices are excluded from analysis because of interference from the ventilator valve and large volume acceleration. The remaining 90% of the tidal volume is divided into six slices and compliance and resistance are calculated by multiple linear regression for each slice. (C) Calculated and measured tracheal pressures. They coincide almost totally, indicating good agreement. (D) Compliance-volume plot obtained using the SLICE method [37].

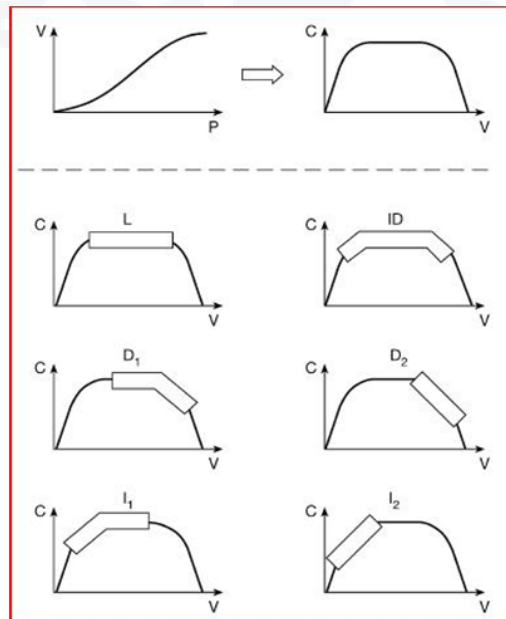


Figure 48: Top panels show an S-shaped P-V curve, with a corresponding trapeziform compliance-volume curve. Below are six predefined shapes of parts of the compliance-volume curve. L is the linear part, with constant compliance, of the SLICE method. ID indicates the increasing-decreasing compliance pattern in the tidal volume. D₁ and D₂ respectively show moderately and severely decreasing compliance with increasing tidal volume. I₁ and I₂ respectively show moderately and severely increasing compliance with increasing tidal volume. The SLICE method gives information on volume-dependent compliance on a breath-by-breath basis [37].

The dynostatic algorithm: Káráson et al. [39] proposed a method for breath-by-breath analysis of alveolar P-V curves [39]. The method is based on the tracheal P-V loop and analysis of pressure and flow at the same lung volume during inspiration and expiration. Inspiratory and expiratory resistance at each volume is assumed equal. Alveolar pressure is calculated using the equation of motion, which is the basis of the dynostatic algorithm. The calculation is repeated for a number of volume values and alveolar pressure is estimated. A plot of alveolar pressure against

volume can be made during dynamic ventilation (Figure 49). In contrast to other methods of dynamic calculation of the alveolar P-V curve, such as the multiple linear regression method, the only assumption is that inspiratory and expiratory resistance are equal at each isovolume, and do not have to be constant throughout inspiration or expiration. The dynostatic algorithm does not require constant flow and gives correct dynamic alveolar P-V curves irrespective of ventilatory mode, without needing an end-inspiratory pause to calculate alveolar pressures.

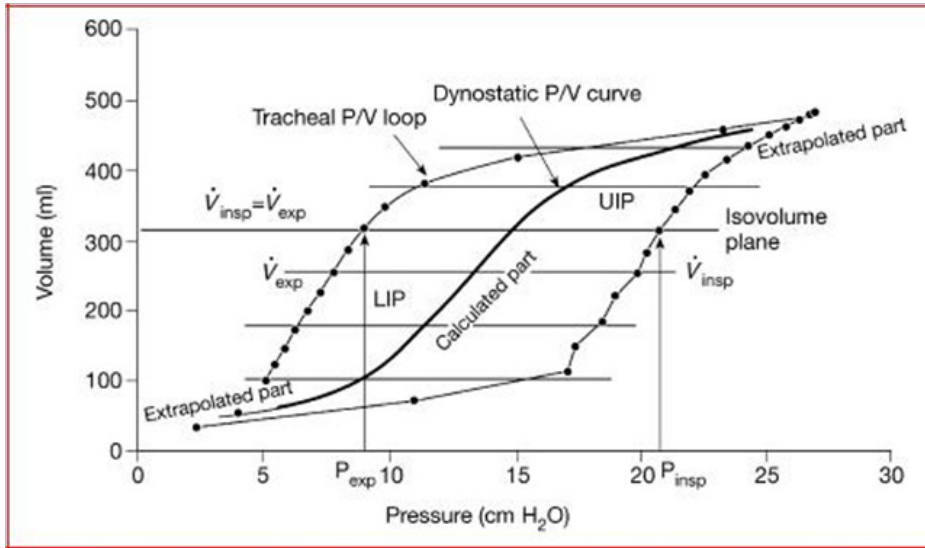


Figure 49: Schematic graph of the mathematical background for the calculation of the dynostatic P-V curve. Alveolar pressure is calculated according to the equation of motion. Every point on the dynostatic curve ($P_{X_{dyn}}$) is calculated using pressure and flow values at isovolume levels (indicated by broken lines) during inspiration and expiration in the tracheal P-V loop [37].

To test the effect when inspiratory and expiratory resistance values are unequal, which contradicts a basic assumption of the dynostatic algorithm, the investigators used a lung model in which the resistances could be varied independently. Within a wide range of $R_{insp}:R_{exp}$ ratios from 2.3:1 to 1:2.3, the dynostatic algorithm P-V curve related very well to the reference alveolar P-V curve in the lung model. In ARDS patients, R_{insp} and R_{exp} are nearly equal. The reason for the good agreement is that the tracheal P-V loop used for the calculations and the inspiratory-expiratory tracheal pressure difference is small (5-7 cm H₂O at mid-tidal volume) where the difference is usually greatest. Thus, even if the expiratory resistance is twice the inspiratory resistance, the alveolar pressure has to be between the inspiratory and expiratory limbs of the tracheal loop and the possibilities for deviation are small. A typical feature of the dynostatic algorithm P-V curve is that compliance is great at low volume and decreases as the volume increases. The decrease in compliance as lung volume increases is much less when compliance is calculated in the conventional way, whereas the final compliance of the dynostatic algorithm P-V curve shows a marked decrease (Figure 50). It had been found that no lower inflection points in patients with

ALI or ARDS, but this may have been because they did not decrease PEEP to zero during measurements. The dynostatic algorithm P-V curve can be regarded as an inspiratory P-V curve superimposed on an expiratory twin P-V curve. Because the time when alveolar pressure value is known, at each lung volume during inspiration and expiration, a plot of alveolar pressure can be made [37].

Pulmonary Mechanics in Intensive Care Patients

Basic principles

Classic respiratory mechanics is based on Newtonian physics as expressed in the equation of motion. The respiratory system is considered to be a resistive and elastic element in series. Any pressure applied to it is either stored as elastic pressure (P_{el}) or dissipated as resistive pressure (P_{res})

$$P(t) = P_{el}(t) + P_{res}(t) \quad (1)$$

Where t indicates a particular time. In its simplest interpretation the elastic element represents lungs and chest wall, while the resistive element represents ventilator

tubing, tracheal tube and airways. It follows that during inflation of the relaxed respiratory system P_{el} can be approximated by alveolar pressure (P_{alv}) and P_{res} by the difference between proximal airway pressure (P_{aw}) and P_{alv} .

$$P_{el}(t) = P_{alv}(t)$$

and

$$P_{res}(t) = P_{aw}(t) - P_{alv}(t)$$

If flow is zero then P_{alv} equilibrates with P_{aw} so that P_{el} can be estimated from airway occlusion pressure. This is how a static recoil pressure-volume curve measurement is made. As P_{el} is a function of volume and P_{res} a function of flow Equation 1 can be rewritten as

$$P(t) = P_o + EV(t) + RV(t)\theta$$

where P_o is the elastic recoil pressure at relaxed end-

expiration. In the clinical literature P_o is often referred to as total PEEP. The constants E and R denote respiratory elastance and resistance and are the factors that scale volume and flow to yield P_{el} and P_{res} , respectively. Clinicians are more likely to use the term compliance (C), which is the inverse of E . During relaxed expiration, flow is generated by P_{alv} (relative to P_{aw}), in that it is determined by the elastic recoil of the respiratory system and by the properties of the resistive element (i.e. properties of airway, tracheal tube and equipment). As both determinants vary with lung volume, so must passive expiratory flow. In normal lungs expiratory flow varies approximately linearly with volume and decreases exponentially with time. Rearranging Equation 4 shows that the slope of the passive expiratory volume flow relationship equals R/E (or $R \cdot C$), which has the units of time. This quantity is the time constant of the respiratory system and defines the time it takes for the elastic element to passively empty approximately 63% of its contents. Inspection of linearity and slope of the expiratory flow-volume curve can be useful when a diagnosis of airway or tracheal tube obstruction is suspected.

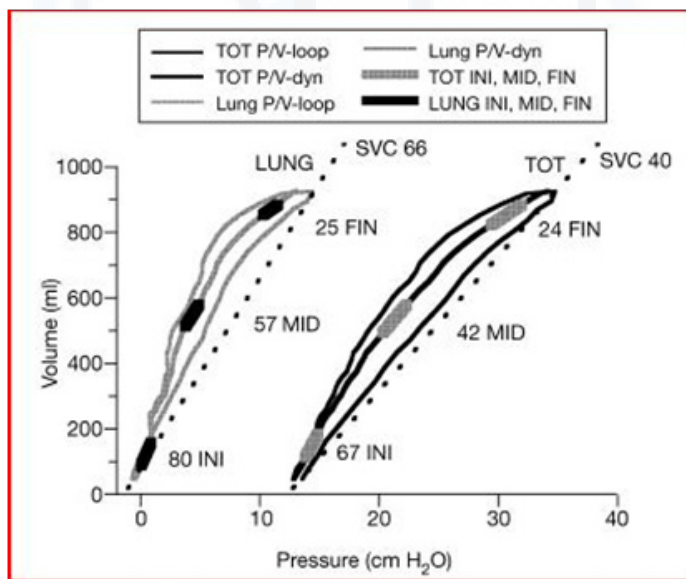


Figure 50: P-V loops in a patient with ALI from the lung and total respiratory system, based on tracheal pressure measurements. Conventionally, compliance is calculated as tidal volume divided by the difference between peak and end-expiratory pressure. The initial (INI), middle (MID) and final (FIN) volume-dependent compliances within the breath for the total respiratory system (TOT) and the lung (LUNG) are shown. Note that initial compliance is markedly greater and final compliance at the end of inspiration is markedly less than conventional single-value compliance (SVC). Calculation of volume-dependent compliance for different parts of the tidal volume could be a sensitive marker for collapse and over-inflation of lung [37].

Assessment of respiratory mechanics in the diagnosis and management of patients with injured lungs

The realization that the physical stress of mechanical ventilation can damage lungs or may amplify non-physical injury mechanisms has generated renewed interest in the mechanics of injured lungs. Publications on this topic have increased exponentially in the last decade (Figure 51)

[40]. An International Consensus Conference held in 1993 defined acute lung injury (ALI) and adult respiratory distress syndrome (ARDS) as conditions characterized by abnormal pulmonary gas exchange in the presence of bilateral pulmonary infiltrates. These features are non-specific, and must be related to the clinical setting and not attributed to left heart failure. ALI and ARDS differ only with respect to the severity of the gas exchange impairment and have a wide variety of causes.

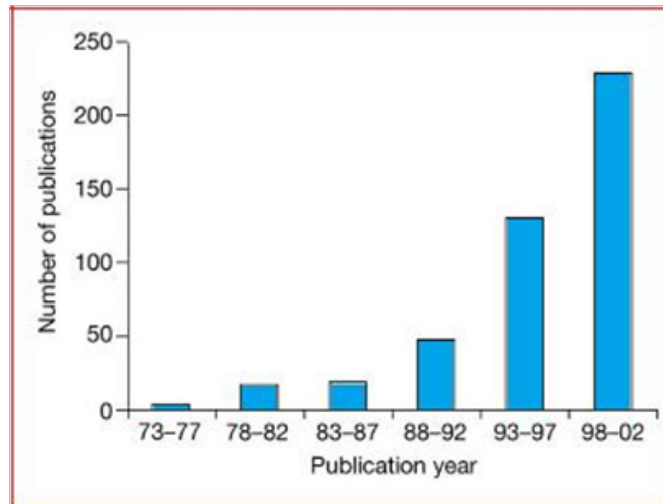


Figure 51: Results of a Medline search of the term 'respiratory mechanics' in association with ALI or ARDS [40].

Injury mechanisms and their consequences on lung mechanics: Irrespective of cause, injured lungs have an abnormal barrier function. The pulmonary capillaries are leaky and the alveolar epithelial cells cannot clear water and solute from the alveolar space properly, with important consequences for the mechanical properties of the lung. Injury and edema increase pulmonary elastance and resistance. Numerous mechanisms have been proposed to explain this. Presently the most popular one is the baby lung concept: alveolar flooding causes collapse of the dependent lung so the greater lung elastance reflects the reduced number and smaller volume of near normal, nondependent, and recruitable units. Other proposed mechanisms include increased surface tension by inactivation of surfactant, airway block by air-liquid interfaces and bubble formation in small airways, reflex-bronchoconstriction, pneumoconstriction caused by release of inflammatory mediators and peri-bronchial edema.

Susceptibility of injured lungs to ventilator-induced lung injury [VILI]: Two attributes of the injured lung explain its susceptibility to additional ventilator induced lung injury:

- a) The number of alveoli that can expand during inspiration is decreased.
- b) The distribution of liquid and surface tension varies in distal airspaces and hence the local impedances to lung expansion are heterogeneous.

The first attribute is the key abnormality in the baby lung concept. It explains the increased risk of lung injury from overdistension of aerated low impedance units. The second attribute, heterogeneity in regional impedances to lung expansion, has several consequences:

- i. One is a large shear stress between neighboring, interdependent units that operate at different volumes. Tissue attachments between large aerated units and smaller neighboring flooded or collapsed units carry

a stress that is substantially greater than the average transpulmonary pressure.

- ii. Another consequence is injury to small airways and alveolar ducts caused by their repeated opening and collapse, by energy dissipation during liquid bridge fracture or from the stress that is imposed on lining cells by the movement of air-liquid interfaces with respiration.

However, the relative contributions of these related injury mechanisms in different diseases are simply not known. Inferences from animal experiments with short-term endpoints are of interest but do not show which mechanism is important in which circumstance. Study of bubble and liquid flow in tubes, although hindered by simplifying assumptions (e.g. rigid tube of uniform diameter, smooth surface), are giving some quantitative data on this problem.

Whole respiratory system mechanics [methods and mechanistic interpretation]: Much literature now describes the static and dynamic pressure volume relationships of injured lungs, and the effects of interventions such as PEEP and recruitment maneuvers (vide supra). A great deal of emphasis has been placed on methods and analytic approach, but, there is little agreement how these measurements can be used clinically. The static respiratory system pressure-volume curve of patients with injured lungs has certain characteristics (Figure 52):

- a) An S-shaped inflation curve with an upper and lower inflection point (UIP and LIP, respectively).
- b) An increased recoil pressure at all lung volumes.
- c) A reduced compliance defined by the slope of the inflation curve between LIP and UIP.

For many years the pressure at LIP was regarded as the critical opening pressure of collapsed lung units and was considered a target of best PEEP. The pressure at UIP, in

turn, was considered to indicate alveolar overdistension that should not be exceeded during mechanical ventilation [41]. These ideas have been challenged because most values from the P-V curve have low specificity. For example, when lungs are rinsed with mineral oils to increase surface tension, the LIP is prominent even though the lung units are open, that is aerated. Similar characteristics are observed when saline filled lungs are inflated with air as happens during a

newborn's first breath. Attention is now on edema, airway liquid and interfacial phenomena as causes of increased opening pressure and lung impedance. In some patients the LIP originates in the chest wall and not the lung. This is likely in patients with small thoracic volumes because the chest wall P-V curve is nonlinear in the low volume range. Nevertheless, even in these patients the contribution of the chest wall to the pressure at LIP is quite small.

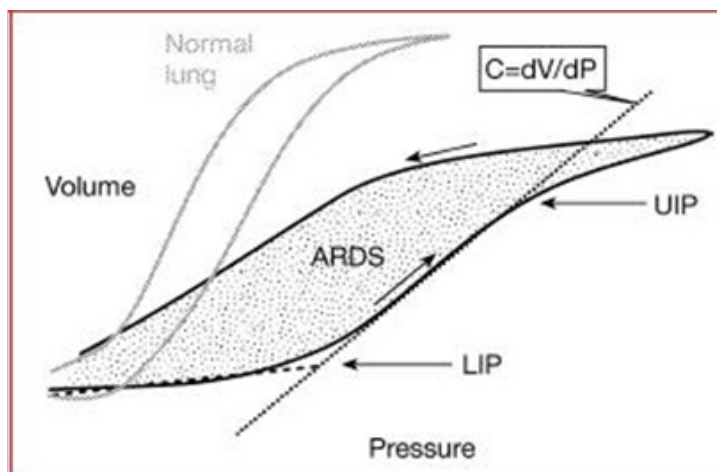


Figure 52: The characteristic PV changes in injured lungs [40].

Because the chest wall may generate P-V artifacts, some have advocated esophageal pressure measurement to guide management in patients with injured lungs. Advocates usually emphasize that even in recumbent patients the change in esophageal pressure (ΔP_{oes}) reflects the average change in lung surface pressure or pleural pressure (ΔP_{pl}). However, support for this statement is from experiments on normal animals. Diseased lungs expand non-uniformly and non-uniform lung expansion is associated with non-uniform distributions of lung surface pressure. This means that the position of the esophageal balloon at which ΔP_{oes} mirrors ΔP_{pl} varies greatly with posture, mode of breathing and with the pattern of respiratory muscle activation. In other words, in injured lungs the calibration of the device with an occlusion test does not guarantee that the signal, that is ΔP_{oes} , will represent ΔP_{pl} under the conditions under which the actual measurements are made. Any concern about erroneous conclusions from esophageal manometry in patients with ARDS is speculative because it is not possible to measure P_{pl} without artifact in humans. However, an example is laid in support of these arguments. It is the apparent large decrease in chest wall compliance of ARDS patients in the prone posture. The investigators defined chest wall compliance as the ratio of tidal volume to ΔP_{oes} . In 15 of 16 supine patients the chest wall compliance estimate was larger than the predicted norm (reaching values up to 0.45 l/cm H_2O) and decreased dramatically upon the assumption of the prone posture. This suggests that in the supine posture the esophageal balloon is near flooded derecruited lung, which does not expand during mechanical ventilation

and therefore does not generate a local pressure swing. Paraspinal lung recruitment associated with the assumption of the prone posture dramatically increases volume and ventilation of peri-esophageal lung regions, leading to a much smaller estimate of chest wall compliance. While it is likely that some regions of the lungs approach their maximal volume at pressures near UIP, the evidence that ventilating patients in this way causes injury provided tidal volume is kept low is circumstantial. The pressures and volumes used to test this hypothesis in experimental animals were generally high and are nowadays rarely used in clinical practice. Therefore, the term overexpansion should be used with caution.

The effects of injury on recoil and on compliance need not be related. This is because abnormal surfactants with increased minimal surface tension and impaired dynamic properties (adsorption, spreading, and compression) cannot cause an appropriate change in surface tension with lung volume. As a result both recoil and compliance of aerated units with abnormal surfactants must increase, while the compliance of flooded and collapsed units must be more or less zero. This is just one of many examples why it is difficult to draw inferences about specific mechanisms from static whole lung P-V curves. This would only be possible if the small-scale distributions of regional elastance were known. In some patients there is a larger than anticipated recoil pressure difference between inflation and deflation, indicating P-V hysteresis. There are several possible mechanisms for P-V hysteresis:

- i. The recruitment and derecruitment of lung units during the maneuver.
- ii. The volume-dependent and time-dependent molecular reorganization of surface active material which coats air-liquid interfaces in alveoli and conducting airways.
- iii. Stress relaxation and stress recovery of airways and lung parenchyma.
- iv. Spurious changes in lung volume on account of gas absorption during the P-V measurement.
- v. The last is a well-described problem of the super-syringe technique.

The clinical literature on ALI and ARDS has generally ignored mechanisms two and three and has attributed all volume- and time-related changes in P-V characteristics to lung recruitment (i.e. the opening of previously closed units). While in injured lungs recruitment is undoubtedly an important cause of airway pressure and time-related changes in lung mechanics, it is certainly not the only one. In a series of classic papers Hildebrandt and colleagues studied the physiologic determinants of the PV loop. In the normal lung, stress relaxation, stress recovery, and hysteresis are surfactant and surface tension phenomena, and they account for changes in lung volume with pressure and time. In other words recruitment maneuvers as they have been described in the critical care literature would be fully expected to alter volume and recoil of normal lungs by recruitment independent mechanisms. Compared with surface properties the fraction of elastic pressure that is lost because of tissue hysteresis is small. However, it is not zero and as emphasized in studies of patients with asthma, can be an important source of relaxation in a lung which is actively constricted. The neglect of alternative mechanisms as explanations for PEEP induced changes in the volume of injured lungs is regrettable, because the reasoning behind the open lung approach is largely based on putative benefits derived from recruitment. However, if P-V measurements cannot distinguish between recruitment of new units and stress relaxation of already recruited units, then clinical decisions will be based on a mechanism (recruitment) that cannot be confidently assessed.

Role of respiratory mechanics testing in clinical decision-making:

As pointed out, most of the recommendations using measurements of mechanics to guide ventilator management are based on physiologic reasoning and not on established clinical efficacy. We should consider factors that determine P-V shape and lung mechanical properties, to assess the soundness of current practice. However, two questions were addressed:

1. Is there a single end-inspiratory pressure beyond which patients should not be mechanically ventilated?
2. Do measurements of respiratory mechanics help in the choice of tidal volume and best PEEP?

There is incontrovertible evidence that mechanical ventilation with large tidal volumes harms the lung. In the

single most definitive study trial on the topic, the ARDS network study, patients were randomized to receive mechanical ventilation with tidal volumes of either 6 or 12 ml/kg predicted body weight. The designers of the study chose to ignore lung mechanics as a guide to ventilator management, and instead scaled tidal volume to predicted body weight, that is an estimate of the size of the normal lung. Because of this design choice, hypotheses about safety limits in end-inspiratory recoil pressure (also referred to as plateau pressure or end-inspiratory hold pressure) cannot be tested post hoc. Certainly, in each group in the study the plateau pressure correlated with the severity of injury (the size of the baby lung) and with outcome. However, it is difficult to separate the effects of V_T assignment and severity of lung impairment on outcomes. Those who argue that there is a safe threshold value of Plateau pressure (often proposed as 30 cm H_2O), below which the choice of V_T becomes less important; implicitly assume that the risk of injury increases as peak lung volume increases [42]. Normal lungs approach their total lung capacity, which may be viewed as their structural limit, at transpulmonary pressures between 30 and 35 cm H_2O . Thus, even in the heterogeneously affected injured lung the most normal and hence low impedance units would not exceed their capacity at plateau pressure less than 30 cm H_2O . Clinical evidence in support of this approach is the observation that in the ARDS Network trial the mortality of patients with the greatest respiratory system compliance was not influenced by V_T assignment: that is, it was identical in the two study arms. However, there are powerful arguments against this reasoning:

- A. The lack of V_T effect on mortality in the high compliance group has limited statistical power.
- B. A post hoc analysis that focused on plateau pressure rather than compliance showed that the V_T effect was preserved across all plateau pressure quartiles.
- C. In spontaneously breathing animals experimentally induced hyperpnoea impairs lung barrier function.
- D. The large alveolar surface area change associated with high V_T breathing inactivates surfactant irrespective of the peak lung volume reached.

The clinical literature provides even less guidance to the question 'do respiratory mechanics measurements aid in the choice of best PEEP'? Most experimental studies on the topic have used measures of pulmonary gas exchange such as the PaO_2/FiO_2 ratio as surrogate outcome variables of clinical benefit. While there is no question that adjustments in PEEP guided by P-V loops may be helpful in optimizing pulmonary gas exchange, it has also become clear that optimizing gas exchange need not convey outcome/survival benefit. Those patients randomized to the high tidal volume group, who ended up having an increased risk of dying, had more improvement in arterial oxygenation on day 1 than patients who were randomized to the low V_T arm and who were more likely to survive.

In summary, measurements of respiratory mechanics in patients with injured lungs can help to identify patients at risk for ventilator induced lung injury. Mechanical ventilation with airway pressures greater than 30-35 cm H₂O should make the clinician re-assess the settings of V_T and PEEP. Until proven otherwise, patients with injured lungs should not receive a V_T more than 8 ml/kg predicted body weight (some would argue 6 ml/kg predicted). Most experts agree that a routine PEEP setting of 5 cm H₂O is too little, but there is no evidence that setting PEEP guided by P-V curves results in better outcomes.

Value of respiratory mechanics in the assessment of respiratory drive and timing

In most cases, when ventilator waveforms are measured, concurrent activity of the respiratory pump is a confounding signal. However, as shown with a simple mechanical analogue (Figure 53) inspection of ventilator waveforms can indicate the performance of the ventilatory pump. Nevertheless, (Figure 53) shows a resistive and elastic

element (the respiratory system) connected to two pressure generators (the mechanical ventilator, pump 1 and the respiratory muscles, pump 2). In the absence of phasic respiratory muscle activity, the airway pressure and flow patterns reflect the choice of ventilator mode and the relaxation characteristics of lungs and chest wall. During lung inflation with constant inspiratory flow, the production of muscle pressure (P_{mus}) by the respiratory pump alters the shape of the inspiratory P_{aw} tracing (shaded area in Figure 53). In contrast during lung inflation with constant pressure P_{mus} would alter the shape of the inspiratory flow profile. Activation of respiratory muscles during lung deflation distorts the expiratory flow profile. Significant differences from the expected pressure volume and flow patterns indicate a large P_{mus} output, which a large patient effort is. In comparison, minor departures indicate decreased respiratory muscle pressure on account of low drive, abnormal neuro-mechanical coupling, muscle weakness, muscle fatigue, or hyperinflation.

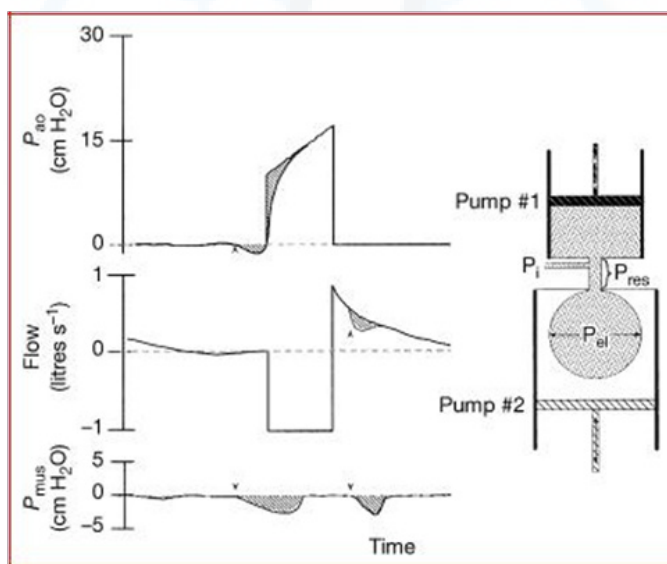


Figure 53: Schematic of inspiratory muscle activity (P_{mus}) on airway pressure and flow during mechanical ventilation in a volume preset mode [40].

Ventilator waveforms can show if respiratory efforts (and hence drive) are increased and if respiratory muscle output is synchronous with machine inflations. Based on this assessment, the care giver must decide if an intervention is required. This depends on the assessment of patient comfort and on the judgment whether the work of breathing is excessive and potentially harmful. Harm may arise either because:

- i. The task is fatiguing (a state that has proven difficult to define and document in the clinical setting).
- ii. Is uncomfortable.
- iii. Causes a dangerous stress response that jeopardizes the balance between oxygen supply and demand in vulnerable tissues.

Once the decision to intervene has been made, therapy consists of a change in ventilator settings with or without the judicious use of sedatives. Changes in ventilator settings can affect respiratory drive and timing through several pathways:

- a) By alleviating shortness of breath (cortical/behavioral feedback).
- b) By correcting hypercapnia and hypoxemia (chemoreceptive feedback).
- c) By affecting amplitude and rate of lung and chest wall expansion (neuromechanical feedback).

Behavioral and chemoreceptive pathways will influence effort and drive while neuromechanical feedback is more

likely to affect breath timing. Failure to reduce excessive patient efforts through increases in ventilator support is usually an indication for sedatives.

Patient-ventilator desynchronize is exceedingly common and if patient discomfort or efforts are not judged excessive, may not require specific therapy. Predisposing factors include all the conditions associated with reduced muscle pressure output and impaired neuro-mechanical feedback. Without careful inspection of pressure volume or flow tracings it is often very difficult to appreciate that a patient generates inspiratory efforts far in excess of machine rate. It may also become apparent that there is no appreciable temporal relationship between efforts and machine breaths. Such patients are often encephalopathic, hypermetabolic, and critically ill. They may be easy to ventilate because they are too weak or their drive is too suppressed to fight the ventilator. Nevertheless, recognition of silent tachypnea is useful because it is the respiratory controller's manifestation of a stress response, predicts futile weaning attempts and guides the use of sedatives, narcotics and paralytics. However, it was confirmed that respiratory waveform analysis is a more effective way of monitoring the dosing of neuromuscular blocking agents than monitoring neuromuscular transmission [40].

Respiratory Muscle Functions during Critical Illness

The salutary effects of maintaining spontaneous breathing during critical illness have been debated since the early 1970s, with the advent of intermittent mandatory ventilation (IMV). Proponents of IMV claimed that this mode could achieve improved patient-ventilator synchrony,

require less need for sedation, and provide faster weaning. The conceptual foundation of IMV, and thus a large measure of its physiologic legitimacy, is that continuous spontaneous breathing by patients with acute respiratory failure is beneficial, a claim, however, that was never substantiated. The invention of airway pressure release ventilation (APRV), in the late 1980s, was accompanied by similar claims of improved respiratory muscle function and reduced time on mechanical ventilation, thus extending the debate surrounding the role of spontaneous breathing during critical illness into contemporary practice. This is hardly surprising, as the inventors of APRV include some of the same investigators who invented and popularized IMV.

Despite substantial laboratory and clinical evidence linking both severely loaded breathing and prolonged inactivity with respiratory muscle damage and weakness, the practical impact of either problem on the duration of mechanical ventilation, particularly in patients with ALI/ARDS, cannot be recognized. This is because the etiology of respiratory muscle weakness in patients undergoing prolonged mechanical ventilation is probably multi-factorial (Figure 54) [43]. Nonetheless, it would seem prudent to curtail unassisted spontaneous breathing early in the course of critical illness if minute ventilation demand is high and there is significant impairment to chest mechanics. On the other hand, passive mechanical ventilation should be avoided, except for the most severe manifestations of respiratory failure. Whenever high levels of assisted ventilation are required, the mandatory rate should be adjusted to assure patients continue to trigger assisted breaths, whereas sedation should be titrated to the lowest level that promotes reasonable patient-ventilator synchrony without suppressing respiratory drive.

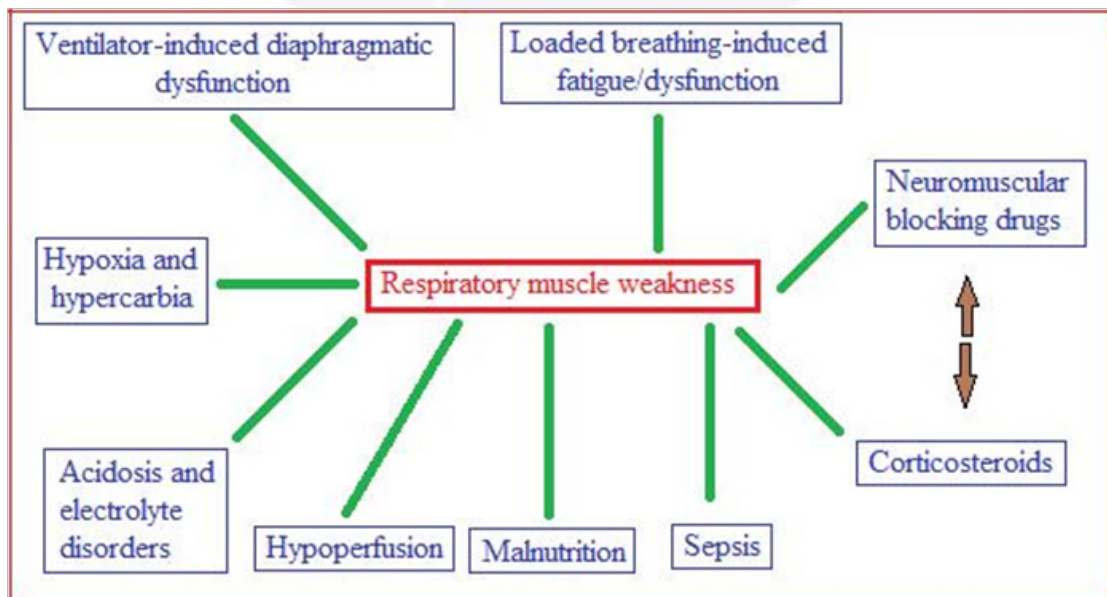


Figure 54: Potential causes of respiratory muscle weakness in mechanically ventilated patients recovering from critical illness [43].

Functioning of respiratory muscle during critical illness

The controversy over the role of spontaneous breathing during critical illness is centered on the clinical relevance of opposite problems. Simply stated, sustained, inactivity of the respiratory muscles results in loss of muscle mass and strength, whereas the sustained imposition of high-tension work causes structural damage and may exacerbate inflammation of the diaphragm. This state has been described as disuse versus use atrophy; both conditions may contribute to prolonged ventilator-dependence in patients with severe respiratory failure and indirectly may impact clinical outcomes.

Discoordinated breathing: Discoordinated breathing was a prominent and early justification for promoting spontaneous breathing throughout the course of critical illness. The origins of this controversy began in the early 1970s, with the observation that approximately 5% of patients recovering from acute respiratory failure showed signs of respiratory muscle discoordination, of varying severity, that could not be attributed to underlying (i.e. primary) neuromuscular disease. Discoordinated breathing first was described briefly in a larger paper on mechanical ventilation and was defined as the onset of expiratory activity while the chest cage was still expanding. It was considered to be idiopathic, was observed to resolve slowly, and in consequence delayed weaning. However, a subsequent, detailed observational study attributed discoordinated breathing to the effects of hyperinflation on diaphragmatic motion in patients with severe COPD. It should be noted that this breathing pattern was described prior to the discovery of intrinsic PEEP, with its associated threshold loading, uncaptured inspiratory efforts, and recruitment of abdominal expiratory muscles that also might contribute to the clinical impression of discoordinated breathing. Yet the supporter of IMV emphasized discoordinated breathing and prolonged weaning following passive mechanical ventilation as a justification for promoting spontaneous breathing throughout the course of mechanical ventilation. They claimed that almost all patients requiring ventilatory support for more than 24 hours develop discoordination of abdominal and accessory muscles of respiration that may prolong dependence on the ventilator and does not occur in patients who breathe spontaneously throughout their treatment with IMV. Although discoordinated breathing was not attributed directly to muscle deconditioning from use of passive mechanical ventilation, the linkage of these 2 phenomena was strongly implied.

Respiratory muscle fatigue: Like other skeletal muscles, the diaphragm is subject to fatigue, defined as loss of a muscle's capacity for developing force and/or velocity, resulting from activity under loaded conditions, and which is reversible with rest. For the respiratory system, that muscular force translates into the pleural pressure necessary to sustain minute ventilation at a level achieving eucapnia. Fatigue is distinguished from muscle weakness, as the latter

denotes the inability to develop a targeted force in a rested muscle. Unlike other skeletal muscles, in which rest can reverse fatigue, the diaphragm must remain continuously active to sustain life. As the primary muscle of ventilation it also must be capable of extremely high work output to accomplish sneezing, coughing, and bodily exertion. The solution to this unique problem is reflected in the proportional composition of muscle fibers. Approximately 55% of the diaphragm consists of Type 1 (slow twitch) muscle fibers that are highly resistant to fatigue, but generate relatively low levels of force. These fibers represent the portion of the diaphragm that is continuously active during normal breathing. The remaining 45% of the diaphragm consists of 2 fibers that are sequentially recruited in proportion to increasing levels of minute-ventilation demand and/or work of breathing. This muscle tissue consists of fast twitch Type 2a (intermediate fatigue-resistant/intermediate force-generating capacity) and Type 2b (low fatigue-resistant/highest force-generating) fibers. The accessory muscles of respiration also possess a similar composition of fiber types (Respiratory Muscle Fatigue Workshop Group 1990).

This structural composition of the respiratory muscles suggests a time-limited work level under loaded conditions whereby minute ventilation can be sustained. Under these conditions, hypercapnia represents either fatigue of the inspiratory muscles or an adaptive strategy to preserve some degree of muscular function so as to prevent a dramatic failure.

Anyhow, fatigue is defined further as either low frequency or high frequency, according to the muscle fibers involved and the duration of degraded muscle performance. In addition, the descriptor incipient fatigue [*initial fatigue*] has been used to describe situations in which voluntary respiratory muscle contractions are limited by central inhibition in the face of excessive work demands, but external electrical diaphragmatic stimulation is capable of eliciting stronger contractions. In contrast, overt fatigue [*obvious fatigue*] refers to the inability of external electrical stimulation to evoke stronger respiratory muscle contractions. During normal tidal breathing, respiratory muscles are normally stimulated at a frequency range of 10-20 Hz, whereas stimulation at higher frequencies (e.g. 60-100 Hz) results in more forceful contractions. High-frequency fatigue, as it involves fast-twitch fibers and forceful contractions, is believed to be caused by the accumulation of inorganic phosphate and the failure of electrical conduction to the contractile fibers in the muscle, as well as intramuscular acidosis. Recovery from high-frequency fatigue generally occurs within 15 minutes. In contrast, low-frequency fatigue is believed to be caused by muscle-fiber injury, recovery from which may take several days [44].

Diaphragmatic function during loaded breathing

Excessive loading of the inspiratory muscles induces acute fatigue, from which complete recovery requires 24-48 hours, even when that load is experienced for relatively brief periods. At functional residual capacity the inspiratory

muscles can sustain increased work loads indefinitely, as long as the inspiratory change in trans-diaphragmatic pressure (ΔP_{di}) is less than 40% of maximum. Beyond this, fatigue eventually ensues at a time point inversely related to magnitude of the load. When subjects are allowed to recruit all of their inspiratory muscles, fatigue-onset occurs when the imposed work load increases to between 50-70% of the maximal inspiratory pressure. Furthermore, the time to fatigue-onset also depends upon the percentage of the respiratory cycle committed to inspiration. However, for any ΔP_{di} , the time to fatigue-onset decreases as inspiratory time increases. This is represented by the tension-time index of the diaphragm, which is the product of the ratio of ΔP_{di} to maximum P_{di} and percent-inspiratory time. That is:

$$TTIdi = (\Delta P_{di} / P_{di-max}) \times (T_i / T_{total})$$

in which TTIdi signifies respiratory muscle oxygen consumption, as well as reflecting limitations in muscle perfusion that affect oxygen supply, removal of metabolites, and maintenance of local electrolyte balance. A value exceeding 0.15 is considered the critical cut-off value for the development of fatigue.

Of particular interest is the presence of disorganized breathing during diaphragmatic fatigue. In normal subjects at fatigue-onset, the breathing pattern has been observed to become irregular and disorganized, whereby inspiration is accomplished in steps (cogwheel pattern). When all inspiratory muscles are allowed to function during fatiguing loads in normal subjects with over time the partitioning of work alternates between the diaphragm and the intercostals/ accessory muscles (respiratory alterans) occurred. This gives the distinct impression of discoordination that becomes more salient with pronounced recruitment of the abdominal muscles during expiration. Respiratory alterans has been observed clinically in patients with inspiratory muscle fatigue, including those with ALI/ARDS, so that the perception of disorganized breathing may signify impending fatigue from excessive muscle loading rather than deconditioning per se. nevertheless, reversal of muscle fatigue requires rest. However, it is uncertain in clinical practice whether this necessitates completely shutting-down the inspiratory muscle with passive mechanical ventilation, or just reducing the power of breathing to normal or subnormal levels for a certain period of time. For example, following induction of diaphragmatic fatigue in normal subjects, recovery was 75% complete within 3 hours and 100% complete by 25 hours with subjects spontaneously breathing at normal workloads. By extension, the failure to adequately reduce inspiratory muscle work load suggests that a state of chronic respiratory muscle fatigue may occur. Proponents of IMV have advocated use of a mandatory rate that will just prevent acidemia. This raises a concern that prolonged ventilator-dependence following acute respiratory failure may, in part, be a consequence of insufficient mechanical support. In some circumstances chronic fatigue may persist for several days or even weeks.

Loaded breathing and diaphragmatic injury: As mentioned earlier, sustained high-tension work causes structural damage to and inflammation of the diaphragm. It is found that the exhaustive contractions in the usual skeletal muscle are causing structural damage as well as degenerative changes in muscle tissue that persists for a week following the event. This appears to be more prominent in highly oxidative, fatigue-resistant (Type 1) fibers. The associated inflammatory response has been shown to persist for several days in human skeletal muscle. Delayed inflammation or secondary injury to both the diaphragm and parasternal intercostal muscles has been demonstrated 3 days following brief periods of fatigue-inducing inspiratory resistive loading. Moreover, delayed injury appears to increase the susceptibility of the respiratory muscles to repeated injury. Anyhow, structural damage to the respiratory muscles from loaded breathing also causes oxidative stress and stimulates proinflammatory cytokine production. Normal subjects breathing at 75% of their maximal inspiratory pressure for less than one hour have significant elevations in plasma levels of tumor necrosis factor alpha, interleukin-1B and interleukin-6, as well lymphocyte activation. TNF- α also has been shown to reduce diaphragmatic force generation.

It was found that the high-load inspiratory resistive breathing below the fatigue level (i.e. tension-time index of 0.12) for 2 hours a day produced cell membrane disruption and sarcomere damage primarily to Type-1 fibers. Diaphragmatic tissue biopsies from elective thoracic surgery patients exposed to brief periods of fatigue-induced threshold-loaded breathing were found to have sarcomere damage. Interestingly, the damage was more pronounced in patients with chronic lung disease. It was speculated that the greater susceptibility to damage observed in these patients may have resulted from in-coordination or co-contraction of agonist and antagonistic muscle groups, or from eccentric loads (i.e. differential contraction intensity between diaphragmatic sub-segments). Anyhow, three days following exposure to a brief period (1.5 hours) of fatiguing inspiratory resistive loads (i.e. tension-time index of 0.22) diaphragm exhibited a marked increase in shredded and necrotic diaphragmatic fibers as well as inflammatory cell infiltration. Ischemia causes increased reactive oxygen species production that, in turn, stimulates cellular proteolytic enzyme systems, leading to muscle degradation. In addition when assessing the risk of muscle fiber damage from loaded breathing in the context of ALI/ARDS, it is interesting to note that the application of passive mechanical ventilation with sepsis actually eliminated cell damage and improved diaphragmatic performance. This is most likely explained by the fact that sepsis induces sarcolemma damage and respiratory muscle weakness; so that loaded breathing probably aggravates the damage further [45].

Ventilator-induced diaphragmatic dysfunction

Numerous clinical studies have confirmed that prolonged skeletal muscle inactivity results in atrophy, weakness, and neuromuscular impairment. In brief, skeletal muscle disuse decreases muscle volume and weight with a corresponding loss of total muscle contractile proteins, as well as mitochondria and sarcoplasmic reticulum that impairs energy production and calcium activity, respectively. Disuse atrophy is caused by decreased protein synthesis and/or increased proteolysis within muscle tissue. More active skeletal muscles have a higher propensity to develop atrophy from prolonged inactivity. As the diaphragm maintains a constant activity level between 30-40%, it appears to be

particularly susceptible to disuse atrophy [46]. Ventilator-induced diaphragmatic dysfunction is defined as the loss of diaphragmatic force-generating capacity specifically related to the use of passive mechanical ventilation. It is characterized by structural damage to muscle fibers from oxidative stress, as well as muscle atrophy. Evidence from animal models of ventilator-induced diaphragmatic dysfunction suggests that several pathways are involved. Prolonged diaphragmatic quietness results in both decreased protein synthesis and increased muscle tissue proteolysis. Whereas decreased production of insulin-like growth factor-1 reduces the expression of protein kinases responsible for protein synthesis, the genesis of structural damage to the diaphragm is more complex (Figure 55).

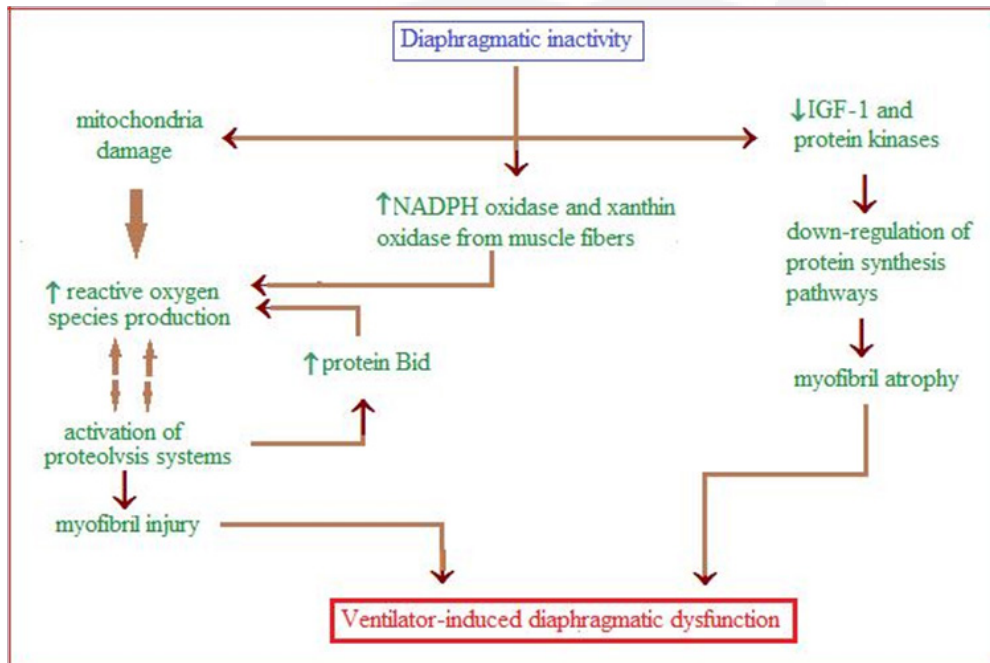


Figure 55: Cellular mechanisms implication in ventilator-induced diaphragmatic dysfunction. BID: BH3-Interacting Death Domain Protein; NADPH: Reduced Nicotinamide Adenine Dinucleotide Phosphate; IGF-1: Insulin-Like Growth Factor [43].

Diaphragmatic muscle fiber damage results from increased levels of reactive oxygen species. However, this is not associated with either inflammatory cell infiltration or increased production of pro-inflammatory cytokines. Damage to the mitochondria appears to be a significant source of reactive oxygen species. The other major source of reactive oxygen species comes from activation of cellular proteolytic systems that also are activated by increased levels of reactive oxygen species. Of these, the mutually reinforcing caspase and calpain systems are believed to drive reactive oxygen species production, resulting in protein degradation, the primary targets being the contractile elements of the diaphragm (i.e. actin and myosin). Furthermore, activation of the caspase and calpain systems may activate the protein Bid (BH3-interacting death domain protein), causing further mitochondrial damage, and thus potentiating reactive oxygen species production [43].

Work of Breathing and Breathing Pattern in ALI/ARDS

ALI/ARDS is characterized by decreased lung compliance (C_L) and, in many patients, decreased chest wall compliance (C_{CW}). Decreased compliance in ALI/ARDS is associated with tachypnea and implies that elastic work of breathing is elevated. This assumption is based on the theory of minimal work, which presuming that the respiratory frequency (f) adopted by a patient to achieve a target alveolar ventilation represents a strategy to minimize inspiratory effort and maximize muscular efficiency by balancing the elastic and resistive components of work of breathing. Therefore, to minimize elastic work of breathing during spontaneous breathing, patients with ALI/ARDS should maintain minute ventilation (V_E) with a relatively rapid f and small tidal volume (V_T). However, lung resistance is increased in ALI/ARDS

and with the additional resistance of the artificial airway may influence the spontaneous breathing pattern (Figure 56) [47]. Anyhow, when elevated, the ratio of respiratory frequency to tidal volume (f/V_T) ratio adopted by a patient during a brief trial of spontaneous breathing is an accurate

predictor of subsequent weaning failure. Thus, it may be an indirect marker of excessive inspiratory muscle work load, impending muscle fatigue, or simply reflects muscle weakness.

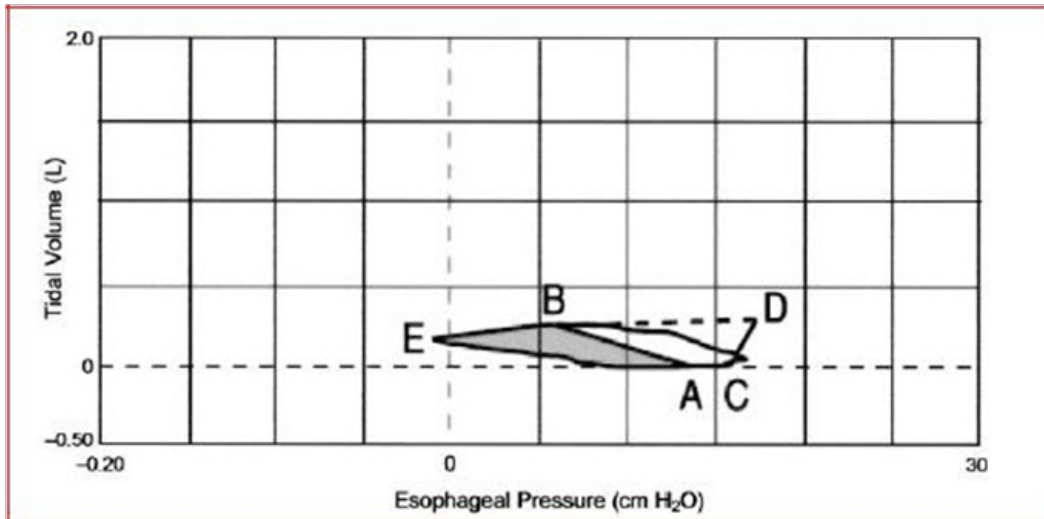


Figure 56: Campbell diagram of work of breathing in a patient with acute respiratory distress syndrome from necrotizing fasciitis and sepsis, with a respiratory system compliance of 26 ml/cm H₂O and a chest wall compliance of 164 ml/cm H₂O. Line CD represents the chest wall compliance curve obtained under conditions of passive ventilation, and is placed by the pulmonary mechanics monitor at the end-expiratory baseline pressure. Line AB represents the lung compliance; point A represents the onset of inspiratory flow, and point B represents the point of maximum tidal volume. Point E represents the maximum negative esophageal pressure. The shaded area AEBA represents the resistive work of breathing. Area CABDC represents the elastic work of breathing done on both the lung and the chest wall [48].

The spontaneous breathing pattern of patients with ALI/ARDS was consistent with the theory of minimal work: that the respiratory frequency (f) adopted by a patient to achieve a target V_E represents a strategy to minimize inspiratory effort. In the presence of reduced respiratory system compliance (C_{RS}) and elevated elastic work of breathing, the body's attempt to minimize effort and maximize efficiency should manifest as a rapid shallow breathing pattern. Accordingly, it was found that f/V_T was directly related to elastic work of breathing and inversely related to ΔP_{es} (P_{es} = peak esophageal pressure).

It should be emphasized that the negative relationship between effort (ΔP_{es} and pressure time product [PTP]) and f/V_T also occurred in the context of both prolonged illness and diminished inspiratory muscle strength. On average, all patients were investigated 14 days into their course of ALI/ARDS and had a maximal inspiratory pressure (MIP) that was 45-70% of normal range values (72-110 cm H₂O). The strong inverse relationship between respiratory muscle strength (MIP) and f/V_T also suggests that rapid shallow breathing in ALI/ARDS may indicate either inspiratory muscle weakness or impending fatigue in the face of an overwhelming work load. This interpretation is supported by the direct relationship between both f/V_T with minute ventilation difference between mechanical ventilation

and spontaneous breathing ($\Delta \dot{V}_E$ (MV-SB)) and with the duration of ALI/ARDS in the multivariate analysis. That peak inspiratory flow rate (V_I) was the best single predictor of f/V_T in the univariate analysis may signify that the capacity to generate a high peak V_I is intimately related to V_T size. In fact, peak inspiratory flow as a predictor of V_T achieved an r^2 of 0.42 ($p < 0.001$). However, in their theory of minimal work, Otis et al framed the f response according to the magnitude and distribution of elastic and resistive loads in terms of target alveolar ventilation. It had been suggested that Otis's prediction extends to conditions of severe pathology. During spontaneous breathing, the patients seemingly could not achieve their target alveolar ventilation, as they accrued a V_E deficit of 3.5-6 l/min that, in turn, was a significant predictor of f/V_T .

Since the first descriptions of ARDS, the implication has been that rapid shallow breathing reflects lung stiffness, and the inverse correlation between f/V_T and compliance had been support this observation. That lung compliance (C_L) was a stronger predictor of f/V_T than C_{RS} may be explained by the fact that the average C_L of patients was 35-60% of normal range values (70-122 ml/cm H₂O), whereas C_{CW} at worst was 69% of normal range values (118-179 ml/cm H₂O). In contrast to patients with ARDS, those with ALI had less severe injury, as measured by the lung injury score,

and significantly higher C_{RS} and C_L . However, this did not translate into a significantly lower elastic work of breathing, which may be explained by the fact that patients with ALI also breathed at a higher V_T . The relative contributions of elastic and resistive work of breathing to the total inspiratory work of breathing were 57% and 43%, respectively, and were not different between patients with ARDS and those with ALI. It had been found that in normal subjects the elastic work of inspiration accounted for 63% of the total work of breathing, whereas 29% was expended overcoming resistive forces, and 8% in overcoming the viscoelastic resistance to tissue deformation. Interestingly, the proportion of work distribution in ALI/ARDS was similar to that found in normal subjects. It was speculated that the abnormally low C_{RS} may have been balanced by increased resistance from the artificial airway, along with increased airway and tissue resistance often found in patients with ARDS [48].

The Normal Alveoli

Respiratory unit

Figure 57 [49] shows the respiratory unit (also called respiratory lobule), which is composed of a respiratory

bronchiole, alveolar ducts, atria, and alveoli. There are about 300 million alveoli in the two lungs, and each alveolus has an average diameter of about 0.2 millimeter (Figure 58) [50]. The alveolar walls are extremely thin, and between the alveoli is an almost solid network of interconnecting capillaries, shown in (Figure 59 & 60). Indeed, because of the extensiveness of the capillary plexus, the flow of blood in the alveolar wall has been described as a sheet of flowing blood. Thus, it is obvious that the alveolar gases are in very close proximity to the blood of the pulmonary capillaries. Further, gas exchange between the alveolar air and the pulmonary blood occurs through the membranes of all the terminal portions of the lungs, not merely in the alveoli themselves. All these membranes are collectively known as the respiratory membrane, also called the pulmonary membrane.

Respiratory Membrane: (Figure 61) shows the ultrastructure of the respiratory membrane drawn in cross section on the left and a red blood cell on the right. It also shows the diffusion of oxygen from the alveolus into the red blood cell and diffusion of carbon dioxide in the opposite direction. Note the following different layers of the respiratory membrane:

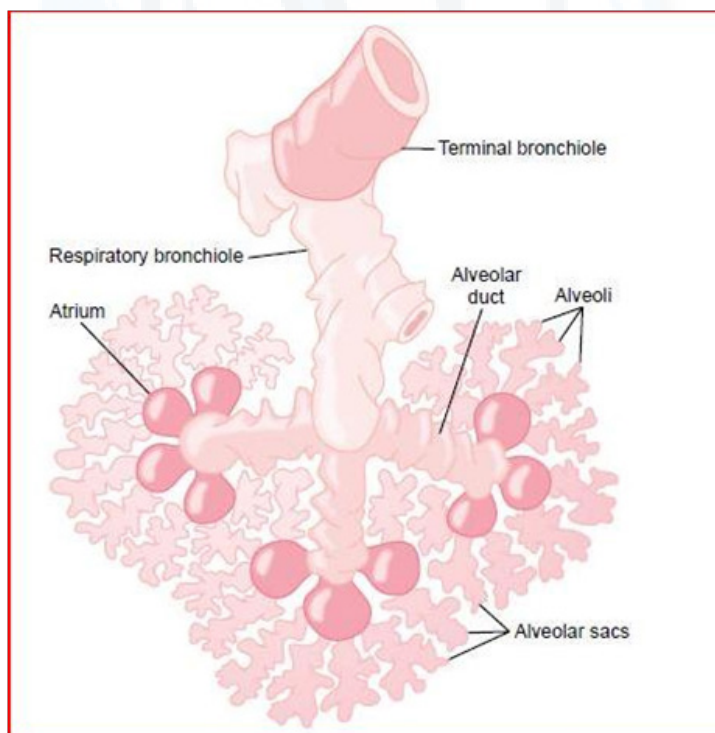


Figure 57: Respiratory unit [49].

- A layer of fluid lining the alveolus and containing surfactant that reduces the surface tension of the alveolar fluid.
- The alveolar epithelium composed of thin epithelial cells.
- An epithelial basement membrane.
- A thin interstitial space between the alveolar epithelium and the capillary membrane.
- A capillary basement membrane that in many places fuses with the alveolar epithelial basement membrane.
- The capillary endothelial membrane.

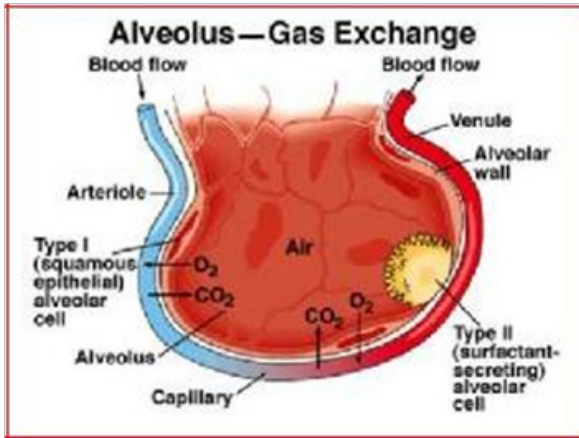


Figure 58: Schematic representation of normal alveolus [50].

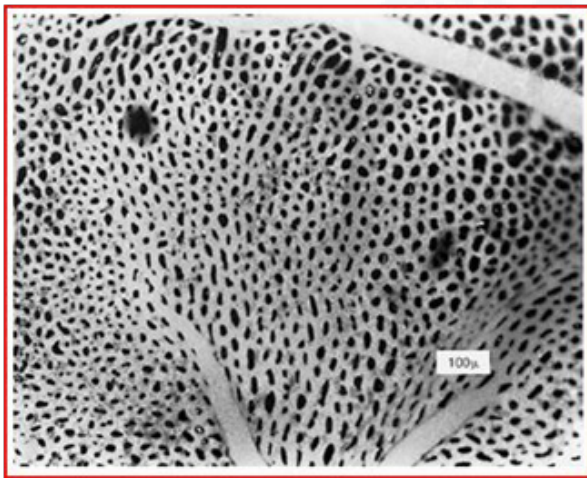


Figure 59: Surface view of capillaries in an alveolar wall [49].

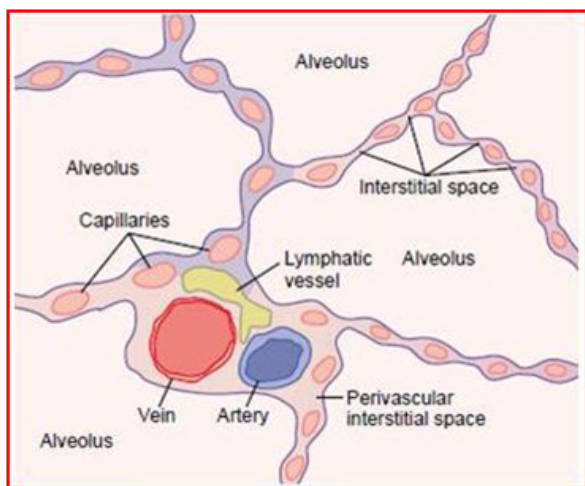


Figure 60: Cross-sectional view of alveolar walls and their vascular supply [49].

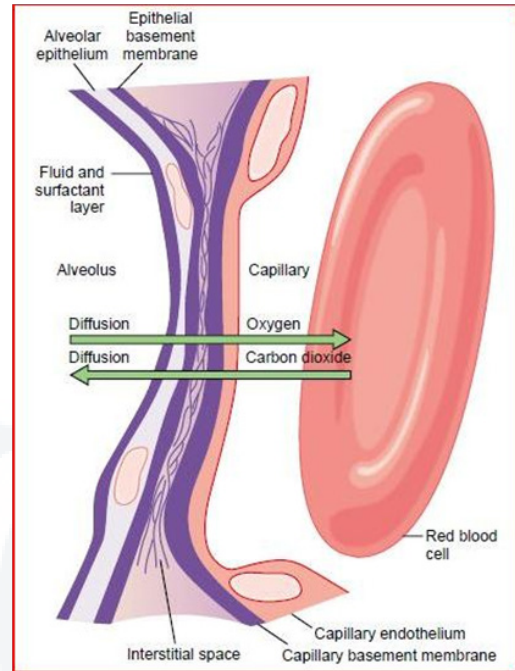


Figure 61: Ultrastructure of the alveolar respiratory membrane, shown in cross section [49].

Despite the large number of layers, the overall thickness of the respiratory membrane in some areas is as little as 0.2 micrometer, and it averages about 0.6 micrometer, except where there are cell nuclei. From histological studies, it has been estimated that the total surface area of the respiratory membrane is about 70 square meters in the normal adult human male. This is equivalent to the floor area of a 25-by-30-foot room. The total quantity of blood in the capillaries of the lungs at any given instant is 60 to 140 milliliters. Now imagine this small amount of blood spread over the entire surface of a 25-by-30-foot floor, and it is easy to understand the rapidity of the respiratory exchange of oxygen and carbon dioxide. The average diameter of the pulmonary capillaries is only about 5 micrometers, which means that red blood cells must squeeze through them. The red blood cell membrane usually touches the capillary wall, so that oxygen and carbon dioxide need not pass through significant amounts of plasma as they diffuse between the alveolus and the red cell. This, too, increases the rapidity of diffusion [49].

Nasal Potential Difference to Detect Na⁺ Channel Dysfunction in Acute Lung Injury

At present nasal potential difference (NPD) has been optimized for the measurement of Cl⁻ transport in a relatively healthy outpatient population for the purpose of diagnosing cystic fibrosis. The optimal method of measuring baseline nasal potential difference and thus Na⁺ channel function has been a secondary consideration in the cystic fibrosis literature. However, a few studies have examined the effects of components of the measurement technique on baseline/

basal NPD. Baseline/basal NPD as measured on the floor of the nose are similar to that measured under the inferior turbinate. Room temperature solutions are equivalent to body temperature solutions and ECG cream is similar to agar for completing the electrical circuit. Measurement of nasal potential difference involves the placement of a double-lumen catheter, which acts as the measuring the luminal electrode, in the nose. A reference (electrically contra-luminal) electrode is placed either subcutaneously (using an electrolyte/agar-filled needle) or over an area of abraded skin, typically on the forearm. Abrading the skin

breaks the epithelial skin barrier and short-circuits the skin potential, allowing electrical contact to the sub-epithelial space. The measuring electrode catheter is placed either under the inferior turbinate or along the floor of the nose and the site of greatest potential difference is sought. The catheter is secured at this site. Different solutions are infused through the double lumen catheter to activate or inhibit specific ion channels and enable *in vivo* ion channel function to be investigated. For Na^+ transport, the following measurements can be made (Figure 62):

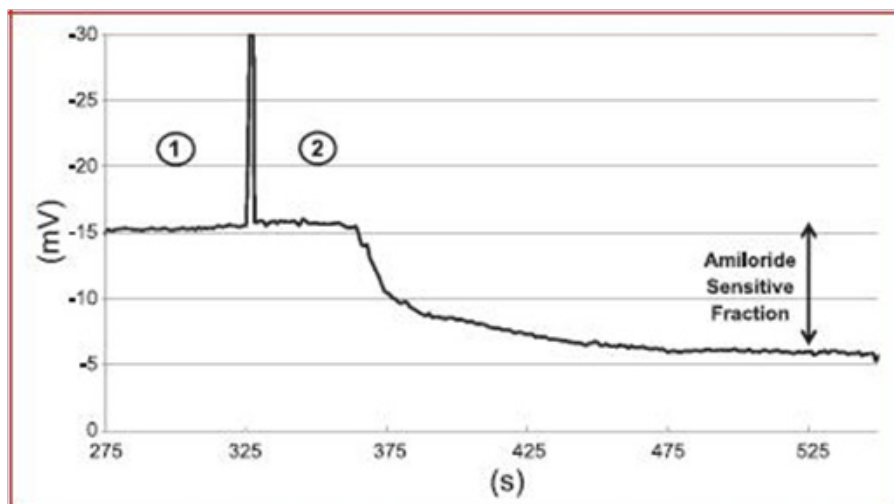


Figure 62: Typical NPD tracing from a healthy volunteer. 1 = Perfusion with Ringers solution; 2 = perfusion with amiloride solution; vertical line indicates onset of amiloride perfusion [3].

- Baseline NPD: This is a composite value of all ion transport but is predominantly reflective of Na^+ transport.
- Amiloride infusion: Amiloride (0.1 mM) blocks the ENaC class (highly selective cation channel, poorly selective cation channel, nonselective cation channel) of Na^+ channels, leading to luminal Na^+ retention and a fall in nasal potential difference (due to the accumulation of the positively charged Na^+ cation making a negative potential difference less negative).

Nasal potential difference as a substitute measure of alveolar ion channel function

There are several reasons that why the nasal potential difference potentially could serve as a noninvasive, surrogate measure of alveolar ion channel function:

- Alveolar cell type 1 (AT1) and AT2 cells to adjust the volume of alveolar lining fluid by alternating between Cl^- secretion and Na^+ absorption. This changing requirement for respiratory liquid layer depth is reflected by the changing epithelial potential difference through the respiratory tract. Just as the surface fluid layer thins from proximal airway to alveolus, so too does the potential difference become smaller. Lower airway potential difference measurements show tracheal

potential differences of approximately -30 mV with a decrease of ~ 10 mV in large proximal bronchi and a further ~ 6 mV decrease in more distal segmental and sub-segmental bronchi. Alveolar potential difference has been determined in cell-based and animal studies as being less than -10 mV (Figure 63). This relationship of decreasing respiratory potential difference has been consistently demonstrated *in vivo* and *ex vivo*, in both animal and human studies.

- Indirect evidence for the utility of nasal potential difference as a surrogate measure of more distal ion channel function comes from human studies of disorders of the airway liquid layer. Cystic fibrosis is the archetypal respiratory ion channel disorder. It is a genetic disease of cystic fibrosis transmembrane regulator with autosomal recessive inheritance. To date over 1600 mutations have been described, leading to varying amounts of the cystic fibrosis transmembrane regulator gene being expressed and cystic fibrosis transmembrane regulator protein being produced, assembled, trafficked to the cell membrane, inserted, and functioning correctly. The exact pathophysiology of cystic fibrosis remains debated; however, the low airway surface liquid volume theory proposes that cystic fibrosis transmembrane regulator dysfunction

causes excessive airway Na^+ resorption via ENaC and an inability to secrete Cl^- to increase airway surface liquid height when necessary. This results in decreased airway surface liquid causing a dry, inspissated mucus layer, which hinders airway clearance and promotes a cycle of repeated airway infection, bronchial damage, and the development of bronchiectasis. Nasal potential difference readings from patients with cystic fibrosis typically demonstrate a large baseline nasal potential difference [approximately -45 mV to -70 mV], a large amiloride-sensitive fraction, and a lack of response to low Cl^- and isoprenaline perfusion. This identifies Na^+ hyper-absorption, an inability of cystic fibrosis transmembrane regulator to allow Cl^- movement, and the interdependency of ENaC and cystic fibrosis transmembrane regulator function. Cystic fibrosis patients with lower, more normal nasal potential differences have a milder phenotype than those with higher nasal potential differences. Systemic pseudohypoaldosteronism is a rare autosomal recessive disorder of ENaC caused by loss-of-function mutations. Excessive airway surface liquid occurs due to an inability to absorb Na^+ and thus water from the air space. This is partly compensated for by increased removal via mucociliary clearance. The excess air space fluid causes luminal narrowing, wheezing and repeated pulmonary infection. Baseline nasal potential difference is approximately one-third that of healthy controls and not affected by amiloride, reflecting abnormal ENaC-mediated Na^+ absorption. In addition, nasal surface liquid Na^+ concentration is increased and liquid volume more than doubled compared with healthy volunteers [51].

- c. Further indirect evidence comes from human studies associating abnormal nasal potential difference with alveolar dysfunction in the form of pulmonary edema. Neonatal RDS is a form of pulmonary edema suffered by premature babies. Both surfactant and ENaC subunit production are dependent on gestational age, and if birth occurs before sufficient production has occurred respiratory dysfunction is likely. Respiratory distress syndrome occurs with a deficiency of both surfactant and ENaC, whereas transient tachypnea of the newborn occurs with ENaC deficiency alone. Premature babies with RDS have lower mRNA levels of all three ENaC subunits than premature babies without RDS. Similarly, premature babies with RDS have lower nasal potential differences than otherwise healthy premature babies. As these babies grow older their nasal potential difference increases in keeping with enhanced ENaC production. Dexamethasone upregulates ENaC expression and pretreatment for the premature fetus decreases the incidence of RDS, nevertheless, via numerous mechanisms. Babies with transient tachypnea of the newborn have a lower amiloride-sensitive fraction of nasal potential difference than healthy babies, with this value recovering to normal after 3 days. Interestingly, newborn babies' nasal potential difference varies with mode of delivery. High-altitude pulmonary edema is a form of pulmonary edema typically suffered at altitudes above 2500 m. The pathophysiology is complex, consisting of excessive hypoxic pulmonary vasoconstriction, endothelial stress failure, excessive inflammation, nitric oxide dysfunction, and, importantly, impaired amiloride-sensitive Na^+ transport. When measured at low altitude, mountaineers prone to the development of high-altitude pulmonary edema have significantly reduced baseline nasal potential difference compared with those resistant to the condition. This reduction was due to the amiloride-sensitive fraction of Na^+ transport, localizing the defective Na^+ movement to the ENaC class of Na^+ channels. Pre-treating this group of high-altitude pulmonary edema prone mountaineers with salmeterol, a β_2 -agonist known to upregulate respiratory Na^+ transport, more than halved the incidence of high-altitude pulmonary edema upon re-exposure to high altitude. When High-altitude pulmonary edema prone and resistant mountaineers underwent nasal potential difference measurement at high altitude, both groups had reduced baseline nasal potential differences compared with their low-altitude values. This decrease was due to impaired amiloride-insensitive Na^+ transport and localized the defect to cyclic nucleotide-gated channels. These findings suggest that a constitutive defect in the ENaC class of Na^+ channels, by interfering with the mechanism of alveolar fluid clearance, may predispose certain individuals to the development of pulmonary edema and that an acquired transient defect in cyclic nucleotide-gated channels, perhaps due to an environmental factor such as hypoxia, may compound this constitutive defect and further impair alveolar fluid clearance [52-61].
- d. There is direct evidence from animal studies that nasal epithelial function may be a surrogate for alveolar epithelium. Transgenic mice, with endogenous murine α -ENaC replaced by partly functional rat α -ENaC, have been used to investigate the possible role of a constitutively impaired ENaC in the generation of pulmonary edema. These mice grow normally and appear otherwise healthy until physiologically challenged. The baseline nasal potential difference of these mice is reduced by $\sim 50\%$, with the defect, as expected, being linked to the amiloride-sensitive fraction. Similarly, the rate of alveolar fluid clearance is reduced by $\sim 50\%$ compared with wild-type mice. When subjected to experimentally induced lung injury, the transgenic mice are more prone to the development of pulmonary edema, develop a more severe pulmonary edema, and exhibit slower rates of alveolar fluid clearance. Nasal potential difference was also significantly correlated with alveolar fluid clearance. Further comparison of nasal potential difference and alveolar fluid clearance comes from another mouse

study investigating the effects of inducible nitric oxide synthase (iNOS), a possible regulator of amiloride-sensitive Na^+ channels, on alveolar fluid clearance. iNOS (+/+) mice had higher nasal potential difference and similar alveolar fluid clearance values to iNOS (-/-)

mice. In the presence of amiloride both nasal potential difference and alveolar fluid clearance decreased in the controls but there was little change in the knockout mice, again suggesting that nasal Na^+ transport reflects alveolar Na^+ transport.

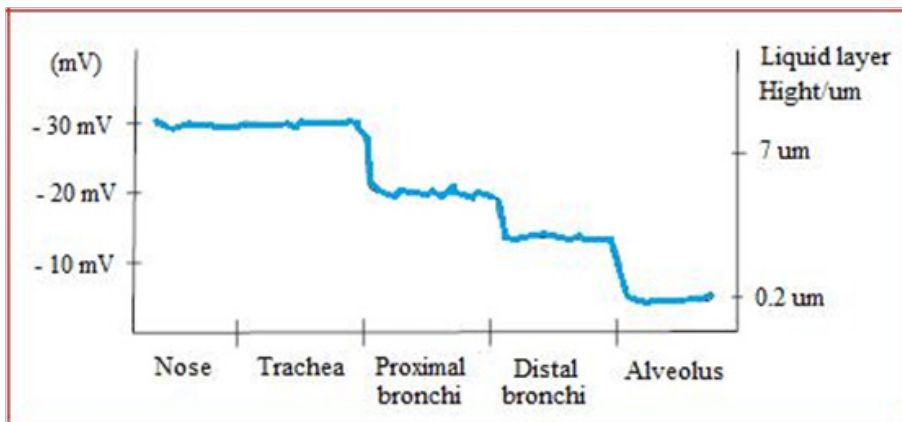


Figure 63: Schematic representation of respiratory potential differences with associated height of respiratory liquid [3].

Several factors could limit the relationship between measured nasal potential difference and alveolar ion transport, especially in the intensive care unit. The nasal epithelium is subjected to a different environment than the alveolus. It has been suggested that altered nasal potential differences seen at high altitude may be reflective of a lack of stimulated Cl^- secretion at this cold dry climate. This is less likely to be of significance in an ICU. Abrasion of the nasal epithelium abolishes nasal potential difference and therefore placement of nasogastric and nasotracheal tubes may affect nasal potential difference measurements. However, nasal potential difference does not vary between nostrils, allowing either nostril to be used [3].

References

- O'Brodovich H, Yang P, Gandhi S, Otulakowski G (2008) Amiloride-insensitive Na^+ and fluid absorption in the mammalian distal lung. *Am J Physiol Lung Cell Mol Physiol* 294(3): L401-L408.
- Bardou O, Trinh NTN, Brochiero E (2009) Molecular diversity and function of K^+ channels in airway and alveolar epithelial cells. *Am J Physiol Lung Cell Mol Physiol* 296(2): L145-L155.
- Mac Sweeney R, Fischer H, McAuley DF (2011) Nasal potential difference to detect Na^+ channel dysfunction in acute lung injury. *Am J Physiol Lung Cell Mol Physiol* 300(3): L305-L318.
- Zhou G, Dada LA, Sznajder JI (2008) Regulation of alveolar epithelial function by Hypoxia. *Eur Respir Jm* 31(5): 1107-1113.
- Blanco G, Mercer R (1998) Isozymes of the Na-K-ATPase: heterogeneity in structure, diversity in function. *Am J Physiol* 275(5 Pt 2): F633-F650.
- Johnson LN, Koval M (2009) Cross-talk between pulmonary injury, oxidant stress, and gap junctional communication. *Antioxid. Redox Signal* 11(2): 355-367.
- Abraham V, Chou ML, George P, Pooler P, Zaman A, et al. (2001) Heterocellular gap junctional communication between alveolar epithelial cells. *Am J Physiol Lung Cell Mol Physiol* 280(6): L1085-L1093.
- Hastings RH, Folkesson HG, Matthay MA (2004) Mechanisms of alveolar protein clearance in the intact lung. *Am J Physiol Lung Cell Mol Physiol* 286(4): L679-L689.
- Folkesson HG, Hedin L, Westrom BR (1992) Lung to blood passage of human growth hormone (hGH) after intratracheal instillation: stimulation of growth in hypophysectomized rats. *J Endocrinol* 134(2): 197-203.
- West JB (1969) Ventilation-perfusion inequality and overall gas exchange in computer models of the lung. *Respir Physiol* 7(1): 88-110.
- Galvin I, Drummond GB, M. Nirmalan M (2007) Distribution of blood flow and ventilation in the lung: gravity is not the only factor. *Brit J Anaesth* 98(4): 420-428.
- Chang H, Lai-Fook SJ, Domino KB, Schimmel C, Hildebrandt J, et al. (2002) Spatial distribution of ventilation and perfusion in anesthetized dogs in lateral postures. *J Appl Physiol* 92(2): 745-762.
- Eyzaguirre C, Zapata P (1984) Perspectives in carotid body research. *J Appl Physiol Respir Environ Exerc Physiol* 57(4): 931-957.
- Vinhaes ENG, Dolhnikoff M, Saldiva PH (2002) Morphological changes of carotid bodies in acute respiratory distress syndrome: a morphometric study in humans. *Braz J Med Biol Res* 35(10): 1119-1125.
- Ganter CG, Jakob SM, Takala J (2006) Pulmonary capillary pressure: A review. *Minerva Anesthesiol* 72(1-2): 21-36.

16. Nunes S, Ruokonen E, Takala J (2003) Pulmonary capillary pressures during the acute respiratory distress syndrome. *Intensive Care Med* 29(12): 2174-2179.
17. Sartori C, Matthay MA (2002) Alveolar epithelial fluid transport in acute lung injury: new insights. *Eur Respir J* 20(5): 1299-1313.
18. Rokaw MD, Sarac E, Lechman E, West M, Angeski J, et al. (1996) Chronic regulation of transepithelial Na⁺ transport by the rate of apical Na⁺ entry. *Am J Physiol* 270(2 Pt 1): C600-C607.
19. Middleton JP (1996) Direct regulation of the Na,K pump by signal transduction mechanisms. *Miner Electrolyte Metab* 22(5-6): 293-302.
20. Modelska K, Matthay MA, Brown LA, Deutch E, Lu LN, et al. (1999) Inhibition of beta-adrenergic-dependent alveolar epithelial clearance by oxidant mechanisms after hemorrhagic shock. *Am J Physiol* 276(5 Pt 1): L844-L857.
21. Conner ER, Ware LB, Modin G, Matthay MA (1999) Elevated pulmonary edema fluid concentrations of soluble intercellular adhesion molecule-1 in patients with acute lung injury: biological and clinical significance. *Chest* 116(Suppl 1): 83S-84S.
22. Ware LB, Golden JA, Finkbeiner WE, Matthay MA (1999) Alveolar epithelial fluid transport capacity in reperfusion lung injury after lung transplantation. *Am J Respir Crit Care Med* 159(3): 980-988.
23. Dudek SM, Garcia JGN (2001) Cytoskeletal regulation of pulmonary vascular permeability. *J Appl Physiol* 91(4): 1487-1500.
24. Tapon N, Hall A (1997) Rho, Rac, and Cdc42 GTPases regulate the organization of the actin cytoskeleton. *Curr Opin Cell Biol* 9(1): 86-92.
25. Garcia JGN, Schaphorst KL, Verin AD, Vepa S, Patterson CE, et al. (2000) Diperoxovanadate alters endothelial cell focal contacts and barrier function: role of tyrosine phosphorylation. *J Appl Physiol* 89(6): 2333-2343.
26. Petrache I, Verin AD, Crow MT, Birukova A, Liu F, et al. (2001) Differential effect of MLC kinase in TNF- α induced endothelial cell apoptosis and barrier dysfunction. *Am J Physiol Lung Cell Mol Physiol* 280(6): L1168-L1178.
27. Siflinger-Birnboim A, Johnson A (2003) Protein kinase C modulates pulmonary endothelial permeability: a paradigm for acute lung injury. *Am J Physiol Lung Cell Mol Physiol* 284(3): L435-L451.
28. Zhou L, Graeff RW, McCray PB, Simonet WS, Whitsett JA (1996) Keratinocyte growth factor stimulates CFTR-independent fluid secretion in the fetal lung in vitro. *Am J Physiol* 271(6 Pt 1): L987-L994.
29. Abraham V, Chou ML, DeBolt KM, Koval M (1999) Phenotypic control of gap junctional communication by cultured alveolar epithelial cells. *Am J Physiol* 276(5 Pt 1): L825-L834.
30. LaRochelle WJ, Sakaguchi K, Atabay N, Cheon HG, Takagi Y, et al. (1999) Heparan sulfate proteoglycan modulates keratinocyte growth factor signalling through interaction with both ligand and receptor. *Biochemistry* 38(6): 1765-1771.
31. Ware LB, Matthay MA (2002) Keratinocyte and hepatocyte growth factors in the lung: roles in lung development, inflammation, and repair. *Am J Physiol Lung Cell Mol Physiol* 282(5): L924-L940.
32. Oswari J, Matthay MA, Margulies SS (2001) Keratinocyte growth factor reduces alveolar epithelial susceptibility to in vitro mechanical deformation. *Am J Physiol Lung Cell Mol Physiol* 281(5): L1068-L1077.
33. Itakura A, Kurauchi O, Morikawa S, Okamura M, Furugori K, et al. (1997) Involvement of hepatocyte growth factor in formation of bronchoalveolar structures in embryonic rat lung in primary culture. *Biochem Biophys Res Commun* 241(1): 98-103.
34. Karbing DS, Kjergaard S, Smith BW, Espersen K, Allerod C, et al. (2007) Variation in the PaO₂/FiO₂ ratio with FiO₂: mathematical and experimental description, and clinical relevance. *Crit Care* 11(6): R118.
35. Gluck E, Sarrigianidis A, Dellinger RP (2002) Mechanical ventilation. In: Parrillo JE, Dellinger RP, et al. (Eds.), *Critical Care Medicine*. (2nd edn), Mosby, USA, pp. 137-161.
36. Stenqvist O (2003) Practical assessment of respiratory mechanics. *Brit J Anaesth* 91(1): 92-105.
37. Krasov S, Soendergaard S, Lundin S, Wiklund J, Stenqvist O (2001) Direct tracheal airway pressure measurements are essential for safe and accurate dynamic monitoring of respiratory mechanics. A laboratory study. *Acta Anaesthesiol Scand* 45(2): 173-179.
38. Krasov S, Soendergaard S, Lundin S, Wiklund J, Stenqvist O (2000) A new method for non-invasive, manoeuvre-free determination of static pressure-volume curves during dynamic/therapeutic mechanical ventilation. *Acta Anaesthesiol Scand* 44(5): 578-585.
39. de Chazal I, Hubmayr RD (2003) Novel aspects of pulmonary mechanics in intensive care. *Brit J Anaesth* 91(1): 81-91.
40. Roupie E, Dambrosio M, Servillo G, Mentec H, el Atrous S, et al. (1995) Titration of tidal volume and induced hypercapnia in acute respiratory distress syndrome. *Am J Resp Crit Care Med* 152(1): 121-128.
41. Tobin MJ (2001) Medical progress: advances in mechanical ventilation. *N Engl J Med* 344(26): 1986-1996.
42. Kallet RH (2011) Patient-ventilator interaction during acute lung injury, and the role of spontaneous breathing: part 1: respiratory muscle function during critical illness. *Respir Care* 56(2): 181-189.
43. Laghi F, Cattapan SE, Jubran A, Parthasarathy S, Warshawsky P, et al. (2003) Is weaning failure caused by low frequency fatigue of the diaphragm? *Am J Respir Crit Care Med* 167(2): 120-127.
44. Laghi F (2002) Curing the septic diaphragm with the diaphragm. *Am J Respir Crit Care Med* 165(2): 145-146.
45. Petrof BJ, Jaber S, Matecki S (2010) Ventilator-induced diaphragmatic dysfunction. *Curr Opin Crit Care* 16(1): 19-25.
46. Kallet RH, Katz JA (2003) Respiratory system mechanics in acute respiratory distress syndrome. *Respir Care Clin N Am* 9(3): 297-319.
47. Kallet RH, Hemphill JC, Dicker RA, Alonso JA, Campbell AR, et al. (2007) The spontaneous breathing pattern and work of breathing of patients with acute respiratory distress syndrome and acute lung injury. *Respir Care* 52(8): 989-995.

48. Guyton AC, John EH (2006) Textbook of Medical Physiology. (11th edn), Elsevier.
49. Tamarkin (2011) Anatomy and physiology. Springfield, Massachusetts, USA.
50. Kerem E, Bistrizer T, Hanukoglu A, Hofmann T, Zhou Z, et al. (1999) Pulmonary epithelial sodium-channel dysfunction and excess airway liquid in pseudohypoaldosteronism. *N Engl J Med* 341(3): 156-162.
51. Glenny RW, Lamm WJE, Bernard SL, et al. (2000) Selected contribution: redistribution of pulmonary perfusion during weightlessness and increased gravity. *J Appl Physiol* 89: 1239-1248.
52. Hickling KG (2002) Reinterpreting the pressure-volume curve in patients with acute respiratory distress syndrome. *Curr Opin Critical Care* 8: 32-38.
53. Kallet RH (2003) Pressure-volume curves in the management of acute respiratory distress syndrome. *Respir Care Clin N Am* 9: 321-341.
54. Nunes S, Uusaro A, Takala J (2004) Pressure-volume relationships in acute lung injury: methodological and clinical implications. *Acta Anaesthesiol Scand* 48: 278-286.
55. Pedley TJ, Kamm RD (1997) Dynamics of gas flow and pressure flow relationships. In *The Lung: Scientific Foundations*, (2nd edn), Edited by Crystal RG, West JB, Barnes PJ, Wiebel EW. Lippincott- Raven, Philadelphia, USA, pp. 1365-1380.
56. Respiratory Muscle Fatigue Workshop Group (1990) Report: respiratory muscle fatigue. *Am Rev Respir Dis* 142(2): 474-480.
57. Rignault S, Haefliger JA, Waeber B, Liaudet L, Feihl F (2007) Acute inflammation decreases the expression of connexin40 in mouse lung. *Shock* 28: 78-85.
58. Tantucci C, Duguet A, Giampiccolo P, Similowski T, Zelter M, et al. (2002) The best peak expiratory flow is flow-limited and effort-independent in normal subjects. *Am J Resp Crit Care Med* 165: 1304-1308.
59. van de Woestijne KP, Zapletal A (1970) The maximum expiratory flow volume curve: peak flow and flow dependent portion. In *Airway Dynamics, Physiology, and Pharmacology*. Thomas: Springfield, IL: 61-83.
60. Ware LB, Matthay MA (2005) Acute pulmonary edema. *N Engl J Med* 353: 2788-2796.